UNIVERSITY OF SOUTHAMPTON

FACULTY OF ENGINEERING AND APPLIED SCIENCE

INSTITUTE OF SOUND AND VIBRATION RESEARCH

NONLINEAR DYNAMIC BEHAVIOUR OF FULLY CLAMPED BEAMS AND RECTANGULAR ISOTROPIC AND LAMINATED PLATES

by

RHALI BENAMAR

Ingénieur de l'école nationale des Ponts et Chaussées

Thesis submitted in fulfilment of the degree of

Doctor of Philosophy

April 1990

CONTENTS

FACULTY OF ENGINEERING AND APPLIED SCIENCE
INSTITUTE OF SOUND AND VIBRATION RESEARCH

Doctor of Philosophy

NONLINEAR DYNAMIC BEHAVIOUR OF FULLY CLAMPED BEAMS AND RECTANGULAR ISOTROPIC AND LAMINATED PLATES

by **Rhali Benamar**

Abstract

The nonlinear vibration of fully clamped beams and rectangular isotropic and laminated plates at large vibration amplitudes is examined in this work. Complementary theoretical and experimental studies have been carried out which show that the mode shapes and natural frequencies are amplitude dependent with accentuated nonlinear behaviour in the case of CFRP plates. A theoretical model has been developed, based on Hamilton's principle and spectral analysis, which allows all of the above cases to be treated in a unified manner and provides a rapid method for calculating the change in mode shapes and natural frequencies at large amplitudes of vibration. Measurements and analyses of the spatial distribution of the response harmonic distortion of a fully clamped rectangular isotropic plate show that the response second harmonic component is spatially distributed according to the second mode shape of the plate tested. An attempt has been made to develop a theoretical model for nonlinear free vibration of beams and plates taking into account the spatial distribution of harmonic distortion.

ACKNOWLEDGEMENTS

So many friends and colleagues at the ISVR and EMI have helped in various ways to make this work possible. I would like to mention particularly:

- Professor R.G. White, for his supervision of this work and for his numerous short and busy trips to Morocco, during which he did, in spite of his busy schedules, give me good advice and encouragement.

- Professor M.M.K. Bennouna, who introduced me to the fascinating area of structural dynamics and to the ISVR.

- Mr. A. Dikouk and Mr. M. Ouazzani, for their assistance during measurements in a very noisy environment at the EMI.

- Mr. J.F. Hawkes for the manufacture of CFRP specimens and adaptation of OVT's.

- Mr. J. Baker, whose technical assistance and constant patience have been of great help during the long and unpleasant experiments on the progressive wave tube at the ISVR.

- Mrs. M. Strickland and Ms. M. Hicks, who agreed to do the last part of the typing and drawing work in a very limited time, and did it in an excellent manner.

My deep and grateful thanks go to my father, who taught me to read, understand and write at a very young age, and provided me with books in so many varied areas; and to my mother, from whom I learned so much, and whose affection is the most precious treasure.

LIST OF TABLES

CHAPTER III

CHAPTER IV

CHAPTER V

CHAPTER VI

CHAPTER VII

CHAPTER VIII

CHAPTER IX

LIST OF FIGURES

LIST OF SYMBOLS

The symbols are generally listed in the order of their first appearance in the text .

CHAPTER I

U,V	in-plane displacements at points (x,y) of the plate in the x and y directions, respectively
W	transverse displacement at point (x,y) of the plae
F	Airy stress functions

CHAPTER II

x,y,z	coordinate system
ω	frequency in rad/s
V_b	bending strain energy
V_a	axial strain energy
T	kinetic energy
$\bar{x}$	vector coordinate ($\bar{x} = x$ in the beam case and $\bar{x} = (x,y)$ in the plate case)
$w(\bar{x},t)$	transverse displacement. $w(\bar{x},t) = w(\bar{x}) \sin \omega t$
$w_i(\bar{x})$	i^{th} basic function used in the series expansion of $w(\bar{x})$
a_i	contribution coefficient of $w_i(\bar{x})$ in the series expansion of w_i
k_{ij}	rigidity tensor general term
m_{ij}	mass tensor general term
b_{ijkl}	geometrical nonlinearity tensor general term
Φ	generalised action over the period $[0, \frac{2\pi}{\omega}]$. $\phi = \int_0^{2\pi/\omega} (V-T)$
δ_{ij}	Kronecker symbol. $\delta_{ij} = 1$ if $i = j$ and $\delta_{ij} = 0$ if $i \neq j$
[K]	rigidity matrix
[B(A)]	nonlinear geometrical rigidity matrix
[M]	mass matrix
{A}	column matrix of the contribution coefficients a_i

CHAPTER IV

V_b bending strain energy

V_a axial strain energy

F axial load induced by large transverse vibrations

T kinetic energy

k_{ij} rigidity tensor general term

b_{ijkl} geometrical nonlinearity tensor general term

m_{ij} mass tensor general term

α non-dimensional parameter. $\alpha = \frac{AH^2}{4I}$

x^* non-dimensional coordinate. $x^* = \frac{x}{L}$

w_i^* non-dimensional clamped-clamped beam basic function

k^*_{ij} non-dimensional rigidity tensor general term

$$k^*_{ij} = \frac{L^3}{EIH^2} k_{ij}$$

m^*_{ij} non-dimensional mass tensor general term

$$m^*_{ij} = \frac{1}{\rho AH^2 L} m_{ij}$$

b^*_{ijkl} non-dimensional geometrical nonlinearity tensor general term

$$b^*_{ijkl} = \frac{L^3}{EIH^2}$$

ω^*_{nl} non-dimensional nonlinear natural frequency parameter.

$$(\omega^*_{nl})^2 = \frac{\rho AL^4}{EI} \omega^2$$

ω_l linear circular frequency

ω_l^* non-dimensional natural frequency parameter

$$(\omega_l^*)^2 = \frac{\rho AL^4}{EI} (\omega_l^*)^2$$

δ_{ij} Kronecker symbol. $\delta_{ij} = 0$ if $i \neq j$ and $\delta_{ij} = 1$ if $i = j$

ω_{ro} amplitude dependent nonlinear natural frequency of the r_0^{th} mode of the simply supported beam

ω_1 amplitude dependent nonlinear natural frequency of the fundamental mode of the simply supported beam.

v_1 eigenfunction parameters of a clamped-clamped beam

G a normalisation factor for non-dimensional clamped-clamped beam functions

CHAPTER V

D	bending stiffness of the plate $D = \dfrac{EH^3}{12(1 - \nu^2)}$
ρ	mass per unit volume of the plate
$W(x,y,t)$	transverse displacement of the plate middle plane at point (x,y) $W(x,y,t) = w(x,y) \sin \omega t$
V_b	bending strain energy
u,v	in-plane displacement in x and y directions respectively
V_a	axial strain energy
$w(x,y)$	transverse displacement spatial function
$w_i(x,y)$	i^{th} basic functions in the transverse displacement series expansion
a_i	contribution coefficient of the function $w_i(x,y)$ in the transverse displacement series expansion
$\{A\}$	column matrix of contribution coefficients
T	transposition of matrix
$\{w\}$	column matrix of basic functions
$\left\{\dfrac{\partial^2 w}{\partial x^2} + \dfrac{\partial^2 w}{\partial y^2}\right\}$	column matrix of functions $\left(\dfrac{\partial^2 w}{\partial x^2} + \dfrac{\partial^2 w}{\partial y^2}\right)$
$[K]$	mass matrix
k_{ij}	rigidity tensor general term
$\left\{\dfrac{\partial w}{\partial x}\right\}$	column matrix of functions $\dfrac{\partial w_i}{\partial x}$
$[C_{ij}(x,y)]$	$n \times n$ square matrix of functins $C_{ij}(x,y)$
$C_{ij}(x,y)$	(x,y) functions defined by $C_{ij}(x,y) = \dfrac{\partial w_i}{\partial x}\dfrac{\partial w_j}{\partial x} + \dfrac{\partial w_i}{\partial y}\dfrac{\partial w_j}{\partial y}$
T	kinetic energy
α	plate aspect ratio. $\alpha = \dfrac{b}{a}$
x^*,y^*	non-dimensional coordinate. $x^* = \dfrac{x}{a}$, $y^* = \dfrac{y}{b}$
$w_i^*(x^*,y^*)$	non-dimensional basic function. $w_i^*(x^*,y^*) = \dfrac{1}{H} w_i(x,y)$
k^*_{ij}	non-dimensional rigidity tensor general term. $k^*_{ij} = \dfrac{b^3}{DaH^2} k_{ij}$
b^*_{ijkl}	non-dimensional geometrical nonlinearity tensor general term. $b^*_{ijkl} = \dfrac{b^3}{DaH^2} b_{ijkl}$

m^*_{ij} non-dimensional mass tensor

$$m^*_{ij} = \frac{1}{\rho H^3 ab} m_{ij}$$

S^* non-dimensional surface $[0,1] \times [0,1]$

ω^* non-dimensional circular frequency parameter

$$\omega^{*2} = \frac{12(1 - \nu^2)\rho b^4}{EH^2} \omega^2$$

α_i the index of the clamped-clamped beam mode intervening in the x direction in the i^{th} plate basic functions

β_i the index of the clamped-clamped beam mode intervening in the y direction in the i^{th} plate basic functions

$f^a_{\alpha_i}$ an α_i'th clamped-clamped beam mode

v_{α_i} clamped-clamped beam parameter

G a normalization factor

$g^a_{\alpha_i}(x^*)$ a non-dimensional α_i'th clamped-clamped beam mode

$g^c_{\alpha_i}(x^*)$ second derivative of $g^a_{\alpha_i}(x^*)$

$g^b_{\alpha_i}(x^*)$ first derivative of $g^a_{\alpha_i}(x^*)$

pinaa, pinca, pincc clamped-clamped beam integrals (equation (5.40), (5.43) and (5.44)) (Notation employed in Fortran programs for clarity)

pin4a, pin4b, pin4c clamped-clamped beam integrals (equations (5.47) to (5.49)) (Notation employed in Fortran programs for clarity)

CHAPTER VII

ω fundamental circular frequency (Rad/s)

$\{w\}$ column matrix of clamped-clamped beam functions

$\{A_1\}$ column matrix of contribution coefficients to the first harmonic

$\{A_2\}$ column matrix of contribution coefficients to the second harmonic

$\{A_q\}$ column matrix of the contribution coefficients to the q^{th} harmonic

a_i^q contribution coefficient for the i^{th} spatial basic function and the q^{th} time harmonic

x,τ spatial and time coordinate

V_b, V_a, T as in Chapter IV

E, I, L, ρ as in Chapter IV

α_{qr} second order tensor for rigidity coupling beween time harmonics

β_{qr} second order tensor for mass coupling beween time harmonics

γ_{qrst} fourth order tensor for nonlinear rigidity coupling between time harmonics

Φ generalised action over the period $[0, 2\pi/\omega]$

$$\Phi = \int_0^{2\pi/\omega} (V - T)$$

Φ_b, Φ_a, Φ_k bending strain, axial strain and kinetic energy contributions to Φ.

CHAPTER VIII

ω fundamental circular frequency (Rads/s)

$\{w\}$ column matrix of fully clamped rectangular plate functions

$\{A_n\}$ column matrix of contribution coefficients to the first harmonic

$\{A_2\}$ column matrix of contribution coefficients to the second harmonic

$\{A_q\}$ column matrix of the contribution coefficients to the q^{th} harmonic

a_i^q contribution coefficient for the i^{th} spatial basic function and the q^{th} time harmonic

x, y, τ spatial and time coordinate

V_b, V_a, T as in Chapter V

E,H,D,a,b as in Chapter V

α_{qr} second order tensor for rigidity coupling beween time harmonics

β_{qr} second order tensor for mass coupling beween time harmonics

γ_{qrst} fourth order tensor for nonlinear rigidity coupling between time harmonics

CHAPTER IX

x,y,z coordinate system

$\bar{U}, \bar{V}, \bar{W}$ total displacements

U,V,W displacements of the mid-plane

$\varepsilon_x, \varepsilon_y, \gamma_{xy}$ tensor strain components

$\{\varepsilon^0\}$ column matrix of strains due to the in-plane displacements u, v, w

$\{K\}$ column matrix of bending or twisting

$\{\lambda^0\}$ column matrix of strains induced by large displacements W.

$\{\varepsilon\}$ column matrix of total strains

$[\bar{Q}]$ 3×3 matrix of transformed reduced stiffnesses

$N_x^{(k)}, N_y^{(k)}, N_{xy}^{(k)}$ force resultant for the k^{th} layer

$M_x^{(k)}, M_y^{(k)}, M_{xy}^{(k)}$ moment resultant for the k^{th} layer

$\{N_k\}$ column matrix of force resultant for the k^{th} layer

$\{M_k\}$ column matrix of moment resultant for the k^{th} layer

$A_{ij.k}, B_{ij.k}, D_{ij.k}$ extensional, coupling and bending stiffness coefficients for the k^{th} layer

A_{ij}, B_{ij}, D_{ij} extensional, coupling and bending stiffness coefficients for the laminated plate

ω, V_a, V_b, T as in Chapter V

$a_i, k_{ij}, m_{ij}, b_{ijkl}$ as in Chapter V

A^*_{ij}, D^*_{ij} non-dimensional extensional and bending stiffness coefficients

$k^*_{ij}, m^*_{ij}, B^*_{ijkl}, \omega_i^*$ as in Chapter V

CHAPTER I

INTRODUCTION

I.1 GENERAL INTRODUCTION TO THE MAIN TOPICS OF THIS WORK

The domain of validity of all linear theories of structural vibrations is limited to vibration amplitudes which are small compared with the thickness of the structure. As the speed of modern machines is increasing and the weight decreasing, large vibration amplitudes often occur in the neighbourhood of resonance frequencies. It is of great interest in such cases to know how far the dynamic characteristics of the structure deviate from those defined via the linear theories. Also, dynamic analysis techniques applied to nonlinear vibration problems can be more accurate if nonlinear analysis methods are available. Qualitative description of nonlinear behaviour can also be very useful in understanding data provided by modal testing. The mode shapes are of particular interest in the study of the dynamic behaviour of a structure, since the axial and bending strains are dependent upon the first and second derivatives of the mode shapes. Large vibration amplitudes of plate-type structures are encountered in many engineering applications, especially in aerospace. The case of fully clamped boundaries can be adequate for idealising many real panel-type situations, as aircraft wing panels [1.1].

A numerical model, derived from the nonlinear differential equation of motion of beams at large deflections has been developed in [1.2] to calculate an amplitude dependent fundamental mode shape of a clamped-clamped beam. Experimental and theoretical studies reported in the above reference have shown that the beam fundamental mode shape was clearly dependent on the amplitude of vibration, especially near to the clamps. High values of increase of beam curvature were noticed near to the clamps causing a highly nonlinear increase in bending strain with increasing deflection instead of the linear rate of increase usually observed in the linear theory. Experimental measurements, reported in [1.2], showed that the dynamic response of a clamped-clamped beam, at large deflections, exhibits a spatial distribution of the response harmonic distortion. Experimental work, reported in [1.3], has shown that the response harmonic distortion, occurring at large vibration amplitudes, can have a significant influence on the fatigue life of structures undergoing large amplitudes of vibrations. An attempt has been made in [1.2] to develop a theoretical model to explain the spatial distribution of the second and third harmonics in the beam case. In [1.4], theoretical results, obtained by a finite element method applied to

nonlinear free vibrations of a simply supported square plate, are presented showing an amplitude dependent spatial distribution of the third harmonic component of the deflection at large vibration amplitudes.

Composite materials with high stiffness-to-weight- ratio, such as those made of fibre reinforced plastics, are becoming increasingly used to build high performance structures which are required for aerospace applications. Carbon fibre reinforced plastics (CFRP) are one type of composite which have been used to advantage in that field. However, experiments reported in [1.5] have shown that a CFRP plate subjected to high level acoustic excitation exhibited more nonlinear behaviour at large amplitudes of vibration than a similar metal plate excited in similar conditions. Also, although the specific modulus of elasticity can be shown to be, for a typical structural fibre volume fraction of 60 %, three times greater for CFRP than for steel or aluminium alloy, the inherent damping of CFRP is, however, low at 60% fibre volume fraction and comparable to that of aluminium alloy [1.6]. So, if resonant behaviour occurs, response amplitude will be relatively high and fatigue could occur. Nonlinear dynamic analysis methods are therefore necessary to have more accurate knowledge of CFRP structural behaviour at large vibration amplitudes.

I.2 REVIEW OF WORK ON LINEAR MODE SHAPES AND NATURAL FREQUENCIES OF THIN ELASTIC PLATES

The determination of the natural frequencies and mode shapes of vibrating plates has been a subject of numerous experimental and theoretical investigations for nearly two centuries, since the experimental work of Chladni was produced in 1787, giving the first known observations of the nodal patterns for completely free square plates [1.7]. Since then, well known investigators, such as Rayleigh, Voight, Love and Ritz, have been associated with this problem [1.7, 1.8]. However, as the partial differential equation governing the transverse vibrations of thin elastic plates has no complete analytical solution, as pointed out by Love and Timoshenko [1.8], no exact solutions have yet been found for most of the boundary condition cases. Consider the case of rectangular plates; 21 combinations of classical boundary conditions exist and exact solutions are known only for the six cases having two opposite edges simply supported. Furthermore, in a survey made by Leissa in 1973 [1.7] it was pointed out that until 1954, when Warburton derived his formulae based on a single-term representation of the deflection mode shapes for the natural frequencies of plates with various boundary conditions, no solution, even approximate, was known for six boundary condition cases. The general accuracy of Warburton's formulae is discussed in

reference [1.7]. Although the clamped boundary conditions are mathematically simple, only approximate solutions are available for the linear mode shapes and resonance frequencies of fully clamped rectangular plates. A brief survey of the techniques and references relative to this case is given in the introduction to Chapter V.

I.3 GENERAL REVIEW OF WORK ON LARGE VIBRATION AMPLITUDES OF PLATES

I.3.1 Introduction

As outlined in reference [1.9] , the subject of nonlinear vibrations has always been a difficult one, since many of the solution characteristics, such as existence, uniqueness and superposition, which are guaranteed for linear vibration problems, are not guaranteed, and often not valid, in the nonlinear case.

The source of nonlinearity may be (1) material, *i.e.,* due to nonlinear stress strain relations; (2) geometrical, *i.e.,* due to the axial load induced by large displacements of a structure restrained at its ends or edges; (3) inertial in the case of structures having a concentrated or distributed mass; (4) due to nonlinear boundary conditions such as a nonlinear spring...*etc.* [1.9,1.10]. The geometrical nonlinear behaviour, which is of main concern in the present work, can be illustrated using curves such as that given in [1.11], in which the static deflection at the centre of a plate fully clamped is plotted versus the applied uniform static load. It is seen that as the load is increased, the deflection is increased almost linearly for small values of the load. For higher load values, the rate of increase of the deflection with increasing load decreases due to the load being more and more resisted by the tensile forces in the midplane of the plate. Thus, the plate stiffness increases with deflection and the plate behaviour can be approximated by that of a nonlinear spring [1.12].

I.3.2 Review of Nonlinear Theory of Large Vibration Amplitude of thin elastic plates

The objective of this section is to make a brief summary of the methods and techniques which have been used in the literature to study the nonlinear vibrations of plates. Rather than attempting a complete survey, which would exceed the scope of the present work, the purpose is to provide some reference points related to various aspects of this problem discussed in section 1.3.2.6 and in Chapter V.

1.3.2.1 Solutions based on the perturbation procedure

In 1956, Chu and Hermann established the set of three nonlinear partial differential equations governing large vibration amplitudes of thin elastic plates [1.13]. These equations, known as the dynamic analogue of the Von Karman equations for the static case, were obtained by substituting the stress displacement relation for large amplitudes of vibration established by Timoshenko into the plate equations of motion. Then, dealing with the simply supported plate, an approximate analytical solution was obtained using a perturbation procedure for the three displacement functions U, V and W. Rehfield in 1973 [1.14] used a perturbation procedure associated with Hamilton's principle to reduce the nonlinear vibration problem to a sequence of linear problems and derived a formula for the nonlinear fundamental natural frequency of a simply supported plate which was in agreement with the results of Chu and Hermann. It should be noted that although the above two methods were based on different approaches, both assumed a single spatial mode.

1.3.2.2 Solutions based on Berger's approximation

In order to solve the static problem, Berger [1.15] proposed, in 1955, an approximation consisting of neglecting the second invariant of the middle surface strain tensor in the total strain energy expression. Nash and Modeer [1.16] applied the same approximations to the dynamic problem and obtained two partial differential equations in terms of the transverse displacement W and the first invariant. The main feature of this approximation is that it leads, when the in-plane inertia terms are neglected, to a great simplification from two coupled fourth order equations (in terms of the transverse displacement W and the stress function F) to a single fourth order equation (in terms of W). Also, a consequence of Berger's approximation is that the sum of the membrane strains is a constant throughout the plate.

Besides Nash and Modeer, wide use was made of the Berger approximation in the study of the nonlinear problem. However, no complete explanation of this approximation was offered. For simply supported plates with immovable edges, comparisons made in [1.10] of the solution obtained by Wah [1.17] and Chu and Hermann [1.13] showed that the errors introduced by the Berger approximation is minimised for plates of aspect ratio of 0.5 for all amplitudes. The error increases as the aspect ratio deviates from 0.5 and the dimensionless displacement amplitude tends to 1. For circular plates restrained at the edges, Huang and Al Khattat found that the Berger approximation leads to accurate results at low amplitudes and that the accuracy decreases as the amplitude increases [1.18].

In the case of fully clamped rectangular isotropic and orthotropic plates, Sathyamoorthy has found that the Berger approximation leads to results comparable with those obtained by the stress function method, associated with an averaging technique for satisfying the in-plane boundary conditions [1.19]. In [1.20], the same averaging technique was used and results are presented for isotropic and orthotropic clamped rectangular plates with immovable edges showing that the difference between both methods decreases as the aspect ratio, defined as the length to width ratio, decreases from about 4 and is a minimum for square plates. In the analyses based upon Berger's approximation, the common approach is to assume a solution as a product of a spatial mode satisfying the boundary conditions and a function of time. Then this assumed solution is substituted into the uncoupled equation of transverse motion, which results in a nonlinear differential equation of the Duffing type in terms of the time function only, which has well known solutions. This procedure is illustrated in [1.19].

I.3.2.3 Solutions based on the stress function method

In this method, very often used to analyse nonlinear vibrations of isotropic and nonhomogeneous plates, the in-plane inertia terms are neglected, which allows an Airy stress function to be defined and the problem results in two coupled nonlinear partial differential equations in terms of the transverse displacement W and F. Again a solution is assumed as a product of a spatial mode satisfying the transverse boundary conditions and a function of time, which is substituted into the compatibility equation, whose solution permits one to obtain an expression of F in terms of constants of integration and the time function. Using the averaging technique presented in [1.20] to satisfy the in-plane boundary conditions, the constants of integration are determined and the resulting expression of F is substituted in the transverse coupled differential equation of motion, which is approximately satisfied using Galerkin's procedure. The resulting differential equation in terms of the time function is of the Duffing type. A summary of this method, still commonly used for both isotropic and orthotropic plates [1.21, 1.22] is presented in [1.9].

I.3.2.4 Solution based on the Finite Element method

The finite element method has been applied to analyse nonlinear vibrations of plates. In [1.4], an incremental Hamilton's principle with the associated element formulation was applied to study the nonlinear vibrations of fully clamped and simply supported plates, in which the transverse displacement involved two time harmonics, the first and the third, and the in-plane displacement involved the second harmonic. A maximum difference of 0.8% was found between the calculated nonlinear resonance frequency in the above reference and results obtained by Chu and Hermann [1.13] for simply supported plates with immovable

edges and an amplitude of vibration equal to the plate thickness. In the case of a fully clamped square plate, results obtained in [1.4] are compared with previous results obtained by the finite element formulation given in [1.23] and [1.24], in which the in-plane displacement was assumed to be zero over the whole plate.

I.3.2.5 Solutions for the case of fully clamped rectangular plates

Using the stress function method associated with the Galerkin technique, Yamaki [1.25] solved the simply supported and fully clamped cases for three combinations of the in-plane boundary conditions i.e. (a) all edges stress free, (b) all edges immovable and (c) all edges movable. In [1.19], solutions obtained are given in graphical form and compared with results obtained using either the Berger approximation or the stress function method for both the isotropic and orthotropic cases. In [1.26], solutions obtained using a finite element formulation in which the in-plane stresses were assumed to be constant for each element are given in graphical form for a fully clamped square plate. In [1.27], results obtained using a finite element formulation associated with a linearisation of the strain displacement relation and an iterative method of solution are given for the three first modes of a clamped-clamped rectangular plate and the fundamental mode of a rectangular plate with an aspect ratio of 2. In [1.4] a finite element formulation based on an incremental Hamilton's principle is used to obtain solutions for a fully clamped square plate. In [1.21], the ultraspherical polynomial approximation method is used, combined with the stress function method as developed in [1.28], to obtain solutions for a fully clamped square plate, and the results are compared with those obtained using the elliptic function method.

I.3.2.6 Conclusions

It appears from the above discussion that in spite of considerable research, no exact solution for the complicated problem of nonlinear vibrations of rectangular plates is known. Various methods involving different types of analytical and numerical approximations have been applied. Among these approximations, the assumption of a single mode of vibration is one of the most widely used. Also, as outlined in [1.9], the large in-plane displacements are generally not considered, and except for the case of simply supported plates treated in [1.13], no solution, even approximate, was found for the in-plane displacements at large amplitudes. Furthermore, among 3^8 combinations of in-plane boundary conditions mentioned in [1.20], only a few appear in the literature, and the completely immovable edge conditions are often enforced by an approximate averaging technique.

On the other hand, it should be noted that the validity of some of the most basic assumptions involved in the above approximate methods, such as the Berger approximation

[1.15], the averaging technique for enforcing the in-plane boundary conditions [1.20], zero in-plane displacements [1.23,1.24], is very difficult to establish rigorously, and the procedure generally adopted is to compare results obtained by a given method to those of previous theories or to experimental data.

I.4 OBJECTIVES OF THE PRESENT WORK

In the present work, the amplitude dependence of the dynamic characteristics and mode shapes of fully clamped beams and rectangular isotropic and laminated plates have been theoretically and experimentally investigated. A theoretical model for large vibration amplitudes of thin straight structures has been developed which appeared as an extension of the Rayleigh-Ritz linear eigenvalue problem to the nonlinear case. Assuming harmonic motion and expanding the displacement in the form of a series of functions, an expression has been derived for the strain energy at large amplitudes. In this expression, in addition to the classical mass and rigidity tensors, a fourth order tensor appeared due to the nonlinearity. However, although the strain energy was a nonlinear functional of the displacement and its derivatives, it was shown that unless finite contribution for a given mode was assumed, the application of Hamilton's principle with the above formulation leads to the linear vibration theory. In the light of this conclusion, the technique adopted was to first assume a given value for one mode contribution. Then, Hamilton's principle was applied in order to determine the other mode contributions. The set of nonlinear algebraic equations obtained by this technique has to be solved numerically in each case, leading to a set of nonlinear mode shapes, each mode being given as function of the maximum amplitude of vibration and the corresponding natural frequency.

A set of nonlinear mode shapes of a clamped-clamped beam, has been obtained via the above model and compared with results from a previous study [1.3]. An investigation has also been made of the assumption that the linear mode shapes of simply supported beams occur in the case of large vibration amplitudes and various formulae proposed in the literature for the nonlinear fundamental natural frequency of a simply supported beam at large deflections are discussed and compared to the results of the present work.

The theoretical model had been applied to fully clamped rectangular plates. Using products of separated x and y clamped-clamped beam functions as basic functions and adopting the solution procedure discussed above, numerical results corresponding to the first nonlinear plate mode shape were obtained, for various values of the plate aspect ratio.

Since the theoretical model presented above is based on the energy expressions at large deflections, it has been possible to extend it to symmetrically laminated CFRP plates using the additive property of the energy and the relationships between stress and strain and between strain and displacement corresponding to each lamina. The expression obtained for the fourth order non-linearity tensor was more complicated than in the homogeneous case. However, numerical results have been obtained corresponding to the first non-linear mode shape of some fully clamped CFRP plates.

The amplitude dependence of the resonance frequency and the spatial distribution of the first and second harmonic components of the dynamic response of fully clamped rectangular homogenous and CFRP plates have been investigated experimentally. Using an electrodynamic point excitation at the middle of the plate and a non-contacting optical vibration transducer, the response signals have been acquired and analysed using FFT and Zoom algorithms. Also, the phase lag between components at different points on the plate have been carefully investigated in order to check the components spatial distribution of the components.

In order to reach higher amplitudes of vibration, a set of tests were carried out , using the ISVR progressive wave tube and acoustic siren facility, in which the plates tested were subjected to high level acoustic excitation, up to 155 dB. Results of such experimental measurements are given and compared to the theory.

On the other hand, using Hamilton's principle and spectral analysis, and assuming a response in which several harmonics were taken into account, the numerical model for nonlinear vibrations of beams and plates presented above has been extended to include the harmonic distortion effects and some numerical results were obtained.

CHAPTER II

THEORETICAL MODEL FOR NONLINEAR FREE VIBRATIONS OF THIN STRAIGHT STRUCTURES AT LARGE VIBRATION AMPLITUDES

II.1 INTRODUCTION

For a large class of vibration problems, analytical solutions do not exist. Among the numerical approximate methods available, the Rayleigh-Ritz method is one of the most widely used in the field of structural vibrations. Although this method can be rigorously derived in the linear case from very general mechanical laws, such as Hamilton's principle, or its equivalent Lagrange's equations, it is quite often presented in terms of minimisation of Rayleigh's quotient, which is the maximum potential energy to maximum reference kinetic energy[1] ratio during one period of vibration, to obtain the linear eigenvalue problem, which leads to the mode shapes and the corresponding natural frequencies of the structure considered [2.1,2.2] . As such, this method is very convenient in many engineering applications, because of its simplicity and ability to be adapted to various situations and to give quick approximations . However, for nonlinear problems, this method has to be adapted because, as will be shown in the theory developed in this chapter, its theoretical justification cannot be extended to the nonlinear case without modification . Also, as illustrated below in equation (2.4), the nonlinear potential energy expression relative to large deflections can contain sine terms with a power greater than two, and consequently, the potential energy can have more than one maximum in a period of vibration. Finally, the harmonic distortion occurring at large vibration amplitudes , which was shown to be spatially distributed, as examined in Chapters VI to VIII, makes the energy exchange between spatial modes and time harmonics much more complicated than in the linear case. Therefore, it was necessary to develop a theoretical model, in order to adapt the Rayleigh-Ritz method to nonlinear problems and this was the objective of the theory reported in this chapter.

---

[1]The reference kinetic energy is the maximum kinetic energy during one period of vibration divided by ω^2 [2.2].

II.2 EXPRESSIONS FOR THE BENDING STRAIN, THE AXIAL STRAIN AND THE KINETIC ENERGIES IN THE NONLINEAR CASE.

Considering thin straight structures, such as beams and plates, the total strain energy can be written as the sum of the strain energy due to bending, denoted here as V_b, plus the axial strain energy due to the axial load induced by large deflections, V_a. As will be illustrated in Chapter IV dealing with beams, in Chapter V dealing with isotropic plates and in Chapter IX dealing with CFRP plates , V_b is in many cases a quadratic functional , *i.e.* a function of functions, of the deflection W and its derivatives; V_a is a fourth order functional of W and its derivatives.

If the time and space functions are supposed to be separable and harmonic motion is assumed, the transverse displacement can be written as:

$$W(\bar{x},t) = w(\bar{x}) \sin\omega t \qquad (2.1)$$

where $\bar{x}$ is the vector coordinate ($\bar{x} = (x,y)$ in the plate case and $\bar{x} = x$ in the beam case). Expanding $w(\bar{x})$ in the form of a finite series :

$$W(\bar{x}) = a_i w_i(\bar{x}) \sin\omega t \qquad (2.2)$$

the total strain energy expression, V, can be obtained. In equation (2.2), and throughout this thesis, we use the usual summation convention explained in Appendix K. Thus, the repeated index i is summed over 1, 2,..., n. with n being the number of the basic spatial functions $w_i(x)$ supposed to contribute to the function $w(\bar{x})$ assumed in equation (2.1). As will be shown in Chapter IV, dealing with beams; in Chapter V, dealing with isotropic plates; and in Chapter IX, dealing with laminated plates, substituting W in the expressions for V_b and V_a and rearranging leads to :

$$V_b = \frac{1}{2} a_i a_j k_{ij} \sin^2\omega t \qquad (2.3)$$

$$V_a = \frac{1}{2} a_i a_j a_k a_l b_{ijkl} \sin^4\omega t \qquad (2.4)$$

where k_{ij} is the classical rigidity tensor and b_{ijkl} is the nonlinearity tensor due to V_a. b_{ijkl} will appear in each case as a functional depending in the beam case on the derivatives with respect to x, and in the plate cases on the partial derivatives with respect to x and y, of the functions w_i, w_j, w_k,and w_l. The kinetic energy T of the structure is given by:

$$T = \frac{1}{2}\omega^2 a_i a_j m_{ij} \cos^2\omega t \qquad (2.5)$$

where m_{ij} is the mass tensor. Expressions of k_{ij} ,m_{ij} and b_{ijkl} corresponding to homogenous beams , homogeneous plates and CFRP plates are given in Chapters IV , V and IX respectively, but are not necessary for the theoretical analysis developed in the remainder of this chapter.

II.3 FREQUENCY EQUATION AT LARGE AMPLITUDES

The dynamic behaviour of the structure is governed by Hamilton's principle, which is symbolically written [2.3]:

$$\partial \int_0^{2\pi/\omega} (V-T) = 0 \qquad (2.6)$$

In which ∂ indicates the variation of the integral. Introducing the assumed series (2.2) into the energy condition (2.6) via equations (2.3) to (2.5) reduces the problem to that of finding the minimum of the function ϕ given by

$$\phi = \int_0^{2\pi/\omega} \{\frac{1}{2} a_i a_j k_{ij} \sin^2\omega t + \frac{1}{2} a_i a_j a_k a_l b_{ijkl} \sin^4\omega t$$

$$- \frac{1}{2}\omega^2 a_i a_j m_{ij} \cos^2\omega t\}\, dt \qquad (2.7)$$

with respect to the undetermined constant a_i. Integrating the trigonometric functions $\sin^2\omega t$, $\sin^4\omega t$ and $\cos^2\omega t$ over the range $[0, \frac{2\pi}{\omega}]$ leads to the following expression:

$$\phi = \frac{\pi}{2\omega}(a_i a_j k_{ij} + \frac{3}{4} a_i a_j a_k a_l b_{ijkl} - \omega^2 a_i a_j m_{ij}) \qquad (2.8)$$

In this expression, ϕ appears as a function of only the undetermined constant, a_i, i=1,..., n. Equation (2.6) reduces to:

$$\frac{\partial \phi}{\partial a_r} = 0 \qquad r = 1,..., n \tag{2.9}$$

which can be written as :

$$\frac{\pi}{2\omega} \Big(\frac{\partial a_j}{\partial a_r} a_j k_{ij} + a_i \frac{\partial a_j}{\partial a_r} k_{ij} + \frac{3}{4} \frac{\partial a_j}{\partial a_r} a_j a_k a_l b_{ijkl} +$$

$$\frac{3}{4} a_i \frac{\partial a_j}{\partial a_r} a_j a_k a_l b_{ijkl} + \frac{3}{4} a_i a_j \frac{\partial a_k}{\partial a_r} a_l b_{ijkl} + \frac{3}{4} a_i a_j a_k \frac{\partial a_l}{\partial a_r} b_{ijkl}$$

$$- \omega^2 \Big(\frac{\partial a_j}{\partial a_r} a_j m_{ij} + a_i \frac{\partial a_j}{\partial a_r} \Big) m_{ij} \Big) = 0 \qquad r = 1,..., n \tag{2.10}$$

As we have :

$$\frac{\partial a_j}{\partial a_r} = \delta_{ir} \; ; \; \frac{\partial a_j}{\partial a_r} = \delta_{jr} \; ; \; \frac{\partial a_k}{\partial a_r} = \delta_{kr} \; ; \; \frac{\partial a_l}{\partial a_r} = \delta_{lr} \tag{2.11}$$

where δ is the Kronecker symbol defined by $\delta ij = 1$ if $i = j$ and $\delta ij = 0$ if $i \neq j$, equations (2.10) lead to :

$$(a_j k_{rj} + a_i k_{ir}) + \frac{3}{4} (a_j a_k a_l b_{rjkl} + a_i a_k a_l b_{irkl} + a_i a_j a_l b_{ijrl} + a_i a_j a_k b_{ijkr})$$

$$- \omega^2 (a_j m_{rj} + a_i m_{ir}) = 0 \qquad r = 1,..., n \tag{2.12}$$

Generally, and this is the case for all the applications of the present theory given in the present work, the tensors k_{ij} and m_{ij} are symmetric, and the tensor b_{ijkl} is such that :

$$b_{ijkl} = b_{klij} \tag{2.13}$$

$$b_{ijkl} = b_{jikl} \qquad (2.14)$$

Taking into account these properties of symmetry, it appears that equations (2.12) are equivalent to the following set of nonlinear algebraic equations:

$$2a_i k_{ir} + 3a_i a_j a_k b_{ijkr} - 2\omega^2 a_i m_{ir} = 0 \qquad r = 1,..., n \qquad (2.15)$$

Putting

$$B_{ij}(\{A\}) = a_k a_l b_{ijkl}\,, \qquad (2.16)$$

the nonlinear geometrical rigidity matrix [B] is defined. Each term of matrix [B] is a quadratic function of the column matrix of coefficients $\{A\} = [a_1 a_2 \ldots a_n]^T$. By introducing matrix [B] in equations (2.15) we get the following matrix equation:

$$2[K]\{A\} + 3[B(\{A\})]\{A\} = 2\omega^2 [M]\{A\} \qquad (2.17)$$

where [K] and [M] are the classical rigidity and mass matrices respectively, which are well known in the linear theories. It should be noticed that, by neglecting the nonlinear term $[B(\{A\})]\{A\}$, equation (2.17) reduces to the classical eigenvalue problem:

$$[K]\{A\} = \omega^2 [M]\{A\} \qquad (2.18)$$

which is the Rayleigh-Ritz formulation of the linear vibration problem.

II.4 DISCUSSION OF THE NUMERICAL MODEL

Equation (2.18) represents a set of n linear equations relating the n coefficients a_i and the frequency ω. As may be expected for such an eigenvalue problem, it leads only to the shape of A and no information can be obtained concerning the amplitude of vibration. So, equation (2.18) determines (n-1) values for the shape of {A} and one value for the corresponding frequency ω. For the nonlinear problem (2.17), as the modulus of {A} is also necessary to determine the physical amplitude of vibration, we have (n+1) unknowns which are the n coefficients of {A} and ω. A further equation has to be added to equations (2.17) in order to complete the formulation. As no dissipation is considered here, such an

equation can be obtained by applying the principle of conservation of energy, which can be written as:

$$V_{max} = T_{max} \tag{2.19}$$

where V_{max} is the maximum value of the strain energy obtained from equations (2.3) and (2.4) for $t = \frac{\pi}{2\omega}$, which leads to $\sin^2\omega t = \sin^4\omega t = 1$, and T_{max} is the maximum value of the kinetic energy obtained from equations (2.5) for $t = 0$, *i.e.* $\cos^2\omega t = 1$. Using the matrix notation, equation (2.19) leads to :

$$\omega^2 = \frac{\{A\}^T[K]\{A\} + \{A\}^T[B(\{A\})]\{A\}}{\{A\}^T[M]\{A\}} \tag{2.20}$$

It is worth noticing that while in the linear case the condition (2.19) is automatically verified, as a consequence of the energy condition (2.6), and can be obtained easily by multiplying the left hand side of equation (2.18) by $\{A\}^T$, in the nonlinear case it leads to equation (2.20) which is an independent equation to be added to the set (2.17) of nonlinear algebraic equations. This can be shown as follows : Substituting equation (2.20) in equation (2.15), we obtain :

$$(\{A\}^T[M]\{A\})\,(2[K]\{A\} + 3[B(\{A\})]\{A\}) - (\{A\}^T[K]\{A\}$$

$$+ \{A\}^T[B(\{A\})]\{A\})\,(2[M]\{A\}) = 0 \tag{2.21}$$

Premultiplying equation (2.21) by $\{A\}^T$ so that all the terms become scalar and rearranging leads to :

$$(\{A\}^T[M]\{A\})\,(2\{A\}^T[K]\{A\} + 3\{A\}^T[B(\{A\})]\{A\}) - (\{A\}^T[K]\{A\}$$

$$+ \{A\}^T[B(\{A\})]\{A\})\,(2\{A\}^T[M]\{A\}) = 0$$

After simplification, we obtain : (2.22)

$$(\{A\}^T[M]\{A\})\,(\{A\}^T[B(\{A\})]\{A\}) = 0 \tag{2.23}$$

The left hand side of equation (2.23) is the product of the maximum values of the kinetic and axial strain energies. As explained in Appendix A, it can strictly vanish only for

$a_1 = a_2 = ... = a_n = 0$. On the other hand, in equation (2.21), for non zero but small values of a_i, the terms $2\{A\}^T[B(\{A\})]\ \{A\}.[M]\{A\}$ and $(\{A\}^T[M]\{A\})(3[B(\{A\})]\{A\})$ can be neglected - since they are proportional to $\{A\}^5$ and the other terms are only proportional to $\{A\}^3$ - leading to the linear eigenvalue problem.

In other words, the set of n nonlinear algebraic equations (2.21) is shown to lead necessarily to the solution $a_1 = a_2 = ... = a_n = 0$. For small values of a_i, it simplifies to equation (2.18) obtained usually for linear systems. So, in order to avoid the situation that the numerical solution of equation (2.21) leads to the linear case, a further condition has to be applied to the displacement amplitude assigning to it a finite value. This can be explained physically by the fact that, since in equation (2.6) no external forces are taken into account, only free vibrations are considered in the present model, and consequently, it does not contain any information concerning the amount of vibration energy stored in the system, or on the mode of excitation. As large vibration amplitudes are of interest in this work, it is not sufficient to use the complete expressions of the potential and kinetic energies at large deflections when deriving the model, since Hamilton's principle still leads to the linear solution corresponding to small vibration amplitudes; a further condition has to be added assigning a finite energy of vibration or finite displacement amplitude to the system. The technique adopted in the present work was to apply the condition (2.6) assuming a given value for the contribution a_{ro} of the function w_{ro} in order to determine the contribution coefficients a_i of the functions w_i for $i \neq r_o$. According to this, the r_o^{th} nonlinear mode shape of the structure, corresponding to the given amplitude coefficient a_{ro}, was obtained by solving the following set of (n-1) nonlinear algebraic equations:

$$2a_ik_{ir} + 3a_ia_ja_kb_{ijkr} - 2\frac{a_ja_jk_{ij} + a_ia_ja_ka_jb_{ijkl}}{a_ia_jm_{ij}}a_im_{ir} = 0 \qquad (2.24)$$

for $r \neq r_o$

where i, j, k and l vary from 1 to n.

The values of a_i, for $i \neq r_o$, obtained by solving equations (2.24) can be substituted in equation (2.20) to obtain the corresponding value of ω^2.

II.5 CONCLUSIONS

A theoretical model for large vibration amplitudes of thin elastic structures has been developed, based on Hamilton's principle and spectral analysis, to obtain numerical results. The theory effectively reduces a nonlinear free vibration problem to a set of nonlinear algebraic equations depending on the classical rigidity and mass matrices, and a fourth order tensor due to the nonlinearity. If the nonlinearity tensor due to finite displacements is neglected, the classical eigenvalue problem known in the linear theory is obtained. By choosing the convenient basic function in each case, and varying the function whose contribution coefficient is assigned, a set of amplitude dependent mode shapes and natural frequencies[1] can be obtained for various structures and boundary conditions. The most significant features of this new approach are that :

(1) It is not subjected to the practical limitation of weak nonlinearity in its formulation as this was the case for some models for nonlinear vibration based on the perturbation procedure developed previously [2.4 , 2.5].

(2) Its formulation is quite simple and does not contain any incremental procedure as in some finite element approaches [2.6] .

(3) Periodic solutions can be obtained directly with any desired accuracy as solutions of the set of nonlinear algebraic equations.

(4) Once the most significantly contributing functions are known, engineering applications can be made easily using data tables or rapid computer programs using only the appropriate functions.

(5) Once the contributions of the functions are calculated, the resulting strains and stresses can be analysed directly, using the analytical expressions for the derivatives of the basic functions.

---

[1]The natural frequencies are defined in the linear theory as the undamped free vibration frequencies of a linear system [2.7]. The model developed in this chapter being concerned with undamped nonlinear free vibrations, the extension of the above definition to nonlinear natural frequencies determined by the present model appears to be justified. It should be noticed that this question has been discussed previously in the literature [2.8,2.9]. The term "nonlinear mode shape" is used here to designate an amplitude dependent deflection shape associated with a given resonance frequency.

(6) It can be extended, as shown in Chapters VII and VIII, in order to take into account nonlinearity features like the spatially distributed harmonic distortion.

The theoretical model developed in this chapter was applied in the present work to study the nonlinear large vibration amplitudes of fully clamped rectangular homogeneous and CFRP plates, clamped-clamped beams and simply supported beams. In each case, the number of mechanical and geometrical parameters required in the numerical treatment was reduced using dimensional analysis. Then, the basic functions were chosen in such a manner to satisfy the corresponding boundary conditions. Finally, equations (2.24) were solved giving the nonlinear mode shapes and natural frequencies of the structure considered.

In Chapters VII and VIII, this model has been extended in order to take into account the spatially distributed harmonic distortion which was experimentally shown to occur at large deflections, as reported in Chapter VI.

The above analysis has also been applied to determine nonlinear behaviour of CFRP plates at large vibration amplitudes. This is treated in Chapter IX.

CHAPTER III

DESCRIPTION AND DISCUSSION OF EXPERIMENTAL TECHNIQUES, MEASUREMENT AND ANALYSIS METHODS

III.1 INTRODUCTION

In the present work, a set of tests was carried out in order to investigate some dynamic response characteristics of fully clamped rectangular plates, both homogeneous and made of carbon fibre reinforced plastics (CFRP), at large vibration amplitudes. This was done in order to obtain experimental data allowing comparison to be made with results obtained by the theoretical models developed throughout this work. Thus, the amplitude dependence of the fundamental mode shape and the corresponding resonance frequencies were examined. Also, the spatial distribution of the harmonic distortion induced by large amplitudes of vibration was carefully investigated in an attempt to allow a better understanding of this important aspect of the dynamical behaviour of fully clamped beams and plates at large vibration amplitudes and more appropriate theoretical models to be developed for nonlinear vibrations of thin straight structures.

As this work was carried out both at the ISVR[1] and the EMI[2], two rigs were built so that experimental work could be carried out continuously. The ISVR rig will be referred to below as rig 1 and the EMI rig as rig 2.

In this chapter, a discussion is given of the testing techniques, measurement and analysis methods adopted in the present work. Description of the specimens, the clamping conditions, the modes of excitation and calibration of response measuring devices is given in Section III.2. In Section III.3.1, the problems posed when applying usual modal testing methods to nonlinear systems are briefly discussed and a method for estimating the amplitude dependent mode shapes is presented in section III.3.2. FFT analyses of the measured mode shapes , including phase lag determination between time harmonics at several points on the plates, were carried out to assess the spatial distribution of the harmonic distortion induced by large vibration amplitudes for the plates tested in the region of the fundamental resonance. This is discussed in Sections III.3.3 and III.3.4.

---

[1]ISVR - Institute of Sound and Vibration Research, University of Southampton, England.
[2]EMI - Ecole Mohammadia d'Ingenieurs, Rabat, Morocco.

III.2 EXPERIMENTAL DETAILS

III.2.1 Description of the specimens

In the present work, several plates were tested. The choice of the specimens dimensions was governed by :

1) The aspect ratio was required to be of approximately 0.67 (or $\frac{1}{0.67}$ =1.5) since for this value, often adopted in experimental tests on plates [3.1-3.3], the fully clamped rectangular plate possesses well separated resonances, as can be seen in results given in [3.4]. This was a condition for concentrating the experimental study on the response near to the first mode, as discussed in Section III.2.3.2.

2) The dimensions of the plates tested were chosen so that the permitted test area would allow a reasonable number of test points without requiring extremely heavy frames. Also, the width of the plates tested on rig 1 was limited to some extent by the working section in the acoustic tunnel.

III.2.1.1 Isotropic plates

Experimental measurements were carried out at the ISVR on several 220 × 366 mm rectangular plates made of aircraft type aluminium alloy DTDS070 having thicknesses of 1.06, 1.16 and 0.51 mm. Several plates with various thicknesses were made, as required during the experimental investigations. The first reason was related to the amplitude of vibrations which had to be as large as possible, in order to allow nonlinear effects, such as deformation shapes and the spatial distribution of harmonic distortion, to be experimentally investigated. So, plates with decreasing thicknesses were manufactured according to the materials available, and a thickness of 0.51 mm was the minimum adopted, to avoid induced membrane effects. The second reason was fatigue which occurred in two plates subjected to high levels of acoustic excitation and made it necessary to manufacture other plates for further tests.

A 586 × 424 × 1.2 mm thick steel plate was manufactured and tested on experimental rig 2. The isotropic plates tested in the present work are numbered from 1 to 5. The plate numbers and their geometrical and mechanical characteristics are summarized in Table 3.1.

III.2.1.2 CFRP plate

An eight layered carbon fibre reinforced plastic plate was manufactured and moulded using the ISVR facilities. The dimensions of the test specimen employed was chosen according to the clamping rig 2 dimensions and were specified as follows :

overall size	586 × 424 mm
dimensions within the clamped edges	480 × 320 mm
thickness	1 mm
lay-up	$[0\ \pm 45\ 90]_S$

The initial preparation of CFRP plates consists of hand stacking a given number of sheets of aligned carbon fibres preimpregnated with resin, the so-called pre-preg sheets, with fibres orientated according to the desired plate lay-up. Then the plate is moulded in a heated press. In this work, high tensile surface treated carbon fibres XAS and epoxy resin 914C with a 60% fibre volume fraction were used.Then, the ISVR ultrasonic scanning facility described in [3.10] was used to inspect the plates for possible defects due to poor bonding or delamination initiation between individual layers.

III.2.2 Description of the clamping conditions

The theoretical clamped boundary conditions are difficult to achieve perfectly in experimental tests and many arrangements are described in the literature [3.1,3.5] and [3.6]. In the present work, in order to approach reasonably such theoretical clamped boundary conditions, the plates were clamped between two heavy steel frames. The dimensions of the two frames used on rig 1 and rig 2 are given in Figures 3.1 and 3.2 respectively. The permitted test areas were of 220 × 366 mm and 324 × 486 respectively. A set of bolts was spaced along the four edges of the frames as shown in Figures 3.1 and 3.2. In all tests, the clamping bolts were tightened progressively to a constant torque loading of given value using a torque wrench. The torque loading was increased up to a value of 100 Nm, for which the measured first linear resonance frequency for the homogeneous plate tested was considered as being close enough to the theoretical value.

III.2.3 Description of the methods of excitation

III.2.3.1 Introduction

High levels of excitation are necessary to excite a fully clamped rectangular plate so that vibration amplitudes well above the plate thickness can occur. Such levels were obtained using acoustic excitation provided by the ISVR progressive wave tube facility as described below. However, because of the practical difficulties involved in measuring the plate response to acoustic excitation at different points using only one or two transducers, such as maintaining a constant pressure level for a period of time long enough to enable data to be acquired on line many times, or moving the OVT[1] head across a vibrating plate in a high noise environment, which can involve some risk if the plate exhibits fatigue, it was necessary to carry out a set of investigations using an electrodynamic point exciter. A further reason for using both types of excitation was that some nonlinearity was noticed in the behaviour of the acoustic tunnel, as mentioned previously in [3.7] and although this nonlinearity was considered as not affecting significantly the response measurements, it was hoped that an additional check on dynamic behaviour could be obtained using another type of excitation.

III.2.3.2 Electrodynamic point excitation

The electrodynamic exciter adopted in the present work was similar to that used previously to study the nonlinear vibrations of a clamped-clamped beam [3.8] It consisted of a light coil attached to a light plastic screw which was glued to the plate. The coil protruded into the flux gap of an annular permanent magnet, thus forming an electrodynamic exciter which imposed no added stiffness and little additional mass on the plate. Details of arrangement of the coil and magnet are given in Figure 3.3. The excitation point was chosen at the centre of the plate, which is a nodal point for all antisymmetrical modes in either the longitudinal or the horizontal direction, in order to eliminate the contribution of all these modes to the plate dynamic response. Also, the plates tested had well separated resonances, as stated above. This allowed the excitation frequencies to be chosen in the region of the fundamental resonance, determined by the frequency response tests, decribed in Chapter VI, in order to reduce as far as possible the contribution of higher modes and concentrate on the study of the effects of large vibration amplitudes on the fundamental mode. On the other hand, the excitation frequencies had to be kept far enough from the unstable region in which the jump phenomenon could occur. Also, it should be noted that in mode shape measurements, the tests were systematically carried out by

[1] Optical vibration transducer (OVT) presented in Section III.2.4

increasing the excitation frequency up to a value for which high vibration amplitudes were obtained in the left side of the region of the fundamental resonance.

III.2.3.3 Acoustic excitation

As stated in the above section, the ISVR acoustic tunnel facility was used to drive the plates to high amplitudes of vibration. A detailed description of this facility is given in [3.9] . A brief description can be given as follows: the pressure of a jet of compressed air is modulated by a siren driven by an electrodynamic assembly. The siren is connected via a horn to a hard walled parallel duct with an absorbing termination. The plate specimens are mounted in a supporting frame using an aperture in the wall of the duct. Then the plate can be subjected at grazing incidence to either harmonic or random acoustic excitation. The exciting pressure signal level, nature and amplitude depend on the current through the siren, which was limited by the safe current in the coil. Measurement of the applied SPL was made by a half inch microphone mounted inside the tunnel close to the test panel surface and levels up to 155 dB were reached. The rig-tunnel interface was similar to that described in reference [3.10] but no axial compressive load was applied to the plates tested.

III.2.4 Description of the response measuring devices

Nonlinear vibrations are very sensitive to all kinds of perturbation which could induce the jump phenomenon to occur. Only noncontacting transducers were appropriate for measuring the nonlinear plate response investigated in the present work. Also, it was necessary to have a transducer capable of measuring displacements through a wide range including very small values, such as those obtained near to the clamps, which can be lower than 10^{-1} millimetres, and values up to a few millimetres, reached at the plate centre. All of the above requirements have motivated the adoption of a non-contacting optical vibration transducer (OVT), similar to that mentioned in [3.8] and [3.11] to measure the plate dynamic response along sections of the plate area. Calibration curves of the OVT's used throughout this work, carried out either statically using a dial indicator to measure the distance between the OVT probe and the surface of the plate, or dynamically using a travelling microscope and a small square CFRP plate attached to a shaker, are given in figures (3.4) to (3.8), which correspond to three OVT's used in the present work. All curves show linear dependence between the output voltage of the OVT's and the distance between the OVT probe and the test surface and a linearity range large enough for the displacement amplitudes considered in each case. Also, white paint was applied uniformly

on all the measuring surfaces to ensure the same absolute calibration at all points of the plates since some dependence of the OVT's absolute calibration on the nature of the reflecting surface has been mentioned previously [3.12] . A guided support, shown in Figure 3.9, was mounted on the frames of rig 2 to carry the OVT head and permitted displacement measurements to be made at any point on the plate. A simpler guiding system, consisting of a long machined beam, carrying the OVT head and sliding on two machined bars situated on the frames, along the longitudinal direction, was used on rig 1. Care has be taken to check that the calibration of the OVT used in that case was independent of the static distance, d_0, between the plate and the OVT head, as shown in Figures 3.4 and 3.5 corresponding to $d_0 = 7.9$ and 11.6 mm respectively. Due to the heavy weight of the frames used, no undesirable vibrations of the frame and OVT support were noticed which could have affected the plate displacement signals measured by the OVT. Phase measurements were necessary for assessing the nature of the second harmonic spatial distribution, as discussed in Chapter VI. In order to obtain a consistent phase information, two OVT's had to be used, positioned at pairs of symmetrical points with respect to the plate centre, in order to allow both signals to be acquired simultanously.

III.3 DETAILS OF DATA ACQUISITION AND ANALYSIS

III.3.1 Introduction

Although considerable progress has been made since the 1970's in developing experimental and computational techniques for data analysis [3.13], the theory of modal testing still remains only strictly valid for linear systems and some modal analysts still attribute to nonlinearity all otherwise inexplicable effects encountered in their work [3.14]. However, as pointed out in [3.15] , a classification of phenomena exhibited by nonlinear systems can be made as follows: (i) phenomena that distort the linear response and (ii) phenomena that are unique to nonlinear systems and therefore cannot be predicted by linear theory or dealt with using linear data analysis techniques. In [3.16] and [3.17] a survey of the current research on the experimental techniques applied to nonlinear systems is made and about 50 references are cited which are directed to the first category of nonlinear behaviour *i.e.* distortion of the linear response due to nonlinearity. A summary of such techniques is given in [3.15].

In the present experimental work, both categories of nonlinear phenomena were encountered and had to be dealt with in the case of fully clamped rectangular plates

vibrating at large displacements near to the fundamental mode. The first category included: (i) the amplitude dependence of the first resonance frequency investigated using frequency response tests, (ii) the amplitude dependence of the fundamental mode shape analysed using either the peak amplitude method or by separating the first harmonic component. The second category included: (a)the plate response harmonic distortion which was examined by separation of harmonics obtained using either the ISVR digital data analysis facility (DAC) or a B & K analyser, (b) the second harmonic spatial distribution whose determination was based on both zoom FFT modulus and phase measurements and analysis. Also, in the light of the theoretical results obtained in this work, an attempt has been made to extend to the nonlinear case an existing method for linear mode shape estimation from experimental data.

III.3.2 Nonlinear mode shape estimation method

To estimate the linear mode shape from experimental data, a method is proposed in [3.3] which minimises the estimation error. In this method, it is assumed that the experimental mode shape is only known within a scaling constant. A squared error e^2 is defined as :

$$e^2 = \frac{(\phi_a - a\phi_e)^T(\phi_a - a\phi_e)}{\phi_a{}^T\phi_a} \qquad (3.1)$$

where ϕ_a is a reference analytical mode shape, ϕ_e the measured mode shape and a is a scaling constant . Minimising e^2 with respect to a leads to :

$$a = \frac{\phi_a{}^T\phi_e}{\phi_e{}^T\phi_e} \qquad (3.2)$$

However, as outlined in the above section, no general method for estimating amplitude dependent mode shapes is available. In [3.8], dealing with nonlinear clamped-clamped beam vibrations, the NAG library routine E02ADF was used to fit Chebyshev polynomials to the measured clamped-clamped beam response data points. Several degrees of the fitted polynomial were tried and some difficulty was found in obtaining estimates having consistent second derivatives. As a conclusion of the above work, it was suggested that a theoretical expression of the amplitude dependent mode shape and its derivatives can lead to better estimates. Also, in numerical results obtained here, from application of the theory developed in the previous chapter to fully clamped beams and plates, the amplitude dependent mode shapes appeared as combinations of the linear mode shapes with

amplitude dependent coefficients. In the light of the above remarks, an attempt has been made to adapt the estimation method presented above to the nonlinear case as follows: The experimental mode shape is expanded as a series :

$$\phi_e = a_i \phi_i \tag{3.3}$$

where the ϕ_i 's are the linear mode shapes of the structure considered and the summation convention defined in the previous chapter is used. The coefficients a_i are determined by minimising the error defined as:

$$e^2 = \frac{(a_i\phi_i - \phi_e)^T(a_i\phi_i - \phi_e)}{\phi_e{}^T\phi_e} \tag{3.4}$$

with respect to the a_i's. Assuming orthogonality of the ϕ_i's, which is the case for the functions used for the beam and plate analyses in the present work, the minimisation leads to:

$$a_i = \phi_i{}^T\phi_e \tag{3.5}$$

which gives directly the estimated contribution coefficient for each mode as product of the experimental mode and the corresponding function. Substituting back expression (3.5) into the error equation and using the orthogonality of the ϕ_i's, the mimimum square error is obtained as:

$$e^2 = 1 - \frac{a_i a_i}{\phi_e{}^T\phi_e} \tag{3.6}$$

in which the repeated index i is summed over 1 to n in the term $a_i a_i$. It appears that the minimum obtained using the present estimation is lower than that obtained using only one mode. This method was applied in the present work to the measured plate response in order to obtain amplitude dependent contribution coefficients as discussed in Chapter VI.

III.3.3 Details of digital data analysis of experimental measurements

A digital data analysis facility was used for signal processing in this work. The time history of the OVT displacement signals measured along various sections in the length and the width directions of the plate, was acquired on line at a sampling rate of 2400 samples/s and stored in files. The Fourier transform (FFT) of each file was evaluated and modulus and phase were plotted against frequency. To obtain the phase lag between the second

harmonic components at several pairs of symmetrical points with respect to the plate centre, in the longitudinal and the horizontal directions, two OVT 's were used to acquire the response signals simultanously at each point of such pairs. As the normal Fourier transform routines failed in calculating consistent values for the phase of the second harmonic component, zoom analysis, with a resolution of 0.625 10^{-2} Hz was applied to extract values of the phase of the second harmonics for each pair. The resolution was increased in several attempts until accurate comparison of phase values was possible as discussed in Chapter VI.

III.3.4 Details of analogue data analysis

As no digital data analysis is yet available at the EMI, some measurements were carried out using an analogue double channel B & K analyser (type 2032) and the response signal autospectrum was plotted in the regions of the first and higher harmonic components. Examples of such plots, indicating various parameters used in the analysis are presented in Chapter VI. Details concerning this analyser are given in [3.18].

III.4 CONCLUSIONS

As has been discussed in this chapter, various testing and analysis techniques have been applied in the present work to study large displacement vibration amplitudes of fully clamped rectangular plates. As discussed in Chapters VI, each method has succeeded to some extent in revealing a particular aspect of such a complicated problem. However, as the linear case, assumed in the usual modal testing practice, remains overall a theoretical limit for the dynamical behaviour of real structures, further investigations are needed in order to develop a more accurate and systematic approach, including test techniques, measurement and analysis methods, dealing with the whole range of nonlinear systems.

CHAPTER IV

EFFECTS OF LARGE VIBRATION AMPLITUDES ON THE MODE SHAPES AND NATURAL FREQUENCIES OF FULLY CLAMPED AND SIMPLY SUPPORTED BEAMS.

IV.1 INTRODUCTION

Although the theoretical model presented in Chapter II was first developed for analysing the effects of large amplitudes of vibration on the mode shapes and natural frequencies of fully clamped rectangular plates, it has been applied in the present chapter to the case of clamped clamped and simply supported beams . This was done partly in order to test the model, since results of a previous study concerned with beams are available. In particular, experimental and theoretical work, reported in [4.1], has shown that the beam fundamental mode shape was clearly dependent on the amplitude of vibration, especially near to the clamps. High values of increase of beam curvatures were also noticed near to the clamps causing a highly nonlinear increase in bending strain with increasing deflection instead of the linear rate of increase usually observed in the linear theory. The present model was expected to lead to similar conclusions. Also, in the study mentioned above, due to the complexity of the two nonlinear algebraic equations obtained from the partial differential equation of beams at large vibration amplitudes, some difficulty remained when fundamental nonlinear mode shape data had to be obtained at a certain amplitude to thickness ratio [4.2]. It was hoped that the present model will provide such data for vibration amplitudes varying continuously from very small displacements to several times the beam thickness. It was also hoped that it will allow new results, corresponding to higher order clamped clamped beam mode shapes *i.e.* second, third and so on, to be obtained.

IV.2 GENERAL FORMULATION

Consider transverse vibrations of the beam shown in Figure 4.1 having the following characteristics:

E : Young's modulus
ρ : mass per unit length

L	:	length of the beam
A	:	area of the cross section
I	:	the second moment of area of cross section
W(x,t)	:	transverse displacement $W(x,t) = w(x).\sin\omega t$
H	:	thickness of the beam

The bending strain energy V_b is:

$$V_b = \frac{1}{2}\int_0^L EI\left(\frac{\partial^2 W}{\partial x^2}\right)^2 dx \qquad (4.1)$$

and the axial strain energy V_a of a beam with hinged ends at large vibration amplitudes is [4.3]:

$$V_a = \frac{L}{2EA}F^2 \qquad (4.2)$$

where F is the axial load induced by large transverse vibration given by

$$F = EA\frac{\Delta L}{L} = \frac{EA}{L}\int_0^L \frac{1}{2}\left(\frac{\partial W}{\partial x}\right)^2 dx \qquad (4.3)$$

Substituting equation (4.3) in equation (4.2) gives :

$$V_a = \frac{EA}{8L}\left(\int_0^L \left(\frac{\partial W}{\partial x}\right)^2 dx\right)^2 \qquad (4.4)$$

The kinetic energy is

$$T = \frac{1}{2}\rho A\int_0^L \left(\frac{\partial W}{\partial t}\right)^2 dx \qquad (4.5)$$

Assuming harmonic motion and using the notation of Chapter II, the displacement series given by equation (2,2) is substituted in equations (4.1) , (4.4) and (4.5), which leads to :

$$V_b = \frac{1}{2} a_i a_j k_{ij} \sin^2 \omega t \tag{4.6}$$

$$V_a = \frac{1}{2} a_i a_j a_k a_l b_{ijkl} \sin^4 \omega t \tag{4.7}$$

$$T = \frac{1}{2} \omega^2 a_i a_j m_{ij} \cos^2 \omega t \tag{4.8}$$

where k_{ij} is the classical rigidity tensor and b_{ijkl} is the nonlinearity tensor due to V_a and m_{ij} the mass tensor. k_{ij} ,b_{ijkl} and m_{ij} are given by :

$$k_{ij} = \int_0^L \frac{\partial^2 w_i}{\partial x^2} \frac{\partial^2 w_j}{\partial x^2} dx \tag{4.9}$$

$$b_{ijkl} = \frac{EA}{4L} \int_0^L \frac{\partial w_i}{\partial x} \frac{\partial w_j}{\partial x} dx \int_0^L \frac{\partial w_k}{\partial x} \frac{\partial w_l}{\partial x} dx \tag{4.10}$$

$$m_{ij} = \rho A \int_0^L w_i \, w_j \tag{4.11}$$

α being the non-dimensional parameter $\alpha = \frac{AH^2}{4I}$, by putting :

$$w_i(x) = H \, w_i^* \frac{x}{L} = H w_i^* (x^*) \tag{4.12}$$

we get:

$$\frac{k_{ij}}{k_{ij}^*} = \frac{EIH^2}{L^3} \tag{4.13}$$

$$\frac{b_{ijkl}}{b^{*}_{ijkl}} = \frac{EIH^2}{L^3} \tag{4.14}$$

$$\frac{m_{ij}}{m^{*}_{ij}} = \rho AH^2L \tag{4.15}$$

where k^{*}_{ij}, b^{*}_{ijkl} and m^{*}_{ij} are non-dimensional tensors given by:

$$k^{*}_{ij} = \int_0^1 \frac{\partial^2 w_i^*}{\partial x^{*2}} \frac{\partial^2 w_j^*}{\partial x^{*2}} dx^* \tag{4.16}$$

$$b^{*}_{ijkl} = \alpha \int_0^1 \frac{\partial w_i^*}{\partial x^*} \frac{\partial w_j^*}{\partial x^*} dx^* \int_0^1 \frac{\partial w_k^*}{\partial x^*} \frac{\partial w_l^*}{\partial x^*} dx^* \tag{4.17}$$

$$m^{*}_{ij} = \int_0^1 w_i^* w_j^* \tag{4.18}$$

Substituting equations (4.16) to (4.18) in equation (2,20) leads to:

$$\omega^2 = \left(\omega^{*}_{nl}\right)^2 . \frac{EI}{\rho AL^4} \tag{4.19}$$

where ω^{*}_{nl} is a non-dimensional nonlinear natural frequency parameter given by:

$$\left(\omega^{*}_{nl}\right)^2 = \frac{a_i a_j k^{*}_{ij} + a_i a_j a_k a_l b^{*}_{ijkl}}{a_i a_j m^{*}_{ij}} \tag{4.20}$$

By substituting equations (4.13) to (4.15), (4.19) and (4.20) in equations (2.24) we obtain the following non-dimensional set of nonlinear algebraic equations:

$$2a_i k^{*}_{ir} + 3a_i a_j a_k b^{*}_{ijkr} - 2\frac{a_i a_j k^{*}_{ij} + a_i a_j a_k a_l b^{*}_{ijkl}}{a_i a_j m^{*}_{ij}} a_i m^{*}_{ir} = 0 \tag{4.21}$$

for $r \neq r_o$

whose solution determines the r_0^{th} nonlinear mode shape. It should be noted that, as the beam linear frequency ω_l is such that :

$$\omega_l^2 = \left(\omega_l^*\right)^2 . \frac{EI}{\rho AL^4} \qquad (4.22)$$

in which ω_l^* is non-dimensional linear frequency parameter determined only by the beam boundary conditions [4.8 and 4.10], we obtain from equations (4.19) and (4.22):

$$\omega = \frac{\omega_{nl}^*}{\omega_l^*} \omega_l \qquad (4.23)$$

Equation (4.23) shows that nonlinear natural frequencies of a beam can be obtained using numerical values of ω_{nl}^* calculated by the present model, which depend on the parameter α and the basic functions used for a given boundary conditions; and the numerical values of ω_l^* , which depend only on the beam boundary conditions; and a measured value of ω_l,when the mechanical characteristics of the beam are unknown. For a uniform beam with a rectangular cross section, $\alpha = 3$ so that the solutions obtained for this value are applicable to any rectangular cross sectioned beam.

IV.3 SIMPLY SUPPORTED BEAM

Although clamped-clamped boundary conditions are of main concern in this study, simply supported boundaries were examined using the same model. This was done in order to have an additional check test for the model, which would be expected to lead to the same conclusion, often adopted in the literature, assuming that the mode shape in the simply supported case is amplitude independent [4.1,4.4,4.6].

Using the notation of Chapter II, let the functions w_i be the linear mode shapes of SS-SS beam given by:

$$w_i(x) = H\sin i\pi \frac{x}{L} = H\sin i\pi t = H\, w^*_i(t) \qquad (4.24)$$

The general expression for the nonlinearity tensor b^*_{ijkl} is given by:

$$b^*_{ijkl} = \alpha \int_0^1 (i\pi\cos(i\pi t))\,(j\pi\cos(j\pi t))dt \int_0^1 (k\pi\cos(k\pi t))\,(1\pi\cos(1\pi))dt$$
$$= \tfrac{1}{4}\alpha\, ijkl\pi^4\, \delta_{ij}\, \delta_{kl} \qquad (4.25)$$

where δ_{ij} is the Kronecker symbol defined by $\delta_{ij} = 0$ if $i \neq j$ and $\delta_{ij} = 1$ if $i = j$. The general expression for the rigidity tensor k^*_{ij} is given by:

$$k^*_{ij} = \int_0^1 ((i\pi)^2 \sin(i\pi t))\,((j\pi)^2 \sin(j\pi t))\,dt = i^2j^2\pi^4\,\tfrac{1}{2}\,\delta_{ij} \qquad (4.26)$$

and the general term for the mass tensor is:

$$m^*_{ij} = \int_0^1 \sin(i\pi t)\,\sin(j\pi t)\,dt = \tfrac{1}{2}\,\delta_{ij} \qquad (4.27)$$

By substituting expressions (4.25) to (4.27) in equation (2.21) we get

$$\left\{4\,r^4 + 3\alpha r^2\,(i^2a_i^2) - 2\,\frac{2\,(a_i^2 i^4) + \alpha\,(i^2a_i^2)\,(k^2a_k^2)}{a_i a_i}\right\} a_r = 0 \quad \text{for } r \neq r_o \qquad (4.28)$$

It appears that a solution of equations (4.26) is

$$a_r = 0 \qquad \text{for} \qquad r \neq r_o \qquad (4.29)$$

which means that the mode shape of a SS-SS beam is amplitude independent. This agrees with results discussed in the literature [4.1,4.4,4.6].

The relationship between vibration displacement amplitude and frequency is given by equation (4.20) in which all the a_i terms equal to zero except a_{ro}. So, we obtain from Equations (4.19) and (4.20) for the r_o^{th} mode:

$$\omega_{ro} = \sqrt{\frac{EI}{\rho A}} \left(\frac{\pi}{L}\right)^2 r_0^2 \sqrt{1 + \frac{AH^2 a_{r0}^2}{8I}} \qquad (4.30)$$

for the fundamental mode shape $r_o = 1$. The above equation can then be written as

$$\omega_1 = \sqrt{\frac{EI}{\rho A}} \left(\frac{\pi}{L}\right)^2 \sqrt{1 + \frac{Ac^2}{8I}} \qquad (4.31)$$

where $c = a_1 H$ is the amplitude coefficient of $\sin \frac{\pi x}{L}$ in the expression (2.2) in which the function given by equation (4.24) is substituted. For a rectangular cross section beam, $\frac{H^2 A}{I} = 12$ and equation (4.31) can be written as:

$$\omega_1 = \sqrt{\frac{EI}{\rho A}} \left(\frac{\pi}{L}\right)^2 \sqrt{1 + \frac{3c^2}{2H^2}} \qquad (4.32)$$

The model obtained in reference [4.1], applying the harmonic balance method to the nonlinear differential equation of beams at large vibration amplitudes leads to the same relationship as equation (4.32). Using Galerkin's method in [4.5] and Hamilton's principle in [4.6], a different numerical value, equal to $\frac{9}{4}$, was determined for the coefficient of $\frac{c^2}{H^2}$. All of the above methods involve numerical approximations. They are also based on the assumption that harmonic motion takes place at large vibration amplitudes. As will be discussed later, this approximation is not absolutely rigorous, even in the simplest case of a SS-SS beam[1]. However, it seems that under this assumption, formula (4.32) is the most accurate since it is based on equation (2.19) which is rigorously exact for a conservative system.

---

[1]This can be checked by putting a solution in the form $W(x,t) = \sin\omega t \sin \pi \frac{x}{L}$ in the nonlinear differential equation of large vibrations of beams [4.13].

IV.4 CLAMPED-CLAMPED BEAM

The theoretical model established in Chapter II, referred to below as model I,was used in the present work to study the amplitude dependence of the first, second and third nonlinear mode shapes of a clamped-clamped beam and their derivatives. Applying the harmonic balance method to the nonlinear differential equation of motion of beams at large deflections, a set of two nonlinear algebraic equations has been found in reference [4.1]. Using the latter model, referred to here as model II, the amplitude dependence of the fundamental mode shape of a clamped-clamped beam was obtained in reference [4.1] and compared with experimental data. In reference [4.7], results obtained from the latter model, corresponding to the second and third nonlinear clamped clamped mode shapes are given. So, in the work presented below, a general comparison is made between results obtained from the two models, relating to the first three nonlinear mode shapes.

IV.4.1 Numerical Details of the Clamped-Clamped Beam Analyses

Taking into account the clamped-clamped boundary conditions considered here and the shape of the amplitude dependent nonlinear clamped-clamped beam fundamental mode shape found in reference [4.1], the chosen basic functions w_i were proportional to the linear clamped-clamped beam functions f_i^a given by:

$$f_i^a(x) = \frac{\text{ch } v_i \frac{x}{L} - \cos v_i \frac{x}{L}}{\text{ch } v_i - \cos v_i} - \frac{\text{sh } v_i \frac{x}{L} - \sin v_i \frac{x}{L}}{\text{sh } v_i - \sin v_i} \qquad (4.33)$$

where v_i for i = 1, 2, ... are eigenfunction parameters for a clamped-clamped beam. The values of the parameters v_i, determined by the clamped clamped boundary conditions [4.8], were computed by solving numerically the transcendental equation ch v_i cos v_i = 1 using Newton's method [4.9,4.10]. Numerical values for the parameters v_i computed using a Fortran program are summarised in Tables 4.1.1 and 4.1.2 for i varying from 1 to 12. The non-dimensional clamped-clamped beam functions w_i^* were defined as :

$$w_i^*(x^*) = \frac{1}{G} f_i^{a*}(x^*) \qquad (4.34)$$

in which G is a scaling constant, $x^* = \frac{x}{L}$ and :

$$f_i^{a*}(x^*) = \frac{ch\ v_i x^* - \cos v_i x^*}{ch\ v_i - \cos v_i} - \frac{sh\ v_i x^* - \sin v_i x^*}{sh\ v_i - \sin v_i} \qquad (4.35)$$

A Fortran routine called CALC was used for computing values taken by the functions f_i^a, and their first and second derivatives, denoted here f_i^{b*} and f_i^{c*} respectively, when x* varies through the range [0,1] with a step of 0.0125 . Then, the functions w_i^* and their first and second derivatives were computed by dividing the calculated values of f_i^a, f_i^b and f_i^c by the scaling factor G given by :

$$G = \sqrt{\int_0^1 \left(f_i^{a*}\right)^2} \qquad (4.36)$$

The integral $\int_0^1 \left(f_i^{a*2}\right)$ was calculated numerically using Simpson's method [4.11] by a routine called SOMM. Due to the orthogonality of the functions f_i^a, the above normalisation procedure leads to:

$$m_{ij}^* = \int_0^1 w_i^*\ w_j^* = \delta_{ij} \qquad (4.37)$$

so that the non-dimensional mass matrix is identical to the identity matrix. The functions w_i^*, i = 1, ..., 5 are represented in Figure 4.2. The parameters k_{ij}^* and b_{ijkl}^* of equations (4.16) and (4.17) have been computed numerically by a routine called PREP, which is listed with all the above mentioned routines in Appendix B.

As equations (4.21) are a set of nonlinear algebraic equations, they have been solved numerically using the Harwell library routine NSO1A. This routine is based on a hybrid iteration method combining the steep descent and Newton's method and which do not require a very good initial estimate of the solution [4.12]. A Fortran routine, called CALFUN, written for calculating the residuals at each iteration, is listed in Appendix B. In addition, the steep calculation procedure was adopted in order to facilitate convergence. So, for the r^{th} nonlinear mode shape, the first calculation was done in the neighbourhood of the known linear solution by attributing a small numerical value a to the coefficient a_r of the basic function w_r^* and a zero value to the contributions of the other functions . The resulting solution was used as an initial estimate for the following step corresponding to

$a + \Delta a$. Thus, by choosing in each case the convenient value of the step Δa, the r^{th} nonlinear mode shape has been calculated at various maximum vibration amplitude to beam thickness ratios extending up to a given value. The limit of error residuals was imposed to be lower than 10^{-16} in all cases.

IV.4.2 Discussion of Numerical Results for Clamped-Clamped Beam

To obtain, via model I, the fundamental nonlinear mode shape of a clamped-clamped beam, the first six symmetric clamped-clamped beam functions were used. The corresponding parameters v_i, i = 1, 3, ..., 12 are given in Table 4.1.1. For a rectangular cross sectioned beam, corresponding to $\alpha = 3$, the non dimensional parameter defined in Section IV.2, some computed values of $a_3, a_5, ..., a_{11}$, corresponding to a_1 varying from 0.05 up to 2, are given in Table (4.2.1). For each solution $a_1, a_3, ..., a_{11}$, the corresponding value of the nonlinear frequency parameter $\left(\frac{\omega^*_{nl}}{\omega^*_l}\right)_1$ associated with the first nonlinear mode shape is also given. Comparison of experimental nonlinear clamped-clamped mode shape data obtained in [4.2] for a non-dimensional vibration amplitude at the beam centre of 2.04 and results obtained from solution of the set of nonlinear algebraic equation (4.21) corresponding to the same non-dimensional amplitude is given in Figure 4.3. It can be seen that the curve for the measured normalised mode shape is well above the normalised theoretical linear mode shape but very close to the normalised nonlinear theoretical mode shape, calculated via the present model.

For the second mode shape, the first six antisymmetric C-C beam functions were used. The corresponding parameters v_i, i = 2, 4. ..., 12 are given in Table (4.1.2). Varying a_2 from 0.05 up to 1.9, some computed values of $a_4, a_6, ..., a_{12}$ are summarised in Table 4.2.2 with the corresponding value of the nonlinear frequency parameter $\left(\frac{\omega^*_{nl}}{\omega^*_l}\right)_2$ associated with the second nonlinear mode shape for a beam with a rectangular cross section.

For the third mode shape, the first six symmetric clamped-clamped beam functions were used. For a rectangular cross sectioned beam, corresponding to $\alpha = 3$, some computed values of $a_1, a_5, a_7, ..., a_{11}$, corresponding to a_3 varying from 0.05 up to 1.7 are given in

Table 4.2.3. For each solution a_1, a_3, ..., a_{11}, the corresponding value of the nonlinear frequency parameter $\left(\frac{\omega^*_{nl}}{\omega^*_l}\right)_3$ associated with the third nonlinear mode shape is also given.

In Figures 4.3.1 to 4.3.3, the basic function coefficients are plotted versus frequency for the first, second and third mode shapes. It can be seen that near the linear frequency of a given mode only the corresponding basic function has a significant contribution. At large amplitudes, the higher order mode contribution coefficients and resonance frequencies increase. The normalised first, second and third nonlinear mode shapes corresponding to maximum normalised amplitude values given in Tables 4.3.1 to 4.3.3 are plotted in Figures 4.4.1 to 4.4.3. It can be seen that all are amplitude dependent. This agrees with theoretical and experimental results obtained in reference [4.1] for the fundamental mode shape. On the other hand, the curvatures, defined as the second derivative of the mode shape, are plotted in Figures 4.5.1 to 4.5.3. All figures show high rates of increase of the curvatures near to the clamps. It can also be seen, from Figure (4.4.2), that the zero slope point shifts towards the clamps. In other words, the nonlinear mode shapes appeared to be increasingly approaching the form of hinged-hinged beam mode shapes at higher amplitudes of vibration. This confirms the result obtained in [4.1] for the first nonlinear mode shape and results reported in [4.7] obtained via model II for the second and third nonlinear clamped-clamped mode shapes.

IV.5 CONCLUSIONS

A theoretical model for large vibration amplitudes of thin elastic beams has been developed, based on Hamilton's principle and spectral analysis, to obtain numerical results. The theory effectively reduces a nonlinear beam free vibration problem to a set of nonlinear algebraic equations depending on the classical rigidity and mass matrices, and a fourth order tensor due to the nonlinearity. Using in each case the appropriate basic functions, the theory has been applied to simply supported and clamped-clamped beams Numerical data, corresponding to the first three clamped-clamped mode shapes were computed using a Fortran program, whose main routines are listed in Appendix B, for a wide range of vibration amplitudes

As has been shown in this work, the clamped-clamped beam mode shapes based upon the linear theory can be different from those obtained if nonlinear effects due to large vibration amplitudes are taken into account. This confirms that it can be inaccurate to

assume a solution of the form $w(x,t) = q_1(t)f_1(x)$, with $f_1(x)$ as the theoretical mode of vibration of a clamped-clamped beam at small deflection oscillations.

On the other hand, the increase in natural frequency as calculated via the theoretical model, which takes into account the nonlinear ridigity tensor in calculating the change in the resonance frequency, exhibited the same trends as the previously measured resonance frequency data [4.1]. This leads to the conclusion that the definition of the generalised parameters in the linear theory are not applicable at large deflections. This is confirmed by the fact that their application, based upon measured mode shape data, would lead, as shown in [4.1], to a predicted decrease in the nonlinear resonance frequency instead of the increase observed in practice. Particularly, the definition of the generalised stiffness in the nonlinear case should take into account the stiffness due to the axial load induced by large deflections.

The general trends of the dependence of the three first nonlinear mode shapes and their derivatives on the amplitude of vibration were qualitatively similar for both models. However, numerical values of the resonance frequency obtained via the two models were slightly different. This may be explained by the difference in the approximations involved in each model. In particular, model II depends on the way in which the high order sine terms are expanded when applying the harmonic balance method [4.1]. Model I depends on the range chosen in integrating (V-T) when applying Hamilton's principle (equation (2.6)). Both assume that harmonic motion takes place at large deflections. This assumption is approximate even in the case of a SS-SS beam, as has been shown. Also in the case of clamped-clamped beams, experimental measurements showed response harmonic distortion at large deflection amplitudes. Further investigations were carried out in order to develop a theoretical nonlinear vibration model, taking into account harmonic distortion of the time function as well as the amplitude dependent spatial function. This is presented in Chapter VII.

The amplitude-dependent normalised mode shapes of clamped-clamped beams had higher values near to the clamps at large deflection amplitudes. The curvatures increased considerably close to the clamps with increasing deflection amplitude, which means that the bending strain can have a higher rate of increase with increasing amplitude in such nonlinear cases, compared to the bending strain in the linear state.

CHAPTER V

THEORETICAL MODEL FOR NONLINEAR NATURAL FREQUENCIES AND MODE SHAPES OF FULLY CLAMPED RECTANGULAR THIN ELASTIC PLATES

V.1 INTRODUCTION

The previous chapter was concerned with the nonlinear natural frequencies and mode shapes of beams. These are very useful as theoretical and experimental test pieces, but engineering interest is concerned mainly with panel-type structures [5.1]. As stated in the introduction, although in the case of fully clamped rectangular plate, the boundary conditions are mathematically simple, compared with the simply supported or free boundaries, it has no exact analytical solution. Even in the linear case, approximate numerical methods, like finite difference techniques, the Galerkin technique, Weinstein's method, integral equations and series methods have been used in the literature to study the linear mode shapes and natural frequencies of fully clamped rectangular plates. A comprehensive treatment of the linear problem and references corresponding to all the above mentioned methods are given in the monograph of Leissa [5.2] and in a more recent review in [5.3]. A detailed presentation of a series method, based on a Levy-type solution and the superposition theorem is given in [5.4]. The Rayleigh-Ritz method has been adopted in the study of the linear problem in references [5.5] to [5.7].

Although a large number of studies have been carried out on nonlinear plate vibrations, as mentioned in the introduction, each problem has received a special treatment involving some particular approximations. Some of the models available, such as those proposed in [5.8] and [5.9], are based on the perturbation procedure, and consequently, are practically limited to the first order effects of finite displacements upon natural frequency. Also, in most of the studies carried out on non-linear vibrations of rectangular plates, the common approach to such problems had been to assume a spatial function, usually the linear mode shape, and seek a solution for the time variable, assuming that the space and time functions can be separated. The objective of the work described in this Chapter was to develop a theory for analysing the effects of nonlinear vibrations of fully clamped thin elastic rectangular plates, due to large transverse displacement amplitudes, on the mode shapes and their corresponding natural frequencies. Such a theory was expected to lead to results qualitatively similar to these, obtained both theoretically and

experimentally, from a previous study dealing with the clamped-clamped beam case [5.10], and to confirm experimental results reported in [5.11] dealing with fully clamped rectangular plates, *i.e.* the dependence of the fully clamped rectangular plate mode shapes and resonance frequencies on the amplitude of vibration which induces stress patterns different to these predicted by the linear theory. Thus, a theoretical model based on Hamilton's principle and spectral analysis has been developed for large vibration amplitudes of fully clamped rectangular plates. It was then put in its general form given in Chapter II, which made it possible to be tested in the beam case, as presented in Chapter IV.

In this Chapter, the theoretical formulation of the plate large displacement vibration problem is presented, which leads to a numerical model, to which the analysis of Chapter II can be applied. By assuming harmonic motion and expanding the transverse displacement in the form of finite series of functions, the bending strain energy V_b, the axial strain energy V_a and the kinetic energy T are expressed in section V.2.1. In sections V.2.2 to V.2.4, by discretisation of the expressions of V_a, V_b and T, the tensors m_{ij}, k_{ij} and b_{ijkl} are defined. Section V.3 presents the non-dimensional formulation of the problem and details of the numerical solution. Numerical solutions corresponding to the first nonlinear mode shape for different values of the plate aspect ratio are discussed and compared to previous results in section V.4.

V.2 GENERAL FORMULATION

V.2.1 Expression of the bending strain, axial strain and kinetic energies in the plate case

V.2.1.1 Expression of the bending strain energy

Consider the transverse vibration of the plate shown in Figure 5.1 having the following characteristics :

a, b, S : length, width and area of the plate
x,y : plate coordinates in the length and the width directions respectively
H : thickness of the plate
E : Young's modulus
ν : Poisson's ratio
D : bending stiffness of the plate $D = \frac{EH^3}{12(1-\nu^2)}$
ρ : mass per unit volume of the plate

Using the notation of Chapter II, the strain energy due to bending, V_b, is given by [5.12] :

$$V_b = \frac{1}{2}\int_S D\left(\frac{\partial^2 W}{\partial x^2}+\frac{\partial^2 W}{\partial y^2}\right)^2 + 2(1-\nu)\left(\left(\frac{\partial^2 W}{\partial xy}\right)^2 - \frac{\partial^2 W}{\partial x^2}\frac{\partial^2 W}{\partial y^2}\right)dS \qquad (5.1)$$

in which W(x,y,t) is the transverse displacement function and dS = dxdy is the elementary surface. In the fully clamped boundaries case, the bending strain energy expression (5.1) can be shown, using integration by parts and the boundary conditions, to simplify to [5.13]:

$$V_b = \frac{1}{2}\int_S D\left(\frac{\partial^2 W}{\partial x^2} + \frac{\partial^2 W}{\partial y^2}\right)^2 dS \qquad (5.2)$$

V.2.1.2 Expression of the Axial Strain Energy

The expression of the axial strain energy induced by large deflections contains terms involving the first partial derivatives of the in-plane displacements U and V with respect either to x or y and terms involving only the first partial derivative of the transverse displacement W with respect either to x or y [5.14]. U and V are known to be of one order higher than W, and consequently $\frac{\partial U}{\partial x}$ and $\frac{\partial V}{\partial y}$ are of the same order as $\left(\frac{\partial W}{\partial x}\right)^2$ and $\left(\frac{\partial W}{\partial y}\right)^2$ in the expressions for the axial strains ε_{xa} and ε_{ya}. However, even so, solutions given in the static case in [5.14] and in the nonlinear dynamic case in [5.8] for a simply supported plate suggest that the contribution of the in-plane displacements to the nonlinear strain energy is small compared with terms involving only $\left(\frac{\partial W}{\partial x}\right)^2$ and $\left(\frac{\partial W}{\partial y}\right)^2$. So, an approximation has been adopted in the present work consisting of neglecting the contribution of the in-plane displacements in the expression for the nonlinear strain energy due to the axial loads induced by large deflections. Such an assumption has been adopted previously in some finite element formulations as discussed in Section V.4.5. Numerical results obtained here are compared with previous results and the domain of validity of such

an approximation is discussed in Section V.4.5. The axial strain energy induced by large deflection, V_a, is then given by [5.14] :

$$V_a = \frac{3D}{2H^2} \int_S \left[\left(\frac{\partial W}{\partial x}\right)^2 + \left(\frac{\partial W}{\partial y}\right)^2 \right]^2 dS \qquad (5.3)$$

V.2.1.3 Expression of the kinetic energy

The kinetic energy of the plate, T, is :

$$T = \frac{1}{2} \rho H \int_S \left(\frac{\partial W}{\partial t}\right)^2 dxdy \qquad (5.4)$$

in which axial and rotary inertia terms are neglected. In expressions (5.3) and (5.4), transverse shear deformation and rotary inertia are neglected in the analysis since past investigations have shown that these effects only contributed significantly in lowering the natural frequency of panels having thickness-to-span ratios greater than 0.5 [5.15].

V.2.2 Discretisation of the bending strain energy expression

If the time and space functions are supposed to be separated and harmonic motion is assumed, the transverse displacement can be written as:

$$W(x,y,t) = w(x,y) \sin\omega t \qquad (5.5)$$

where (x,y) is the vector coordinate. Expanding w(x,y) in the form of a finite series :

$$w(x,y) = a_i w_i(x,y) \qquad (5.6)$$

in which the usual summation convention defined in Chapter II is used, the discretisation of the strain energy expression, V_b, can be made. Using matrix notation, equation (5.6) can be written as :

$$W(x,y,t) = \{A\}^T \{w\} \sin \omega t \qquad (5.7)$$

where $\{w\}^T=[w_1(x,y)\ w_2(x,y) \ldots w_n(x,y)]$ is the basic spatial function matrix depending on the vector coordinate (x,y) and $\{A\}^T = [a_1\ a_2 \ldots a_3]$ is the contribution coefficients matrix. Substituting expression (5.7) into equation (5.2) corresponding to the clamped boundary conditions leads to :

$$V_b = \frac{1}{2}\int_S D\left[\{A\}^T\left\{\frac{\partial^2 w}{\partial x^2} + \frac{\partial^2 w}{\partial y^2}\right\}\right].\left[\{A\}^T\left\{\frac{\partial^2 w}{\partial x^2} + \frac{\partial^2 w}{\partial y^2}\right\}\right] dS\ \sin^2\omega t \qquad (5.8)$$

where :

$$\left\{\frac{\partial^2 w}{\partial x^2} + \frac{\partial^2 w}{\partial y^2}\right\}^T = \left[\frac{\partial^2 w_1}{\partial x^2} + \frac{\partial^2 w_1}{\partial y^2} \quad \frac{\partial^2 w_2}{\partial x^2} + \frac{\partial^2 w_2}{\partial y^2} \quad \ldots \quad \frac{\partial^2 w_n}{\partial x^2} + \frac{\partial^2 w_n}{\partial y^2}\right] \qquad (5.9)$$

is a matrix depending on the second partial derivatives of the functions w_i. As terms between brackets in equation (5.8) are scalar, we have :

$$\{A\}^T.\left\{\frac{\partial^2 w}{\partial x^2} + \frac{\partial^2 w}{\partial y^2}\right\} = \left\{\frac{\partial^2 w}{\partial x^2} + \frac{\partial^2 w}{\partial y^2}\right\}^T \{A\} \qquad (5.10)$$

Using equation (5.10) and the property of associativity of matrix multiplication, equation (5.8) can be written as :

$$V_b = \frac{1}{2}\{A\}^T\left\{\int_S D\left\{\left\{\frac{\partial^2 w}{\partial x^2} + \frac{\partial^2 w}{\partial y^2}\right\}.\left\{\frac{\partial^2 w}{\partial x^2} + \frac{\partial^2 w}{\partial y^2}\right\}^T\right\} dS\right\}\{A\}^T \sin^2\omega t \qquad (5.11)$$

The integral term is identical to the rigidity matrix of the plate. Thus, equation (5.2) can be written as :

$$V_b = \frac{1}{2}\ \{A\}^T\ [K]\ \{A\}\ \sin^2\omega t = \frac{1}{2}\ a_i a_j k_{ij}\ \sin^2\omega t \qquad (5.12)$$

in which k_{jj} is the general term of matrix [K] given by:

$$k_{ij}= \int_S D\left(\frac{\partial^2 W_i}{\partial x^2} + \frac{\partial^2 W_i}{\partial y^2}\right)\left(\frac{\partial^2 W_j}{\partial x^2} + \frac{\partial^2 W_j}{\partial y^2}\right) dxdy \qquad (5.13)$$

and indices i and j are summed over 1, ..., n.

V.2.3 Discretisation of the axial strain energy expression

From quations (5.3) and (5.7) one obtains :

$$V_a = \frac{3D}{2H^2} \sin^4\omega t \int_S \left\{ \left[\{A\}^T\left\{\frac{\partial w}{\partial x}\right\}\right]\left[\{A\}^T\left\{\frac{\partial w}{\partial x}\right\}\right] + \left[\{A\}^T\left\{\frac{\partial w}{\partial y}\right\}\right]\left[\{A\}^T\left\{\frac{\partial w}{\partial y}\right\}\right] \right\}^2 dS \quad (5.14)$$

where $\left\{\frac{dw}{dx}\right\}^T = \left[\frac{dw_1}{dx}\ \frac{dw_2}{dx}\ \ \frac{dw_n}{dx}\right]$ is the matrix of the first derivatives of the functions w_i. The factors between brackets in equation (5.14) can be transformed in a manner similar to that applied in equation (5.10) to these of equation (5.8), leading to :

$$V_a = \frac{3D}{2H^2} \sin^4\omega t \int_S \left\{\{A\}^T\left[\left\{\frac{\partial w}{\partial x}\right\} \cdot \left\{\frac{\partial w}{\partial x}\right\} + \left\{\frac{\partial w}{\partial y}\right\} \cdot \left\{\frac{\partial w}{\partial y}\right\}^T\right]\{A\}^T\right\}^2 dS$$

$$= \frac{3D}{2H^2} .\sin^4\omega t \int_S \left\{ \{A\}^T\ [C_{ij}(x,y)]\ \{A\}^T \right\}^2 dS \qquad (5.15)$$

where $[C_{ij}(x,y)]$ is a matrix whose general term C_{ij} is a function of (x,y) given by :

$$C_{ij}(x,y) = \frac{\partial w_i}{\partial x} \cdot \frac{\partial w_j}{\partial x} + \frac{\partial w_i}{\partial y} \cdot \frac{\partial w_j}{\partial y} \qquad (5.16)$$

so that equation (5.15) can be written as :

$$V_a = \frac{3D}{2H^2} \sin^4\omega t \int_S \left\{ a_i a_j\, C_{ij}(x,y) \right\} \left\{ a_k a_l\, C_{kl}(x,y) \right\} dS$$

$$= \frac{3D}{2H^2} \sin^4\omega t\ a_i a_j a_k a_l \int_S \left\{ C_{ij}(x,y) \right\} \left\{ C_{kl}(x,y) \right\} dS = \frac{1}{2} .\sin^4\omega t\ a_i a_j a_k a_l\, b_{ijkl} \qquad (5.17)$$

in which the fourth order tensor b_{ijkl} is given by :

$$b_{ijkl} = \frac{3D}{H^2} \int_S \left(\frac{\partial w_i}{\partial x} \frac{\partial w_j}{\partial x} + \frac{\partial w_i}{\partial y} \frac{\partial w_j}{\partial y} \right) \left(\frac{\partial w_k}{\partial x} \frac{\partial w_l}{\partial x} + \frac{\partial w_k}{\partial y} \frac{\partial w_l}{\partial y} \right) dS \qquad (5.18)$$

V.2.4 Discretisation of the kinetic energy expression

Substituting equation (5.7) in equation (5.4) leads to:

$$T = \frac{1}{2}\rho H \omega^2 \cos^2 \omega t \int_S w^2 dxdy = \frac{1}{2}\rho H \omega^2 \cos^2 \omega t \int_S \left[\{A\}^T \{w\} \right] \left[\{A\}^T \{w\} \right] dxdy$$

$$= \frac{1}{2}\rho H \omega^2 \cos^2 \omega t \ \{A\}^T \left[\int_S \{w\}^T \{w\} dxdy \right] \{A\} \qquad (5.19)$$

The integral term is the mass matrix whose general term m_{ij} is given by :

$$m_{ij} = \rho H \int_S w_i \, w_j dxdy \qquad (5.20)$$

so that T can be written as in expression (4.8), in which m_{ij} is given by equation (5.20).

V.3 NON-DIMENSIONAL FORMULATION AND NUMERICAL DETAILS

V.3.1 Non-dimensional formulation

To simplify the study of the influence of various geometrical and mechanical parameters on the plate nonlinear behaviour and the numerical treatment of the nonlinear algebraic equations, non-dimensional formulation of the nonlinear vibration problem has been made as follows: α being the aspect ratio of the plate, $\alpha = \frac{b}{a}$, by putting :

$$w_i(x,y) = H \, w_i^*\left(\frac{x}{a}, \frac{y}{b}\right) = H w_i^*(x^*, y^*) \qquad (5.21)$$

where x* and y* are non-dimensional coordinates $x^* = \frac{x}{a}$ and $y^* = \frac{y}{b}$, we obtain :

$$k_{ij} = \frac{DaH^2}{b^3} k^*_{ij} \tag{5.22}$$

$$b_{ijkl} = \frac{DaH^2}{b^3} b^*_{ijkl} \tag{5.23}$$

$$m_{ij} = \rho H^3 ab.\, m^*_{ij} \tag{5.24}$$

where k^*_{ij}, b^*_{ijkl} and m^*_{ij} are non-dimensional generalised parameters given by:

$$k^*_{ij} = \int_{S^*} \left(\alpha 2 \frac{\partial^2 w^*_i}{\partial x^{*2}} + \frac{\partial^2 w^*_i}{\partial y^{*2}}\right)\left(\alpha 2 \frac{\partial^2 w^*_i}{\partial x^{*2}} + \frac{\partial^2 w^*_i}{\partial y^{*2}}\right) dx^* dy^* \tag{5.25}$$

$$b^*_{ijkl} = 3 \int_{S^*} \left(\alpha 2 \frac{\partial w^*_i}{\partial x^*}\frac{\partial w^*_j}{\partial x^*} + \frac{\partial w^*_i}{\partial y^*}\frac{\partial w^*_j}{\partial y^*}\right)\left(\alpha 2 \frac{\partial w^*_k}{\partial x^*}\frac{\partial w^*_l}{\partial x^*} + \frac{\partial w^*_k}{\partial y^*}\frac{\partial w^*_l}{\partial y^*}\right) dx^* dy^* \tag{5.26}$$

The mass tensor m^*_{ij} is given by :

$$m^*_{ij} = \int_{S^*} w^*_i \; w^*_j dx^* dy^* \tag{5.27}$$

where (S*) is the non-dimensional surface $[0,1] \times [0,1]$. By substituting expressions (5.25)-(5.27) in equation (2.14) established in Chapter II, we obtain :

$$\omega^2 = \frac{D}{\rho H b^4}\; \omega^{*2} = \frac{EH^2}{12(1-\nu^2)\rho b^4}\; \omega^{*2} \tag{5.28}$$

where ω^{*2} is the non-dimensional frequency parameter given by :

$$\omega^{*2} = \frac{a_i a_j k^*_{ij} + a_i a_j a_k a_l b^*_{ijkl}}{a_i a_j m^*_{ij}} \tag{5.29}$$

The pararameters k^*_{ij}, b^*_{ijkl} and m^*_{ij} given in the plate case by equations (5.25)-(5.27) depend only on the plate aspect ratio α and the chosen basic functions w^*_i. Also, it should be noticed that, as outlined in [5.3] in the linear case, the nonlinear frequency parameter ω^* does

not depend on the Poisson's ratio ν, since none of the pararameters k^*_{ij}, b^*_{ijkl} and m^*_{ij} depend on it, but the nonlinear frequency itself depends in all cases on ν, via the plate bending stiffness $D = \frac{EH^3}{12(1-\nu^2)}$ as shown in equation (5.28).

A set of nonlinear algebraic equations, identical to equations (2.24) established in Chapter II, in which the dimensional parameters are replaced by the non-dimensional ones, has to be solved for each value of the plate aspect ratio α and the assigned r_0^{th} mode contribution a_{ro} to obtain the amplitude dependent r_0^{th} nonlinear plate mode shape.

V.3.2 Choice and normalisation of basic functions

The basic functions used in the nonlinear rectangular plate analysis were obtained as products of x- and y-clamped-clamped beam functions. These functions which satisfy all the fully clamped theoretical boundary conditions, *i.e.* zero displacement and zero slope along the four plate edges, have been used in previous studies on fully clamped rectangular plate vibration [5.2] and have been demonstrated in many cases to be appropriate for the determination of plate natural frequencies [5.3].Thus the i^{th} plate (x,y) function used in the present work was proportional to $f^a_{\alpha i}(x) \, . \, f^a_{\beta i}(y)$, where $f^a_{\alpha i}$ is a clamped-clamped beam function given by :

$$f^a_{\alpha(i)}(x) = \frac{\text{ch } \nu_{\alpha i} \frac{x}{L} - \cos \nu_{\alpha i} \frac{x}{L}}{\text{ch } \nu_{\alpha i} - \cos \nu_{\alpha i}} - \frac{\text{sh } \nu_{\alpha i} \frac{x}{L} - \sin \nu_{\alpha i} \frac{x}{L}}{\text{sh } \nu_{\alpha i} - \sin \nu_{\alpha i}} \qquad (5.30)$$

and αi and βi are indices depending on i as follows : When using n^2 plate basic functions obtained as products of the first n clamped-clamped beam functions, the indices $\alpha(i)$ and $\beta(i)$ vary from 1 to n and the index i varies from 1 to n^2. The relationship between αi, βi and i used in the Fortran programs was:

$$i = n*(\alpha i - 1)) + \beta i \qquad (5.31)$$

$\nu_{\alpha i}$ for $\alpha i = 1,2,..,n$ are eigenfunction parameters for a clamped-clamped beam defined in Chapter IV (equation (4.33)). The non-dimensional fully clamped rectangular plate functions w^*_i were defined as :

$$w_i^*(x^*,y^*) = \frac{1}{G} f_{\alpha i}^{a^*}(x^*) \quad f_{\beta i}^{a^*}(y^*) \tag{5.32}$$

in which $x^* = \frac{x}{L}$, $y^* = \frac{y}{L}$ and:

$$f_{\alpha_i}^{a^*}(x^*) = \frac{\text{ch } v_i x^* - \cos v_i x^*}{\text{ch } v_i - \cos v_i} - \frac{\text{sh } v_i x^* - \sin v_i x^*}{\text{sh } v_i - \sin v_i} \tag{5.33}$$

and G is a normalisation scaling factor given below. A Fortran routine called CALC was used for computing values taken by the functions $f\alpha_i^a$, and their first and second derivatives, as explained in Chapter IV. The functions w_i^* and their first and second derivatives were computed by dividing the calculated values of $f\alpha_i^a$, $f\alpha_i^b$ and $f\alpha_i^c$ by the scaling factor G given by :

$$G = \sqrt{\int_{s^*} \left(f_{\alpha i}^{a^*}(x^*) \quad f_{\beta i}^{a^*}(y^*) \right)^2 dx^* dy^*} \tag{5.34}$$

By use of Fubini's theorem [5.16], the x* and y* variables could be separated in the above double integral which allowed G to be calculated as:

$$G = \sqrt{\int_0^1 \left(f_{\alpha i}^{a^*}(x^*) \right)^2 dx^*} \sqrt{\int_0^1 \left(f_{\beta i}^{a^*}(x^*) \right)^2 dx^*} \tag{5.35}$$

The simple integrals, such as $\int_0^1 \left(f_{\alpha(i)}^{a^*}(x^*) \right)^2 dx^*$ and those appearing in the remainder of this section were calculated numerically using Simpson's method by a routine called SOMM. By putting :

$$g_{\alpha i}^{a^*}(x^*) = \frac{f_{\alpha i}^{a^*}(x^*)}{\sqrt{\int_0^1 \left(f_{\alpha i}^{a^*}(x^*) \right)^2 dx^*}} \tag{5.36}$$

the non-dimensional plate function $w_i^*(x^*,y^*)$ can be written as:

$$w_i^*(x^*,y^*) = g_{\alpha i}^{a^*}(x^*)\ \ g_{\beta i}^{a^*}(y^*) \tag{5.37}$$

V.3.3 Numerical details of the m_{ij}, k_{ij} and b_{ijkl} tensor calculations

In this section, the numerical calculation procedure used for calculating k_{ij}^*, b_{ijkl}^* and m_{ij}^* is presented. It was based on Fubini's theorem, which allows a double integral depending on a function in which the x- and y-variables are separated to be calculated as product of two simple integrals, each depending only on one of the two variables.

V.3.3.1 Mass tensor m_{ij}

Substituting equations (5.37) in equation (5. 27) leads to :

$$m_{ij}^* = \int_{S^*} g_{\alpha i}^{a^*}(x^*)\ g_{\beta i}^{a^*}(y^*)\ g_{\alpha j}^{a^*}(x^*)\ f_{\beta j}^{a^*}(y^*)\, dx^* dy^*$$

$$= \left[\int_0^1 g_{\alpha i}^{a^*}(x^*)\ g_{\alpha j}^{a^*}(x^*) dx^*\right]\left[\int_0^1 g_{\beta i}^{a^*}(y^*)\ g_{\beta j}^{a^*}(y^*) dy^*\right] \tag{5.38}$$

which can be written as :

$$m_{ij}^* = \text{pinaa}(\alpha_i,\alpha_j)\ .\ \text{pinaa}(\beta_i,\beta_j) \tag{5.39}$$

in which pinaa(αi,αj) is the simple integral given by:

$$\text{pinaa}(\alpha_i,\alpha_j) = \int_0^1 g_{\alpha i}^{a^*}(x^*)\ g_{\alpha j}^{a^*}(x^*)\ dx^* \tag{5.40}$$

This notation might appear unusual but it is employed here and in the programs for clarity.

V.3.3.2 Rigidity tensor k^*_{ij}

Substituting Equations (5.37) in equation (5.25) and denoting $g^{c*}_{\alpha i}$ the second derivatives of the function $g^{a*}_{\alpha i}$ leads to, Fubini's theorem being used :

$$k^*_{ij} = \alpha 4\left[\int_0^1 g^{c*}_{\alpha i}(x^*)\, g^{c*}_{\alpha j}(x^*)dx^*\right]\left[\int_0^1 g^{a*}_{\beta i}(y^*)\, g^{a*}_{\beta j}(y^*)dy^*\right]$$

$$+ \alpha 2\left[\int_0^1 g^{c*}_{\alpha i}(x^*)\, g^{a*}_{\alpha j}(x^*)dx^*\right]\left[\int_0^1 g^{a*}_{\beta i}(y^*)\, g^{c*}_{\beta j}(y^*)dy^*\right]$$

$$+ \alpha 2\left[\int_0^1 g^{a*}_{\alpha i}(x^*)\, g^{c*}_{\alpha j}(x^*)dx^*\right]\left[\int_0^1 g^{c*}_{\beta i}(y^*)\, g^{a*}_{\beta j}(y^*)dy^*\right]$$

$$+ \left[\int_0^1 g^{a*}_{\alpha i}(x^*)\, g^{a*}_{\alpha j}(x^*)dx^*\right]\left[\int_0^1 g^{c*}_{\beta i}(y^*)\, g^{c*}_{\beta j}(y^*)dy^*\right] \qquad (5.41)$$

Equation (5.39) can be written as :

$$k^*_{ij} = \alpha 4 pincc(\alpha_i,\alpha_j)\,.\,pinaa(\beta_i,\beta_j) + \alpha 2 pinca(\alpha_i,\alpha_j)\,.\,pinca(\beta_j,\beta_i) +$$
$$\alpha 2 pinca(\alpha_j,\alpha_i)\,.\,pinca(\beta_i,\beta_j) + pinaa(\alpha_i,\alpha_j)\,.\,pincc(\beta_i,\beta_j) \qquad (5.42)$$

in which pincc and pinca are simple integrals given by :

$$pincc(\alpha_i,\alpha_j) = \int_0^1 g^{c*}_{\alpha i}(x^*)\, g^{c*}_{\alpha j}(x^*)\, dx^* \qquad (5.43)$$

$$pinca(\alpha_i,\alpha_j) = \int_0^1 g^{c*}_{\alpha i}(x^*)\, g^{a*}_{\alpha j}(x^*)\, dx^* \qquad (5.44)$$

V.3.3.3 Nonlinear rigidity tensor b^{*}_{ijkl}

Substituting equations (5.37) in equation (5.26) and denoting $g^{b*}_{\alpha i}$ and $g^{c*}_{\alpha i}$ the first and second derivatives of the function $g^{a*}_{\alpha i}$ leads to, Fubini's theorem being used:

$$b^{*}_{ijkl} = 3\ \alpha^4\left[\int_0^1 g^{b*}_{\alpha i}(x^*)g^{b*}_{\alpha j}(x^*)g^{b*}_{\alpha k}(x^*)\ g^{b*}_{\alpha l}\ (x^*)dx^*\right]\left[\int_0^1 g^{a*}_{\beta i}(y^*)g^{a*}_{\beta j}(y^*)g^{a*}_{\beta k}(x^*)g^{a*}_{\beta l}\ (x^*)dy^*\right]$$

$$3\ \alpha^2\left[\int_0^1 g^{b*}_{\alpha i}(x^*)g^{b*}_{\alpha j}(x^*)g^{a*}_{\alpha k}(x^*)\ g^{a*}_{\alpha (l)}\ (x^*)dx^*\right]\left[\int_0^1 g^{a*}_{\beta i}(y^*)g^{a*}_{\beta j}(y^*)g^{b*}_{\beta k}(x^*)g^{b*}_{\beta l}\ (x^*)dy^*\right]$$

$$3\ \alpha^2\left[\int_0^1 g^{a*}_{\alpha i}(x^*)g^{a*}_{\alpha j}(x^*)g^{b*}_{\alpha k}(x^*)\ g^{b*}_{\alpha l}\ (x^*)dx^*\right]\left[\int_0^1 g^{b*}_{\beta i}(y^*)g^{b*}_{\beta j}(y^*)g^{a*}_{\beta k}(x^*)g^{a*}_{\beta l}\ (x^*)dy^*\right]$$

$$3\left[\int_0^1 g^{a*}_{\alpha i}(x^*)g^{a*}_{\alpha j}(x^*)g^{a*}_{\alpha k}(x^*)\ g^{a*}_{\alpha l}\ (x^*)dx^*\right]\left[\int_0^1 g^{b*}_{\beta i}(y^*)g^{b*}_{\beta j}(y^*)g^{b*}_{\beta k}(y^*)g^{b*}_{\beta l}\ (y^*)dy^*\right] \qquad (5.45)$$

which can be written as :

$$b^{*}_{ijkl} = 3\alpha^4[\text{pin4b}(\alpha_i,\alpha_j,\alpha_k,\alpha_l)\text{pin4a}(\beta_i,\beta_j,\beta_k,\beta_l)]$$
$$+3\alpha^2[\text{p2a2b}(\alpha_k,\alpha_l,\alpha_i,\alpha_j)\text{p2a2b}(\beta_k,\beta_l,\beta_i,\beta_j)] +3\alpha^2[\text{p2a2b}(\alpha_i,\alpha_j,\alpha_k,\alpha_l)\text{p2a2b}(\beta_i,\beta_j,\beta_k,\beta_l)]$$
$$+[\text{pin4a}(\alpha_i,\alpha_j,\alpha_k,\alpha_l)\text{pin4b}(\beta_i,\beta_j,\beta_k,\beta_l)] \qquad (5.46)$$

in which pin4a, pin4b and p2a2b are simple integrals given by :

$$\text{pin4a}(\alpha_i,\alpha_j,\alpha_k,\alpha_l) = \int_0^1 g^{a*}_{\alpha i}(x^*)g^{a*}_{\alpha j}(x^*)g^{a*}_{\alpha k}(x^*)\ g^{a*}_{\alpha l}\ (x^*)dx^* \qquad (5.47)$$

$$\text{pin4b}(\alpha_i,\alpha_j,\alpha_k,\alpha_l) = \int_0^1 g^{b*}_{\alpha i}(x^*)g^{b*}_{\alpha j}(x^*)g^{b*}_{\alpha k}(x^*)\ g^{b*}_{\alpha l}\ (x^*)dx^* \qquad (5.48)$$

$$p2a2b(\alpha_i,\alpha_j,\alpha_k,\alpha_l) = \int_0^1 g^{a*}_{\alpha i}(x^*)g^{a*}_{\alpha j}(x^*)g^{b*}_{\alpha k}(x^*)\, g^{b*}_{\alpha l}(x^*)dx^* \qquad (5.49)$$

V.3.3.4 Conclusions

It appears from expressions (5.38) to (5.49) that k^*_{ij}, b^*_{ijkl} and m^*_{ij} can be calculated as products (or sums of products) of simple integrals. This reduces considerably the computation time since $2n^4$ double integrals for k^*_{ij} and m^*_{ij}, and n^8 double integrals for b^*_{ijkl} are needed when using n^2 basic functions; but only $3n^2 + 3\,n^4$ simple integrals have to be calculated. Also, due to the orthogonality of the beam basic functions, a further simplification can be noticed: the mass matrix is identical to the identity matrix and all the nondiagonal terms of the rigidity matrix are equal to zero. A fortran routine, called Prep, was written for calculating the non-dimensional parameters for the fully clamped rectangular plate, which is listed in Appendix C.

V.4 FIRST NONLINEAR MODE SHAPE

V.4.1 Numerical details

To obtain the fundamental nonlinear mode shape of a fully clamped rectangular thin elastic plate, 25 basic functions obtained as products of the first five clamped-clamped beam mode shapes were used. As a set of 24 nonlinear algebraic equations had to be solved numerically for various values of the amplitude of vibration and plate aspect ratios, it was necessary to find an appropriate routine. Most of the iterative methods available are either relatively quick but require for convergence a good estimate of the solution, such as Newton's method, or slow but can converge even if the first estimate is quite far from the solution, such as the gradient method. The Harwell library routine NS01A was used since it is based on a hybrid method combining the steep descent and Newton's methods and consequently participates to the advantages of both methods [5.17]. The routine CALFUN, calculating residuals, was similar to that mentioned in the clamped-clamped beam case and listed in Appendix C. Also, a step procedure, similar to that described in Chapter IV, was adopted for ensuring a quick convergence when varying the amplitude, which allowed solutions to be obtained with quite small number of iterations (an average of 30 for 24 equations).

V.4.2 Convergence of the spectral expansion

Typical results referring to five values of the plate aspect ratio α and to a maximum amplitude to thickness ratio of 0.5 are given in Table 5.1. It can be seen that the only significant contributions are, as may be expected due to the symmetry of the plate first mode shape, those corresponding to the nine first symmetric basic functions in both the x and y directions. It should be noticed that the above nine symmetric functions, are these whose contributions to the first linear mode shape of fully clamped square plates are considered as significant in results published by Leissa from Young's work, based on Rayleigh-Ritz analysis [5.2]. For the range of vibration amplitudes considered in the numerical results given below, the non symmetric basic functions in either the x or y directions had contributions which were at least 10^{-3} times the smallest contribution of the symmetric basic functions, in both x and y directions. This corresponds in terms of curvatures to a maximum ratio of at least 75 $\left(= 10^3 \frac{v_1^2}{v_5^2} \right)$[1].To check that the addition of non-symmetric clamped-clamped beam functions does not affect the results, calculations were made with only nine symmetric-symmetric functions obtained as product of the first three symmetric clamped-clamped beam functions defined in the linear theory. The results show no significant change in both the value of the resonance frequency and the basic function contributions. So, the conclusion has been made that the nonlinear fundamental mode shape can be obtained with enough accuracy using the nine first symmetric-symmetric basic functions, which simplifies significantly the computation effort, since calculations of the nonlinearity tensor b^*_{ijkl} involve $25^4=3.9\ 10^5$ terms when using 25 basic functions, but only $9^4=6.5\ 10^3$ terms when using 9 basic functions.

V.4.3 Comparison of solutions obtained from the nonlinear model for small amplitudes with known linear solutions

In Table 5.2, numerical solutions of the set of nonlinear algebraic equations corresponding to the nonlinear vibration problem, obtained for $a_{11} = 0.05$. are compared to results given in [5.2] from Rayleigh-Ritz analysis of the linear problem corresponding to a square plate. It can be seen that both resonance frequencies and contribution coefficients

[1]The curvatures involve second derivatives, which introduce a multiplication factor of v_i^2 as can be seen in equation (5.33).

obtained from nonlinear analysis for small vibration amplitudes are very close to those obtained from linear analysis. Also, in Table 5.3, nonlinear frequency parameters obtained here from nonlinear analysis for a_{11}=0.05 are compared with previously linear frequency parameters published in the above reference corresponding to various plate aspect ratios and a good agreement can be seen. It may be worth outlining here, from the numerical methods point of view, that a classical eigenvalue problem, solved usually by classical numerical methods, such as Jacobi's method, appears here as a limit of a nonlinear problem, described by a set of nonlinear algebraic equations, whose solution tends to the eigenvalue problem solution when the amplitude tends to zero.

V.4.4 General presentation of numerical results

Numerical results corresponding to the assigned contribution a_{11} varying from 0.05 to 2, which corresponds to a maximum amplitude vibration to thickness ratio varying from ($0.05 \times 1.5^2 = 0.11$) to ($2 \times 1.5^2 = 4.5$) and α = 0.2, 0.4, 0.6, 0.8, 1 are summarised in Tables 5.4 to 5.8. In each table, a_{ij} represents the contribution of the basic function obtained as product of the i^{th} and j^{th} x and y clamped-clamped basic functions. w^*_{max} is the maximum non-dimensional amplitude, obtained at the plate centre and $\frac{\omega^*_{nl}}{\omega^*_l}$ is the ratio of the nonlinear non-dimensional frequency parameter defined in equation (5.29) to the linear non-dimensional frequency parameter obtained by the same equation for small values of the contribution coefficients and listed in Table 5.3. It can be noticed that in nonlinear numerical results corresponding to the square plate (α=1), the contribution coefficients a_{ij} are, as may be expected due to the complete symmetry of the problem in this case, identical to a_{ji} (for i = 1,2,3 and j = 1,2,3) for all values of vibration amplitudes. This was considered as an additional check of good convergence of the iterative method used for solving the set of nonlinear algebraic equations.

V.4.5 Comparison of the Amplitude-Frequency Dependence Calculated via the Present Theory with Previous Results

In order to estimate the accuracy of the results obtained by the present theory and the effects of the approximations adopted, a detailed comparison was made of all the results found in the literature (references [5.8] and [5.18] to [5.24]) and the present ones. Most of the results available are concerned with a clamped square plate and only few deal with plates of various aspect ratios. Also, as discussed in the Introduction, although various techniques

are used, no results were found for the amplitude dependence of the mode shapes. Consequently, the comparison was restricted to the amplitude dependence of the resonance frequency. Even so, such comparison was thought to lead to acceptable conclusions, especially with respect to the zero in-plane displacement assumption, since the nonlinear resonance frequency is governed, as has been shown in the present work, by the strain energy due to the axial load induced by large amplitudes, and hence the importance of the terms neglected in the strain energy expression must be reflected on the nonlinear frequency estimates. Table 5.9.1 summarises a set of results corresponding to a fully clamped square plate obtained during the period 1961 to 1989 for displacement amplitude at the plate centre to thickness ratios up to 1, and 1.5 for results from [5.21]. As these results were based on various analytical assumptions and numerical techniques of solution, a general comparison was made by calculating the average and the standard deviation of the nonlinear frequency estimates obtained by various methods for each amplitude of vibration, as shown in Table 5.9.2. Good agreement can be seen between different results and although the standard deviation increases with amplitude, it remains within a reasonable range. For nondimensional displacement amplitudes up to 1 it does not exceed 1.3%. It can be seen also that results obtained in the present work are very close to the average and to results obtained in [5.20] by the finite element method assuming zero in-plane displacements. This may suggest that the importance of the contribution of these displacements to the axial strain energy may be estimated by the difference between results obtained in [5.20] and results obtained in [5.23] since both are based on the finite element method with zero and non-zero in-plane displacements, respectively. This would lead to the conclusion that the assumption of zero in-plane displacement leads to accurate results for finite but small amplitudes and remains acceptable for amplitudes up to once the plate thickness. Comparison of the value obtained here and that taken from [5.21] for an amplitude of 1.5 times the thickness show a standard deviation somewhat below 2%. Results obtained here for an aspect ratio of 0.5 are compared to results obtained in [5.20]and [5.21] in Table 5.9.3. The corresponding average and standard deviation is given in Table 5.9.4, which shows a maximum standard deviation of 0.26 %.

V.4.6 Amplitude-frequency dependence

It can be seen from Tables 5.4 to 5.8 that the rate of increase in nonlinear fundamental frequency with increasing displacement is very low at small amplitudes. For all values of the plate aspect ratio, it is somewhat more than 1% for displacement amplitudes slightly exceeding 0.2 times the plate thickness. This can lead to the conclusion

that the practical use of the linear frequencies for such amplitudes can be of acceptable accuracy, although it must limit the expected frequency estimate accuracy to a reasonable range. However, for amplitudes as great as nearly once the thickness, the rate of increase in resonance frequencies is about 18% and the nonlinear effect has to be taken into account.

V.4.7 Amplitude dependence of the plate fundamental mode shape

In Figures 5.2.1-5.2.5, normalised sections of the nonlinear fundamental mode shape, corresponding to $y^* = 0.5$ and $\alpha = 1.0, 0.8, 0.6, 0.4, 0.2$ are plotted for the values of the maximum non-dimensional amplitudes w^*_{max} given in Table 5.10. All curves show the amplitude dependence of the mode shape and an increase of curvatures near to the clamps. The same curves corresponding to $y^*=0.05$ given in Figures 5.3.1-5.3.5 show that the shape of nonlinear mode shape sections in the neighbourhood of the clamps can be very different to that usually expected in the linear theory, especially those parallel to the width direction and for small values of the plate ratio aspect. Similar curves are given in Figures 5.4.1-5.4.5 and 5.5.1-5.5.5corresponding to $x^* = 0.5$; $\alpha = 1,0.8, 0.6, 0.4, 0.2$ and $x^* = 0.05$; $\alpha = 1,0.8, 0.6, 0.4, 0.2$ respectively. It can be generally noticed that the deformation of the mode shape, for a given value of the normalised amplitude of vibration, increases as the aspect ratio α decreases.

V.4.8 Analysis of bending stresses associated with the fundamental nonlinear mode shape

The maximum bending strains ε_{xb} and ε_{yb} obtained for $z = \frac{H}{2}$ are given by :

$$\varepsilon_{xb} = \frac{H}{2}\left(\frac{\partial^2 W}{\partial x^2}\right) \tag{5.50}$$

$$\varepsilon_{yb} = \frac{H}{2}\left(\frac{\partial^2 W}{\partial y^2}\right) \tag{5.51}$$

using the classical thin plate assumption of plane stress state and Hooke's law, the stresses can be obtained as :

$$\sigma_{x\,b} = \frac{EH}{2(1-\nu^2)}\left[\left(\frac{\partial^2 W}{\partial x^2}\right) + \nu\left(\frac{\partial^2 W}{\partial y^2}\right)\right] \tag{5.52}$$

$$\sigma_{y\,b} = \frac{EH}{2(1-\nu^2)}\left[\left(\frac{\partial^2 W}{\partial y^2}\right) + \nu\left(\frac{\partial^2 W}{\partial x^2}\right)\right] \tag{5.53}$$

Using the non-dimensional parameters defined in the previous section, non-dimensional stresses σ^*_{xb} and σ^*_{yb} can be defined by :

$$\sigma^*_{xb} = \alpha^2\left(\frac{\partial^2 W^*}{\partial x^{*2}}\right) + \nu\left(\frac{\partial^2 W^*}{\partial y^{*2}}\right) \tag{5.54}$$

$$\sigma^*_{yb} = \left(\frac{\partial^2 W^*}{\partial y^{*2}}\right) + \nu\,\alpha^2\left(\frac{\partial^2 W^*}{\partial x^{*2}}\right) \tag{5.55}$$

with the relationships between dimensional and non-dimensional stresses given by :

$$\sigma = \frac{EH^2}{2(1-\nu^2)b^2}\,\sigma^* \tag{5.56}$$

which is valid for both dimensional and non-dimensional pairs of stresses defined by equations (5.50) to (5.56).

The non-dimensional bending stress distribution is plotted in Figures 5.6.1- 5.6.4 for y* = 0.05.0.2, 0.375 and 0.5. It can be seen in Figure 5.6.1 that the bending stress can exhibit in the neighbourhood of the clamps a distribution with positive values along the whole section, due to the Poisson's ratio effect and to high curvatures in the y directions. Figures 5.6.2-5.6.4 show a high increase of the bending stress near to the clamps, compared with the rate of increase expected in the linear theory. This behaviour in the plate central line is similar to that obtained in [5.10] and in the present work (Chapter IV) in the clamped-clamped beam case.

V.5 CONCLUSIONS

The theoretical model for large vibration amplitudes of thin elastic structures established in Chapter II and applied to clamped-clamped beams in Chapter IV had been extended to the case of fully clamped thin elastic plates. In the same manner to the beam case examined in Chapter IV, the theory reduces a nonlinear free vibration problem to a set of non-linear algebraic equations depending on the classical rigidity and mass matrices, and a nonlinear term in which appears a fourth order tensor due to the non-linearity, and a cubic factor with respect to the contribution coefficients. Numerical data corresponding to various values of the plate aspect ratio and to the first and second nonlinear fully clamped rectangular plate mode shapes were computed using a Fortran program, whose main routines are listed in Appendix C, for a wide range of vibration amplitudes

As has been shown in this work, the fully clamped rectangular plate mode shapes based upon the linear theory can be different from those obtained if nonlinear effects due to large vibration amplitudes are taken into account. This confirms that it can be inaccurate to assume a solution of the form $w(x,y,t) = q_1(t)f_1(x,y)$, with $f_1(x,y)$ as the theoretical mode of vibration of a fully clamped rectangular plate at small deflection oscillations.

On the other hand, the increase in natural frequency as calculated via the theoretical model, which takes into account the nonlinear ridigity tensor in calculating the change in the resonance frequency, exhibited the same trends as the measured resonance frequency data (Chapter VI). This leads to the conclusion, as in the beam case, that the definition of the generalised parameters in the linear theory are not applicable at large deflections. Particularly, the definition of the generalised stiffness in the nonlinear case should take into account the stiffness due to the axial load induced by large deflections.

A systematic comparison of nonlinear frequency parameters obtained here for displacements up to 1.5 times the plate thickness and aspect ratios of 1 and 0.5 with all previous available results obtained by various methods has shown a reasonable agreement. Numerical results given here for higher amplitudes and lower aspect ratios must be considered with some reservation until further investigations determine accurately how other nonlinear effects, such as high inplane displacements or change of material behaviour from elastic to plastic may affect the results.

The amplitude-dependent normalised mode shapes of fully clamped rectangular plates had higher values near to the clamps at large deflection amplitudes. The curvatures

increased considerably close to the clamps with increasing deflection amplitude, which means that the bending strain can have a higher rate of increase with increasing amplitude in such nonlinear cases, compared to the bending strain in the linear state.

CHAPTER VI

MEASUREMENT OF THE RESPONSE OF FULLY CLAMPED RECTANGULAR ISOTROPIC AND CFRP PLATES IN A FREQUENCY RANGE COVERING THE FUNDAMENTAL MODE AT LARGE VIBRATION AMPLITUDES

VI.1 INTRODUCTION

In the present Chapter, results of experimental investigations carried out on fully clamped rectangular homogeneous and CFRP plates are presented and discussed. Measurements of the resonance frequency amplitude dependence are presented in Section VI.2. The investigation of the effects of large amplitudes of vibration on the mode shapes using the peak amplitude method and the nonlinear mode shape estimation method discussed in Chapter III are presented in Section VI.3. In Section VI.4, details are given concerning the harmonic distortion measurements and analysis. In Section VI.5, the separated fundamental mode amplitude dependence obtained using either electrodynamic or acoustic excitation is examined. The investigation of the second harmonic spatial distribution including modulus and phase measurements is presented in Section VI.6. Investigations of the response at large vibration amplitudes of a CFRP plate is presented in Section VI.7.and a general discussion of experimental results and conclusions are given in Section VI.7.

VI.2 AMPLITUDE DEPENDENCE OF THE RESONANCE FREQUENCY

According to the ISO standard recommendation, "resonance of a system in forced oscillation exists when any change, however small, in the frequency of excitation causes a decrease in a response of the system" [6.1]. As discussed previously in the literature [6.2] and [6.3], this definition, valid for linear systems, cannot be applied in the nonlinear case, because of the qualitative difference in the behaviour of nonlinear systems, due to the existence of multivalued regions in the frequency response curve and the possible occurrence in that region of the associated jump phenomena [6.4]. In [6.5], dealing with nonlinear clamped-clamped beam vibrations, the resonance frequency was defined as the frequency at which maximum vibration amplitude was observed when the excitation frequency was increased through the range of interest during a frequency response test. In the present work, this definition was adopted and a set of tests have been carried out on a

fully clamped rectangular homogeneous plate in which the excitation frequency was increased, using a sweep oscillator, for a given value of the current in the coil attached to the plate centre, until the jump phenomenon occurred and the corresponding values of the frequency and peak displacement amplitude were noted. The electronic apparatus used in such experiments is represented in Figure 6.1. The jump phenomenon was observed at frequencies higher than the linear resonance frequency which was obtained for low excitation levels.

Results obtained at points of non-dimensional coordinates (x*,y*) = (0.5,0.5), (0,35,0.35), (0.225,0.225) of plate 1 presented in Chapter III clamped on rig 2 are summarised in Table (6.1) and plotted in Figures 6.2 to 6.4 with the corresponding theoretical curves obtained via the theory developed within the present work . It can be seen that the measured resonance frequency was very close to the theoretical value given in Table 3.1. As the excitation level increased, the measured resonance frequency increased and both theoretical and experimental curves show a nonlinear behaviour of the hardening spring type. In all figures, the theoretical resonance frequency values were higher than the experimental ones, as may be expected, due to the theoretical approximation involved in the Rayleigh-Ritz series expansion, which is known to lead to upper bound frequency estimates, and the effect of clamp flexibility and the coil mass. The trends of increase in resonance frequency with increasing normalised amplitude are very similar for each pair of theoretical and experimental curves, although some irregularities can be noticed in Figures 6.3 and 6.4 corresponding to the points (x*,y*) = (0.35,0.35) and (0.225,0.225) which are probably due to the higher sensitivity of small measured values to experimental errors and the accentuated effect of clamp flexibility due to the proximity of the plate edges.

VI.3 FIRST NONLINEAR MODE SHAPE[1] MEASUREMENTS BASED ON THE PEAK AMPLITUDE METHOD

As a first attempt to investigate experimentally the effects of large amplitudes of vibration on the fully clamped rectangular plate first mode shape, an electrodynamic exciter, made of a coil and magnet arrangement such as that described in Chapter III, was attached to the centre of plate 2 and the peak amplitude method was used to measure the plate response at

[1]Throughout the experimental part of this work, the term "mode shape" is used to describe the dynamic deflection shape in the neighbourhood of a resonance frequency. Strictly, this is not the mode shape, as there are small off-resonance contributions from other modes when the measurements are made by the peak amplitude method. The terminology used here is in accordance with that generally used when measurements are made on lightly damped systems.

various points for several values of the input current in the coil and the excitation frequency. Results of such measurements, carried out for maximum normalised non-dimensional amplitudes of 0.47, 0.72, and 0.91 are summarised in Tables 6.2 to 6.4, respectively. As for each value of the maximum amplitude, the response at 90 points had to be measured, which was quite a long process, the displacement amplitude at the plate centre was measured after each set of measurements, indicating very small variation in each case, as can be seen in Tables 6.3 and 6.4. The corresponding normalised values, with respect to maximum amplitude vibration measured at the plate centre, are given in Tables 6.5 to 6.7. The measured and normalised values are ordered in the same manner for all tables and the coordinates of the corresponding points are given in Table 6.2. Although the displacement amplitudes involved in such measurements, obtained using a coil and a magnet exciter, are still relatively small, compared with amplitudes obtained using acoustic excitation, an amplitude dependence of the normalised values can be noticed, with a general trend of increase for almost all the measurement points, with increasing the displacement amplitude at the plate centre, with a particular accentuation in the region of the clamps. In order to obtain a global estimation of the trends exhibited in such nonlinear behaviour, an attempt has been made, using the nonlinear mode shape estimation method presented in Chapter III, for estimating the basic function contribution coefficients . A Fortran routine was written, called DATAA, which is listed in Appendix D, for calculating the mode shape estimates. Results obtained numerically for amplitudes of 0.47, 0.72 and 0.91 corresponding to the four plate basic functions obtained as products of the first two symmetric-symmetric beam functions in the x and y directions are summarised in Table 6.8 and the corresponding normalised contribution coefficients with respect to the predominant contribution of the first basic function are summarised in Table 6.9. In Table 6.10, values of the rate of increase of each basic function contribution with amplitude are given. A clear trend of increase of the contribution coefficients of the second and higher basic functions can be noticed, with increasing amplitude of vibration. This qualitatively conforms to theoretical results obtained in the previous chapter. However, as the functions 3, and 6 to 9, where the notation defined in equation (5.31) is used, involve the 5^{th} clamped-clamped beam function in either the plate width or length directions, which exhibits five changes in sign along that direction, no attempt was made to estimate the corresponding contribution coefficients, as this was not expected to lead to consistent results, due to numerical and experimental errors. Using the estimated function contributions, the non-dimensional bending stress defined in equation (5.56) was calculated at $(x^*,y^*) = (0.5,0)$ for the three amplitudes considered. Table 6.11 summarizes values of the theoretical non-dimensional bending stress, obtained by the numerical model presented in Chapter V, the estimated non-dimensional bending stress obtained here and

the corresponding theoretical and estimated rate of increase of the bending stress with amplitude of vibration. It can be seen that good agreement exits between theoretical and experimental rates of increase of the bending stress with amplitude. However, the absolute theoretical bending stresses are about 2.5 times higher than the experimental values. Such a high ratio of the predicted to measured bending strains has been reported in the literature for conventional aluminium alloy panels and seems to be related to the effect of the flexibility of the practical clamps, compared with the perfect clamped boundary conditions assumed in the theory [6.6-6.8].

VI.4 DETAILS OF THE HARMONIC DISTORTION ANALYSIS

The separation of harmonic components in the nonlinear response of the clamped-clamped beam investigated in [6.5] has led to similar conclusions concerning the fundamental component spatial distribution. However, as the plate response time signals observed on the oscilloscope during the amplitude measurements were distorted, depending on the measurement point, it was necessary to examine the effect in the plate case using FFT techniques for extracting the harmonic components at various points on the plates tested. So, the plate responses at various points were acquired on line using an analogue to digital converter. A sampling rate of 2400 samples per second was adopted, which allowed frequencies up to 600 Hz to be examined, according to the DAC system recommendations. An antialiasing filter was used to filter frequencies higher than the above value and avoid any aliasing effects [6.9]. The stored files were then analysed, using an FFT algorithm available in the DAC system [6.10]. The electronic apparatus used in such measurements is represented in Figure 6.5.1 to 6.5.3 corresponding to acoustic excitation and digital data acquisition, electrodynamic excitation and digital data acquisition and electrodynamic excitation and a B & K 2032 analyser measurements and analysis respectively. As the number of files involved in such measurements was quite high, a systematic procedure was adopted in numbering of the acquired files which allowed the analyses to be made automatically using the routine Xzoom listed in Appendix E.

A set of measurements was carried out on plate 3 clamped on rig 1 for an excitation frequency of 105.5 Hz and a current in the coil of 0.2 Amps. The resulting non-dimensional amplitude was equal to 0.94 at the plate centre. Response time signals, acquired along the plate centre line parallel to the longitudinal direction at points $(x^*,y^*) = (0.5,0.5)$, $(0.80,0.5)$, $(0.88,0.5)$ and $(0.936,0.5)$ are plotted in Figures 6.6.1

to 6.6.4. The modulus of the corresponding FFT output is plotted on a linear scale in Figures 6.7.1 to 6.7.4 and on a logarithmic scale in Figures 6.8.1 to 6.8.4. Response time signals acquired along the centre line parallel to the horizontal direction at points (x*,y*) = (0.5,0.091) and (0.5,0.318) are plotted in Figures 6.6.5 and 6.6.6. The modulus of the corresponding FFT output is plotted in Figures 6.7.5 and 6.7.6 in linear scale and 6.8.5 and 6.8.6 in logarithmic scale. Examining the above figures, the following remarks can be made. The plate response was distorted and several harmonics appeared in the logarithmic scale plots, with a predominance of the second harmonic. Also, the harmonic distortion along the centre line parallel to the width direction was very small compared with points close to the plate edge on the central line parallel to the length direction. A more laborious but systematic procedure was adopted to obtain a general qualitative result concerning the harmonic distortion spatial distribution, which is presented in Section VI.7.

VI.5 AMPLITUDE DEPENDENCE OF THE SEPARATED FIRST COMPONENT

The amplitude dependence of the fundamental mode was investigated using either electrodynamic excitation and an analogue B & K analyser or acoustic excitation and the ISVR digital acquisition and analysis facility (DAC). Results of experiments of the first category carried out on plate 3 on rig 1 for maximum non-dimensional amplitudes of 0.3 and 0.7 are plotted in Figures 6.9.1 and 6.9.2, and results of the second category carried out on plates 4 and 5 using the ISVR acoustic test facility are plotted in Figures 6.9.3 and 6.9.4. In each figure, the measured mode along a section parallel to the width direction (x* = 0.5 for Figures 6.9.1 to 6.9.3 and x* = 0.28 for Figure 6.9.4 is normalised and compared to the theoretical linear mode shape. Indications concerning the excitation frequencies, levels of excitation and amplitudes of vibration are given in figures. An example of FFT output of the acoustic pressure signals is given in the Figure 6.10 corresponding to measurements represented in Figures 6.9.3. It can be seen in the mode shape plots (Figures 6.9.1 to 6.9.4) that for an amplitude ratio of 0.3, which is relatively small, the measured mode shape is very close to the theoretical mode. As the amplitude increases, the normalised measured values increase and the mode shape deformation becomes clearer, confirming the trends observed in the theoretical results obtained in the previous Chapter.

VI.6 SECOND HARMONIC SPATIAL DISTRIBUTION

A systematic procedure was adopted for analysing the spatial distribution of the harmonic distortion. Modulus and phase measurements have been made for several sections of the plate parallel to the length and the width directions and for various values of displacement amplitude up to a value approximately equal to the plate thickness. As the second and higher harmonics were relatively small, numerical values of the corresponding modulus and phase calculated via a normal Fourier transform were sensitive to the resolution in the frequency domain, which was restricted due to the limitation imposed to the time history signal. Hence, FFT analysis was first used to obtain approximate values of harmonics and zoom analysis was then used in the neighbourhood of each harmonic to obtain accurate values of modulus and phase. It was observed from plots similar to those given in Figures 6.11.1 to 6.14.4 that for the frequency range of interest and chosen amplitudes of vibration, the spatial distribution of the second harmonic of the dynamic response was very similar to the second mode shape of the fully clamped rectangular plate considered, whose predominant component is the product of the second and first clamped-clamped beam mode shapes in the length and width directions respectively. As an example, the normalised first harmonic spatial distribution, obtained along the centre line parallel to the length direction of plate 3, and for a maximum amplitude of 0.9 times the thickness, is plotted in Figure 6.11.1. It has, as should be expected, the form of the first mode shape of the plate. The second harmonic spatial distribution is plotted in Figure 6.11.2. It can be seen that its shape is very similar to that of the second mode shape of a fully clamped rectangular plate in the length direction. The phase lags between the first harmonic components for the pairs of points (A,A') and (B,B') shown in Figures 6.11.1 and 6.11.2 were 0.05 and 0.06 rad respectively, while the phase lags between the second harmonic components were 3.16 and 3.19 rad respectively. These values confirmed that the second harmonic components for each pair were vibrating out of phase. Examples of OVT output time history signals obtained at symmetrical points $(x^*,y^*) = (.72,.5)$ and (.28,.5) are given in Figures (6.12.1) and (6.12.2). The corresponding modulus and phase plots obtained from zoom analysis in the neighbourhood of the second harmonic are given in Figures 6.13.1 and 6.13.2.

As the maximum amplitude of the second harmonic component was seen to occur at about $x^* = 0.25$ and $x^* = 0.75$, which is close to the maximum of the second mode in the length direction, measurements in the width direction were carried out, using two O.V.T.s along the Sections $x^* = 0.3$ and $x^* = 0.7$ for y varying simultaneously from 11 cm to 1.5 cm and 11 cm to 20.5 cm respectively, at intervals of 1 cm. This was done since

measurements at the centre of the plate have led to small harmonic distortion and no consistent phase information could be obtained. The corresponding normalised spatial distributions of the first and second harmonic components are plotted in Figures 6.14.1 to 6.14.4. It can be seen that both the first and second harmonic distributions have a shape similar to the first fully clamped rectangular plate mode shape in the width direction. The phase lags obtained between the second harmonics of all symmetrical points showed that they were vibrating out of phase, confirming the identification of the mode excited at the second harmonic component as the second mode shape of the plate considered.

VI.7 MEASUREMENTS OF A CFRP PLATE RESPONSE NEAR TO THE FUNDAMENTAL MODE

Measurements were carried out on the CFRP plate described in Chapter III on rig 2. The plate was excited by a coil and magnet in the neighbourhood of its first resonance determined by frequency response tests. The response measurements and separation of harmonics was made using the B & K analyser 2032. The normalised separated first harmonic component spatial distribution is plotted in Figures 6.15.1 and 6.15.2 for non-dimensional amplitudes of 0.5 and 0.8 together with the normalised theoretical linear mode shape. It can be seen that normalised measured values are higher than the theoretical values and increase with increasing amplitude. Comparison of Figures 6.15.1 and 6.15.2 with Figures 6.9.1 and 6.9.2 shows that the CFRP plate exhibits for similar amplitudes of vibration a more accentuated nonlinearity characterised by higher normalised values than for the isotropic plates. The normalised second harmonic spatial distribution corresponding to the above two sets of measurements is represented in Figure 6.15.3. A shape similar to the plate second mode in the length direction can be observed. Also, the normalised second harmonic spatial distribution appears to be amplitude dependent, with a shift of the maximum points towards the clamps. This recalls the amplitude dependence of the second clamped-clamped nonlinear mode obtained theoretically in Chapter IV (Figure 4.5.2).

VI.8 CONCLUSIONS

The measurements presented above show how the nonlinear behaviour of fully clamped rectangular plates at large dynamic displacement amplitudes can be complex and different from those expected in linear theory. In spite of this, some results have been obtained with respect to some aspects of such complicated problems, but many questions

remain to be investigated. Measurements of change in resonance frequency with amplitude of vibration exhibited similar trends to the theoretical results obtained in the previous chapter. Also, in spite of the sensitivity of estimated mode shapes to experimental and numerical errors, which made accurate quantitative indications difficult to obtain, trends of increase of the higher mode contribution coefficients and the corresponding bending stress were observed. Considering the separated fundamental component of the plate response, it was observed that its spatial distribution deviated from the linear mode as the amplitude increased so that the curvatures increased near to the clamps. A systematic investigation of the harmonic distortion spatial distribution has shown that the plate second mode can be excited, due to nonlinear effects, although the excitation force is applied in the nodal point of this mode and the excitation frequency is close to the fundamental resonance frequency. This new qualitative result, based on both modulus and phase measurements, may be due to the second harmonic of the excitation frequency, whose presence is due to nonlinear effects, being close to the second resonance frequency of the plate. However, as the nonlinear resonance frequencies for all modes are amplitude dependent, an exchange between higher harmonic spatial distributions may be expected as the amplitude grows and the resonance frequencies shift to the right on the frequency axis. Also, different second and higher harmonic spatial distributions may be found for plates of different aspect ratios, since the distribution of modes is aspect ratio dependent.

Measurements carried out on a CFRP plate have led to results similar to those obtained for the isotropic plates tested for both the first and second harmonic spatial distribution, with a more accentuated nonlinear behaviour, which seems to be due to higher inplane stiffnesses, as discussed in Chapter IX.

A complementary discussion of other aspects of the experimental work and suggestions for further investigations are given in the general conclusions.

CHAPTER VII

THEORETICAL MODEL FOR NONLINEAR FREE VIBRATIONS OF CLAMPED-CLAMPED BEAMS TAKING INTO ACCOUNT THE HARMONIC DISTORTION AT LARGE DEFLECTIONS

VII.1 INTRODUCTION

The purpose of the work presented in this chapter was to develop a theoretical model for nonlinear vibrations dealing with amplitude dependent clamped-clamped beam mode shapes, but also providing a means of analysing the spatially distributed harmonic distortion occurring at large deflections. Previous analytical and experimental investigations, reported in [7.1], had shown that a clamped-clamped beam vibrating nonlinearly can have harmonic response solutions at $1\frac{1}{2}$, 2, 3,.. of the excitation frequency. Results of FFT analyses of measurements of a clamped-clamped beam response near to its fundamental resonance, reported in [7.2], showed that the response second and third harmonic distortion was spatially distributed with a distribution somewhat similar to some clamped-clamped mode shapes. In the light of this experimental result, and of measurements reported in the previous Chapter in the plate case, the spatial distribution of the second harmonic and higher harmonic components of the dynamic response of a clamped-clamped beam have been examined theoretically as follows: assuming a response in which the displacement functions were expanded as a series of products of spatial and harmonic time functions having as frequencies increasing multiples of the fundamental circular frequency ω; Hamilton's principle was applied in order to determine the contribution coefficients in the assumed series, introducing in addition to the nonlinearity tensor b_{ijkl} due to the axial tension in the middle line of the beam, obtained in Chapter IV, two second order tensors α_{qr} and β_{qr} and a fourth order tensor γ_{qrst} which represent a weighting coefficient for the coupling between time harmonics in the set of nonlinear algebraic equations obtained for the nonlinear vibration problem. The so-developed model appeared as an extension of the numerical model for nonlinear free vibrations of beams and plates established in Chapter II which included the time harmonic distortion effects.

VII.2 GENERAL EXPRESSION FOR THE DISPLACEMENT FUNCTION

Extending the numerical model developed in Chapter II for large vibration amplitudes of fully clamped beams and plates, and using the definitions and notation given in the above reference, the transverse displacement function W(x,t) is now written as:

$$W(x,t) = \{A_1\}^T \{w\} \sin \omega t + \{A_2\}^T \{w\} \sin 2\omega t + \ ... +$$

$$\{A_q\}^T \{w\} \sin q\omega t + ... + \{A_p\}^T \{w\} \sin p\omega t \qquad (7.1)$$

where $\{w(x)\}^T = \left[w_1(x)\ w_2(x,)..\ w_n(x)\right]$ is the basic spatial function matrix depending on the abscissa x and $\{A_q\}^T = \left[a_1^q\ a_2^q \ ...\ a_n^q\right]$ is the matrix of coefficients of $\{w(x)\}$ corresponding to the q^{th} harmonic. In the above expression, n is the number of the spatial functions supposed to contribute to the dynamic response of the structure considered and p is the number of harmonics taken into account. In order to avoid confusion of any indices, in the remainder of this Chapter, the integer indices qrst and ijkl will be used for the time harmonics and the basic spatial functions respectively. The time variable will be denoted by τ to avoid confusion with the integer index t. In reduced notation, equation (7.1) can be written as:

$$W(x,\tau) = \{A_q\}^T \{w\} \sin q\omega\tau \qquad (7.2)$$

where the repeated integer index q is summed over 1, ..., p.

VII.3 EXPRESSION OF THE BENDING STRAIN, AXIAL STRAIN AND KINETIC ENERGIES IN THE BEAM CASE

In this section, the general form obtained by discretisation of the bending strain, the axial strain and the kinetic energy expressions, when the displacement function given in equation (7.2) is adopted, is developed in order to allow the frequency equation to be obtained by application of Hamilton's principle in the next Section. The beam notation defined in Chapter IV is adopted in the following analysis.

VII.3.1 Discretisation of the bending strain energy expression.

Substituting the displacement function given in equation (7.2) into equation (4.1) giving the beam bending strain energy expression leads to:

$$V_b = \frac{1}{2}\int_0^L EI\left[\{A_q\}^T \cdot \left\{\frac{d^2w}{dx^2}\right\} \sin q\omega\tau\right].\left[\{A_r\}^T \cdot \left\{\frac{d^2w}{dx^2}\right\} \sin r\omega\tau\right]dx \qquad (7.3)$$

where $\left\{\frac{d^2w}{dx^2}\right\}^T = \left[\frac{d^2w_1}{dx^2}\ \frac{d^2w_2}{dx^2}\ \ \frac{d^2w_n}{dx^2}\right]$ is the column matrix of the second derivatives of the functions w_i. As we have :

$$\{A_q\}^T\left\{\frac{d^2w}{dx^2}\right\} = \left\{\frac{d^2w}{dx^2}\right\}^T\{A_q\} \qquad (7.4)$$

Equation (7.3) can be written after transformation as :

$$V_b = \frac{1}{2}\{A_q\}^T\left\{\int_0^L EI\left\{\left\{\frac{d^2w}{dx^2}\right\}.\left\{\frac{d^2w}{dx^2}\right\}^T\right\}dx\right\}\{A_r\}^T \sin q\omega\tau \sin r\omega\tau \qquad (7.5)$$

The integral term is identical to the beam rigidity matrix . Therefore, equation (7.5) can be written as :

$$V_b = \frac{1}{2}\ \{A_q\}^T [K]\ \{A_r\} \sin q\omega\tau \sin r\omega\tau \qquad (7.6)$$

q and r are summed over 1, ..., p.

VII.3.2 Discretisation of the axial strain energy expression

Substituting the displacement function given by equation (7.2) into equation (4.4) giving the beam strain energy due to the axial load leads to:

$$V_a = \frac{EA}{8L}\left[\int_0^L \left[\{A_q\}^T\ \left\{\frac{dw}{dx}\right\} \sin q\omega\tau\right].\left[\{A_r\}^T\ \left\{\frac{dw}{dx}\right\} \sin r\omega\tau\right]dx\right] .$$

$$\left[\int_0^L \left[\{A_s\}^T\ \left\{\frac{dw}{dx}\right\} \sin s\omega\tau\right].\left[\{A_t\}^T\ \left\{\frac{dw}{dx}\right\} \sin t\omega\tau\right]dx\right] \qquad (7.7)$$

where $\left\{\frac{dw}{dx}\right\}^T = \left[\frac{dw_1}{dx}\ \frac{dw_2}{dx}\ \ \frac{dw_n}{dx}\right]$ is the column matrix of the first derivatives of the functions w_i. Each of the two factors put between brackets in the above product is similar to the integral appearing in equation (7.3) in which $\left\{\frac{d^2w}{dx^2}\right\}$ is replaced by $\left\{\frac{dw}{dx}\right\}$; so that both can be transformed as detailed above in equations (7.3) to (7. 5), leading to:

$$V_a = \frac{EA}{8L}\left[\{A_q\}^T\left\{\int_0^L \left\{\left\{\frac{dw}{dx}\right\}.\left\{\frac{dw}{dx}\right\}^T\right\}dx\right\}\{A_r\}^T\right]\sin q\omega\tau \sin r\omega\tau \ .$$

$$\left[\{A_s\}^T\left\{\int_0^L \left\{\left\{\frac{dw}{dx}\right\}.\left\{\frac{dw}{dx}\right\}^T\right\}dx\right\}\{A_t\}^T\right]\sin s\omega\tau \sin t\omega\tau \qquad (7.8)$$

Using the matrix notation, V_a takes the following form :

$$V_a = \left(\{A_q\}^T[L]\{A_r\}\right)\left(\{A_s\}^T[L]\{A_t\}\right)\sin q\omega\tau \sin r\omega\tau \sin s\omega\tau \sin t\omega\tau \qquad (7.9)$$

where [L] is n square matrix whose general term L_{ij} is :

$$L_{ij} = \sqrt{\frac{EA}{4L}}\int_0^L \frac{dw_i}{dx}\frac{dw_j}{dx}\,dx \qquad (7.10)$$

and where q, r, s and t are summed over 1, ..., p.

VII.3.3 Discretisation of the kinetic energy expression

Substituting the displacement function given in equation (7.2) into equation (4.5) giving the beam kinetic energy expression leads to :

$$T = \frac{1}{2}\int_0^L \rho A q r \omega^2 \left[\{A_q\}^T\ \{w\}\cos q\omega\tau\right].\left[\{A_r\}^T\ \{w\}\cos r\omega\tau\right]dx \qquad (7.11)$$

As detailed above in equations (7.3) to (7.5) for V_b, equation (7.11) can be written as :

$$T = \frac{1}{2} qr\omega^2 \{A_q\}^T \left\{ \int_0^L \rho A \{\{w\}.\{w\}^T\} dx \right\} \{A_r\}^T \cos q\omega\tau \cos r\omega\tau \qquad (7.12)$$

The integral term is identical to the beam mass matrix . So, Equation (7.12) can be written as

$$T = \frac{1}{2} \omega^2 \{A_q\}^T [M_{qr}] \{A_r\} \cos q\omega\tau \cos r\omega\tau \qquad (7.13)$$

where $[M_{qr}]$ is a generalised qr mass matrix corresponding to the coupling between the q^{th} and r^{th} time harmonics given by:

$$[M_{qr}] = qr.\,[M] \qquad (7.14)$$

where [M] is the usual mass matrix.

VII.4 NUMERICAL MODEL

VII.4.1 General expressions for the bending strain, axial strain and kinetic energies

Reintroducing the tensors k_{ij}, b_{ijkl} and m_{ij} defined in Chapter IV for a beam, the bending strain energy , the axial strain energy and the kinetic energy expressions given in equations (7.6), (7.9) and (7.13) can be written in the following general form :

$$V_b = a_i^q \, a_j^r \, k^{ij} \, . \sin q\omega\tau \sin r\omega\tau \qquad (7.15)$$

$$V_a = a_i^q \, a_j^r \, a_k^s \, a_l^t \, b^{ijkl} \sin q\omega\tau \sin r\omega\tau \sin s\omega\tau \sin t\omega\tau \qquad (7.16)$$

$$T = \omega^2 \, a_i^q \, a_j^r \, m^{ij} \, \omega^2 \cos q\omega t \cos r\omega t \qquad (7.17)$$

in which the indices i, j, k, and l are summed over 1 to n and the repeated indices q, r, s and t are summed over 1 to p.

VII.4.2 Frequency equation

To obtain the frequency equation for a vibrating beam at a circular frequency ω, Hamilton's principle can be applied as follows:

$$\delta \int_0^{2\pi/\omega} \{\tfrac{1}{2} a_i^q a_j^r k^{ij} \sin q\omega\tau \sin r\omega\tau + \tfrac{1}{2} a_i^q a_j^r a_k^s a_l^t b^{ijkl} \sin q\omega\tau \sin r\omega\tau \sin s\omega\tau \sin t\omega\tau$$

$$-\tfrac{1}{2}\omega^2 a_i^q a_j^r qr\, m^{ij}\, \omega^2 \cos q\omega\tau \cos r\omega\tau\} d\tau = 0 \qquad (7.18)$$

Put

$$\alpha_{qr} = \int_0^{2\pi/\omega} \sin q\omega\tau \sin r\omega\tau \, d\tau \qquad (7.19)$$

$$\beta_{qr} = qr \int_0^{2\pi/\omega} \cos q\omega\tau \cos r\omega\tau \, d\tau \qquad (7.20)$$

$$\gamma_{qrst} = \int_0^{2\pi/\omega} \sin q\omega\tau \sin r\omega\tau \sin s\omega\tau \sin t\omega\tau \, d\tau \qquad (7.21)$$

The problem (7.18) reduces to that of minimising, with respect of the undetermined coefiicients a_i^q, the function Φ defined by:

$$\Phi = \Phi_b + \Phi_a - \omega^2 \Phi_k \qquad (7.22)$$

where Φ_b, Φ_a and Φ_k can be written in reduced notation as:

$$\Phi_b = a_i^q a_j^r k^{ij} \alpha_{qr} \qquad (7.23)$$

$$\Phi_a = a_i^q a_j^r a_k^s a_l^t b^{ijkl} \gamma_{qrst} \qquad (7.24)$$

$$\Phi_k = a_i^q a_j^r m^{ij} \beta_{qr} \qquad (7.25)$$

As mentioned in Chapter IV, the matrices [K] and [M] are diagonal due to the choice of clamped-clamped beam mode shapes as basic functions. Also, the tensors α_{qr} and β_{qr} are diagonal and proportional to the Kronecker tensor δ_{qr}, Φ_b and Φ_a can be written as:

$$\Phi_b = \left(a_i^q\right)^2 k^{ii} \alpha_{qq} \qquad i = 1, ..., n \qquad q = 1, ..., p \qquad (7.26)$$

$$\Phi_k = \left(a_i^q\right)^2 m^{ii} \beta_{qq} \qquad i = 1, ..., n \qquad q = 1, ..., p \qquad (7.27)$$

In order to obtain the minimum of the function Φ defined in equations (7.22) to (7.25), the set of equations obtained by writing:

$$\frac{\partial \Phi}{\partial a_i^q} = 0 \qquad r = 1, ..., p \qquad i = 1, ..., n \tag{7.28}$$

has to be solved numerically. As we have:

$$\frac{\partial \Phi_b}{\partial a_i^q} = 2\ a_i^q\ k^{ii}\ \alpha_{qq} \qquad \text{(no summation involved)} \tag{7. 29}$$

$$\frac{\partial \Phi_b}{\partial a_i^q} = 4\ a_j^r a_k^s a_l^t\ b^{ijkl}\ \gamma_{qrst} \tag{7.30}$$

$$\frac{\partial \Phi_k}{\partial a_i^q} = 2\ a_i^q\ m^{ii}\ \beta_{qq} \qquad \text{(no summation involved)} \tag{7. 31}$$

Equation (7.28) can be written as:

$$2\ a_i^q\ k^{ii}\ \alpha_{qq} + 4\ a_j^r\ a_k^s\ a_l^t\ b^{ijkl}\ \gamma_{qrst} - 2\ \omega^2\ a_i^q\ m^{ii}\ \beta_{qq} = 0$$

$$q = 1, ..., p \qquad i = 1, ..., n \tag{7.32}$$

which is a set of n × p nonlinear algebraic equations obtained by varying i and q through 1,., n and 1,.,p respectively. In each equation, the dummy indices j, k, l and r, s, t are summed over 1to n and 1 to p respectively.

VII.4.3 Discussion of the numerical model

In the set (7.32), n × p + 1 unknowns have to be determined which are the n × p coefficients and ω, while only n × p equations are available. To overcome a similar difficulty in the model presented in Chapter II dealing with nonlinear vibrations with no consideration of harmonic distortion, the principle of conservation of energy was applied to equate the maximum total strain energy and the maximum kinetic energy of the vibrating structure, which has led to the remaining equation necessary for closing the formulation. For the present problem, the maximum stored kinetic energy expression can be obtained easily since at t = 0, the total strain energy, *i.e.* $V_b + V_a$, is equal to zero as may be seen from equation (7. 15) and (7.16), and consequently, all the structure mechanical energy is stored as a kinetic energy the expression for which can be obtained by putting t = 0 in equation (7.13), which leads to :

$$T_{max} = \frac{1}{2}\,\omega^2 \{A_q\}^T [M_{qr}] \{A_r\} \qquad (7.33)$$

However, the general maximum strain energy expression would be more difficult to obtain since at $t = \frac{\pi}{2\omega}$, cosine terms in expressions (7.17) whose argument is $q\omega \frac{\pi}{2\omega} = q\frac{\pi}{2}$ do not vanish, as this was the case in the previous model, for even values of q. Consequently, the technique adopted here was slightly different from that adopted in Chapter II. Instead of assigning only a given value to the first spatial basic function contribution, the spatial basic function contributions corresponding to the first time harmonic and ω were chosen as one of the solutions obtained from the theory discussed in Chapter IV. Then, the contribution vectors $\left[a_1^2\ a_2^2\ \ldots\ a_n^2\right]$ to $\left[a_1^p\ a_2^p\ \ldots\ a_n^p\right]$ were calculated by solving the above set of nonlinear algebraic equations in which i varies from 1 to n and p varies only from 2 to p.

VII.4.4 Choice of the basic functions

It is well known that the success of the Rayleigh-Ritz method in leading to a good estimate of the natural frequencies and mode shapes for a given problem depends to a large extent on the suitability of the basic functions used for the investigated mode shapes. In the present unexplored problem, the spatial distribution of the second and third harmonics for a clamped-clamped beam were investigated, and the only experimental data available are those given in [7.2], in which no phase information is given. This made it difficult to know exactly which mode corresponded to the measured second and third harmonic spatial distribution. Also, in a previous study on large vibration amplitudes of beams, a partial differential equation of motion was obtained, with a cubic stiffness term, which was identical to the Duffing equation. It is well known that the solution of such a nonlinear equation, leads to multivalued regions, in the amplitude response curves, in which the jump phenomenon can occur [7.3-7.7]. Also, in contrast with the linear case, the steady-state solution in the nonlinear case can depend on the initial conditions [7.3]. So, it was not excluded that for the present complicated nonlinear problem more than one solution could exist. Therefore, several basic function combinations were investigated, corresponding to the choices of basic functions presented in the following sections

VII.4.5 Non-dimensional formulation and numerical details

The non-dimensional formulation of the present problem was made as in Chapter IV, leading to expressions for the non-dimensional tensors m^*_{ij} , k^*_{ij} , b^*_{ijkl} and ω^* given by equations (4.16) to (4.18), and to a set of nonlinear algebraic equations identical to equations (7.32) in which the dimensional parameters are replaced by the non-dimensional ones mentioned above. The tensors α_{qr}, β_{qr}, γ_{qrst} defined by equations (7.19) to (7.21) had been calculated numerically using the trigonometric relations established in Appendix F The tensors m^*_{ij} , k^*_{ij} and b^*_{ijkl} were calculated using the Fortran routine PREPB, listed in Appendix B. The library routine NS01A presented in the previous chapters was used to solve the set of nonlinear algebraic equations (7.32). A routine called CALFUNBH, listed in Appendix G, was written for calculating the residuals, necessary for NS01A at each iteration.

VII.5 NUMERICAL SOLUTION

VII.5.1 First solution

Calculations have been made for a clamped-clamped beam of rectangular cross Section. The first 11 linear clamped-clamped beam functions have been used as basic spatial functions and the number of time harmonics was restricted to three due to the numerical complexity of the treatment of high numbers of nonlinear algebraic equations. As explained in Section VII.4.3, the first harmonic spatial distribution and the corresponding frequency were chosen as one of the solutions obtained from the theory discussed in Chapter IV. The second and third harmonic spatial distributions were calculated by solving the corresponding 22 nonlinear algebraic equations. A summary of numerical solutions obtained for various amplitudes of vibration is given in Table 7.1 in which only the contribution coefficient of symmetric functions to the third harmonic are given, since the contribution coefficients obtained for the second harmonic spatial distribution were very small (in all cases lower than 10^{-14}) and the contribution coefficients of antisymmetric functions to the third harmonic are at least 10^{-1} times the smallest contribution coefficients of the symmetric functions. The third harmonic spatial distribution appears as an amplitude dependent combination of symmetrical linear clamped-clamped beam mode shapes. In all cases, the preponderant coefficients are those of the first and third symmetrical clamped-clamped beam mode shapes with an increasing third to first

contribution ratio with amplitude as can be seen in the normalised third harmonic spatial distribution plotted in Figure 7.1.

VII.5.2 Second solution

Investigations have been made for a numerical solution in which only the second to the eleventh linear clamped-clamped beam functions would contribute to the second and third harmonic spatial distribution. As explained above, the first harmonic spatial distribution and the corresponding frequency were chosen as one of the solutions obtained from the theory discussed in Chapter IV. The second and third harmonic spatial distributions were calculated by solving the corresponding 20 nonlinear algebraic equations. A summary of numerical solutions obtained for various amplitudes of vibration is given in Table 7.2 in which only the contribution coefficients of symmetric functions to the third harmonic are given, since the contribution coefficients obtained for the second harmonic spatial distribution were very small (in all cases lower than 10^{-14}) and the contribution coefficients of antisymmetric functions to the third harmonic are at least 10^{-1} times the smallest contribution coefficients of the symmetric functions. The third harmonic spatial distribution appears as an amplitude dependent combination of third and higher symmetrical linear clamped-clamped beam mode shapes. In all cases, the preponderant coefficients are those of the third clamped-clamped beam mode shape, with an increase of curvatures near to the clamps and shift of the nodal point toward the clamps, as can be seen in Figure 7.2.

VII.6 DISCUSSION OF NUMERICAL RESULTS AND CONCLUSIONS

In this chapter, a theoretical model had been presented for large amplitude free vibrations of clamped-clamped beams which attempted to analyse the harmonic distortion spatial distribution, noticed previously in an experimental study dealing with nonlinear vibrations of a clamped-clamped beam. Numerical results have been obtained showing second and third harmonic amplitude dependent spatial distributions. However, at the present stage, the following comments can be made :

1) As has been shown in the numerical results presented in the previous sections, the second harmonic had a very small contribution. Although this agrees with theoretical results obtained via a model developed in [7.2], based on the partial

differential equation of large vibration amplitudes of beams, the measured second harmonic contribution reported in the above reference remains unexplained. Further investigations dealing with the response problem may clarify this point.

2) Although the amplitude dependence of the beam reponse harmonic distortion has not been mentioned in the above reference or in any of the available papers, this may be due to experimental errors affecting measurements of a very small quantity. However, amplitude dependent third harmonic spatial distribution has been obtained for some plates in [7.8]. Also,the amplitude dependence of the harmonic distortion has been noticed in experimental measurements carried out within the present work on a fully clamped rectangular CFRP plate reported in Chapter IX.

3) As in the Rayleigh-Ritz method, qualitative choice of the basic functions has to be made according to the type of problems considered. Further experimental measurements of the harmonic distortion spatial distribution in the nonlinear response of clamped-clamped beams may decide whether the first, the second, or both theoretically possible combinations of linear mode shapes obtained here is experimentally observable.

CHAPTER VIII

THEORETICAL MODEL FOR NONLINEAR FREE VIBRATION OF FULLY CLAMPED RECTANGULAR PLATES TAKING INTO ACCOUNT THE HARMONIC DISTORTION AT LARGE VIBRATION AMPLITUDES

VIII.1 INTRODUCTION

In this chapter, an attempt is made to apply the theoretical model including spatially distributed harmonic distortion developed for clamped-clamped beams to the case of fully clamped rectangular plates, for which experimental results discussed in Chapter VI have shown that large vibration amplitudes induce a harmonic distortion of the response with a spatial distribution of the second harmonic component similar to the plate second mode shape. In Section VIII.2, the discretisation of the bending strain, axial strain and kinetic energies is carried out, leading to a general form similar to that obtained in the beam case in Chapter VII. In Section VIII.3, numerical results obtained via this model are presented and and a general discussion and conclusion is given in Section VIII.4

VIII.2 DISCRETISATION OF THE BENDING STRAIN, AXIAL STRAIN AND KINETIC ENERGIES IN THE PLATE CASE

Extending the numerical model developed in Chapter VII for large vibration amplitudes of fully clamped beams including a spatial distribution of the harmonic distortion induced by large amplitudes of vibration to the case of fully clamped rectangular plates, and using the definitions and notation given in Chapter V, the transverse displacement function W(x,y,t) is now written as:

$$W(x,y,t) = \{A_1\}^T \{w\} \sin \omega t + \{A_2\}^T \{w\} \sin 2\omega t + \; +$$

$$\{A_q\}^T \{w\} \sin q\omega t + \ldots + \{A_p\}^T \{w\} \sin p\omega t \qquad (8.1)$$

where $\{w(x,y)\}^T = \left[w_1(x,y)\ w_2(x,y) .. \ w_n(x,y)\right]$ is the basic spatial function matrix depending on the vector coordinate (x,y) and $\{A_q\}^T = \left[a_1^q\ a_2^q \ \ldots \ a_n^q\right]$ is the matrix of coefficients of $\{w(x,y)\}$ corresponding to the q^{th} harmonic. In the above expression, n is the number of the spatial functions supposed to contribute to the plate dynamic response

and p is the number of harmonics taken into account. As was explained in the previous chapter, the integer indices qrst and ijkl will be used for the time harmonics and the spatial basic functions respectively. The time variable will be denoted τ to avoid confusion with the integer index t. In reduced notation, equation (8.1) can be written as:

$$W(x,y,\tau) = \{A_q\}^T \{w\} \sin q\omega\tau \tag{8.2}$$

where the repeated integer index q is summed over 1, ..., p.

VIII.2.1 Discretisation of the bending strain energy expression

In this section, the general form obtained by discretisation of the bending strain energy expression, when the displacement function given in equation (8.2) is adopted, is developed for the plate case. The plate notation defined in V is adopted in the remainder of this chapter. Substituting expression (8.1) into equation (5.2) giving the bending strain energy expression for a fully clamped plate leads to:

$$V_b = \frac{1}{2}\int_S D\left[\{A_q\}^T \cdot \left\{\frac{\partial^2 w}{\partial x^2} + \frac{\partial^2 w}{\partial y^2}\right\} \sin q\omega\tau\right]\cdot\left[\{A_r\}^T \cdot \left\{\frac{\partial^2 w}{\partial x^2} + \frac{\partial^2 w}{\partial y^2}\right\}\sin r\omega\tau\right] dS \tag{8.3}$$

where $\left\{\frac{\partial^2 w}{\partial x^2} + \frac{\partial^2 w}{\partial y^2}\right\}^T = \left[\frac{\partial^2 w_1}{\partial x^2} + \frac{\partial^2 w_1}{\partial y^2} \quad \frac{\partial^2 w_2}{\partial x^2} + \frac{\partial^2 w_2}{\partial y^2} \quad \cdots \quad \frac{\partial^2 w_n}{\partial x^2} + \frac{\partial^2 w_n}{\partial y^2}\right]$ is the column matrix of the second derivatives of the functions w_i's. As we have :

$$\{A_q\}^T \cdot \left\{\frac{\partial^2 w}{\partial x^2} + \frac{\partial^2 w}{\partial y^2}\right\} = \left\{\frac{\partial^2 w}{\partial x^2} + \frac{\partial^2 w}{\partial y^2}\right\}^T \{Ar\} \tag{8.4}$$

After transformation, equation (8.3) can be written as :

$$V_b = \frac{1}{2}\{A_q\}^T \left\{\int_S D \left\{\left\{\frac{\partial^2 w}{\partial x^2} + \frac{\partial^2 w}{\partial y^2}\right\} \cdot \left\{\frac{\partial^2 w}{\partial x^2} + \frac{\partial^2 w}{\partial y^2}\right\}^T\right\} dS\right\} \{A_r\} \sin q\omega\tau \sin r\omega\tau \tag{8.5}$$

The integral term is identical to the rigidity matrix of the structure considered. So, equation (8.5) can be written as :

$$V_b = \frac{1}{2} \{A_q\}^T [K] \{A_r\} \sin q\omega\tau \sin r\omega\tau \qquad (8.6)$$

q and r are summed over 1, ..., p.

VIII.2.2 Discretisation of the axial strain energy expression

Substituting expression (8.2) into equation (5.3) giving the expression of the axial strain energy leads to:

$$V_a = \frac{3D}{2H^2} \cdot$$

$$\int_S \left[\{A_q\}^T \left\{\frac{\partial w}{\partial x}\right\} \sin q\omega\tau \{A_r\}^T \left\{\frac{\partial w}{\partial x}\right\} \sin r\omega\tau + \{A_q\}^T \left\{\frac{\partial w}{\partial y}\right\} \sin q\omega\tau \{A_r\}^T \left\{\frac{\partial w}{\partial y}\right\} \sin r\omega\tau \right]$$

$$\left[\{A_s\}^T \left\{\frac{\partial w}{\partial x}\right\} \sin s\omega\tau \{A_t\}^T \left\{\frac{\partial w}{\partial x}\right\} \sin t\omega\tau + \{A_s\}^T \left\{\frac{\partial w}{\partial y}\right\} \sin s\omega\tau \{A_t\}^T \left\{\frac{\partial w}{\partial y}\right\} \sin t\omega\tau \right] dS \qquad (8.7)$$

where $\left\{\frac{\partial w}{\partial x}\right\}^T = \left[\frac{\partial w_1}{\partial x} \frac{\partial w_2}{\partial x} \quad \frac{\partial w_n}{\partial x}\right]$ is the matrix of the first derivatives of the functions w_i's.

Using a transformation similar to that of equation (8.4), the above equation can be written as :

$$V_a = \frac{3D}{2H^2} \cdot$$

$$\int_S \left[\{A_q\}^T \left\{ \left\{\frac{\partial w}{\partial x}\right\} \left\{\frac{\partial w}{\partial x}\right\}^T \right\} \{A_r\} + \{A_q\}^T \left\{ \left\{\frac{\partial w}{\partial y}\right\} \left\{\frac{\partial w}{\partial y}\right\}^T \right\} \{A_r\} \right] \sin q\omega\tau . \sin r\omega\tau$$

$$\left[\{A_s\}^T\left\{\left\{\frac{\partial w}{\partial x}\right\}\left\{\frac{\partial w}{\partial x}\right\}^T\right\}\{A_t\}+\{A_s\}^T\left\{\left\{\frac{\partial w}{\partial y}\right\}\left\{\frac{\partial w}{\partial y}\right\}^T\right\}\{A_t\}\right]\sin s\omega\tau.\sin t\omega\tau dS \quad (8.8)$$

This expression is expanded in tensorial form in Section VIII.2.4

VIII.2.3 Discretisation of the kinetic energy expression.

Substituting expression (8.1) into equation (5.4) giving the kinetic strain energy expression for a plate fully clamped leads to:

$$T=\frac{1}{2}\int_S \rho H q r \omega^2 \left[\{A_q\}^T . \{w\}\cos q\omega t\right].\left[\{A_r\}^T\{w\}\cos q\omega t\right]dS \quad (8.9)$$

As detailed above in equations (8.3) to (8.5), equation (8.9) can be written as :

$$T=\frac{1}{2}qr\omega^2\{A_q\}^T\left\{\int_S \rho H\left\{\{w\}.\{w\}^T\right\}dS\right\}\{A_r\}^T\cos q\omega\tau\cos r\omega\tau \quad (8.10)$$

The integral term is identical to the plate mass matrix of the structure considered. So, equation (8.10) can be written as

$$T=\frac{1}{2}\omega^2\{A_q\}^T[M]_{qr}\{A_r\}\cos q\omega t\cos r\omega t \quad (8.11)$$

where $[M]_{qr}$ is the generalised qr mass matrix corresponding to the coupling between the q^{th} and r^{th} time harmonics and is given by:

$$[M]_{qr}=qr\,.\,[M] \quad (8.12)$$

where [M] is the usual mass matrix.

VIII.2.4 General expressions for the bending strain, axial strain and kinetic energies for fully clamped rectangular plates.

Reintroducing the tensors k_{ij}, b_{ijkl} and m_{ij} defined in Chapter V for a plate, the bending strain energy, the axial strain energy and the kinetic energy expressions given in equations (8.6), (8.8) and (8.10) can be written in the following general form:

$$V_b = a_i^q \, a_j^r \, k^{ij} \, . \sin q\omega\tau \sin r\omega\tau \tag{8.13}$$

$$V_a = a_i^q \, a_j^r \, a_k^s \, a_l^t \, b^{ijkl} \sin q\omega\tau \sin r\omega\tau \sin s\omega\tau \sin t\omega\tau \tag{8.14}$$

$$T = \omega^2 \, a_i^q \, a_j^r \, m^{ij} \, \omega^2 \cos q\omega t \cos r\omega t \tag{8.15}$$

in which the indices i, j, k, and l are summed over 1 to n and the indices q, r, s and t are summed over 1 to p. Expressions (8.13) to (8.15) are identical to that obtained in Chapter VII in the beam case, therefore, the frequency equation established in the previous chapter can be applied to the plate case, leading to a set of nonlinear algebraic equations identical to (7.32) in which the tensors k_{ij}, b_{ijkl} and m_{ij} are given by their expressions established in chapter V.

VIII.3 NON-DIMENSIONAL FORMULATION AND NUMERICAL DETAILS

The non-dimensional formulation of the present problem was made as in Chapter V, leading to the introduction of the non-dimensional tensors m^*_{ij} , k^*_{ij} , b^*_{ijkl} and ω^* and to a set of nonlinear algebraic equations identical to equations (7.32) in which the dimensional parameters are replaced by the non-dimensional ones mentioned above. The tensors α_{qr}, β_{qr}, γ_{qrst} defined by equations (7.19) to (7.21) have been calculated numerically using the trigonometric relations established in appendix F, presented in the previous chapter. The tensors m^*_{ij} , k^*_{ij} and b^*_{ijkl} were calculated using the Fortran routine PREPP, listed in Appendix C. The library routine NS01A presented in the previous chapters was used to solve the set of nonlinear algebraic equations (7.32). A routine called CALFUNPH was written for calculating the residuals, necessary for NS01A at each iteration,for the present formulation.

VIII.3.1 Numerical solutions

Calculations have been made for a fully clamped rectangular plate with an aspect ratio of 0.6. The first nine plate functions obtained as products of the first three linear clamped-clamped beam functions in the two directions of the plate have been used as basic spatial functions. This was done to allow contributions of both symmetric and antisymmetric functions in both directions. The number of time harmonics was restricted to three due to the numerical complexity of the treatment of high numbers of nonlinear

algebraic equations. As explained in Section VII.4.3, the first harmonic spatial distribution and the corresponding frequency were chosen as one of the solutions obtained from the theory discussed in Chapter V. The second and third harmonic spatial distributions were calculated by solving the corresponding 18 nonlinear algebraic equations. A summary of numerical solutions obtained for various amplitudes of vibration is given in Table 8 in which only the contribution coefficients of the third harmonic are given, since the contribution coefficients obtained for the second harmonic spatial distribution were very small (in all cases lower than 10^{-12}) . The third harmonic spatial distribution appears as an amplitude dependent combination of modes. In all cases, the preponderant coefficients were those of plate functions obtained as products of symmetric clamped-clamped beam mode shapes in both directions.

VIII.4 CONCLUSIONS

A theoretical model has been developed for the analysis of harmonic distortion spatial distribution induced by large vibration amplitudes of fully clamped rectangular plates. The numerical treatment was restricted to a limited number of functions due to the long computation times necessary in the iterative process of solution of a high number of nonlinear algebraic equations involving many second and fourth order tensors. The numerical solution obtained from solution of 18 nonlinear algebraic equations allows the following remarks to be made:

1) The second harmonic contribution to the free response was very small, compared with that obtained experimentally in Chapter VI from forced response analysis. This result is, however, similar to that obtained by the present model and in a previous study, based on a different analytical approach, for the beam case, as discussed in Chapter VII.

2) An interaction was shown to be possible between the first and higher symmetric-symmetric modes, leading to an amplitude dependent third harmonic spatial distribution. This result is similar to that obtained in [5.23] by the finite element method for the free response of a simply supported plate.

On the other hand, it should be noticed that no phase lag between the first and higher harmonics was assumed in the present simplified model. Further investigations may be carried out assuming a displacement function of the form:

$$W(x,y,\tau) = \{A_q\}^T \{w\} \sin(q\omega\tau + \phi_q)$$

This is likely to lead to more general results, since the exchange of energy between V_a, V_b and T would depend on the ϕ_q, as can be seen in the equations obtained from (8.13) to (8.15) in which phase terms are added.

CHAPTER IX

THEORETICAL MODEL FOR NONLINEAR NATURAL FREQUENCIES AND MODE SHAPES OF FULLY CLAMPED RECTANGULAR CFRP PLATES

IX.1 INTRODUCTION

As stated in the Introduction, composite materials such as these made of carbon fibre reinforced plastics CFRP, are being widely used for replacing classical materials, not only in aerospace, which has been their most important application, but in many other areas [9.1], because of their advantage of high stiffness,high strength and weight saving. However, previous experimental studies have shown that CFRP beams and plates exhibit a more accentuated nonlinear behaviour at large amplitudes of vibration than these made of isoptropic materials [9.2,9.3]. An increase of 100% in the first resonance frequency of a thin plate with increasing the acoustic excitation level from 130 dB to 154 dB is reported in [9.2], while the corresponding increase for an aluminium alloy plate was 35%. The purpose of the work reported in this Chapter was to apply the analytical and numerical techniques developed in the previous Chapters in order to examine that effect. In Section IX.2, the constitutive equation of a laminated plate at large amplitudes of vibration is established as follows: using the nonlinear strain-displacement equation from classical plate theory and the stress-strain relation for each lamina, the stresses in each lamina were expressed as a function of the plate middle plane displacements and the lamina extensional, coupling and bending stiffnesses. Then, by integrating the above stress-displacement relationships through the whole thickness of a laminate, the constitutive equation of laminated plates at large deflections was obtained. In Section IX.3, the axial strain energy due to large deflection amplitudes is expressed and the bending strain energy expression is obtained. In Section IX.4, the discretisation of the above expressions is made using a harmonic time function and an expansion in the form of a finite series for the spatial function. It is shown that the axial strain energy expression for laminated plates still leads to a fourth order tensor b_{ijkl} whose general expression is given and compared with the isotropic case and with some special laminated plates. In all cases, the theory developed in Chapter II appeared to be applicable for analysing the effects of large vibration amplitudes on the mode shapes and natural frequencies of laminated plates. In Section IX.5, details are given concerning the non-dimensional formulation and numerical treatment of this problem. Then, a solution obtained from nonlinear analysis for a particular plate lay-up and stiffnesses and small vibration amplitudes is given and compared with The Engineering

Science data unit (ESDU) published solution obtained from a linear analysis. In Section IX.6, solutions obtained for large vibration amplitudes for the plate tested in the present work are presented and discussed.

IX.2 CONSTITUTIVE EQUATION OF A LAMINATED ISTOTROPIC PLATE AT LARGE DEFLECTIONS

IX.2.1 Strain-displacement relationships at large deflections

Consider the transverse vibration of the plate shown in Figure 9.1 of dimensions a, b and h with a coordinate system taken such that xy-plane coincides with the midplane of the plate. The thickness coordinate z is measured downward from the midplane. Considering the classical plate theory, the displacements are [9.4]:

$$\overline{\overline{U}} = U - z\frac{\partial W}{\partial x} \qquad \overline{\overline{V}} = V - z\frac{\partial W}{\partial x} \qquad \overline{W} = W \tag{9.1}$$

where $\overline{\overline{U}}$, $\overline{\overline{V}}$ and $\overline{W}$ are total displacements, and U, V and W are displacements of the midplane. In the thin plate theory, the strain-displacements relation for large deflections are given by:

$$\varepsilon_x = \frac{\partial U}{\partial x} + \frac{1}{2}\left(\frac{\partial W}{\partial x}\right)^2 - z\left(\frac{\partial^2 W}{\partial x^2}\right) \tag{9.2}$$

$$\varepsilon_y = \frac{\partial V}{\partial y} + \frac{1}{2}\left(\frac{\partial W}{\partial y}\right)^2 - z\left(\frac{\partial^2 W}{\partial y^2}\right) \tag{9.3}$$

$$\gamma_{xy} = \frac{\partial U}{\partial y} + \frac{\partial V}{\partial x} + \frac{\partial W}{\partial x}\cdot\frac{\partial W}{\partial y} - 2z\frac{\partial^2 W}{\partial xy} \tag{9.4}$$

in which the terms depending on z are due to the bending of the plate and the remaining terms are due to the tension in the middle plane of the plate [9.5]. Using matrix notation, equations (9.2) to (9.4) can be written as:

$$\begin{bmatrix} \varepsilon_x \\ \varepsilon_y \\ \gamma_{xy} \end{bmatrix} = \begin{bmatrix} \frac{\partial U}{\partial x} \\ \frac{\partial V}{\partial y} \\ \frac{\partial U}{\partial x} + \frac{\partial V}{\partial y} \end{bmatrix} + z \begin{bmatrix} -\frac{\partial^2 W}{\partial x^2} \\ -\frac{\partial^2 W}{\partial y^2} \\ -2\frac{\partial^2 W}{\partial xy} \end{bmatrix} + \begin{bmatrix} \frac{1}{2}(\frac{\partial W}{\partial x})^2 \\ \frac{1}{2}(\frac{\partial W}{\partial x})^2 \\ \frac{\partial W}{\partial x}\frac{\partial W}{\partial y} \end{bmatrix} \qquad (9.5)$$

Put :

$$\{\varepsilon^o\} = \begin{bmatrix} \varepsilon_X^0 \\ \varepsilon_Y^0 \\ \gamma_{XY}^0 \end{bmatrix} = \begin{bmatrix} \frac{\partial U}{\partial x} \\ \frac{\partial V}{\partial y} \\ \frac{\partial U}{\partial x} + \frac{\partial V}{\partial y} \end{bmatrix} \qquad (9.6)$$

$$\{\kappa\} = \begin{bmatrix} \kappa_x \\ \kappa_y \\ \kappa_{xy} \end{bmatrix} = \begin{bmatrix} -\frac{\partial^2 W}{\partial x^2} \\ -\frac{\partial^2 W}{\partial y^2} \\ -2\frac{\partial^2 W}{\partial xy} \end{bmatrix} \qquad (9.7)$$

$$\{\lambda^0\} = \begin{bmatrix} \lambda_x^0 \\ \lambda_y^0 \\ \lambda_{xy}^0 \end{bmatrix} = \begin{bmatrix} \frac{1}{2}(\frac{\partial W}{\partial x})^2 \\ \frac{1}{2}(\frac{\partial W}{\partial x})^2 \\ \frac{\partial W}{\partial x}\frac{\partial W}{\partial y} \end{bmatrix} \qquad (9.8)$$

Equation (9.5) can be written as :

$$\begin{bmatrix} \varepsilon_x \\ \varepsilon_y \\ \gamma_{xy} \end{bmatrix} = \begin{bmatrix} \varepsilon_X^0 \\ \varepsilon_Y^0 \\ \gamma_{XY}^0 \end{bmatrix} + z \begin{bmatrix} \kappa_x \\ \kappa_y \\ \kappa_{xy} \end{bmatrix} + \begin{bmatrix} 0 \\ \lambda_X \\ 0 \\ \lambda_y \\ 0 \\ \lambda_{xy} \end{bmatrix} \qquad (9.9)$$

or in a more contracted form :

$$\{\varepsilon\} = \{\varepsilon^0\} + z\{\kappa\} + \{\overset{0}{\lambda}\} \qquad (9.10)$$

where the middle surface strain term appears as the sum of the linear term $\{\varepsilon^0\}$ and the nonlinear term due to large deflections $\{\lambda^0\}$.

IX.2.2 Stress-strain relationships at large deflections for the k^{th} lamina

Consider a laminated plate having n layers, as shown in Figure 9.1, oriented about a reference plane such that the distance of the outer surface of the k^{th} layer is h_k and the inner surface is h_{k-1} from the reference surface. The stress-strain relationship through the thickness for such a laminate can be obtained as follows: By substitution of the strain variation through the thickness of the lamina , Equation (9.5), in the strain stress relation for a given lamina, say the k^{th} laminae, established in [9.6], the stress in the k^{th} layer can be expressed in terms of the laminate middle surface strain and curvatures as :

$$\begin{bmatrix}\sigma_x\\ \sigma_y\\ \tau_{xy}\end{bmatrix}_k = \begin{bmatrix}\overline{Q_{11}}\,\overline{Q_{12}}\,\overline{Q_{16}}\\ \overline{Q_{12}}\,\overline{Q_{22}}\,\overline{Q_{26}}\\ \overline{Q_{16}}\,\overline{Q_{26}}\,\overline{Q_{66}}\end{bmatrix}_k \cdot \left\{ \begin{bmatrix}\varepsilon_x^0\\ \varepsilon_y^0\\ \gamma_{xy}^0\end{bmatrix} + z\begin{bmatrix}\kappa_x\\ \kappa_y\\ \kappa_{xy}\end{bmatrix} + \begin{bmatrix}\overset{0}{\lambda_x}\\ \overset{0}{\lambda_y}\\ \overset{0}{\lambda_{xy}}\end{bmatrix} \right\} \qquad (9.11)$$

in which terms of matrix $\left[\overline{Q}\right]$ can be obtained by the relationships given in [9.6], as a function of the k^{th} layer fibre orientation and the reference lamina mechanical characteristics; the reference lamina being a lamina for which the principle material axes are aligned with the natural body axes of the problem. z vary through the range $[h_k, h_{k-1}]$.

IX.2.3 Resultant forces and moments through the k^{th} lamina

The force and moment resultant for the k^{th} layer are obtained by integrating the inplane stresses over the layer thickness, which leads to :

$$N_x^{(k)} = \int_{h_{k-1}}^{h_k} \sigma_x^{(k)} \, dz \tag{9.12}$$

$$N_y^{(k)} = \int_{h_{k-1}}^{h_k} \sigma_y^{(k)} \, dz \tag{9.13}$$

$$N_{xy}^{(k)} = \int_{h_{k-1}}^{h_k} \sigma_{xy}^{(k)} \, dz \tag{9.14}$$

$$M_x^{(k)} = \int_{h_{k-1}}^{h_k} \sigma_x^{(k)} \, z \, dz \tag{9.15}$$

$$M_y^{(k)} = \int_{h_{k-1}}^{h_k} \sigma_y^{(k)} \, z \, dz \tag{9.16}$$

$$M_{xy}^{(k)} = \int_{h_{k-1}}^{h_k} \sigma_{xy}^{(k)} \, z \, dz \tag{9.17}$$

by substituting equation (9.11) into equations (9.12) to (9.17), we obtain the resultant forces and the moments in the lamina :

$$\{N\}_k = [A]_k \left[\{\varepsilon^o\} + \{\lambda^0\}\right] + [B]_k \{\kappa\} \tag{9.19}$$

$$\{M\}_k = [B]_k \left[\{\varepsilon^o\} + \{\lambda^0\}\right] + [D]_k \{\kappa\} \tag{9.20}$$

where $\{N\}_k^T = [N_x \; N_y \; N_{xy}]$ and $\{M\}_k^T = [M_x \; M_y \; M_{xy}]$ are the resultant forces and moments vectors, respectively, and :

$$A_{ij.k} = \overline{Q_{ij.k}} \cdot (h_k - h_{k-1}) \tag{9.21}$$

$$B_{ij.k} = \frac{1}{2}\overline{Q_{ij.k}} \cdot (h_k^2 - h_{k-1}^2) \tag{9.22}$$

$$D_{ij.k} = \frac{1}{3}\overline{Q_{ij.k}} \cdot (h_k^3 - h_{k-1}^3) \tag{9.23}$$

In the small displacements theory, $A_{ij.k}$, $B_{ij.k}$ and $D_{ij.k}$ are the so called extensional stiffness coefficients, coupling stiffness coefficients and bending stiffness coefficients corresponding to the k^{th} layer. However, because of the presence of the term $\{\lambda^0\}$ due to large deflections in equations (9.19) and (9.20), there is coupling in the nonlinear case between bending and extension even in the cases in which the classical coupling stiffness coefficients B_{ij} vanish. Thus the constitutive equation of large amplitudes of vibration of the k^{th} lamina in a laminated anisotropic plate may be written in matrix form as :

$$\begin{bmatrix} N \\ \\ M \end{bmatrix}_k = \begin{bmatrix} [\overline{A}] & [\overline{B}] \\ \\ [\overline{B}] & [\overline{D}] \end{bmatrix}_k \cdot \begin{bmatrix} \{\varepsilon^0\} + \{\lambda^0\} \\ \\ \{\kappa\} \end{bmatrix} \tag{9.24}$$

IX.2.4 Resultant forces and moments through the laminated plate

The inplane forces and bending moments resultant in a plate are obtained by integrating the inplane stresses over the plate thickness. In the case of a layered plate, this leads to a summation over the layers, which gives from equation (9.24) :

$$\begin{bmatrix} N \\ \\ M \end{bmatrix} = \begin{bmatrix} [A] & [B] \\ \\ [B] & [D] \end{bmatrix} \cdot \begin{bmatrix} \{\varepsilon^0\} + \{\lambda^0\} \\ \\ \{\kappa\} \end{bmatrix} \tag{9.25}$$

in which matrices [A], [B] and [D] are given by their general term :

$$A_{ij} = (\overline{Q_{ij}})_k \cdot (h_k - h_{k-1}) \tag{9.26}$$

$$B_{ij} = \frac{1}{2}(\overline{Q_{ij}})_k \cdot (h_k^2 - h_{k-1}^2) \tag{9.27}$$

$$D_{ij} = \frac{1}{3}(\overline{Q_{ij}})_k \cdot (h_k^3 - h_{k-1}^3) \qquad (9.28)$$

where the repeated index k is summed over the layers number n.

IX.3 BENDING STRAIN, AXIAL STRAIN AND KINETIC STRAIN ENERGY EXPRESSIONS FOR LAMINATED PLATES AT LARGE VIBRATION AMPLITUDES

IX.3.1 Bending strain energy expression for laminated plates

The strain energy due to the bending of a plate can be obtained as :

$$V_b = \frac{1}{2}\int_S \{M\}^T\{\kappa\}dS \qquad (9.29)$$

where S is the plate surface [0,a] × [0,b] and dS the elementary surface dxdy. For symmetrical laminates, *i.e.* laminates that are symmetric in both geometry and material properties about the middle surface, all the coupling stiffnesses, *i.e.* Bij can be shown to be zero (since B_{ij} is an even function of the z-coordinate) . Hence [B] = 0 and from Equation (9.25) :

$$\{M\} = [D].\{\kappa\} \qquad (9.30)$$

Substitution of equations (9.7) and (9.30) into (9.29) leads to the bending strain energy expression for a laminated plate [9.7]:

$$V_b = \frac{1}{2}\int_S \left\{ D_{11}\left(\frac{\partial^2 W}{\partial x^2}\right)^2 + 2D_{12}\frac{\partial^2 W \partial^2 W}{\partial y^2\, \partial x^2} + D_{22}\left(\frac{\partial^2 W}{\partial y^2}\right)^2 + 4D_{16}\frac{\partial^2 W \partial^2 W}{\partial x^2\, \partial xy} + 4D_{26}\frac{\partial^2 W \partial^2 W}{\partial y^2\, \partial xy} + 4D_{66}\left(\frac{\partial^2 W}{\partial xy}\right)^2 \right\} dS \qquad (9.31)$$

IX.3.2 Kinetic strain energy expression

The kinetic energy of the plate when neglecting the axial inertial terms and the rotary inertia terms is :

$$T = \frac{1}{2}\rho H \int_S \left(\frac{\partial W}{\partial t}\right)^2 dxdy \qquad (9.32)$$

IX.3.3 Axial strain energy expression for laminated plates at large vibration amplitudes

The potential energy of the plate under the action of inplane loading is given by [9.8]:

$$V_a = \frac{1}{2}\int_S \left(N_x \overset{0}{\lambda_x} + N_y \overset{0}{\lambda_y} + N_{xy} \overset{0}{\lambda_{xy}}\right) dxdy \qquad (9.33)$$

Substituting the strains $\overset{0}{\lambda_x}$, $\overset{0}{\lambda_y}$ and $\overset{0}{\lambda_{xy}}$ from equation (9.8) into equation (9.33), we obtain the potential energy due to the inplane loads induced by large transverse vibrations:

$$V_a = \frac{1}{2}\int_S \left\{N_x \left(\frac{\partial W}{\partial x}\right)^2 + N_y \left(\frac{\partial W}{\partial y}\right)^2 + 2 N_{xy} \left(\frac{\partial W}{\partial x}\frac{\partial W}{\partial y}\right)\right\} dxdy \qquad (9.34)$$

Now, in order to obtain the expression for V_a depending only on the transverse displacement W , the stress resultants N_x, N_y and N_{xy} have to be expressed as a function of W via equation (9.25). The term $\{\varepsilon^o\}$ being neglected as in the isotropic case discussed in Chapter V, this leads to :

$$[N] = [A]\{\lambda^o\} + [B]\{\kappa\} \qquad (9.35)$$

As stated above, for symmetrically laminated plates, $B_{ij} = 0$. Thus, by putting [B] = 0 in equation (8.35) and substituting the resulting equation in equation (9.34), we obtain:

$$V_a = \frac{1}{2}\int_S \left\{ \frac{A_{11}}{4}\left(\frac{\partial w}{\partial x}\right)^4 + \frac{A_{22}}{4}\left(\frac{\partial w}{\partial y}\right)^4 \right.$$

$$\left. + \left[\frac{A_{12}}{2} + A_{66}\right]\left(\frac{\partial w}{\partial y}\right)^2\left(\frac{\partial w}{\partial x}\right)^2 + A_{16}\left(\frac{\partial w}{\partial x}\right)^3\frac{\partial w}{\partial y} + A_{26}\frac{\partial w}{\partial y}\left(\frac{\partial w}{\partial y}\right)^3 \right\} dS \qquad (9.36)$$

It should be noticed that the axial strain energy expression for laminated plates given above differs from that of isotropic plates given in equation (5.2) by the presence in the former of the terms $\left(\frac{\partial w}{\partial x}\right)^3\frac{\partial w}{\partial y}$ and $\frac{\partial w}{\partial y}\left(\frac{\partial w}{\partial y}\right)^3$ and the influence of different coefficients for each term. However, as will be shown in the next section, the nonlinearity will still appear in the numerical model via a fourth order tensor b_{ijkl} although its expression will contain in the general anisotropic case more terms and higher derivatives than in the homogeneous case.

IX.4 DISCRETISATION OF THE BENDING STRAIN, AXIAL STRAIN AND KINETIC ENERGY EXPRESSIONS IN THE CFRP PLATE CASE

If the time and space functions are supposed to be separated and harmonic motion is assumed, the transverse displacement can be written as:

$$W(x,t) = w(x) \sin \omega t \qquad (9.37)$$

where x is the vector coordinate i.e. $\bar{x} = (x,y)$, Expanding w(x,y) in the form of a finite series :

$$w(x,y) = a_i w_i(x,y) \qquad (9.38)$$

in which the usual summation convention defined in Chapter II is used, discretisation of the strain and kinetic energy expressions can be carried out leading to the expressions for the tensors k_{ij}, m_{ij}, b_{ijkl} given in the following sections.

IX.4.1 Discretisation of the bending strain energy expression

By using the tensor notation, substituting equation (9.37) into (9.38) and then into equation (9.31) and rearranging leads to :

$$V_b = \frac{1}{2} a_i a_j k_{ij} \sin^2 \omega t \qquad (9.39)$$

where k_{ij} is given by :

$$k_{ij} = \frac{1}{2} \int_S \left\{ D_{11} \frac{\partial^2 w_i}{\partial x^2} \frac{\partial^2 w_j}{\partial x^2} + D_{22} \frac{\partial^2 w_i}{\partial y^2} \frac{\partial^2 w_j}{\partial y^2} + D_{12} \left[\frac{\partial^2 w_i}{\partial x^2} \frac{\partial^2 w_j}{\partial y^2} + \frac{\partial^2 w_i}{\partial y^2} \frac{\partial^2 w_j}{\partial x^2} \right] \right.$$
$$\left. + 2D_{16} \left[\frac{\partial^2 w_i}{\partial x^2} \frac{\partial^2 w_j}{\partial xy} + \frac{\partial^2 w_i}{\partial xy} \frac{\partial^2 w_j}{\partial x^2} \right] + 2D_{26} \left[\frac{\partial^2 w_i}{\partial y^2} \frac{\partial^2 w_j}{\partial xy} + \frac{\partial^2 w_i}{\partial xy} \frac{\partial^2 w_j}{\partial y^2} \right] + 4D_{66} \frac{\partial^2 w_i}{\partial xy} \frac{\partial^2 w_j}{\partial xy} \right\} dS \qquad (9.40)$$

In the terms between brackets in the above expression, pairs of terms obtained by interchanging i and j were used instead of one term. This was done in order to make the k_{ij} tensor symmetric, as required by the general theory presented in Chapter II, without changing the sum $\frac{1}{2} a_i a_j k_{ij}$ coresponding to V_b.

IX.4.2 Discretisation of the axial strain energy expression

Using the tensor notation, substituting equation (9.37) into equation (9.38) and then into (9.36) and rearranging leads to :

$$V_a = \frac{1}{2} a_i a_j a_k a_l b_{ijkl} \sin^4 \omega t \qquad (9.41)$$

where b_{ijkl} is given by :

$$b_{ijkl} = \frac{1}{2}\int_S \left\{ \frac{A_{11}}{4}\left[\frac{\partial w_i}{\partial x}\frac{\partial w_j}{\partial x}\frac{\partial w_k}{\partial x}\frac{\partial w_l}{\partial x}\right] + \frac{A_{22}}{4}\left[\frac{\partial w_i}{\partial y}\frac{\partial w_j}{\partial y}\frac{\partial w_k}{\partial y}\frac{\partial w_l}{\partial y}\right] \right.$$

$$+\left[\frac{A_{12}}{4}+\frac{A_{66}}{2}\right]\left\{\left[\frac{\partial w_i \partial w_j}{\partial x\,\partial x}\cdot\frac{\partial w_k \partial w_l}{\partial y\,\partial y}\right]+\left[\frac{\partial w_i \partial w_j}{\partial y\,\partial y}\cdot\frac{\partial w_k \partial w_l}{\partial x\,\partial x}\right]\right\}$$

$$+\frac{A_{16}}{2}\left\{\left[\frac{\partial w_i}{\partial x}\frac{\partial w_j}{\partial x}\frac{\partial w_k}{\partial x}\frac{\partial w_l}{\partial y}\right]+\left[\frac{\partial w_i}{\partial x}\frac{\partial w_j}{\partial x}\frac{\partial w_k}{\partial y}\frac{\partial w_l}{\partial x}\right]\right\}$$

$$\left.+\frac{A_{26}}{2}\left\{\left[\frac{\partial w_i}{\partial x}\frac{\partial w_j}{\partial y}\frac{\partial w_k}{\partial y}\frac{\partial w_l}{\partial y}\right]+\left[\frac{\partial w_i}{\partial y}\frac{\partial w_j}{\partial x}\frac{\partial w_k}{\partial y}\frac{\partial w_l}{\partial y}\right]\right\}\right\} dS \qquad (9.42)$$

As mentioned above for k_{ij}, some terms have been written twice, with interchanging i and j, in order to obtain a bijkl tensor fulfilling the symmetry requirements assumed in equations (2.13) and (2.14), which does not change the sum $\frac{1}{2}a_i a_j a_k a_l b_{ijkl}$ giving V_a

IX.4.3 Discretisation of the kinetic energy expression

Using the tensor notation, substituting equation (9.37) into equation (9.38) and then into (9.32) and rearranging leads to :

$$T = \frac{1}{2}a_i a_j m_{ij} \sin^2\omega t \qquad (9.43)$$

where m_{ij} is given by an expression identical to that given in equation (5.20).

IX.5 NON-DIMENSIONAL FORMULATION

In order to formulate the vibration problem of fully clamped rectangular CFRP plates corresponding to large deflections in non-dimensional terms, the non-dimensional functions defined in equation (5.21) and the non-dimensional aspect ratio $\alpha = \frac{b}{a}$ were used. As the numerical treatment of the set of nonlinear algebraic equations to be solved is sensitive to the order of magnitude of the terms involved, since either overflows or underflows can appear when calculating the inverse of the Jacobian matrix used in Newton's method or in

calculating residuals, it was necessary to set the axial and bending stiffnesses A_{ij} and B_{ij} to a reasonable order of magnitude by putting:

$$A^*_{ij} = \frac{A^*_{ij}}{HE} \tag{9.44}$$

$$D^*_{ij} = \frac{D^*_{ij}}{H^3E} \tag{9.45}$$

where H is the plate thickness and E is a reference Young's modulus, whose numerical value was taken as 7E 10^{10} N/m, which is a typical value for aluminium alloys. Using the non-dimensional parameters as defined above, the non-dimensional tensors k^*_{ij}, b^*_{ijkl} and m^*_{ij} can be obtained as :

$$k_{ij} = \frac{aH^5E}{b^3}.k^*_{ij} \tag{9.46}$$

$$b_{ijkl} = \frac{aH^5E}{b^3}.b^*_{ijkl} \tag{9.47}$$

$$m_{ij} = \rho\, H^3ab.m^*_{ij} \tag{9.48}$$

where m^*_{ij} is given by equation (5,27). k^*_{ij} and b^*_{ijkl} are given by:

$$k^*_{ij} = \frac{1}{2}\int_S \Bigg\{ D^*_{11}\alpha^4\left[\frac{\partial^2 w^*_i}{\partial x^{*2}}\frac{\partial^2 w^*_j}{\partial x^{*2}}\right] + D^*_{22}\left[\frac{\partial^2 w^*_i}{\partial y^{*2}}\frac{\partial^2 w^*_j}{\partial y^{*2}}\right] + D^*_{12}\alpha^2\left[\frac{\partial^2 w^*_i}{\partial x^{*2}}\frac{\partial^2 w^*_j}{\partial y^{*2}} + \frac{\partial^2 w^*_i}{\partial y^{*2}}\frac{\partial^2 w^*_j}{\partial x^{*2}}\right]$$

$$+ 2D^*_{16}\alpha^3\left[\frac{\partial^2 w^*_i}{\partial x^{*2}}\frac{\partial^2 w^*_j}{\partial x^*y^*} + \frac{\partial^2 w^*_i}{\partial x^*y^*}\frac{\partial^2 w^*_j}{\partial x^{*2}}\right] + 2D^*_{26}\alpha\left[\frac{\partial^2 w^*_i}{\partial y^{*2}}\frac{\partial^2 w^*_j}{\partial x^*y^*} + \frac{\partial^2 w^*_i}{\partial x^*y^*}\frac{\partial^2 w^*_j}{\partial y^{*2}}\right]$$

$$+ 4\,D^*_{66}\alpha^2\left[\frac{\partial^2 w^*_i}{\partial xy}\frac{\partial^2 w^*_j}{\partial xy}\right]\Bigg\}\, dS \tag{9.49}$$

$$b^*_{ijkl} = \frac{1}{2}\int_{S^*}\left\{\frac{A^*_{11}}{4}\alpha^4\left[\frac{\partial w^*_i}{\partial x^*}\frac{\partial w^*_j}{\partial x^*}\frac{\partial w^*_k}{\partial x^*}\frac{\partial w^*_l}{\partial x^*}\right]+\frac{A^*_{22}}{4}\left[\frac{\partial w^*_i}{\partial y^*}\frac{\partial w^*_j}{\partial y^*}\frac{\partial w^*_k}{\partial y^*}\frac{\partial w^*_l}{\partial y^*}\right]\right.$$

$$+\left[\frac{A^*_{12}}{4}+\frac{A^*_{66}}{2}\right]\alpha^2\left\{\left[\frac{\partial w^*_i}{\partial x^*}\frac{\partial w^*_j}{\partial x^*}\cdot\frac{\partial w^*_k}{\partial y^*}\frac{\partial w^*_l}{\partial y^*}\right]+\left[\frac{\partial w^*_i \partial w^*_j}{\partial y^* \partial y^*}\cdot\frac{\partial w^*_k \partial w^*_l}{\partial x^* \partial x^*}\right]\right\}$$

$$+\frac{A^*_{16}}{4}\alpha^3\left\{\left[\frac{\partial w^*_i}{\partial x^*}\frac{\partial w^*_j}{\partial x^*}\frac{\partial w^*_k}{\partial x^*}\frac{\partial w^*_l}{\partial y^*}\right]+\left[\frac{\partial w^*_i}{\partial x^*}\frac{\partial w^*_j}{\partial x^*}\frac{\partial w^*_k}{\partial y^*}\frac{\partial w^*_l}{\partial x^*}\right]\right\}$$

$$\left.+\frac{A^*_{26}}{2}\alpha\left\{\left[\frac{\partial w^*_i}{\partial x^*}\frac{\partial w^*_j}{\partial y^*}\frac{\partial w^*_k}{\partial y^*}\frac{\partial w^*_l}{\partial y^*}\right]+\left[\frac{\partial w^*_i}{\partial y^*}\frac{\partial w^*_j}{\partial x^*}\frac{\partial w^*_k}{\partial y^*}\frac{\partial w^*_l}{\partial y^*}\right]\right\}\right\}dS^* \qquad (9.50)$$

Substituting equations (9.46) to (9.48) in equation (2.20) leads to :

$$\omega^2 = \frac{H^2 E}{\rho b^4}\,\omega^{*2} \qquad (9.51)$$

So, for given fibre and matrix properties, lay-up, layer thicknesses and plate aspect ratio, the D* and A* matrices have to be estimated and put in the routine PREPC, presented below, in order to calculate the parameters k^*_{ij}, b^*_{ijkl} and m^*_{ij} given in the CFRP plate case by equations (9.49) to (9.50) . Then, a set of nonlinear algebraic equations, identical to equations (2.24) established in Chapter II, in which the dimensional parameters are replaced by non-dimensional parameters, has to be solved for each value of the assigned r_0^{th} mode contribution a_{r0} in order to obtain the amplitude dependent r_0^{th} nonlinear CFRP plate mode shape. Worth noticing is the fact that, for some special lay-up cases, simplifications in the b_{ijkl} and k_{ij} expressions can occur. For example, for cases in which [B] = 0 and D16 = D26 = A16 = A26 = 0, such as that of specially orthotropic plates, the above expressions of k^*_{ij} and b^*_{ijkl} can be written in a much simpler form than that given above.

IX.6 FIRST NONLINEAR MODE SHAPE

IX.6.1 Numerical details

To obtain the fundamental nonlinear mode shape of a fully clamped rectangular thin CFRP plate, the first nine basic functions obtained as products of the first three symmetric clamped-clamped beam mode shapes were used, since the analysis of the isotropic case has

shown that the contribution of the non-symmetric functions in either the x or y directions to the first nonlinear mode shape are, as may be expected due to the symmetry of this mode, negligible. So, the first three non-dimensional plate functions defined in Chapter V, and an estimated values for the D^*_{ij} and A^*_{ij} matrices, obtained using the plate lay-up and a single layer properties by a program called Lami [9.9] (ESDU 83035), were used to calculate the tensors k^*_{ij} and b^*_{ijkl} . A Fortran routine, called PREPC, was written for calculating these parameters using a method similar to that detailed in the isotropic case in Chapter V. The routine PREPC is listed in Appendix H. To solve the set of nonlinear algebraic equations,obtained for the nonlinear problem in Chapter II (Equation (2,24)) , the library routine NS01A presented in the previous chapters was used and numerical solutions were obtained for the nonlinear mode shapes and resonance frequencies of laminated plates considered at large vibration amplitudes.

IX.6.2 Comparison between results of nonlinear analysis obtained for small vibration amplitudes and published linear results

In [9.9] (ESDU 83036) a method is presented for calculating the linear mode shapes and resonance frequencies of laminated plates. A Fortran program is also listed and an example of output is given relative to a symmetric laminates with 16 layers, a thickness of 2.72 mm, a density of 1540 kg/m^3 and a lay-up given by [45 0 - 45 45 -45 0 -45 45]$_S$. lay up. The characteristics of this plate were used in the program written here to examine the nonlinear case. The input estimated A and D stiffness matrices used in the nonlinear case and results obtained from solution of the nonlinear algebraic equations for $a_{11} = 0.005$ are given in Appendix I. Good agreement can be noticed between the natural frequency calculated from nonlinear analysis for a value of 0.005 of the assigned contribution a_{11} and the linear natural frequency given in the above reference (A frequency of 792.9 Hz was given in [8.10] for the plate linear frequency and a value of 795.7 was found here for a small displacement amplitude)

IX.6.3 General presentation of numerical results

Numerical results corresponding to the assigned contribution a_{11} varying from 0.05 to 1.05 which corresponds to a maximum amplitude vibration to thickness ratio varying from ($0.05 \times 1.5^2 = 0.11$) to ($1.05 \times 1.5^2 = 2.36$) for a symmetrically laminated plate whose lay-up, geometrical and mechanical characteristics are given in Appendix J are summarised in Tables 9.1 in which a_{ij} represents the contribution of the basic function obtained as product of the i^{th} and j^{th} x and y clamped-clamped basic functions ω^* is the nonlinear non-dimensional frequency parameter defined in equations (5.29) A general trend of increase can be noticed for the contribution coefficients with increasing the assigned

contribution coefficient a_{11} with higher values than these obtained for an isotropic plate having the same aspect ratio, as can be seen from comparison of Tables 5.6 and 9 which indicates a more accentuated deformation of the mode shapes at high amplitudes.

IX.6.4 Amplitude-frequency dependence

The numerical results listed in Table 9 show an increase of the non-dimensional nonlinear frequency parameter with increasing a_{11} which is much higher than that obtained for an isotropic plate of identical aspect ratio. In Figure 9.2, the non-dimensional nonlinear frequency parameter obtained for the CFRP plate considered in Appendix I is compared to that obtained for an isotropic plate. It can be seen that for an amplitude equal to twice the plate thickness, the increase of nonlinear natural frequency for the isotropic plate is somewhat above 50% while the corresponding increase for the C.F.R.P plate is about 100%, which is in qualitative agreement with results obtained in 9.2 for the increase of resonance frequency with increasing acoustic excitation level.

IX.7 CONCLUSIONS

As has been shown in this chapter, the theoretical model presented in Chapter II for nonlinear vibration of thin straight structures can be extended to laminated plates, permitting the calculation of the amplitude dependent fundamental mode shape and the corresponding natural frequencies. As has been stated in the Introduction, the assumption of a single spatial mode is the basis of most of the studies on nonlinear plate vibration. The high dependence on displacement amplitude of the contribution coefficients and the natural frequency obtained here for the CFRP plate considered show how this assumption can be particularly innaccurate for laminated plates. The higher nonlinearity exhibited by composite plates appears to be due to higher inplane stiffnesses, inducing higher contributions of the axial strain energy at large amplitudes to the total strain energy, as can be seen from comparison of the non-dimensional inplane and flexural stiffnesses input in the routine PREPC in Appendix I. This is an unfortunate characteristic of the higher performance of composites which may be remedied by improving the damping qualities of such materials, as discussed in [9.11].

CHAPTER X

CONCLUSIONS AND SUGGESTIONS FOR FURTHER INVESTIGATIONS

As stated in the Introduction, considerable research has taken place in the last few decades on the nonlinear dynamic behaviour of plates at large vibration amplitudes. Due to the analytical and physical complexity of such problems, various methods of approximation and techniques for solution have been proposed. The assumption of a single spatial mode of vibration has been widely used as a starting point of many investigations, with the consequence of reducing the effects of nonlinearity to the amplitude dependence of the resonance frequency. Results obtained in the present work have shown how such an assumption can be inaccurate. The fully clamped rectangular plate fundamental mode shape calculated via the nonlinear theoretical model was clearly displacement amplitude dependent. Also, in spite of the sensitivity of the estimated mode shapes to experimental and numerical errors, an amplitude dependence of the estimated mode shapes from measured data was observed. Similar trends of increase of higher mode contribution coefficients were obtained both theoretically and experimentally at large amplitudes, leading to a nonlinear increase of the hardening spring type of the bending stress at the plate edge with increasing amplitude of vibration. This has a practical consequence that the rate of increase of bending stress with increasing displacement amplitude is higher than that predicted by the linear theory.

Although the finite element method remains the only way for dealing with plates with complicated shapes, previous comparisons relative to linear rectangular plate vibration have shown that the Rayleigh-Ritz method needs much less computational effort. The theoretical model for nonlinear vibration presented in Chapter II was an attempt to extend the Rayleigh-Ritz method to the nonlinear case, which has permitted the treatment of many cases of thin straight structures in a unified manner. To avoid using an incremental procedure, Hamilton's principle was applied in the neighbourhood of a given mode with a given finite displacement and the corresponding nonlinear mode was obtained directly as a solution of the set of nonlinear algebraic equations. Also, by changing the mode considered, various nonlinear mode shapes could be obtained, *i.e.*, the second, third and so on, as has been illustrated in the beam case.

Application of the theoretical model to the case of simply supported beams has led to an amplitude independent nonlinear mode shape, which is an assumption often adopted in the literature, and to nonlinear frequency formulae identical to some results previously obtained

and slightly different to some others. This situation seems to be unavoidable, since the exact solution of such a nonlinear problem is unknown, and may not even exist. However, in spite of the slight differences noted, the general agreement of the formulae obtained here with previous results showed that the change in resonance frequency at large amplitudes is quantitatively related to the increase in the generalised stiffness, due to the contribution to the total strain energy of the axial load induced by large displacements. This contribution term is the only difference beween the expression obtained here for the frequency and that used in the linear theory. Further results obtained in the other cases considered here have confirmed this conclusion.

In a previous study on the nonlinear dynamic behaviour of a clamped-clamped beam, theoretical and experimental investigations have shown that the fundamental mode shape was amplitude dependent, with an increase of curvatures near to the clamps. Solutions obtained from the theoretical model developed within the present work applied to clamped-clamped beams exhibited similar behaviour and a good agreement was found between the calculated nonlinear fundamental mode shape and previous experimental data. This showed that the expansion of the displacement function in terms of linear modes of vibration, which are intrinsic properties of the structure, can still be convenient in the nonlinear case. Numerical results obtained from the present analysis have shown that, as the amplitude of vibration increases, these modes combine in such manner to satisfy general mechanical laws, expressed by Hamilton's principle. The use of such an expansion has provided a quick method for calculating the nonlinear fundamental mode components as solution of a set of five nonlinear algebraic equations for various beam cross section shapes and a wide range of amplitudes of vibration. Such components may be used to obtain directly the first and second derivatives of a mode shape, necessary for estimating the change in bending and axial stresses with increasing amplitude of vibration. Also, the second and third nonlinear mode shapes of clamped-clamped beams were obtained in a similar manner, and exhibited an amplitude dependence with a general trend of increase of curvature near to the clamps and displacements of the nodal points towards the clamps with increasing displacement amplitude. Further experimental investigations dealing with the beam response near to the second and higher modes may confirm such theoretical results. Also, the case of beams with variable cross section can be considered in the theoretical model using the appropriate strain energy expressions.

Since no exact solution is known for the mode shapes and natural frequencies of fully clamped rectangular plates, various methods have been developed previously to obtain approximate solutions. The Rayleigh-Ritz method associated with basic functions obtained

as products of beam mode shapes in the two directions of the plate has led to accurate results in terms of function contribution coefficients to the linear modes of vibration and the corresponding natural frequencies. Numerical results obtained in the present work from solution of 25 nonlinear algebraic equations have shown how the linear solutions obtained for small amplitudes for the mode shape contribution coefficients and the natural frequency estimates deviate from their initial values as the amplitude of vibration increases. A systematic comparison of nonlinear frequency parameters obtained here for displacements up to 1.5 times the plate thickness and aspect ratios of 1 and 0.5 with all previous available results obtained by various methods has shown a reasonable agreement. Numerical results given here for high amplitudes and lower plate aspect ratios must be considered with some reservation until further investigations determine accurately how other nonlinear effects, such as high inplane displacements or change of material behaviour from elastic to plastic may affect the results. Although consideration of such effects exceeded the scope of the present work, it is thought that extension of the present theory to include the first effect may be made using adequate inplane displacement functions and taking into account their contribution to the total strain energy. Solutions obtained from such a formulation may determine accurately the contribution of the inplane displacements to the axial stresses and contribute to clarification of the question of the domain of validity of the Berger approximation, which has been a subject of much discussion in the literature. Also, higher nonlinear modes of fully clamped rectangular plates may be considered, by solving in each case the appropriate set of nonlinear algebraic equation.

Many aspects of the experimental work have been discussed in the conclusion of Chapter VI. Generally, good qualitative agreement was found between the trends of mode shape and resonance frequency amplitude dependence which were obtained theoretically and experimentally. However, a significant difference was noticed between estimated and theoretical bending stresses. This seems to be related to the effects of the boundary conditions, as has been discussed in the literature. Further investigations, dealing with nonlinear behaviour of plates with elastic constraints at the edge may lead to a more realistic representation of the boundary conditions. The investigation of the second harmonic spatial distribution has shown that the second mode can be excited, due to the nonlinearity, even if the excitation frequency is close to the fundamental mode and the excitation force is applied in a nodal point of the second mode. This shows how the nonlinear behaviour can be different from that represented by linear theory. Consideration of the amplitude dependence of the spatial distribution of harmonic distortion and various aspect ratios may reveal other aspects of this problem. As the quantities involved in the second and higher harmonics are very small for isotropic plates, the use of CFRP plates in such investigations may lead to a

better qualitative understanding of the problem, since nonlinear effects are much more accentuated for this type of plates, as has been shown in the present work.

The theoretical model for nonlinear vibrations of beams and plates including a modal expansion of the harmonic distortion has led to numerical results showing a possible interaction between the first and third harmonics, leading to an amplitude dependent third component spatial distribution. However, in contrast with experimental results, no significant contribution of the second harmonic was found in both cases. This may be due to a possible qualitative difference in the nonlinear behaviour of the free response considered in the theory and the measured forced response. Further investigation, dealing with the problem of the response at high amplitudes may clarify this point.

Numerical results obtained from the application of the theoretical model to the case of fully clamped CFRP plates has led to results in qualitative agreement with the measured data, showing a more accentuated nonlinear behaviour due to relatively high inplane stiffnesses. Investigations directed towards increasing the damping of such materials, via use of matrix materials with more appropriate viscoelasic properties, may offer, to some extent, a remedy to this disadvantage.

REFERENCES

CHAPTER I

1.1 C.E. Teh 1982 *Ph.D. Thesis*, Institute of Sound and Vibration Research. Dynamic behaviour and acoustic fatigue of isotropic and anisotropic panels under combined acoustic excitation and static in-plane compression.

1.2 M.M.K. Bennouna and R.G. White 1984 *Journal of Sound and Vibration* **96**(3), 309-331. The effects of large vibration amplitudes on the fundamental mode shape of a clamped-clamped uniform beam.

1.3 M.M.K. Bennouna and R.G. White 1984 *Journal of Sound and Vibration* **96**(3), 281-308. The effects of large vibration amplitudes on the dynamic strain response of a clamped-clamped beam with consideration of fatigue life.

1.4 S.L. Lau, Y.K. Cheung and S.Y. Wu 1984 *Journal of Applied Mechanics* **51**, 837-844. Nonlinear vibrations of thin elastic plates. Part 1: Generalized incremental Hamilton's principle and element formulation.

1.5 R.G. White 1978 *Composites*, 251-258. A comparison of some statistical properties of the responses of aluminium alloy and carbon fibre reinforced plates to acoustic excitation.

1.6 R.G. White 1985 *Proceedings of the third international conference on composite structures*. Some influence of material properties on the dynamic response of C.F.R.P. structures. Paisley College of Technology.

1.7 A.W. Leissa 1973 *Journal of Sound and Vibration* **31**(3), 257-293. The free vibration of rectangular plates.

1.8 R.F. McLean 1982 In *Applied Mathematical Analysis: Vibration Theory* (ed. G.F. Roach), 23-55. The biharmonic equation and its finite difference approximations.

1.9 A.W. Leissa 1984 *Proc. of the 2nd International Conference on Recent Advances in Structural Dynamics*, University of Southampton, Vol. 1, 241-260. Nonlinear analysis of plate and shell vibrations.

1.10 A.H. Nayfeh and D.T. Mook 1979 *Nonlinear Oscillations*. John Wiley & Sons.

1.11 S.P. Timoshenko and S.W. Krieger 1959 *Theory of Plates and Shells*, 407. McGraw-Hill.

1.12 E.J. Kirchman and J. Greenspon 1957 *Journal of the Acoustical Society of America*, 854-857. Nonlinear response of aircraft panels in acoustic noise.

1.13 H.N. Chu and G. Hermann 1956 *Journal of Applied Mechanics*, 532-540. Mechanics, influence of large amplitudes on free flexural vibrations of rectangular elastic plates.

1.14 L.W. Rehfield 1973 *Int. J. Solids and Structures*, 581-590. Nonlinear free vibrations of elastic structures.

1.15 H.M. Berger 1955 *Journal of Applied Mechanics*, 465-472. A new approach to the analysis of large deflections of plates.

1.16 W. A. Nash and J. R. Modeer 1959 *Proc.Symp.Theor.Thin Elast.Shells*, 331-354 Certain approximate analyses of the nonlinear behaviour of plates and shallow shells.

1.17 T. Wah 1963 *Int. Journal of Mechanical Sciences* **5**, 425-438. Large amplitude flexural vibration of rectangular plates.

1.18 C.L. Huang and I.M. Al Khattat 1977 *Int. J. Non-linear Mechanics*, **12**, 297-306. Finite amplitude vibrations of a circular plate.

1.19 M. Sathyamoorthy 1978 Letter to the editor of *Journal of Sound and Vibration* **58**(2), 301-304. Nonlinear vibration of rectangular plates.

1.20 G. Prathap and T.K. Varadan 1978 *Journal of Sound and Vibration* **56**(4), 521-530. On the nonlinear vibration of rectangular plates.

1.21 G. Chandrasekharappa and H.R. Srirangarayan 1989 *AIAA Journal* **27**(5), 665-667. Nonlinear free vibration of elastic plates.

1.22 J. Robinson and Chuh Mei 1989 *Proc. AIAA Conference* San Antonio. Paper 89-1104. The influence of nonlinear damping on the random response of panels by time domain simulation.

1.23 G.V. Rao, K.K. Raju and I.S. Raju. 1976 *Computers and Structures* **6**, 169-172. Finite element formulation for the large amplitude free vibrations of beams and orthotropic circular plates.

1.24 J.N. Reddy 1979 *Proceedings of 3rd Int. Conference on Finite Element Methods*, New South Wales. Simple finite elements with relaxed continuity for nonlinear analysis of plates.

1.25 M. Yamaki 1961 *ZAMM* **41**, 501-510. Influence of large amplitudes on flexural vibrations of elastic plates.

1.26 C. Mei 1973 *Computer and Structures* **3**, 163-174. Finite element displacement method for large amplitude free flexural vibration of beams and plates.

1.27 G.V. Rao, I.S. Raju and K.K. Raju 1976 *Computers and Structures* **6**, 163-167. A finite element formulation for large amplitude flexural vibrations of thin rectangular plates.

1.28 H.F. Bauer 1968 *Trans. ASME Journal of Applied Mechanics* **35**, 47-52. Nonlinear response of elastic plates to pulse excitation.

CHAPTER II

[2.1] G.B. Warburton 1976 *The dynamical behaviour of structures,* 146. Pergamon

[2.2] L.Meirovitch 1986 *Elements of vibration analysis*, 267-168. McGraw-Hill Book Company.

[2.3] Kyuichiro Washizu 1975 *Variational methods in Elasticity and Plasticity*, 1-3. Pergamon Press.

[2.4] H.N. Chu and G. Herrmann 1956 *Journal of Applied Mechanics* **23,** 532-540. Influence of large amplitudes on free flexural vibrations of rectangular elastic plates.

[2.5] L.W. Rehfield 1973 *Int. J. Solids Structures*, **9**, 581-590. Nonlinear free vibrations of elastic structures.

[2.6] Lau, S.L., Cheung, Y.K. and Wu, S.Y. 1984 *Journal of Applied Mechanics* **51,** 837-851. Nonlinear vibration of thin elastic plates.

[2.7] D.J.Ewins 1984 *Modal testing; Theory and Practice*, 59. Research Studies Press

[2.8] R.G. White 1971 *J. of Sound and Vibration* **16**, 255. Effects of nonlinearity due to large deflections in the resonance testing of structures.

[2.9] A. Tondl 1971 *J. Sound Vibration* **17**, 429. Notes on the paper 'Effects of non-linearity due to large deflections in the resonance testing of structures'

CHAPTER III

[3.1] R.G. White and C.E. Teh 1981 *Journal of Sound and Vibration* **75**(4),527-547 Dynamic behaviour of isotropic plates under combined acoustic excitation and static inplane compression. *Journal of Sound and Vibration* **75**(4), 527-547.

[3.2] R.G. White 1988 *Proceedings of the 25th structural dynamics and materials conference.* Williamsburg U.S.A., April 18-20, 253-260. The acoustic excitation and fatigue of composites plates.

[3.3] D.L. Gregory and D.O. Smallwood 1986 Natural frequencies and mode shapes of a free rectangular plate as a function of the aspect ratio.

[3.4] A.W. Liessa 1969 *NASA-SP 160* , 58-67. Vibration of plates.

[3.5] R.F. McLean 1982 *University of Strathclyde seminars in applied mathematical analysis: Vibration theory*, 23-55. The biharmonic equation and its finite difference approximations. (G.F. Roach : editor). Shiva Publishing Limited.

[3.6] R.G. White 1975 *Journal of the Royal Aeronautical Society* 318-325. Some measurements of the dynamic properties of mixed, carbon fibre reinforced, plastic beams and plates.

[3.7] RG. White 1978 *Composites*, 251-258. A comparison of some statistical properties of the response of aluminium alloy and C.F.R.P. plates to acoustic excitation.

[3.8] M.M. Bennouna and R.G. White 1984 *Journal of Sound and Vibration*, (3), 309-331. The effects of large vibration amplitudes on the fundamental mode shape of a clamped-clamped uniform beam.

[3.9] B.L. Clarkson and A. Pietrusewics 1963 *ASD-TDR-63-91* The university of Southampton random siren facility.

[3.10] C.E. Teh 1982 *Ph.D. Thesis,* Institute of Sound and Vibration Research. Dynamic behaviour and acoustic fatigue of isotropic and anisotropic panels under combined acoustic excitation and static inplane compression.

[3.11] G. C. Wright 1971 *Institute of Sound and Vibration research technical report no 51.* The dynamic properties of fibre reinforced plastic beams.

[3.12] M.M.K. Bennouna 1982 *Ph.D. Thesis,* Institute of Sound and Vibration Research. Nonlinear dynamic behaviour of a clamped-clamped beam with consideration of fatigue life.

[3.13] D.J.Ewins 1984 *Modal testing; Theory and Practice*, 59. Research Studies Press

[3.14] H. Vold 1989 *ASD-TDR-63-91 Proceedings of the 7th IMAC* , Las Vegas U.S.A. Insight not numbers - keynote address.

[3.15] L. D. Zavodney 1987 *Proceedings of the 5th IMAC.* Can the modal analyst afford to be ignorant of nonlinear vibration phenomena?

[3.16] G.R. Tomlinson 1985 *Proceedings of the 4th IMAC*, Orlando, 837-843. Detection, identification and qualification of nonlinearity in modal analysis- a review

[3.17] H.R. Busby, C. Nopporn and R. Singh 1986 *Journal of Sound and Vibration,* **180**(3), 415-427. Experimental modal analysis of nonlinear systems: a feasibility study.

[3.18] R.B. Randall and B. Teh 1987 *Frequency Analysis,* 117 Bruel & Kjaer.

CHAPTR IV

[4.1] M.M. Bennouna 1981 *Ph.D. Thesis*, ISVR, Southampton University, 97. Nonlinear behaviour of a clamped-clamped beam with consideration of fatigue life.

[4.2] M.M. Bennouna and R.G. White 1984 *Journal of Sound and Vibration* (3), 309-331. The effects of large vibration amplitudes on the fundamental mode shape of a clamped-clamped uniform beam.

[4.3] L. H. Donnell 1976 *Beams, Plates and Shells*, 71. MacGraw-Hill.

[4.4] J.D. Ray and C.W. Bert 1969 *Journal of Engineering for Industry* 91B, 997-1004. Nonlinear vibrations of a beam with pinned ends.

[4.5] H.N. Chu and G. Hermann 1956 *Journal of Applied Mechanics* **23**, 532-540. Influence of large amplitudes on free flexural vibrations of rectangular elastic plates.

[4.6] L.W. Rehfield 1973 *Int. J. Solids Structures*, **9**, 581-590. Nonlinear free vibrations of elastic structures.

[4.7] R. Benamar M.M. Bennouna and R.G. White. To be published in *Journal of Sound and Vibration*..The effects of large vibration amplitudes on the fundamental mode shape of a thin elastic structures. Part I: Simply supported and clamped-clamped beams.

[4.8] L.Meirovitch **1986** *Elements of vibration analysis* , 267, 161. McGraw-Hill Book Company.

[4.9] P. Henrici 1964 *Elements of numerical analysis* , 77. John Wiley & Sons.

[4.10] W.T. Thomson *Theory of vibration with applications*, 465-469. George Allen & Unwin Ltd.

[4.11] P. Henrici 1964 *Elements of numerical analysis, 251.* John Wiley & Sons.

[4.12] M.J.D. Powell 1965 *Computer Journal* . A method for minimising a sum of squares of nonlinear functions without calculating derivatives.

[4.13] J. A. Bennett and J. G. Eisley 1970 *American Institute of Aeronautics and Astronautics Journal* **8**, 734-739. A multiple degree-of-freedom approach to nonlinear beam vibrations.

CHAPTER V

[5.1] R.G. White 1975 *Journal of the Royal Aeronautical Society,* 318-325. Some measurements of the dynamic properties of mixed, carbon fibre reinforced, plastic beams and plates

[5.2] A.W. Leissa 1969 *NASA-SP 160* , 58-67. Vibration of plates.

[5.3] A.W. Leissa 1973 *Journal of Sound and Vibration* **31**, 257-293. Free vibrations of rectangular plates.

[5.4] D.J. Gorman 1982 *Free vibration analysis of rectangular plates,* 69-100. Elsevier North Holland, Inc.

[5.5] G.B. Warburton 1954 *Proc.Inst.Mech.Eng*, ser.A, **168**(12), 371-384. The vibration of rectangular plates.

[5.6] D. Young :1950 *J. Appl. Mech*, **17**(4), 448-453. Vibrations of rectangular plates by the Ritz method.

[5.7] J. Nagaraja and S.S. Rao 1953 *J. Aeron. Sci,* **20**(12), 855-856. Vibration of rectangular plates.

[5.8]. H.N. Chu and G. Herrmann 1956 *Journal of Applied Mechanics* **23**, 532-540. Influence of large amplitudes on free flexural vibrations of rectangular elastic plates.

[5.9] L.W. Rehfield 1973 *Int. J. Solids Structures*, Vol. 9, 581-590. Nonlinear free vibrations of elastic structures.

[5.10] M.M. Bennouna and R.G. White 1984 *Journal of Sound and Vibration*, (3), 309-331. The effects of large vibration amplitudes on the fundamental mode shape of a clamped-clamped uniform beam.

[5.11] R.G. White 1971 *J. SoundVib.* **16**(2), 255-267. Effects of nonlinearity due to large deflections in the resonance testing of structures.

[5.12] L.H. Donnell 1976 ***Beams, Plates and Shells***,203. McGraw-Hill.

[5.13] S.P. Timoshenko 1959 *Theory of plates and shells,* 345. Mc Graw-Hill.

[5.14] S.P. Timoshenko 1959 *Theory of plates and shells* , 419 Mc Graw-Hill.

[5.15] C.E. Teh 1989 *Ph.D. Thesis,* Institute of Sound and Vibrations Research. Dynamic behaviour and acoustic fatigue of isotropic and anisotropic panels under combined acoustic excitation and static inplane compression.

[5.16] R. Courant 1947 *Differential and Integral Calculus*, vol. 2. Blackie & Sons Ltd.

[517] M.J.D. Powell 1965 *Computer Journal.* A method for minimising a sum of squares of non-linear functions without calculating derivatives.

[5.18] M. Yamaki 1961 *ZAMM* **41**, 501-510. Influence of large amplitudes on flexural vibrations of elastic plates.

[5.19] C. MEI 1973 *Computer and Structures* **3**, 163-174. Finite element displacement method for large amplitude free flexural vibration of beams and plates.

[5.20] G.V. Rao, I.S. Raju and K.K. Raju 1976 *Computers and Structures* **6**, 163-167. A finite element formulation for large amplitude flexural vibrations of thin rectangular plates.

[5.21] M. Sathyamoorthy 1978 Letter to the editor of *Journal of Sound and Vibration* **58**(2), 301-304. Nonlinear vibration of rectangular plates.

[5.22] J.N. Reddy 1979 *Proceedings of 3rd Int. Conference on Finite Element Methods*, New South Wales. Simple finite elements with relaxed continuity for nonlinear analysis of plates.

[5.23] S.L. Lau, Y.K. Cheung and S.Y. Wu 1984 *Journal of Applied Mechanics* **51**, 837-844. Nonlinear vibrations of thin elastic plates. Part 1: Generalized incremental Hamilton's principle and element formulation.

[5.24] G. Chandrasekharappa and H.R. Srirangarayan 1989 *AIAA Journal* **27**(5), 665-667. Nonlinear free vibration of elastic plates.

CHAPTER VI

[6.1] ISO Standard Recommendation ISO/TC 108. Secr.-40, 108E. Vibration and shock - terminology.

[6.2] R.G. White 1971 *Journal of Sound and Vibration* **16**, 255. Effects of non-linearity due to large deflections in the resonance testing of structures.

[6.3] A. Tondl 1971 *Journal of Sound and Vibration* **17**, 429-436. Notes on the paper "Effects of non-linearity due to large deflections in the resonance testing of structures".

[6.4] A.H. Nayfeh and D.T. Mook 1979 *Nonlinear Oscillations.* John Wiley & Sons.

[6.5] M.M.K. Bennouna and R.G. White 1984 *Journal of Sound and Vibration* 96(3), 309-331. The effects of large vibration amplitudes on the fundamental mode shape of a clamped-clamped uniform beam.

[6.6] T.K Brewer 1988 *Master of Engineering*, Engineering Mechanics. Old Dominion University. The effects of elastic boundary conditions on the dynamic response of rectangular plates.

[6.7] L.A. Roussos, K.E. Heitman and C.E. Rucker 1986 Presented at the *10th AIAA Aeroacoustic conference*, Seattle, AIAA paper no 86-1931. Predicted and measured strain response of rectangular panels.

[6.8] L.A. Roussos, T.K. Brewer *Presented at AIAA Dynamics Specialists conference*, Monterey, April 9-10,R.B. Effects of the boundary conditions on dynamic strain Response of rectangular panels.

[6.9] Randall and B. Teh 1987 *Frequency Analysis*, 30. Brüel and Kjaer.

[6.10] G. Jewell 1987 *Signal Processing and Control Group, ISVR, University of Southampton.* A description of DATS Modules.

CHAPTER VII

[7.1] W.Y. Tseng and J. Dungundji 1970 *J. Appl. Mech* June. 292. Nonlinear vibrations of a beam under harmonic excitation.

[7.2] M.M. Bennouna and R.G. White 1984 *Journal of Sound and Vibration*, (3), 309-331. The effects of large vibration amplitudes on the fundamental mode shape of a clamped-clamped uniform beam.

[7.3] A. H. Nayfeh and D.T. Mook 1979 *Nonlinear oscillations*, 162-171. John Wiley and Sons.

[7.4] J.J. Stoker 1950 *Nonlinear vibrations.* Interscience Publishers Inc. NewYork

[7.5] Cunningham 1958 *Nonlinear analysis*. McGraw Hill Electrical and electronic engineering series.

[7.6] C. Hayashi 1966 *Nonlinear oscillations in physical systems.* McGraw Hill.

[7.7] F. Dinca and C. Teodosin 1970 *Nonlinear and random vibrations.* Academic Press, Inc.

[7.8] D.J. Gorman 1982 *Free vibration analysis of rectangular plates*, 69-100. Elsevier North Holland, Inc.

CHAPTER IX

[9.1] S.W. Tsai 1988 *Composites Design.* 4th edition Think Composites pp.1-2.

[9.2] R.G. White 1978 *Composites*, 251-258. A comparison of some statistical properties of the response of aluminium alloy and C.F.R.P. plates to acoustic excitation.

[9.3] M.M. Bennouna 1981 *Ph.D. Thesis*, ISVR, University of Southampton, 92,258. Nonlinear behaviour of a clamped-clamped beam with consideration of fatigue life.

[9.4] J. E. Ashton and J.M. Whitney 1970 *Theory of laminated plates*, 12. Technomic Publication.

[9.5]. Timoshenko 1959 *Theory of plates and shells*, 416. McGraw-Hill.

[9.6] R. M. Jones 1975 *Mechanics of composite material*, 51. International Student Edition.

[9.7] J. E. Ashton and J.M. Whitney 1970 *Theory of laminated plates*, 35. Technomic Publication.

[9.8]. Timoshenko 1959 *Theory of plates and shells*, 419. Mc Graw-Hill

[9.9] Engineering Science Data Unit (ESDU) 1983 Estimation of the stiffnesses and apparent elastic properties of laminated flat plates. Item number 83035 .

[9.10] Engineering Science Data Unit (ESDU) 1983 Natural frequencies of rectangular, specially orthotropic laminated plates. Item number 83036 pp. 16 to 18[9.10] ESDU83036.

[9.11] R.G. White 1985 *Proceedings of the Third International Conference on Composite Structures*. Some influence of material properties on the dynamic response of C.F.R.P. structures. Paisley college of Technology.

APPENDIX A

MATHEMATICAL PROOF REQUIRED FOR CHAPTER 2

Equation (4.4) gives the axial strain energy expression in the beam case as :

$$Va = \frac{EA}{8L}\left(\int_0^L \left(\frac{\partial W}{\partial x}\right)^2 dx\right)^2$$

If the displacement function W is expanded in the form of the series given in equation (2.2):

$$W(x) = a_i \bar{w}_i(x) \quad \sin\omega t$$

Substituting W in the expressions for V_a and rearranging leads to :

$$V_a = \frac{1}{2} a_i a_j a_k a_l b_{ijkl} \sin^4\omega t$$

which can be written in matrix notation as :

$$V_a = \frac{1}{2} \{A\}^T [B(A)] \{A\} \sin^4\omega t$$

So, if we have, as a consequence of equation (2.23) :

$$\{A\}^T [B(A)] \{A\} = 0$$

this leads to:

$$\left(\int_0^L \left(\frac{\partial W}{\partial x}\right)^2 dx\right)^2 = 0$$

or :

$$\int_0^L \left(\frac{\partial W}{\partial x}\right)^2 dx = 0$$

Therefore :

$$W = 0 \text{ almost everywhere}$$

Due to continuity, the above result leads to:

$$a_i \bar{w_i}(x) = 0$$

As the functions w_i are independent, we obtain :

$$a_i = 0 \quad \text{for} \quad i=1,...,n$$

In the plate case, V_a is given by equation (5.2):

$$V_a = \frac{3D}{2H^2} \int_S \left(\left(\frac{\partial W}{\partial x}\right)^2 + \left(\frac{\partial W}{\partial y}\right)^2\right)^2 dS$$

and an analysis similar to that stated above can be made, leading to the same conclusion..

APPENDIX B

MAIN ROUTINES FOR FUNDAMENTAL CLAMPED-CLAMPED BEAM NONLINEAR MODE SHAPE CALCULATIONS

THE MAIN PROGRAM

```
C BEAM16
      IMPLICIT DOUBLE PRECISION (A-H,O-Z)
      DOUBLE PRECISION X(5),F(5),AJINV(5,5),W(2500),RIG(6,6)
     1,MA(6,6),TNL(6,6,6,6),PA(6,161),PC(6,161),XX(6),PNL(40,161)
     1,PCNL(40,161),PNLN(40,161),FI(11),FREQ(40),RA
      OPEN(UNIT=13,NAME='M1P61.DAT',STATUS='NEW')
      OPEN(UNIT=14,NAME='M1P62.DAT',STATUS='NEW')
      OPEN(UNIT=15,NAME='M1P63.DAT',STATUS='NEW')
      OPEN(UNIT=16,NAME='M1P64.DAT',STATUS='NEW')
      OPEN(UNIT=17,NAME='M1P65.DAT',STATUS='NEW')
      OPEN(UNIT=18,NAME='M1P66.DAT',STATUS='NEW')
      OPEN(UNIT=19,NAME='M1P67.DAT',STATUS='NEW')
      OPEN(UNIT=20,NAME='M1P68.DAT',STATUS='NEW')
     IMP1=13
     IMP2=15
     IMP3=14
     IMP6=16
     IMP7=17
     IMP8=18
     IMP9=19
     IMP=20
      CALL PREP(IMP1,IMP6,RIG,TNL,MA,PA,PC,FI)
     DO  999 K=40,70
     IF(K.GT.1) GO TO 810
     X(1)=-0.108D-4
     X(2)=0.732548D-3
     X(3)=0.558D-5
     X(4)=-0.598D-4
     X(5)=-0.108D-4
 810 Y=DBLE(K)/DBLE(20)
     PRINT *,Y
     N=5
     STEP=0.0015D0
     ACC=0.0000000000000001D0
     MAXFUN=800
     DMAX=10.D0
     CALL
NS01A(N,X,F,AJINV,STEP,DMAX,ACC,MAXFUN,0,W,IMP2,Y,MA,RIG,TNL
     1,NI,RA,RESID)
      CALL CALFUN(N,X,RIG,TNL,MA,F,Y,IMP,R)
     RESID1=0.D0
     XX(1)=Y
     DO 875 I=1,N
      XX(I+1)=X(I)
     RESID1=RESID1+F(I)*F(I)
 875  CONTINUE
     WRITE(IMP3,800)
 800  FORMAT(2X,//,4X,'PREMIER MODE PROPRE NON LINEAIRE'//)
 801  FORMAT(4X,'CALCUL NO : ',I5,4X,'RA= ',F16.8)
```

```
   WRITE(IMP3,801)K,RA
   WRITE(IMP3,803)Y
803  FORMAT(4X,'RESULTAT POUR A1 = ',F16.8)
   WRITE(IMP3,804)NI
804  FORMAT(4X,'NOMBRE D''ITERATIONS NECESSAIRES : ',I5)
    WRITE(IMP3,8)(I,X(I),F(I),I=1,N)
   WRITE(IMP3,9)RESID1
  8   FORMAT(//4X,'I',7X,'X(I)',12X,'F(I)'//(I5,2E17.8))
 9  FORMAT(/5X,'LA SOMME DES CARRES EST : ',E17.8//)
   FREQ(K)=R/(FI(1)**4)
   FREQ(K)=DSQRT(FREQ(K))
   FREQ(K)=FREQ(K)*30.66
   WRITE(17,9003)K,FREQ(K)
   WRITE(18,9004)K,FREQ(K)
   WRITE(20,9005)K,FREQ(K)
9003 FORMAT(2X,'DISPLACEMENT NO:',I2,//,2X,'FREQUENCY:',F13.6)
9005 FORMAT(2X,'NORMALIZED DISPT NO:',I2,//,2X,'FREQUENCY:',F13.6)
9004 FORMAT(2X,'CURVATURES NO:',I2,//,2X,'FREQUENCY:',F13.6)
   DO 411 KK=1,161,4
    PNL(K,KK)=0.D0
    PCNL(K,KK)=0.D0
   DO 412 I=1,N+1
    PNL(K,KK)=PNL(K,KK)+(XX(I)*PA(I,KK))
    PCNL(K,KK)=PCNL(K,KK)+(XX(I)*PC(I,KK))
412  CONTINUE
   DS=DBLE(KK-1)/DBLE(160)
    WRITE(17,9002)DS,PNL(K,KK)
    WRITE(18,9002)DS,PCNL(K,KK)
411  CONTINUE
    WRITE(19,9002)PNL(K,81),FREQ(K)
    DO 413 KK=1,161,4
   DS=DBLE(KK-1)/DBLE(160)
    PNLN(K,KK)=PNL(K,KK)/PNL(K,81)
    WRITE(20,9002)DS,PNLN(K,KK)
 413 CONTINUE
 999 CONTINUE
9001 CONTINUE
9002 FORMAT(4X,F15.8,5X,F15.8)
    STOP
    END
    DOUBLE PRECISION FUNCTION FA(X)
    DOUBLE PRECISION X
    FA=DEXP(X)+DEXP(-X)
    FA=FA/DBLE(2)
    FA=FA-DCOS(X)
    RETURN
    END
    DOUBLE PRECISION FUNCTION GA(X)
    DOUBLE PRECISION X
    GA=DEXP(X)-DEXP(-X)
    GA=GA/DBLE(2)
    GA=GA-DSIN(X)
    RETURN
    END

    DOUBLE PRECISION FUNCTION FB(X)
    DOUBLE PRECISION X
    FB=DEXP(X)-DEXP(-X)
```

```
      FB=FB/DBLE(2)
      FB=FB+DSIN(X)
      RETURN
      END


      DOUBLE PRECISION FUNCTION FC(X)
      DOUBLE PRECISION X
      FC=DEXP(X)+DEXP(-X)
      FC=FC/DBLE(2)
      FC=FC+DCOS(X)
      RETURN
      END


       SUBROUTINE CALC(F,G,FI,GI,P)
      IMPLICIT DOUBLE PRECISION (A-H,O-Z)
       DIMENSION FI(6),P(6,161),GI(6,2)
      DX=DBLE(1)/DBLE(160)
      DO 330 I=1,6
      DO 331 J=1,161
      X=(DX*DFLOAT(J-1)*FI(I))
       P(I,J)=((F(X)/GI(I,1))-(G(X)/GI(I,2)))
  331 CONTINUE
  330 CONTINUE
      RETURN
      END


      SUBROUTINE SOMM(TAB,RESUL)
      IMPLICIT DOUBLE PRECISION (A-H,O-Z)
      DIMENSION TAB(161)
      S=DBLE(0)
      DX=DBLE(1)/DBLE(160)
      DO 332 I=1,80
      J=2*I-1
      S=S+(TAB(J)+(4*TAB(J+1))+TAB(J+2))
  332 CONTINUE
      RESUL=S*DX/DBLE(3)
      RETURN
      END


       SUBROUTINE CALFUN(N,X,RIG,TNL,MA,F,Y,IMP,R)
C      ********************
C      *PROGRAMME .CALFUN*
C      ********************
C
C
C
      IMPLICIT DOUBLE PRECISION (A-H,O-Z)
       DOUBLE PRECISION X(5),F(5),TNL(6,6,6,6)
      1,A(6),D(6),DTA(6),DTF(6),DTM(6),
      1MA(6,6),RIG(6,6)

      A(1)=Y
      DO 9 I=2,N+1
      A(I)=X(I-1)
```

```
   9 CONTINUE
C
C
C
C
      TA=0.D0
      DO 110 I1=1,N+1
      DO 115 I2=1,N+1
      DO 114 I3=1,N+1
      DO 334 I4=1,N+1
      TA=TA+(TNL(I1,I2,I3,I4)*A(I1)*A(I2)*A(I3)*A(I4))
  334 CONTINUE
  114 CONTINUE
  115 CONTINUE
  110 CONTINUE
C
C
      TF=0.D0
      TM=0.D0
      DO 333 I=1,N+1
      TF=TF+(A(I)*A(I)*RIG(I,I))
      TM=TM+A(I)*A(I)
  333 CONTINUE
C
C
C
      DO 12 I=1,N+1
      DTA(I)=0.D0
   12 CONTINUE
      DO 30 IR=1,N+1
      DO 35 J=1,N+1
      DO 34 K=1,N+1
      DO 29 L=1,N+1
      DTA(IR)=DTA(IR)+(3*A(J)*A(K)*A(L)*TNL(IR,J,K,L))
   29 CONTINUE
   34 CONTINUE
   35 CONTINUE
   30 CONTINUE
C
C
C
      DO 13 J=1,N+1
      DTF(J)=2*A(J)*RIG(J,J)
   13 CONTINUE
C  14 CONTINUE
C
C
C
      DO  15 I=1,N+1
      DTM(I)=0.D0
      DTM(I)=2*A(I)
   15 CONTINUE
C
C
      DO 16 I=1,N+1
      D(I)=0.D0
      D(I)=((DTF(I)+DTA(I))*TM)-(DTM(I)*(TF+TA))
   16 CONTINUE
```

```
      DO 17 I=2,N+1
      F(I-1)=D(I)
   17 CONTINUE
      R=(TF+TA)/TM
      RETURN
      END


      SUBROUTINE PREP(IMP,IMP6,RIG,TNL,MA,PAN,PCN,FI)
      IMPLICIT DOUBLE PRECISION (A-H,O-Z)
      DOUBLE PRECISION MA
      DIMENSION TAB1(161),TAB2(161),TAB3(161)
       DIMENSION PAN(6,161),PBN(6,161),PCN(6,161)
       DIMENSION FI(6),GI(6,2),SURF(6)
       DIMENSION MA(6,6),RIG(6,6),RAG(6,6),TNL(6,6,6,6)
      EXTERNAL FA
      EXTERNAL GA
      EXTERNAL FB
      EXTERNAL FC
       N=6
       FI(1)=4.730040744862704D0
       FI(2)=10.99560783800167D0
       FI(3)=17.27875965739948D0
       FI(4)=23.56194490204046D0
       FI(5)=29.84513020910325D0
       FI(6)=36.12831551628262D0
       DO 301 I=1,N
       GI(I,1)=FA(FI(I))
       GI(I,2)=GA(FI(I))
  301 CONTINUE
       CALL CALC(FA,GA,FI,GI,PAN)
       CALL CALC(FB,FA,FI,GI,PBN)
       CALL CALC(FC,FB,FI,GI,PCN)
       DO 302 I=1,N
       DO 303 K=1,161
       TAB1(K)=PAN(I,K)*PAN(I,K)
  303 CONTINUE
       CALL SOMM(TAB1,SURF(I))
       SURF(I)=DSQRT(SURF(I))
  302 CONTINUE
       DO 304 I=1,N
       DO 305 K=1,161
        PAN(I,K)=PAN(I,K)/SURF(I)
        PBN(I,K)=PBN(I,K)/SURF(I)
        PCN(I,K)=PCN(I,K)/SURF(I)
  305 CONTINUE
  304 CONTINUE
       DO 306 I=1,N
       DO 307 J=1,N
       DO 308 K=1,161
        TAB1(K)=PAN(I,K)*PAN(J,K)
        TAB2(K)=PBN(I,K)*PBN(J,K)*FI(I)*FI(J)
        TAB3(K)=PCN(I,K)*PCN(J,K)*FI(I)*FI(I)*FI(J)*FI(J)
  308 CONTINUE
       CALL SOMM(TAB1,MA(I,J))
       CALL SOMM(TAB2,RAG(I,J))
       CALL SOMM(TAB3,RIG(I,J))
  307 CONTINUE
```

```
306 CONTINUE
   DO 111 I=1,N
   DO 112 J=1,N
   DO 113 K=1,N
   DO 114 L=1,N
    TNL(I,J,K,L)=3*RAG(I,J)*RAG(K,L)
114  CONTINUE
113  CONTINUE
112  CONTINUE
111  CONTINUE
   WRITE(IMP,320)
320  FORMAT(4X,////,19X,' NONLINEAR CALCULUS DATA')
   WRITE(IMP,321)
321  FORMAT(19X,'*****************************',/////)
   WRITE(IMP,322)
322  FORMAT(4X,//,4X,'MODES USED')
   WRITE(IMP,3221)
3221  FORMAT(4X,'*****************************',//)
   DO 323 I=1,N
   WRITE(IMP,324)I,FI(I)
324  FORMAT(7X,'  FI(',I1,')= ',F12.8)
323  CONTINUE
   WRITE(IMP,333)
333  FORMAT(19X,/////,'*****************************',/////)
   IMP6=16
   DO 3520 K=1,161,4
   DXX=0.625D-2
   DS=DFLOAT(K-1)*DXX
    WRITE(IMP6,3521)DS,(PAN(I,K),I=1,5)
3520 CONTINUE
   DO 3720 K=1,161,4
   DXX=0.625D-2
   DS=DFLOAT(K-1)*DXX
    WRITE(IMP6,4521)DS,PAN(6,K)
3720 CONTINUE
   DO 3522 K=1,161,4
   DXX=0.625D-2
   DS=DFLOAT(K-1)*DXX
    WRITE(IMP6,3521)DS,(PBN(I,K),I=1,5)
3522 CONTINUE
   DO 3922 K=1,161,4
   DXX=0.625D-2
   DS=DFLOAT(K-1)*DXX
    WRITE(IMP6,4521)DS,PBN(6,K)
3922 CONTINUE
   DO 3103 K=1,161,4
   DXX=0.625D-2
   DS=DFLOAT(K-1)*DXX
    WRITE(IMP6,3521)DS,(PCN(I,K),I=1,5)
3103 CONTINUE
   DO 3123 K=1,161,4
   DXX=0.625D-2
   DS=DFLOAT(K-1)*DXX
    WRITE(IMP6,4521)DS,PCN(6,K)
3123 CONTINUE
3521  FORMAT(4X,F5.3,2X,F9.6,2X,F9.6,2X,F9.6,2X,F9.6,2X,F9.6)
4521 FORMAT(4X,F5.3,2X,F9.6)
   WRITE(IMP,325)
```

```
      WRITE(IMP,3325)
 3325 FORMAT(4X,'******************',///////)
  325  FORMAT(4X,/////,4X,'MASS MATRIX')
      DO 326 I=1,N
      WRITE(IMP,3326)I
 3326 FORMAT(4X,'I= ',I1,/)
       WRITE(IMP,1182)(MA(I,J),J=1,3)
       WRITE(IMP,2182)(MA(I,J),J=4,6)
  326  CONTINUE
      WRITE(IMP,180)
      WRITE(IMP,1180)
 1180 FORMAT(4X,'******************',///////)
  180  FORMAT(4X,/////,4X,'RIGIDITY MATRIX')
      DO 181 I=1,N
      WRITE(IMP,3326)I
       WRITE(IMP,1182)(RIG(I,J),J=1,3)
       WRITE(IMP,2182)(RIG(I,J),J=4,6)
  181  CONTINUE
      WRITE(IMP,980)
      WRITE(IMP,9180)
  980  FORMAT(4X,'**************************',/////)
 9180  FORMAT(4X,/////'NON L. RIGIDITY MATRIX')
      DO 981 I=1,N
      WRITE(IMP,3326)I
       WRITE(IMP,1182)(RAG(I,J),J=1,3)
       WRITE(IMP,2182)(RAG(I,J),J=4,6)
  981  CONTINUE
 1182    FORMAT(2X,'J=1,..,3    ','*',F16.8,'*',F16.8,'*',F16.8,'*')
 2182    FORMAT(2X,'J=4,..,6    ','*',F16.8,'*',F16.8,'*',F16.8,'*')
      RETURN
      END
```

APPENDIX C

MAIN ROUTINES FOR FUNDAMENTAL FULLY CLAMPED RECTANGULAR PLATE MODE SHAPE CALCULATION

```
C P25CAD

      IMPLICIT DOUBLE PRECISION (A-H,O-Z)
      DOUBLE PRECISION X(8),F(8),AJINV(8,8),W(2500),RF(5),
     1B1(18),RIG(9,9),MA(9,9),TNL(9,9,9,9)
     1,LAMDA,RA
      OPEN(UNIT=13,FILE='HAL1.DAT',STATUS='NEW',ERR=9001)
      OPEN(UNIT=14,FILE='HAL2.DAT',STATUS='NEW',ERR=9001)
      OPEN(UNIT=15,FILE='HAL3.DAT',STATUS='NEW',ERR=9001)
      IMP1=13
      IMP2=15
      IMP3=14
      RF(1)=DBLE(1)/DBLE(5)
      RF(2)=DBLE(2)*RF(1)
      RF(3)=DBLE(3)*RF(1)
      RF(4)=DBLE(4)*RF(1)
      RF(5)=DBLE(5)*RF(1)
      DO 9001 II=1,5
      LAMDA=RF(II)
C     LAMDA=0.6
      PRINT *,LAMDA
      WRITE(IMP1,4000)LAMDA
      WRITE(IMP2,4000)LAMDA
      WRITE(IMP3,4000)LAMDA
 4000 FORMAT(2X,/////,13X,'LAMDA= ',F12.8,/////)
      CALL PREP(IMP1,RIG,TNL,MA,LAMDA)
      B1(1)=0.05D0
      B1(2)=0.10D0
      B1(3)=0.15D0
      B1(4)=0.20D0
      B1(5)=0.25D0
      B1(6)=0.30D0
      B1(7)=0.35D0
      B1(8)=0.40D0
      B1(9)=0.45D0
      B1(10)=0.50D0
      B1(11)=0.55D0
      B1(12)=0.65D0
      B1(13)=0.75D0
      B1(14)=0.85D0
      B1(15)=0.95D0
      B1(16)=1.05D0
      B1(17)=1.50D0
      B1(18)=2.00D0
      DO  999 K=1,18
      IF(K.GT.1) GO TO 810
      X(1)=-0.108D-4
      X(2)=0.732548D-3
      X(3)=0.558D-5
      X(4)=-0.598D-4
      X(5)=-0.108D-4
      X(6)=-0.341D-7
```

```
      X(7)=-0.178D-5
      X(8)=-0.107D-7
  810 Y=B1(K)
      PRINT *,Y
      N=8
      STEP=0.0015D0
      ACC=0.0000000000000001D0
      MAXFUN=800
      DMAX=10.D0
       CALL NS01A(N,X,F,AJINV,STEP,DMAX,ACC,MAXFUN,0,W,IMP2,Y,MA,RIG,TNL
     1,NI,RA,RESID,LAMDA)
       CALL CALFUN(N,X,RIG,TNL,MA,F,Y,IMP,R,LAMDA)
      RESID1=0.D0
      DO 875 I=1,8
      RESID1=RESID1+F(I)*F(I)
  875 CONTINUE
      WRITE(IMP3,800)
  800 FORMAT(2X,//,4X,'PREMIER MODE PROPRE NON LINEAIRE'//)
  801  FORMAT(4X,'CALCUL NO : ',I5,4X,'RA= ',F16.8)
      WRITE(IMP3,801)K,RA
      WRITE(IMP3,803)Y
  803 FORMAT(4X,'RESULTAT POUR A1 = ',F16.8)
      WRITE(IMP3,804)NI
  804 FORMAT(4X,'NOMBRE D''ITERATIONS NECESSAIRES : ',I3)
       WRITE(IMP3,8)(I,X(I),F(I),I=1,8)
      WRITE(IMP3,9)RESID1
    8  FORMAT(//4X,'I',7X,'X(I)',12X,'F(I)'//(I5,2E17.8))
   9 FORMAT(/5X,'LA SOMME DES CARRES EST : ',E17.8//)
  999 CONTINUE
 9001 CONTINUE
      ENDFILE 13
      CLOSE (UNIT=13)
      ENDFILE 14
      CLOSE (UNIT=14)
      ENDFILE 15
      CLOSE (UNIT=15)
      STOP
      END

       SUBROUTINE CALFUN(N,X,RIG,TNL,MA,F,Y,IMP,R,LAMDA)
C      ********************
C      *PROGRAMME .CALFUN*
C      ********************
C
C
C
      IMPLICIT DOUBLE PRECISION (A-H,O-Z)
       DOUBLE PRECISION X(8),F(8),TNL(9,9,9,9)
     1,A(9),D(9),DTA(9),DTF(9),DTM(9),
     1MA(9,9),RIG(9,9),LAMDA
      A(1)=Y
      DO 9 I=2,N+1
      A(I)=X(I-1)
    9 CONTINUE
C
C
C
C
```

```
C
C
      TA=0.D0
      DO 110 I1=1,N+1
      DO 115 I2=1,N+1
      DO 114 I3=1,N+1
      DO 334 I4=1,N+1
      TA=TA+(TNL(I1,I2,I3,I4)*A(I1)*A(I2)*A(I3)*A(I4))
  334 CONTINUE
  114 CONTINUE
  115 CONTINUE
  110 CONTINUE

C
C
      TF=0.D0
      TM=0.D0
      DO 333 I=1,N+1
      DO 444 J=1,N+1
      TF=TF+(A(I)*A(J)*RIG(I,J))
      TM=TM+(A(I)*A(J)*MA(I,J))
  444 CONTINUE
  333 CONTINUE
C
C
C
C
C
      DO 12 I=2,N+1
      DTA(I)=0.D0
   12 CONTINUE
      DO 30 IR=2,N+1
      DO 35 J=1,N+1
      DO 34 K=1,N+1
      DO 29 L=1,N+1
      DTA(IR)=DTA(IR)+(3*A(J)*A(K)*A(L)*TNL(IR,J,K,L))
   29 CONTINUE
   34 CONTINUE
   35 CONTINUE
   30 CONTINUE
C
C
C
      DO 14 I=2,N+1
      DTF(I)=0.D0
      DO 13 J=1,N+1
      DTF(I)=DTF(I)+2*A(J)*RIG(I,J)
   13 CONTINUE
   14 CONTINUE
C
C
C
      DO  15 I=2,N+1
      DTM(I)=0.D0
      DTM(I)=2*A(I)
   15 CONTINUE
C
C
```

```
      DO 16 I=2,N+1
      D(I)=0.D0
      D(I)=((DTF(I)+DTA(I))*TM)-(DTM(I)*(TF+TA))
   16 CONTINUE
      DO 17 I=1,N
      J=I+1
      F(I)=D(J)
   17 CONTINUE
      R=(TF+TA)/TM
      RETURN
      END
      SUBROUTINE PREP(IMP,RIG,TNL,MA,LAMDA)
      IMPLICIT DOUBLE PRECISION (A-H,O-Z)
      DOUBLE PRECISION MA,RIG,TNL
     1,TABC1,TABC2,TABC3,TABC4,TABC5
     1,TABF1,TABF2,TABF3,TABF4,TABF5
      1,PAN,PBN,PCN,PINAA,PINBB,PINAC,PINCA,PINCC,PIN4A,PIN4B,P2A2B
     1,QAN,QBN,QCN,QINAA,QINBB,QINAC,QINCA,QINCC,QIN4A,QIN4B,q2A2B
      1 ,GIf,FI,GI,SURFF,SURFC,lAMDA,H2,H4,PI,Z,SIGNE
      DIMENSION TABC1(41),TABC2(41),TABC3(41),TABC4(41),TABC5(41)
      DIMENSION TABF1(41),TABF2(41),TABF3(41),TABF4(41),TABF5(41)
      DIMENSION PAN(3,41),PBN(3,41),PCN(3,41)
      DIMENSION PINAA(3,3),PINBB(3,3),PINCC(3,3),PINAC(3,3),PINCA(3,3)
      DIMENSION PIN4A(3,3,3,3),PIN4B(3,3,3,3),P2A2B(3,3,3,3)
      DIMENSION QAN(3,41),QBN(3,41),QCN(3,41)
      DIMENSION QINAA(3,3),QINBB(3,3),QINCC(3,3),QINAC(3,3),QINCA(3,3)
      DIMENSION QIN4A(3,3,3,3),QIN4B(3,3,3,3),Q2A2B(3,3,3,3)
      DIMENSION FI(3),GI(3,2),GIF(3,2),SURFF(3),SURFC(3)
      DIMENSION MA(9,9),RIG(9,9),TNL(9,9,9,9)
      EXTERNAL FA
      EXTERNAL GA
      EXTERNAL FB
      EXTERNAL FC
      N=3
      A=0.4857D0
      B=0.3229D0
      H=0.0012D0
      E=21.E10
      RO=9.396D0
      NU=0.3D0
      FI(1)=4.73004074649388606D0
c     FI(2)=7.85320462409583753D0
      FI(2)=10.9956078380016709D0
C     FI(4)=14.1371654912574640D0
      FI(3)=17.2787596573994797D0
C     LAMDA=B/A
C     LAMDA=1.D0
      H2=LAMDA*LAMDA
      H4=H2*H2
      DO 301 I=1,N
      GI(I,1)=FA(FI(I))
      GI(I,2)=GA(FI(I))
      GIF(I,1)=FA(FI(I))
      GIF(I,2)=GA(FI(I))
c     GIF(I,1)=-FA(FI(I))
c     GIF(I,2)=Fb(FI(I))
  301 CONTINUE
      CALL CALC(FA,GA,FI,GI,PAN)
```

```
      CALL CALC(FB,FA,FI,GI,PBN)
      CALL CALC(FC,FB,FI,GI,PCN)
      CALL CALC(FA,GA,FI,GIF,QAN)
      CALL CALC(FB,FA,FI,GIF,QBN)
      CALL CALC(FC,FB,FI,GIF,QCN)
C     CALL CALCF(FC,FB,FI,GIF,QAN)
C     CALL CALCF(GA,FC,FI,GIF,QBN)
C     CALL CALCF(FA,GA,FI,GIF,QCN)
      DO 302 I=1,N
      DO 303 K=1,41
      TABC1(K)=PAN(I,K)*PAN(I,K)
      TABF1(K)=QAN(I,K)*QAN(I,K)
  303 CONTINUE
      CALL SOMM(TABC1,SURFC(I))
      SURFC(I)=DSQRT(SURFC(I))
      CALL SOMM(TABF1,SURFF(I))
      SURFF(I)=DSQRT(SURFF(I))
  302 CONTINUE
      DO 304 I=1,N
      DO 305 K=1,41
      PAN(I,K)=PAN(I,K)/SURFC(I)
      PBN(I,K)=PBN(I,K)/SURFC(I)
      PCN(I,K)=PCN(I,K)/SURFC(I)
      QAN(I,K)=QAN(I,K)/SURFF(I)
      QBN(I,K)=QBN(I,K)/SURFF(I)
      QCN(I,K)=QCN(I,K)/SURFF(I)
  305 CONTINUE
  304 CONTINUE
      DO 306 I=1,N
      DO 307 J=1,N
      DO 308 K=1,41
      TABC1(K)=PAN(I,K)*PAN(J,K)
      TABC2(K)=PBN(I,K)*PBN(J,K)*FI(I)*FI(J)
      TABC3(K)=PCN(I,K)*PCN(J,K)*FI(I)*FI(I)*FI(J)*FI(J)
      TABC4(K)=PAN(I,K)*PCN(J,K)*FI(J)*FI(J)
      TABC5(K)=PCN(I,K)*PAN(J,K)*FI(I)*FI(I)
      TABF1(K)=QAN(I,K)*QAN(J,K)
      TABF2(K)=QBN(I,K)*QBN(J,K)*FI(I)*FI(J)
      TABF3(K)=QCN(I,K)*QCN(J,K)*FI(I)*FI(I)*FI(J)*FI(J)
      TABF4(K)=QAN(I,K)*QCN(J,K)*FI(J)*FI(J)
      TABF5(K)=QCN(I,K)*QAN(J,K)*FI(I)*FI(I)
  308 CONTINUE
      CALL SOMM(TABC1,PINAA(I,J))
      CALL SOMM(TABC2,PINBB(I,J))
      CALL SOMM(TABC3,PINCC(I,J))
      CALL SOMM(TABC4,PINAC(I,J))
      CALL SOMM(TABC5,PINCA(I,J))
      CALL SOMM(TABF1,QINAA(I,J))
      CALL SOMM(TABF2,QINBB(I,J))
      CALL SOMM(TABF3,QINCC(I,J))
      CALL SOMM(TABF4,QINAC(I,J))
      CALL SOMM(TABF5,QINCA(I,J))
  307 CONTINUE
  306 CONTINUE
      DO 309 I1=1,N
      DO 310 J1=1,N
      DO 311 I2=1,N
      DO 312 J2=1,N
```

```
      M1=N*(I1-1)+J1
      M2=N*(I2-1)+J2
      MA(M1,M2)=PINAA(I1,I2)*QINAA(J1,J2)
       RIG1=PINCC(I1,I2)*QINAA(J1,J2)
       RIG2=PINCA(I1,I2)*QINAC(J1,J2)
       RIG3=PINAC(I1,I2)*QINCA(J1,J2)
       RIG4=PINAA(I1,I2)*QINCC(J1,J2)
       RIG5=PINBB(I1,I2)*QINBB(J1,J2)
      RIG23=(RIG2+RIG3)/2
       RIG(M1,M2)=H4*RIG1+(2*H2*RIG23)+RIG4-(2*H2*(1-NU)*(RIG23-RIG5))
  312 CONTINUE
  311 CONTINUE
  310 CONTINUE
  309 CONTINUE
      DO 313 I1=1,N
      DO 314 I2=1,N
      DO 315 I3=1,N
      DO 316 I4=1,N
      DO 317 K=1,41
       RIG2=FI(I1)*FI(I2)*FI(I3)*FI(I4)
       RIG3=FI(I3)*FI(I4)
        TABC1(K)=PAN(I1,K)*PAN(I2,K)*PAN(I3,K)*PAN(I4,K)
        TABC2(K)=PBN(I1,K)*PBN(I2,K)*PBN(I3,K)*PBN(I4,K)*RIG2
        TABC3(K)=PAN(I1,K)*PAN(I2,K)*PBN(I3,K)*PBN(I4,K)*RIG3
       TABF1(K)=QAN(I1,K)*QAN(I2,K)*QAN(I3,K)*QAN(I4,K)
        TABF2(K)=QBN(I1,K)*QBN(I2,K)*QBN(I3,K)*QBN(I4,K)*RIG2
       TABF3(K)=QAN(I1,K)*QAN(I2,K)*QBN(I3,K)*QBN(I4,K)*RIG3
  317 CONTINUE
      CALL SOMM(TABC1,PIN4A(I1,I2,I3,I4))
      CALL SOMM(TABC2,PIN4B(I1,I2,I3,I4))
      CALL SOMM(TABC3,P2A2B(I1,I2,I3,I4))
      CALL SOMM(TABF1,QIN4A(I1,I2,I3,I4))
      CALL SOMM(TABF2,QIN4B(I1,I2,I3,I4))
      CALL SOMM(TABF3,Q2A2B(I1,I2,I3,I4))
  316 CONTINUE
  315 CONTINUE
  314 CONTINUE
  313 CONTINUE
      DO 111 I1=1,N
      DO 112 I2=1,N
      DO 113 I3=1,N
      DO 114 I4=1,N
      DO 115 J1=1,N
      DO 116 J2=1,N
      DO 117 J3=1,N
      DO 118 J4=1,N
      M1=N*(I1-1)+J1
      M2=N*(I2-1)+J2
      M3=N*(I3-1)+J3
      M4=N*(I4-1)+J4
       TNL4=PIN4A(I1,I2,I3,I4)*QIN4B(J1,J2,J3,J4)
       TNL2=P2A2B(I3,I4,I1,I2)*Q2A2B(J1,J2,J3,J4)
       TNL3=P2A2B(I1,I2,I3,I4)*Q2A2B(J3,J4,J1,J2)
       TNL1=PIN4A(J1,J2,J3,J4)*QIN4B(I1,I2,I3,I4)
      TNL5=3*(H4*TNL1+(H2*(TNL2+TNL3))+TNL4)
      TNL(M1,M2,M3,M4)=TNL5
  118 CONTINUE
  117 CONTINUE
```

```
116 CONTINUE
115 CONTINUE
114 CONTINUE
113 CONTINUE
112 CONTINUE
111 CONTINUE
   WRITE(IMP,320)
320 FORMAT(4X,////,19X,'NONLINEAR TERMS')
   WRITE(IMP,321)
321 FORMAT(19X,'*****************************',/////)
   WRITE(IMP,322)
322 FORMAT(4X,//,4X,'MODES USED')
   WRITE(IMP,3221)
3221 FORMAT(4X,'*****************************',//)
   DO 323 I=1,N
   WRITE(IMP,324)I,FI(I)
324 FORMAT(7X,' FI(',I1,')= ',F12.8)
323 CONTINUE
   WRITE(IMP,333)
333 FORMAT(19X,/////,'*****************************',/////)
   IMP6=16
   DO 3520 K=1,41
   DXX=0.25D-1
   DS=DFLOAT(K-1)*DXX
    WRITE(IMP6,3521)DS,(PAN(I,K),I=1,3)
3520 CONTINUE
   DO 3522 K=1,41
   DXX=0.25D-1
   DS=DFLOAT(K-1)*DXX
    WRITE(IMP6,3521)DS,(PBN(I,K),I=1,3)
3522 CONTINUE
   DO 3523 K=1,41
   DXX=0.25D-1
   DS=DFLOAT(K-1)*DXX
    WRITE(IMP6,3521)DS,(PCN(I,K),I=1,3)
3523 CONTINUE
3521 FORMAT(4X,F5.3,2X,F9.6,2X,F9.6,2X,F9.6,2X,F9.6,2X,F9.6)
   WRITE(IMP,325)
   WRITE(IMP,3325)
3325 FORMAT(4X,'******************',///////)
325 FORMAT(4X,/////,4X,' MASS MATRIX')
   DO 326 I=1,9
   WRITE(IMP,3326)I
3326 FORMAT(4X,'I= ',I1,/)
    WRITE(IMP,1182)(MA(I,J),J=1,3)
    WRITE(IMP,2182)(MA(I,J),J=4,6)
    WRITE(IMP,3182)(MA(I,J),J=7,9)
326 CONTINUE
   WRITE(IMP,180)
   WRITE(IMP,1180)
1180 FORMAT(4X,'******************',///////)
180 FORMAT(4X,/////,4X,' RIGIDITY MATRIX')
   DO 181 I=1,9
   WRITE(IMP,3326)I
    WRITE(IMP,1182)(RIG(I,J),J=1,3)
    WRITE(IMP,2182)(RIG(I,J),J=4,6)
    WRITE(IMP,3182)(RIG(I,J),J=7,9)
181 CONTINUE
```

```
1182   FORMAT(2X,'J=1,..,3   ','*',F16.8,'*',F16.8,'*',F16.8,'*')
2182   FORMAT(2X,'J=4,..,6   ','*',F16.8,'*',F16.8,'*',F16.8,'*')
3182   FORMAT(2X,'J=7,..,9   ','*',F16.8,'*',F16.8,'*',F16.8,'*')
C    WRITE(IMP,183)
C    WRITE(IMP,1183)
 183  FORMAT(4X,/////,4X,'INTEGRALES PIN4A(I,J,K,L)')
1183  FORMAT(4X,'************************',/////)
C    DO 184 I=1,3
C    DO 185 J=1,3
C    DO 1185 K=1,3
C     WRITE(IMP,4183)I,J,K
4183  FORMAT(4X,//,2X,' I=',I1,'   J=',I1,'   K=',I1)
C     WRITE(IMP,1184)(PIN4A(I,J,K,L),L=1,3)
1184   FORMAT(2X,/,2X,'( L=1,..,3)   :',4X,F16.8,'*',F16.8,'*',F16.8,'*')
C1185 CONTINUE
C 185 CONTINUE
C 184 CONTINUE
C    WRITE(IMP,187)
C    WRITE(IMP,1187)
 187  FORMAT(4X,/////,4X,'INEGRALES PIN4B(I,J,K,L)')
1187  FORMAT(4X,'************************',/////)
C    DO 188 I=1,3
C    DO 189 J=1,3
C    DO 1189 K=1,3
C     WRITE(IMP,4183)I,J,K
C     WRITE(IMP,1184)(PIN4B(I,J,K,L),L=1,3)
C1189 CONTINUE
C 189 CONTINUE
C 188 CONTINUE
C    WRITE(IMP,190)
C    WRITE(IMP,1190)
  190 FORMAT(4X,/////,4X,'INTEGRALES P2A2B(I,J,K,L)')
 1190 FORMAT(4X,'************************',/////)
C    DO 191 I=1,3
CC   DO 192 J=1,3
C    DO 1192 K=1,3
C     WRITE(IMP,4183)I,J,K
C     WRITE(IMP,1184)(P2A2B(I,J,K,L),L=1,3)
C1192 CONTINUE
C 192 CONTINUE
C 191 CONTINUE
C    WRITE(IMP,193)
C    WRITE(IMP,1193)
  193 FORMAT(4X,/////////,4X,' NONLINEAR TERM  TNL(I,J,K,L)')
 1193 FORMAT(4X,'******************',/////////)
C    DO 194 I=1,9
C    DO 195 J=1,9
C    WRITE(IMP,196)I,J
C    WRITE(IMP,1196)
C    DO 197 K=1,9
C    WRITE(IMP,1197)K
 1197 FORMAT(4X,'K=',I1)
C     WRITE(IMP,4182)(TNL(I,J,K,L),L=1,3)
C     WRITE(IMP,5182)(TNL(I,J,K,L),L=4,6)
C     WRITE(IMP,6182)(TNL(I,J,K,L),L=7,9)
C 197 CONTINUE
C 195 CONTINUE
C 194 CONTINUE
```

```
 4182 FORMAT(2X,'L=1,..,3   ','*',F16.8,'*',F16.8,'*',F16.8,'*')
 5182 FORMAT(2X,'L=4,..,6   ','*',F16.8,'*',F16.8,'*',F16.8,'*')
C6182 FORMAT(2X,'L=7,..,9   ','*',F16.8,'*',F16.8,'*',F16.8,'*',/)
  196 FORMAT(4X,///,4X,'I=',I2,4X,'J=',I2,'*')
 1196 FORMAT(4X,'************',///)
      RETURN
      END
```

APPENDIX D
PROGRAM FOR ESTIMATION OF NONLINEAR MODE SHAPES OF FULLY CLAMPED RECTANGULAR PLATES

```
c dataa.for
    implicit double precision (a-h,o-z)
     dimension vmeas(3,11,12),Dmeas(3,11,12),DNmeas(3,11,12)
     1,xx(12),yy(11),dx(11,12),dy(11,12),contn(3,9)
     1,ds(11,12),py(3,11),px(3,12),cont(3,9),err1(9),err2(9)
      open(unit=13,file='measures.dat',status='old')
      open(unit=15,file='funcy.dat',status='old')
      open(unit=14,file='funcx.dat',status='old')
      open(unit=16,file='PEAKD.dat',status='NEW')
      open(unit=17,file='NPEAKD.dat',status='NEW')
     calib=600.*1.06/dsqrt(dble(2))
     read(13,120)(yy(j),j=2,10)
     print*,(yy(j),j=2,10)
     yy(1)=0.
     yy(11)=220.
     read(13,121)(xx(i),i=1,12)
     print*,(xx(i),i=1,12)
     do 11 ia=1,3
     do 10 i=1,12
     vmeas(ia,1,i)=0.
     vmeas(ia,11,i)=0.
     read(13,120)(vmeas(ia,j,i),j=2,10)
     do 230 jk=2,10
    Dmeas(ia,jk,i)=Vmeas(ia,jk,i)/calib
 230 continue
     WRITE(16,220)(Dmeas(ia,j,i),j=2,10)
 220  FORMAT(8x,9F8.3)
  10  continue
  11  continue
     DO 110 IA=1,3
     DO 111 I=2,11
     DO 112 J=2,10
     DNmeas(ia,j,i)=Vmeas(ia,j,i)/Vmeas(ia,6,7)
 112  CONTINUE
     WRITE(17,220)(DNmeas(ia,Jj,i),Jj=2,10)
 111  CONTINUE
 110  CONTINUE
     do 12 i=2,11
     do 13 j=2,10
     dx(j,i)=(xx(i+1)-xx(i-1))/(367.*2.)
     dy(j,i)=(yy(j+1)-yy(j-1))/(220.*2.)
     ds(j,i)=dx(j,i)*dy(j,i)
     print*,dx(j,i)
     print*,dy(j,i)
     print*,ds(j,i)
  13  continue
  12  continue
     do 15 j=2,10
      read(14,122)py(1,j),py(2,j),py(3,j)
      print*,py(1,j),py(2,j),py(3,j)
  15  continue
     do 16 i=2,11
      read(15,122)px(1,i),px(2,i),px(3,i)
      print*,px(1,i),px(2,i),px(3,i)
```

```
16 continue
   do 17 ia=1,3
   do 18 ii=1,3
   do 19 jj=1,3
   im=3*(ii-1)+jj
   teg=0.
   do 20 i=2,11
   do 21 j=2,10
   teg=teg+(px(ii,i)*py(jj,j)*dmeas(ia,j,i)*ds(j,i))
21 continue
20 continue
   cont(ia,im)=teg
   print*,teg
19 continue
18 continue
17 continue
   do 23 ia=1,3
   dnorm=cont(ia,1)
   do 24 im=1,9
   contn(ia,im)=cont(ia,im)/dnorm
212 FORMAT(5F10.6)
24 continue
23 continue
   do 330 ia=1,3
   WRITE(17,212)(CONT(IA,IIM),IIM=1,5)
330 continue
   do 331 ia=1,3
   WRITE(17,212)(CONTn(IA,IIM),IIM=1,5)
331 continue
   do 30 ic=1,5
   err1(ic)=(contn(2,ic)-contn(1,ic))/abs(contn(1,ic))
   err2(ic)=(contn(3,ic)-contn(1,ic))/abs(contn(1,ic))
30 continue
   do 340 ic=1,5
   write(17,213)err1(ic),err2(ic)
340 continue
213 format(2f10.3)
120 format(9f10.0)
121 format(12f10.0)
122 format(12f10.6)
   stop
   end
```

APPENDIX E
PROGRAM FOR EXTRACTION OF MODULUS AND PHASE OF ZOOM OUTPUT PEAKS

```
DIMENSION X(100),Y(100),Z(100),IM(100)
print*,'please give the set number'
/read(nm)
print*,'please give the number of FILES'
/READ(NN)
DO 10 II=1,NN
/READ(IM(II))
10 CONTINUE
print*,'please give the lower freq'
/read(xl)
print*,'please give the upper freq'
/read(xu)
res=(xu-xl)/800
DO 3 IK=1,NN
/KILL(IM(IK)*10,IM(IK)*10+1,IM(IK)*10+2,IM(IK)*10+3,IM(IK)*10+4)
/KILL(IM(IK)*10-1,IM(IK)*10-2)
/conv(IM(IK),IM(IK)*10-2,2,1248)
/conv(IM(IK)*10-2,IM(IK)*10-1,4,1248)
/zoom(im(ik)*10-1,im(ik)*10,1,xl,xu,res)
/MOPH(IM(IK)*10,IM(IK)*10+1,0)
/CONV(IM(IK)*10+1,IM(IK)*10+2,4)
/THRES(IM(IK)*10+2,IM(IK)*10+3,1,0.001,0.001)
/PEAK(IM(IK)*10+3,IM(IK)*10+4,1)
/GIVE(IM(IK)*10+3,-4,V)
/GIVE(IM(IK)*10+4,-1,N)
N=N/2
DO 1 J=1,N
/GIVE(IM(IK)*10+4,J*2,W)
JJ=(W-xl)/V+1
/GIVE(IM(IK)*10+1,JJ*2,X(J))
/GIVE(IM(IK)*10+4,J*2-1,Y(J))
/GIVE(IM(IK)*10+4,J*2,Z(J))
1 CONTINUE
type*,'set no :',nm
TYPE *,'FILE  NO :',im(IK)
TYPE *,'  FREQ          MOD          PHASE'
DO 2 J=1,N
TYPE *,Z(J),Y(J),X(J)
2 CONTINUE
/KILL(IM(IK)*10,IM(IK)*10+1,IM(IK)*10+2,IM(IK)*10+3,IM(IK)*10+4)
/KILL(IM(IK)*10-1,IM(IK)*10-2)
3 CONTINUE
END
```

APPENDIX F

CALCULATION OF THE TENSORS α_{ij}, β_{ij} and γ_{ijkl}

$$\alpha_{ij} = \int_0^{2\pi/\omega} \sin i\omega t \sin j\omega t \, dt = \frac{1}{2} \int_0^{2\pi/\omega} \{-\cos(i + j)\omega t + \cos(i - j)\omega t\} dt$$

$$= \frac{\pi}{\omega} \delta_{ij}$$

$$\beta_{ij} = ij \int_0^{2\pi/\omega} \cos i\omega t \cos j\omega t \, dt = \frac{1}{2} ij \int_0^{2\pi/\omega} \{\cos(i + j)\omega t + \cos(i - j)\omega t\} dt$$

$$= \frac{\pi}{\omega} (\delta_{ij})(ij)$$

$$\gamma_{ijkl} = \int_0^{2\pi/\omega} (\sin i\omega t \sin j\omega t \sin k\omega t \sin l\omega t) \, dt$$

$$= \frac{1}{4} \int_0^{2\pi/\omega} (\cos(i - j)\omega t - \cos(i + j)\omega t)(\cos(k - l)\omega t - \cos(k + l)\omega t) dt$$

$$= \frac{1}{8} \int_0^{2\pi/\omega} \{\cos(i - j + k - l)\omega t + \cos(i - j - k + l)\omega t - \cos(i - j + k + l)\omega t$$

$$- \cos(i - j - k - l)\omega t - \cos(i + j + k - l)\omega t - \cos(i + j - k + l)\omega t$$

$$+ \cos(i + j + k + l)\omega t + \cos(i + j - k - l)\omega t\} dt$$

$$= \frac{1}{4} \frac{\pi}{\omega} \{\delta_{i+k,j+l} + \delta_{i+l,j+k} - \delta_{i+k+l,j} - \delta_{i,j+k+l} - \delta_{i+j+k,l} - \delta_{i+j+l,k}$$

$$+ \delta_{i+j,k+l}\}$$

where $\delta_{\alpha\beta}$ is the Kronecker symbol.

APPENDIX G
ROUTINES USED IN THE HARMONIC DISTORTION ANALYSIS OF CLAMPED-CLAMPED BEAMS

```
C MAIN PROGRAM

      IMPLICIT DOUBLE PRECISION (A-H,O-Z)
      DOUBLE PRECISION X(22),X1(11),F(22),AJINV(22,22),
     1W(2500),
     1omegag(20),a1G(20),a3G(20),a5G(20),a7g(20),a9G(20),a11G(20),
     1RIG(11,11),MA(11,11),RAG(11,11),
     1PA(11,161),PC(11,161),
     1XX1(6),PNL1(40,161),PCNL1(40,161),PNLN1(40,161),
     1XX2(6),PNL2(40,161),PCNL2(40,161),PNLN2(40,161),
     1XX3(6),PNL3(40,161),PCNL3(40,161),PNLN3(40,161),
     1FI(11),FREQ(40),
     1ALPHA(9,9),BETA(9,9),GAMMA(3,3,3,3)
      OPEN(UNIT=13,NAME='dM1P61.DAT',STATUS='NEW')
      OPEN(UNIT=21,NAME='dparaM.DAT',STATUS='NEW')
      OPEN(UNIT=14,NAME='dM1P62.DAT',STATUS='NEW')
      OPEN(UNIT=15,NAME='dM1P63.DAT',STATUS='NEW')
      OPEN(UNIT=16,NAME='dM1P64.DAT',STATUS='NEW')
      OPEN(UNIT=17,NAME='dM1P65.DAT',STATUS='NEW')
      OPEN(UNIT=18,NAME='dM1P66.DAT',STATUS='NEW')
      OPEN(UNIT=19,NAME='dM1P67.DAT',STATUS='NEW')
      OPEN(UNIT=20,NAME='dM1P68.DAT',STATUS='NEW')
     IMP1=13
     IMP2=15
     IMP3=14
     IMP6=16
     IMP7=17
     IMP8=18
     IMP9=19
     IMP=20
c
c    frequencies
c
     omegag(1)=501.6988D0
     omegag(2)=541.1303D0
     omegag(3)=634.8140D0
     omegag(4)=778.8247D0
     omegag(5)=969.2597d0
     omegag(6)=1203.1479D0
     omegag(7)=1478.5200D0
     omegag(8)=1794.1595D0
     omegag(10)=2543.659d0
     omegag(9)=2627.196d0
     omegag(11)=2798.9331d0
     omegag(12)=3448.915233339d0
     omegag(13)=4623.51113D0
c
c   contributions
c
     A1G(1)=0.05D0
     A1G(2)=0.30D0
     A1G(3)=0.55D0
     A1G(4)=0.80D0
```

```
      A1G(5)=1.05D0
      A1G(6)=1.30D0
      A1G(7)=1.55D0
      A1G(8)=1.80D0
      A1G(10)=2.30D0
      A1G(9)=2.35d0
      A1G(11)=2.45d0
      A1G(12)=2.80d0
      A1G(13)=3.35D0
c
c
c
c
      A3G(1)=0.4765D-5
      A3G(2)=0.9941D-3
      A3G(3)=0.5666D-2
      A3G(4)=0.1564D-1
      A3G(5)=0.3111D-1
      A3G(6)=0.5144D-1
      A3G(7)=0.7571D-1
      A3G(8)=0.1029D0
      A3G(10)=0.1637d0
      A3G(9)=0.170136d0
      A3G(11)=0.18305631d0
      A3G(12)=0.22938023d0
      A3G(13)=0.3044629D0
c
c
c
      A5G(1)=0.5944D-6
      A5G(2)=0.1273D-3
      A5G(3)=0.7684D-3
      A5G(4)=0.2289D-2
      A5G(5)=0.4956D-2
      A5G(6)=0.8920D-2
      A5G(7)=0.1422D-1
      A5G(8)=0.2082D-1
      A5G(10)=0.03746d0
      A5G(9)=0.3934d-1
      A5G(12)=0.57747694d-1
      A5G(11)=0.43213361d-1
      A5G(13)=0.83027447D-1
c
c
c
      A7G(1)=0.1374D-6
      A7G(2)=0.2972D-4
      A7G(3)=0.1835D-3
      A7G(4)=0.5642D-3
      A7G(5)=0.1268D-2
      A7G(6)=0.2378D-2
      A7G(7)=0.3954D-2
      A7G(8)=0.6033D-2
      A7G(10)=0.1174d-1
      A7G(9)=0.12417d-1
      A7G(11)=0.13836693d-1
      A7G(12)=0.19380298d-1
      A7G(13)=0.2969788D-1
```

```
c
c
c
      A9G(1)=0.4423D-7
      A9G(2)=0.9617D-5
      A9G(3)=0.6007D-4
      A9G(4)=0.1879D-3
      A9G(5)=0.4310D-3
      A9G(6)=0.8263D-3
      A9G(7)=0.1407D-2
      A9G(8)=0.2200D-2
      A9G(10)=0.004494d0
      A9G(11)=0.53750601d-2
      A9G(9)=0.4778d-2
      A9G(12)=0.77754614d-2
      A9G(13)=0.12485478D-1
c
c
c
      A11G(1)=0.1749D-7
      A11G(2)=0.3815D-5
      A11G(3)=0.2400D-4
      A11G(4)=0.7581D-4
      A11G(5)=0.1761D-3
      A11G(6)=0.3422D-3
      A11G(7)=0.5914D-3
      A11G(8)=0.9391D-3
      A11G(10)=0.00198d0
      A11G(11)=0.23910658d-2
      A11G(9)=0.21119d-2
      A11G(12)=0.35363289d-2
      A11G(13)=0.59778777D-2
c
c
c
      do 444 i=1,9
      do 445 j=1,9
      if(i.eq.j) go to 446
      alpha(i,j)=0d0
  446 alpha(i,i)=dble(1)
      beta(i,j)=dble(i*j)*alpha(i,j)
  445 continue
  444 continue
      do 447 I=1,3
      do 448 j=1,3
      do 449 k=1,3
      do 450 l=1,3
      aa=dble(0)
      aa=alpha(i+k,j+l)+alpha(i+l,j+k)+alpha(i+j,k+l)
      bb=alpha(i,j+k+l)+alpha(j,i+k+l)+alpha(k,i+j+l)+alpha(l,i+j+k)
      gamma(i,j,k,l)=(aa-bb)/DBLE(4)
  450 continue
  449 continue
  448 continue
  447 continue
      write(21,451)
  451 format(4x,/,'kronecker tensor  alpha',/)
      do 452 i=1,3
```

```
      write(21,454)(alpha(i,j),j=1,3)
  452 continue
      write(21,551)
  551 format(4x,/,'mass coupling tensor beta',/)
      do 552 i=1,3
      write(21,454)(beta(i,j),j=1,3)
  552 continue
   454  format(4x,'j=1,..,3',4x,f16.8,4x,f16.8,4x,F16.8)
      write(21,651)
  651 format(4x,/,'non-linear stiffness coupling tensor gamma',/)
      do 652 i=1,3
      do 653 j=1,3
      do 654 k=1,3
      write(21,655)i,j,k
      write(21,674)(gamma(i,j,k,l),l=1,3)
  654 continue
  653 continue
  652 continue
   674  format(4x,'l=1,..,3',4x,f16.8,4x,f16.8,4x,F16.8)
   655 format(/,4x,'  i=',i1,'  j=',i1,'  k=',i1,/)
       CALL PREP(IMP1,IMP6,RIG,RAG,MA,PA,PC,FI)
c      DO 1001 ILK=1,10,2
      ilk=13
      omega=OMEGAG(ilk)
      X1(1)=A1G(ILK)
      X1(2)=0.0d0
      X1(3)=A3G(ILK)
      X1(4)=0.0d0
      X1(5)=A5G(ILK)
      X1(6)=0.0d0
      X1(7)=A7G(ILK)
      X1(8)=0.0d0
      X1(9)=A9G(ILK)
      X1(10)=0.0d0
      X1(11)=A11G(ILK)
      do 667 i=1,22
  667 x(i)=0d0
      N=22
      STEP=0.0015D0
      ACC=0.0000000000000001D0
      MAXFUN=800
      DMAX=10.D0
       CALL NS01A(N,X,X1,F,AJINV,STEP,DMAX,ACC,MAXFUN,1,W,IMP2,
     1omega,MA,RIG,RAG,alpha,beta,gamma,NI,RESID)
       CALL CALFUNBH(N,X,x1,RIG,RAG,MA,F,omega,alpha,beta,gamma,IMP)
      RESID1=0.D0
      DO 875 I=1,22
      RESID1=RESID1+F(I)*F(I)
  875 CONTINUE
      WRITE(IMP3,800)
  800 FORMAT(2X,//,4X,'PREMIER MODE PROPRE NON LINEAIRE'//)
  801  FORMAT(4X,'CALCUL NO : ',I5,4X,'RA= ',F16.8)
      WRITE(IMP3,801)ilK,omega
      WRITE(IMP3,803)x1(1)
      WRITE(IMP3,804)NI
      write(imp3,802)
  802 format(//,4x,'first harmonic space distribution')
  803 FORMAT(4X,'RESULTAT POUR A1 = ',F16.8)
```

```
    write(imp3,10)(i,x1(i),i=1,11)
804  FORMAT(//,4X,'NOMBRE D''ITERATIONS NECESSAIRES : ',I5)
    write(imp3,805)
805  format(//,4x,'second harmonic space distribution')
     WRITE(IMP3,8)(I,X(I),F(I),I=1,11)
    write(imp3,806)
806  format(//,4x,'third harmonic space distribution')
     WRITE(IMP3,8)(I,X(I),F(I),I=12,22)
    WRITE(IMP3,9)RESID1
    do 5005 ilp=1,11
    xx1(ilp)=x1(ilp)
    xx2(ilp)=x(ilp)
    xx3(ilp)=x(ilp+11)
5005 continue
    WRITE(17,9003)ilk,omegag(ilk)
    WRITE(18,9004)ilk,omegag(ilk)
    WRITE(17,9008)
    WRITE(18,9008)
    DO 411 KK=1,161,4
     PNL1(ilK,KK)=0.D0
     PCNL1(ilK,KK)=0.D0
     PNL2(ilK,KK)=0.D0
     PCNL2(ilK,KK)=0.D0
     PNL3(ilK,KK)=0.D0
     PCNL3(ilK,KK)=0.D0
    DO 412 I=1,11
     PNL1(ilK,KK)=PNL1(ilK,KK)+(XX1(I)*PA(I,KK))
     PCNL1(ilK,KK)=PCNL1(ilK,KK)+(XX1(I)*PC(I,KK))
     PNL2(ilK,KK)=PNL2(ilK,KK)+(XX2(I)*PA(I,KK))
     PCNL2(ilK,KK)=PCNL2(ilK,KK)+(XX2(I)*PC(I,KK))
     PNL3(ilK,KK)=PNL3(ilK,KK)+(XX3(I)*PA(I,KK))
     PCNL3(ilK,KK)=PCNL3(ilK,KK)+(XX3(I)*PC(I,KK))
412  CONTINUE
    DS=DBLE(KK-1)/DBLE(160)
     WRITE(17,9002)DS,PNL1(ilK,KK),PNL2(ilK,KK),PNL3(ilK,KK)
     WRITE(18,9002)DS,PCNL1(ilK,KK),PCNL2(ilK,KK),PCNL3(ilK,KK)
411  CONTINUE
    WRITE(20,9005)ilk,omegag(ilk)
    WRITE(20,9008)
    DO 413 KK=1,161,4
    DS=DBLE(KK-1)/DBLE(160)
     PNLN1(ilK,KK)=PNL1(ilK,KK)/PNL1(ilK,81)
     PNLN2(ilK,KK)=PNL2(ilK,KK)/PNL2(ilK,81)
     PNLN3(ilK,KK)=PNL3(ilK,KK)/PNL3(ilK,81)
      WRITE(20,9002)DS,PNLN1(K,KK),PNLN2(K,KK),PNLN3(K,KK)
 413 CONTINUE
1001 continue
   8   FORMAT(//4X,'I',7X,'X(I)',12X,'F(I)'//(I5,2E17.8))
  9  FORMAT(/5X,'LA SOMME DES CARRES EST : ',E17.8//)
  10   FORMAT(//4X,'I',7X,'X(I)',//(I5,E17.8))
9002 FORMAT(4X,F15.4,5X,3F15.8)
9003 FORMAT(2X,'DISPLACEMENT NO:',I2,//,2X,'FREQUENCY:',F13.6)
9004 FORMAT(2X,'CURVATURES NO:',I2,//,2X,'FREQUENCY:',F13.6)
9005 FORMAT(2X,'NORMALIZED DISPT NO:',I2,//,2X,'FREQUENCY:',F13.6)
9008  FORMAT(2X,'ds',19x,'1st ha',17x,'2nd ha',18x,'Third ha')
    STOP
    END
```

ROUTINE CALFUNBH

```
      SUBROUTINE CALFUNBH(N,X,X1,RIG,rag,MA,F,omega,alpha,beta,gamma,IMP)
C     ******************
C     *PROGRAMME .CALFUN*
C     ******************
C
C
C
      IMPLICIT DOUBLE PRECISION (A-H,O-Z)
      DOUBLE PRECISION X(22),F(22),x1(11),
     1A(3,11),D(3,11),DTA(3,11),DTF(3,11),DTM(3,11),
     1MA(11,11),RIG(11,11),rag(11,11),
     1alpha(9,9),beta(9,9),gamma(3,3,3,3)
C
C       DO 9 I=1,11
      A(1,I)=X1(I)
      A(2,I)=X(I)
      A(3,I)=X(11+I)
    9 CONTINUE
C
C
C       DO 112 IR=2,3
      DO 212 Ii=1,11
      DTA(IR,ii)=0.D0
      DO 312 I2=1,11
      DO 412 I3=1,11
      DO 512 I4=1,11
      DO 612 Ir2=1,3
      DO 712 Ir3=1,3
      DO 812 Ir4=1,3
      dta1=0d0
      dta2=0d0
      DTA1=DBLE(4)*A(ir2,i2)*A(ir3,i3)*A(ir4,i4)
      DTA2=rag(ii,i2)*rag(i3,i4)*gamma(ir,ir2,ir3,ir4)
      dta(ir,ii)=dta(ir,ii)+dta1*dta2
  812 CONTINUE
  712 CONTINUE
  612 CONTINUE
  512 CONTINUE
  412 CONTINUE
  312 CONTINUE
  212 CONTINUE
  112 CONTINUE
C
C
C
      DO 113 ir=2,3
      DO 213 ii=1,11
      dtf(ir,ii)=0d0
      DO 313 ir2=1,3
      DO 413 i2=1,11
      DTF(ir,ii)=DTF(ir,ii)+(DBLE(2)*A(ir2,i2)*RIG(ii,i2)*alpha(ir,ir2))
  413 CONTINUE
  313 CONTINUE
  213 CONTINUE
  113 CONTINUE
C
```

```
C
C
      DO 115 ir=2,3
      DO 215 ii=1,11
      dtm(ir,ii)=0d0
      DO 315 ir2=1,3
      DO 415 i2=1,11
      DTm(ir,ii)=DTm(ir,ii)+(DBLE(2)*A(ir2,i2)*ma(ii,i2)*beta(ir,ir2))
  415 CONTINUE
  315 CONTINUE
  215 CONTINUE
  115 CONTINUE
       DO 116 Ir=2,3
      DO 216 Ii=1,11
      D(Ir,ii)=0.D0
      D(Ir,ii)=DTF(Ir,ii)+DTA(Ir,ii)-(omega*DTM(Ir,ii))
  216 CONTINUE
  116 CONTINUE
      DO 117 iI=1,11
      F(iI)=D(2,iI)
      F(iI+11)=D(3,iI)
  117 CONTINUE
      RETURN
      END
```

APPENDIX H
MAIN ROUTINES FOR NONLINEAR ANALYSIS OF LAMINATED PLATES

```
MAIN Program FOR composites
      IMPLICIT DOUBLE PRECISION (A-H,O-Z)
       DOUBLE PRECISION X(8),F(8),AJINV(8,8),W(2500),RF(5),
      1B1(18),RIG(9,9),MA(9,9),TNL(9,9,9,9)
     1,LAMDA,RA
       OPEN(UNIT=13,NAME='comp61.dat',status='new')
       OPEN(UNIT=14,NAME='comp62.dat',status='new')
       OPEN(UNIT=15,NAME='compl63.dat',status='new')
      IMP1=13
      IMP2=15
      IMP3=14
      RF(1)=DBLE(1)/DBLE(5)
      RF(2)=DBLE(2)*RF(1)
      RF(3)=DBLE(3)*RF(1)
      RF(4)=DBLE(4)*RF(1)
      RF(5)=DBLE(5)*RF(1)
c     DO 9001 II=1,5
      LAMDA=0.5D0
C     LAMDA=RF(5)
C     PRINT *,LAMDA
      WRITE(IMP1,4000)LAMDA
      WRITE(IMP2,4000)LAMDA
      WRITE(IMP3,4000)LAMDA
 4000 FORMAT(2X,/////,13X,'LAMDA= ',F12.8,/////)
      CALL PREP(IMP1,RIG,TNL,MA,LAMDA)
       B1(1)=0.005D0
       B1(2)=0.10D0
       B1(3)=0.15D0
       B1(4)=0.20D0
       B1(5)=0.25D0
       B1(6)=0.30D0
       B1(7)=0.35D0
       B1(8)=0.40D0
       B1(9)=0.45D0
       B1(10)=0.50D0
       B1(11)=0.55D0
       B1(12)=0.65D0
       B1(13)=0.75D0
       B1(14)=0.85D0
       B1(15)=0.95D0
       B1(16)=1.05D0
       B1(17)=1.50D0
       B1(18)=2.00D0
       DO  999 K=1,18,18
       IF(K.GT.1) GO TO 810
       X(1)=-0.108D-4
       X(2)=0.732548D-3
       X(3)=0.558D-5
       X(4)=-0.598D-4
       X(5)=-0.108D-4
       X(6)=-0.341D-7
       X(7)=-0.178D-5
       X(8)=-0.107D-7
    810 Y=B1(K)
```

```
C    PRINT *,Y
     N=8
     STEP=0.0015D0
     ACC=0.00000000000000000000001D0
     MAXFUN=800
     DMAX=10.D0
     CALL
NS01A(N,X,F,AJINV,STEP,DMAX,ACC,MAXFUN,0,W,IMP2,Y,MA,RIG,TNL
    1,NI,RA,RESID,LAMDA)
     do 551 iil=1,9
     do 552 ijl=1,9
     do 553 ikl=1,9
     do 554 ill=1,9
     tnl(iil,ijl,ikl,ill)=0.d0
 554 continue
 553 continue
 552 continue
 551 continue
     CALL CALFUN(N,X,RIG,TNL,MA,F,Y,IMP,R,LAMDA)
     RESID1=0.D0
     DO 875 I=1,8
     RESID1=RESID1+F(I)*F(I)
 875 CONTINUE
     WRITE(IMP3,800)
 800 FORMAT(2X,//,4X,'PREMIER MODE PROPRE NON LINEAIRE'//)
 801  FORMAT(4X,'CALCUL NO : ',I5,4X,'RA = ',e17.8)
     WRITE(IMP3,801)K,RA
     WRITE(IMP3,803)Y
 803 FORMAT(4X,'RESULTAT POUR A1 = ',F16.8)
     WRITE(IMP3,804)NI
 804 FORMAT(4X,'NOMBRE D''ITERATIONS NECESSAIRES : ',I3)
      WRITE(IMP3,8)(I,X(I),F(I),I=1,8)
     WRITE(IMP3,9)RESID1
    8  FORMAT(//4X,'I',7X,'X(I)',12X,'F(I)'//(I5,2E17.8))
  9 FORMAT(/5X,'LA SOMME DES CARRES EST : ',E17.8//)
 999 CONTINUE
 9001 CONTINUE
     STOP
     END
     END
      SUBROUTINE CALFUN(N,X,RIG,TNL,MA,F,Y,IMP,R,LAMDA)
C     ********************
C     *PROGRAMME .CALFUN*
C     ********************
C
C
C
      IMPLICIT DOUBLE PRECISION (A-H,O-Z)
      DOUBLE PRECISION X(8),F(8),TNL(9,9,9,9)
     1,A(9),D(9),DTA(9),DTF(9),DTM(9),
     1MA(9,9),RIG(9,9),LAMDA
      A(1)=Y
      DO 9 I=2,N+1
      A(I)=X(I-1)
    9 CONTINUE
C
C
```

```
C
C
C
      TA=0.D0
      DO 110 I1=1,N+1
      DO 115 I2=1,N+1
      DO 114 I3=1,N+1
      DO 334 I4=1,N+1
      TA=TA+(TNL(I1,I2,I3,I4)*A(I1)*A(I2)*A(I3)*A(I4))
  334 CONTINUE
  114 CONTINUE
  115 CONTINUE
  110 CONTINUE
C
C
C
      TF=0.D0
      TM=0.D0
      DO 333 I=1,N+1
      DO 444 J=1,N+1
      TF=TF+(A(I)*A(J)*RIG(I,J))
      TM=TM+(A(I)*A(J)*MA(I,J))
  444 CONTINUE
  333 CONTINUE
C
C
C
CC
      DO 12 I=2,N+1
      DTA(I)=0.D0
   12 CONTINUE
      DO 30 IR=2,N+1
      DO 35 J=1,N+1
      DO 34 K=1,N+1
      DO 29 L=1,N+1
      DTA(IR)=DTA(IR)+(3*A(J)*A(K)*A(L)*TNL(IR,J,K,L))
   29 CONTINUE
   34 CONTINUE
   35 CONTINUE
   30 CONTINUE
C
CC
C
      DO 14 I=2,N+1
      DTF(I)=0.D0
      DO 13 J=1,N+1
      DTF(I)=DTF(I)+2*A(J)*RIG(I,J)
   13 CONTINUE
   14 CONTINUE
C
C
C
      DO  15 I=2,N+1
      DTM(I)=0.D0
      DTM(I)=2*A(I)
   15 CONTINUE
C
C
```

```
C     CALCUL DE D2 , D3 , ... , D9
C
      DO 16 I=2,N+1
      D(I)=0.D0
      D(I)=((DTF(I)+DTA(I))*TM)-(DTM(I)*(TF+TA))
   16 CONTINUE
      DO 17 I=1,N
      J=I+1
      F(I)=D(J)
   17 CONTINUE
      R=(TF+TA)/TM
      RETURN
      END


      SUBROUTINE PREP(IMP,RIG,TNL,MA,LAMDA)
      IMPLICIT DOUBLE PRECISION (A-H,O-Z)
      DOUBLE PRECISION MA,RIG,TAB1,TAB2,TAB3,TAB4,TAB5,PAN
       1,PBN,PCN,TNL,PINAA,PINBB,PINAC,PINCA,PINCC,PIN4A,PIN4B
       1,P2A2B,FI,GI,SURF,NU,LAMDA,H2,H4,PI,Z,SIGNE
      DIMENSION TAB1(41),TAB2(41),TAB3(41)
     1,TAB4(41),TAB5(41),TAB6(41),TAB7(41)
       DIMENSION PAN(3,41),PBN(3,41),PCN(3,41)
       DIMENSION PINAA(3,3),PINBB(3,3),PINCC(3,3)
       dimension PINAC(3,3),PINCA(3,3),pincb(3,3),pinab(3,3)
        DIMENSION PIN4A(3,3,3,3),PIN4B(3,3,3,3),P2A2B(3,3,3,3)
       DIMENSION P3A1b(3,3,3,3),P3b1a(3,3,3,3)
       DIMENSION FI(3),GI(3,2),SURF(3)
       DIMENSION MA(9,9),RIG(9,9),TNL(9,9,9,9)
      EXTERNAL FA
      EXTERNAL GA
      EXTERNAL FB
      EXTERNAL FC
c
c     stiffness coefficients
c
       a11=0.22009d+9/(2.72*7.d+7)
       a12=0.88116d+8/(2.72*7.d+7)
       a22=0.10695D+9/(2.72*7.d+7)
       a66=0.92644D+8/(2.72*7.d+7)
c
c
c
       d11=0.12355d+3/(2.7**3*7.d+1)
       d12=0.58296d+2/(2.7**3*7.d+1)
       d16=-0.D+0
       d22=0.70140d+2/(2.7**3*7.d+1)
       d26=-0.d+0
       d66=0.61088d+2/(2.7**3*7.d+1)
c
c
       N=3
       A=0.4857D0
       B=0.3229D0
       H=0.001D0
       E=21.E10
       RO=9.396D0
       NU=0.3D0
```

```
      FI(1)=4.73004074649388606D0
C     FI(2)=7.85320462409583753D0
      FI(2)=10.9956078380016709D0
C     FI(4)=14.1371654912574640D0
      FI(3)=17.2787596573994797D0
C     LAMDA=B/A
C     LAMDA=1.D0
      H1=lamda
      H2=LAMDA**2
      h3=lamda**3
      H4=lamda**4
      DO 301 I=1,N
      GI(I,1)=FA(FI(I))
      GI(I,2)=GA(FI(I))
  301 CONTINUE
      CALL CALC(FA,GA,FI,GI,PAN)
      CALL CALC(FB,FA,FI,GI,PBN)
      CALL CALC(FC,FB,FI,GI,PCN)
      DO 302 I=1,N
      DO 303 K=1,41
      TAB1(K)=PAN(I,K)*PAN(I,K)
  303 CONTINUE
      CALL SOMM(TAB1,SURF(I))
      SURF(I)=DSQRT(SURF(I))
  302 CONTINUE
      DO 304 I=1,N
      DO 305 K=1,41
      PAN(I,K)=PAN(I,K)/SURF(I)
      PBN(I,K)=PBN(I,K)/SURF(I)
      PCN(I,K)=PCN(I,K)/SURF(I)
  305 CONTINUE
  304 CONTINUE
      DO 306 I=1,N
      DO 307 J=1,N
      DO 308 K=1,41
      TAB1(K)=PAN(I,K)*PAN(J,K)
      TAB2(K)=PBN(I,K)*PBN(J,K)*FI(I)*FI(J)
      TAB3(K)=PCN(I,K)*PCN(J,K)*FI(I)*FI(I)*FI(J)*FI(J)
      TAB4(K)=PAN(I,K)*PCN(J,K)*FI(J)*FI(J)
      TAB5(K)=PCN(I,K)*PAN(J,K)*FI(I)*FI(I)
      TAB6(K)=PCN(I,K)*PbN(J,K)*FI(I)*FI(I)*fi(j)
      TAB7(K)=PaN(I,K)*PbN(J,K)*FI(j)
  308 CONTINUE
      CALL SOMM(TAB1,PINAA(I,J))
      CALL SOMM(TAB2,PINBB(I,J))
      CALL SOMM(TAB3,PINCC(I,J))
      CALL SOMM(TAB4,PINAC(I,J))
      CALL SOMM(TAB5,PINCA(I,J))
      CALL SOMM(TAB6,PINCb(I,J))
      CALL SOMM(TAB7,PINab(I,J))
  307 CONTINUE
  306 CONTINUE
      DO 309 I1=1,N
      DO 310 J1=1,N
      DO 311 I2=1,N
      DO 312 J2=1,N
      M1=N*(I1-1)+J1
      M2=N*(I2-1)+J2
```

```
      MA(M1,M2)=PINAA(I1,I2)*PINAA(J1,J2)
      RIG1=PINCC(I1,I2)*PINAA(J1,J2)
      RIG2=PINCA(I1,I2)*PINAC(J1,J2)
      RIG3=PINAC(I1,I2)*PINCA(J1,J2)
      RIG4=PINAA(I1,I2)*PINCC(J1,J2)
      RIG5=PINBB(I1,I2)*PINBB(J1,J2)
      RIG6=PINcb(I1,I2)*PINaB(J1,J2)
      RIG7=PINcb(I2,I1)*PINab(J2,J1)
      RIG8=PINab(I1,I2)*PINcB(J1,J2)
      RIG9=PINaB(I2,I1)*PINcb(J2,J1)
      RIGx2x2=D11*H4*RIG1
      RIGx2y2=D12*H2*RIG2
      RIGy2x2=D12*H2*RIG3
      RIGy2y2=D22*RIG4
      RIGx2xy=2*D16*H3*RIG6
      RIGxyx2=2*D16*H3*RIG7
      RIGy2xy=2*D26*H1*RIG8
      RIGxyy2=2*D26*H1*RIG9
      RIGxyxy=4*D66*H2*RIG5
      RIGg1=RIGx2x2+RIGx2y2+RIGy2x2+RIGy2y2
      rigg2=RIGx2xy+RIGxyx2+RIGy2xy+RIGxyy2+rigxyxy
      RIG(M1,M2)=rigg1+rigg2
  312 CONTINUE
  311 CONTINUE
  310 CONTINUE
  309 CONTINUE
      DO 313 I1=1,N
      DO 314 I2=1,N
      DO 315 I3=1,N
      DO 316 I4=1,N
      DO 317 K=1,41
      RIG2=FI(I1)*FI(I2)*FI(I3)*FI(I4)
      RIG3=FI(I3)*FI(I4)
       TAB1(K)=PAN(I1,K)*PAN(I2,K)*PAN(I3,K)*PAN(I4,K)
       TAB2(K)=PBN(I1,K)*PBN(I2,K)*PBN(I3,K)*PBN(I4,K)*RIG2
       TAB3(K)=PAN(I1,K)*PAN(I2,K)*PBN(I3,K)*PBN(I4,K)*RIG3
  317 CONTINUE
      CALL SOMM(TAB1,PIN4A(I1,I2,I3,I4))
      CALL SOMM(TAB2,PIN4B(I1,I2,I3,I4))
      CALL SOMM(TAB3,P2A2B(I1,I2,I3,I4))
  316 CONTINUE
  315 CONTINUE
  314 CONTINUE
  313 CONTINUE
      DO 111 I1=1,N
      DO 112 I2=1,N
      DO 113 I3=1,N
      DO 114 I4=1,N
      DO 115 J1=1,N
      DO 116 J2=1,N
      DO 117 J3=1,N
      DO 118 J4=1,N
      M1=N*(I1-1)+J1
      M2=N*(I2-1)+J2
      M3=N*(I3-1)+J3
      M4=N*(I4-1)+J4
       TNL4=PIN4A(I1,I2,I3,I4)*PIN4B(J1,J2,J3,J4)
       TNL2=P2A2B(I3,I4,I1,I2)*P2A2B(J1,J2,J3,J4)
```

```
      TNL3=P2A2B(I1,I2,I3,I4)*P2A2B(J3,J4,J1,J2)
      TNL1=PIN4A(J1,J2,J3,J4)*PIN4B(I1,I2,I3,I4)
     TNLxxxx=A11*H4*TNL1
     TNLyyyy=A22*TNL4
     TNLxxyy=H2*((A12/4)+(a66/2))*TNL2
     TNLyyxx=H2*((A12/2)+(a66/2))*TNL3
     TNL(M1,M2,M3,M4)=TNLXXXX+TNLYYYY+tnlxxyy+TNLYYXX
 118 CONTINUE
 117 CONTINUE
 116 CONTINUE
 115 CONTINUE
 114 CONTINUE
 113 CONTINUE
 112 CONTINUE
 111 CONTINUE
     WRITE(IMP,320)
 320 FORMAT(4X,////,19X,'DONNEES DU CALCUL NON LINEAIRE')
     WRITE(IMP,321)
 321 FORMAT(19X,'*****************************',/////)
     WRITE(IMP,322)
 322 FORMAT(4X,//,4X,'MODES UNIDIMENSIONNELS UTILISES')
     WRITE(IMP,3221)
3221 FORMAT(4X,'*****************************',//)
     DO 323 I=1,N
     WRITE(IMP,324)I,FI(I)
 324 FORMAT(7X,'  FI(',I1,')= ',F12.8)
 323 CONTINUE
     WRITE(IMP,333)
 333 FORMAT(19X,/////,'*****************************',/////)
     IMP6=16
     DO 3520 K=1,41
     DXX=0.25D-1
     DS=DFLOAT(K-1)*DXX
      WRITE(IMP6,3521)DS,(PAN(I,K),I=1,3)
3520 CONTINUE
     DO 3522 K=1,41
     DXX=0.25D-1
     DS=DFLOAT(K-1)*DXX
      WRITE(IMP6,3521)DS,(PBN(I,K),I=1,3)
3522 CONTINUE
     DO 3523 K=1,41
     DXX=0.25D-1
     DS=DFLOAT(K-1)*DXX
      WRITE(IMP6,3521)DS,(PCN(I,K),I=1,3)
3523 CONTINUE
 3521 FORMAT(4X,F5.3,2X,F9.6,2X,F9.6,2X,F9.6,2X,F9.6,2X,F9.6)
     WRITE(IMP,325)
     WRITE(IMP,3325)
3325 FORMAT(4X,'******************',///////)
 325 FORMAT(4X,/////,4X,'MASS')
     DO 326 I=1,9
     WRITE(IMP,3326)I
3326 FORMAT(4X,'I= ',I1,/)
     WRITE(IMP,1182)(MA(I,J),J=1,3)
     WRITE(IMP,2182)(MA(I,J),J=4,6)
     WRITE(IMP,3182)(MA(I,J),J=7,9)
 326 CONTINUE
     WRITE(IMP,180)
```

```
   WRITE(IMP,1180)
1180 FORMAT(4X,'******************',///////)
 180  FORMAT(4X,/////,4X,' RIGIDITY')
   DO 181 I=1,9
   WRITE(IMP,3326)I
    WRITE(IMP,1182)(RIG(I,J),J=1,3)
    WRITE(IMP,2182)(RIG(I,J),J=4,6)
    WRITE(IMP,3182)(RIG(I,J),J=7,9)
 181  CONTINUE
1182   FORMAT(2X,'J=1,..,3   ','*',e16.8,'*',e16.8,'*',e16.8,'*')
2182   FORMAT(2X,'J=4,..,6   ','*',e16.8,'*',e16.8,'*',e16.8,'*')
3182   FORMAT(2X,'J=7,..,9   ','*',e16.8,'*',e16.8,'*',e16.8,'*')
C   WRITE(IMP,183)
C   WRITE(IMP,1183)
 183  FORMAT(4X,/////,4X,'INTEGRALES PIN4A(I,J,K,L)')
1183  FORMAT(4X,'************************',/////)
C   DO 184 I=1,3
C   DO 185 J=1,3
C   DO 1185 K=1,3
C    WRITE(IMP,4183)I,J,K
4183  FORMAT(4X,//,2X,' I=',I1,'   J=',I1,'   K=',I1)
C    WRITE(IMP,1184)(PIN4A(I,J,K,L),L=1,3)
1184   FORMAT(2X,/,2X,'( L=1,..,3)   :',4X,F16.8,'*',F16.8,'*',F16.8,'*')
C1185 CONTINUE
C 185 CONTINUE
C 184 CONTINUE
C   WRITE(IMP,187)
C   WRITE(IMP,1187)
 187  FORMAT(4X,/////,4X,'INEGRALES PIN4B(I,J,K,L)')
1187  FORMAT(4X,'************************',/////)
C   DO 188 I=1,3
C   DO 189 J=1,3
C   DO 1189 K=1,3
C    WRITE(IMP,4183)I,J,K
C    WRITE(IMP,1184)(PIN4B(I,J,K,L),L=1,3)
C1189 CONTINUE
C 189 CONTINUE
C 188 CONTINUE
C   WRITE(IMP,190)
C   WRITE(IMP,1190)
  190 FORMAT(4X,/////,4X,'INTEGRALES P2A2B(I,J,K,L)')
 1190 FORMAT(4X,'************************',/////)
C   DO 191 I=1,3
CC   DO 192 J=1,3
C   DO 1192 K=1,3
C    WRITE(IMP,4183)I,J,K
C    WRITE(IMP,1184)(P2A2B(I,J,K,L),L=1,3)
C1192 CONTINUE
C 192 CONTINUE
C 191 CONTINUE
C   WRITE(IMP,193)
C   WRITE(IMP,1193)
  193 FORMAT(4X,/////////,4X,'TERME NON LINEAIRE  TNL(I,J,K,L)')
 1193 FORMAT(4X,'******************',/////////)
C   DO 194 I=1,9
C   DO 195 J=1,9
C   WRITE(IMP,196)I,J
C   WRITE(IMP,1196)
```

```
C    DO 197 K=1,9
C    WRITE(IMP,1197)K
 1197 FORMAT(4X,'K=',I1)
C     WRITE(IMP,4182)(TNL(I,J,K,L),L=1,3)
C     WRITE(IMP,5182)(TNL(I,J,K,L),L=4,6)
C     WRITE(IMP,6182)(TNL(I,J,K,L),L=7,9)
C 197 CONTINUE
C 195 CONTINUE
C 194 CONTINUE
  4182  FORMAT(2X,'L=1,..,3    ','*',F16.8,'*',F16.8,'*',F16.8,'*')
  5182  FORMAT(2X,'L=4,..,6    ','*',F16.8,'*',F16.8,'*',F16.8,'*')
C6182  FORMAT(2X,'L=7,..,9    ','*',F16.8,'*',F16.8,'*',F16.8,'*',/)
   196  FORMAT(4X,///,4X,'I=',I2,4X,'J=',I2,'*')
 1196 FORMAT(4X,'************',///)
     RETURN
     END
```

APPENDIX I

COMPARISON OF RESULTS FROM NONLINEAR ANALYSIS OF COMPOSITE PLATES FOR SMALL AMPLITUDES AND PREVIOUS LINEAR RESULTS

In this appendix, a comparison is made of the linear natural frequency of a laminated plate estimated in E.S.D.U. 83036 and the nonlinear natural frequency obtained here for small amplitudes

Input to lami (plate lay-up and layers characteristics)

```
 16,1
0
0,45.
1.7E-4,1.73E+11,7.2E+9,3.76e+9,0.290
0,-45.
1.7E-4,1.73E+11,7.2E+9,3.76e+9,0.290
0,0.
1.7E-4,1.73E+11,7.2E+9,3.76e+9,0.290
0,-45.
1.7E-4,1.73E+11,7.2E+9,3.76e+9,0.290
0,45.
1.7E-4,1.73E+11,7.2E+9,3.76e+9,0.290
0,-45.
1.7E-4,1.73E+11,7.2E+9,3.76e+9,0.290
0,0.
1.7E-4,1.73E+11,7.2E+9,3.76e+9,0.290
0,45.
1.7E-4,1.73E+11,7.2E+9,3.76e+9,0.290
```

OUTPUT OF LAMI

SYMMETRIC LAMINATE 16 LAYERS

PLATE CONSTRUCTION

LAYER NO.	LAYER ANGLE	LAYER THICKNESS	DISTANCE FROM REF. PLANE,BETA)	E(ALPHA) (ALPHA-BETA)	E(BETA)	G(ALPHA- POISSONS RATIO
1	45.0	0.1700E-03	0.1275E-02	0.1730E+12	0.7200E+10	0.3760E+10 0.290
2	-45.0	0.1700E-03	0.1105E-02	0.1730E+12	0.7200E+10	0.3760E+10 0.290
3	0.0	0.1700E-03	0.9350E-03	0.1730E+12	0.7200E+10	0.3760E+10 0.290
4	-45.0	0.1700E-03	0.7650E-03	0.1730E+12	0.7200E+10	0.3760E+10 0.290
5	45.0	0.1700E-03	0.5950E-03	0.1730E+12	0.7200E+10	0.3760E+10 0.290
6	-45.0	0.1700E-03	0.4250E-03	0.1730E+12	0.7200E+10	0.3760E+10 0.290
7	0.0	0.1700E-03	0.2550E-03	0.1730E+12	0.7200E+10	0.3760E+10 0.290
8	45.0	0.1700E-03	0.8500E-04	0.1730E+12	0.7200E+10	0.3760E+10 0.290
9	45.0	0.1700E-03	-.8500E-04	0.1730E+12	0.7200E+10	0.3760E+10 0.290
10	0.0	0.1700E-03	-.2550E-03	0.1730E+12	0.7200E+10	0.3760E+10 0.290
11	-45.0	0.1700E-03	-.4250E-03	0.1730E+12	0.7200E+10	0.3760E+10 0.290
12	45.0	0.1700E-03	-.5950E-03	0.1730E+12	0.7200E+10	0.3760E+10 0.290
13	-45.0	0.1700E-03	-.7650E-03	0.1730E+12	0.7200E+10	0.3760E+10 0.290

```
14    0.0 0.1700E-03 -.9350E-03 0.1730E+12 0.7200E+10 0.3760E+10  0.290
15  -45.0 0.1700E-03 -.1105E-02 0.1730E+12 0.7200E+10 0.3760E+10  0.290
16   45.0 0.1700E-03 -.1275E-02 0.1730E+12 0.7200E+10 0.3760E+10  0.290

 IN-PLANE STIFFNESS SUB-MATRIX A

0.22009E+09 0.88116E+08 0.00000E+00
0.88116E+08 0.10695E+09 0.00000E+00
0.00000E+00 0.00000E+00 0.92644E+08

 COUPLED IN-PLANE AND FLEXURAL STIFFNESS SUB MATRIXB,

0.00000E+00 0.00000E+00 0.00000E+00
0.00000E+00 0.00000E+00 0.00000E+00
0.00000E+00 0.00000E+00 0.00000E+00

 FLEXURAL STIFFNESS SUB-MATRIX D

0.12355E+03 0.58296E+02 0.00000E+00
0.58296E+02 0.70140E+02 0.00000E+00
0.00000E+00 0.00000E+00 0.61088E+02

 THE PLATE STIFFNESS MATRICES SATISFY THE CONDITIONS FOR SPECIAL
ORTHORTROPY
 APPARENT ELASTIC PROPERTIES
 E(ALPHA)=0.5422E+11  E(BETA)=0.2635E+11  G(ALPHA-BETA)0.3406E+11
 POISSONS RATIO(BETA-ALPHA)=0.8239
 POISSONS RATIO(BETA-ALPHA)=0.4004
 PLATE THICKNESS0.2720E-02
```

The output of LAMI is put in the routine PREPC listed in APPENDIX I1 to calculate the nonlinear natural frequencies and mode shapes contributions of the C.F.R.P. plate considered.

The calculated value of the parameter ω^* is $\omega^*=37.6319$. Substituting this value in Equation (9.51), in which E is replaced by the normalisation value used in Equations (9.44) and (9.45), the circular frequency ω can be obtained as :

$$\omega^2 = \frac{7\ 10^{10}\ 2.72^2\ 10^{-6}\ 37.6319}{1540.0.15^4}$$

which leads to the frequency f

$$f=\frac{\omega}{2\pi} = 795.7 \text{ Hz}$$

which is in good agreement with the value of 792.9 Hz given in [9.9]

APPENDIX J

CHARACTERISTICS USED IN NONLINEAR ANALYSIS OF THE CFRP PLATES CONSIDERED IN TABLE (9)

INPUT TO LAMI 8,1
0
0,90.
0.000125,1.205e+11,9.63e+9,3.58e+9,0.32
0,-45.
0.000125,1.205e+11,9.63e+9,3.58e+9,0.32
0,45.
0.000125,1.205e+11,9.63e+9,3.58e+9,0.32
0,0.
0.000125,1.205e+11,9.63e+9,3.58e+9,0.32

OUTPUT OF LAMI

SYMMETRIC LAMINATE 8 LAYERS

PLATE CONSTRUCTION

LAYER NO.	LAYER ANGLE	LAYER THICKNESS	DISTANCE FROM REF. PLANE	E(ALPHA)	E(BETA)	G(ALPHA-BETA)	POISSONS RATIO (ALPHA-BETA)
1	90.0	0.1250E-03	0.4375E-03	0.1205E+12	0.9630E+10	0.3580E+10	0.320
2	-45.0	0.1250E-03	0.3125E-03	0.1205E+12	0.9630E+10	0.3580E+10	0.320
3	45.0	0.1250E-03	0.1875E-03	0.1205E+12	0.9630E+10	0.3580E+10	0.320
4	0.0	0.1250E-03	0.6250E-04	0.1205E+12	0.9630E+10	0.3580E+10	0.320
5	0.0	0.1250E-03	-.6250E-04	0.1205E+12	0.9630E+10	0.3580E+10	0.320
6	45.0	0.1250E-03	-.1875E-03	0.1205E+12	0.9630E+10	0.3580E+10	0.320
7	-45.0	0.1250E-03	-.3125E-03	0.1205E+12	0.9630E+10	0.3580E+10	0.320
8	90.0	0.1250E-03	-.4375E-03	0.1205E+12	0.9630E+10	0.3580E+10	0.320

IN-PLANE STIFFNESS SUB-MATRIX A

0.51768E+08 0.16941E+08 0.00000E+00
0.16941E+08 0.51768E+08 0.00000E+00
0.00000E+00 0.00000E+00 0.17414E+08

COUPLED IN-PLANE AND FLEXURAL STIFFNESS SUB MATRIXB,

0.00000E+00 0.00000E+00 0.00000E+00
0.00000E+00 0.00000E+00 0.00000E+00
0.00000E+00 0.00000E+00 0.00000E+00

FLEXURAL STIFFNESS SUB-MATRIX D

0.19102E+01 0.11956E+01 -.43666E+00
0.11956E+01 0.71501E+01 -.43666E+00
-.43666E+00 -.43666E+00 0.12350E+01

THE PLATE STIFFNESS MATRICES DO NOT SATISFY THE CONDITIONS FOR SPECIAL ORTHOTROPY
APPARENT ELASTIC PROPERTIES
E(ALPHA)=0.4622E+11 E(BETA)=0.4622E+11 G(ALPHA-BETA)0.1741E+11
POISSONS RATIO(BETA-ALPHA)=0.3272
POISSONS RATIO(BETA-ALPHA)=0.3272
PLATE THICKNESS0.1000E-02

APPENDIX K

DETAILS CONCERNING THE SUMMATION CONVENTION USED IN CHAPTERS II, IV, V AND IX

The usual summation convention, called Einstein's convention, is very useful for simplifying the writing of complex algebraic expressions, involving a summation of products, whose factors are dependent on one, two or more indices varying over a given range 1 to n, n being a given integer number.

According to this convention, if an index i appears in two factors of an algebraic expression, this means implicitly that this expression involves a summation of all the products obtained by giving to the index i all the integer values of the range 1 to n. This permits avoidance of the use of one sign Σ for each index involved, which makes the formula much easier to write and to read. For example, using this convention, the sum

$$V_b = \sum_{i=1}^{n} \sum_{j=1}^{n} a_i a_j k_{ij} \tag{K.1}$$

for the expression of the classical bending strain energy is written as:

$$V_b = a_i a_j k_{ij} \tag{K.2}$$

Now, let us use this convention to obtain, for example, expression (4.9) for the rigidity tensor k_{ij} of a beam. In order to substitute the transverse displacement expression (2.2) into the bending strain energy expression for a beam, (4.1). Notice first that:

$$\left(\frac{\partial^2 w}{\partial x^2}\right)^2 = \left(\frac{\partial^2 w}{\partial x^2}\right)\left(\frac{\partial^2 w}{\partial x^2}\right) \tag{K.3}$$

Also, $\frac{\partial^2 w}{\partial x^2}$ can be written either as:

$$\frac{\partial^2 w}{\partial x^2} = a_i \frac{\partial^2 w_i}{\partial x^2} \tag{K.4}$$

or

$$\frac{\partial^2 w}{\partial x^2} = a_j \frac{\partial^2 w_j}{\partial x^2} \tag{K.5}$$

as in both formulae (K.4) and (K.5) the index is summed over 1 to n. Substituting equations (K.4) and (K.5) in (K.3) and then in (4.1) leads to

$$V_b = \frac{1}{2} \int_0^L EI\, a_i \left(\frac{\partial^2 w_i}{\partial x^2}\right) a_j \left(\frac{\partial^2 w_j}{\partial x^2}\right) dx \qquad \text{(K.6)}$$

in which both indices are summed over 1 to n and it is obvious that equation (K.6) can be written as

$$V_b = a_i a_j \int_0^L \frac{1}{2} EI \frac{\partial^2 w_i}{\partial x^2} \frac{\partial^2 w_j}{\partial x^2} \qquad \text{(K.7)}$$

in which the indices i and j are still repeated and hence summed over 1 to n. The identification of (K.7) with (K.2) leads obviously to (4.9).

Plate	E (N/m^2) ($\times 10^{10}$)	ρ kg/m^3	ν	a (mm)	b(mm)	α	H (mm)	ω^*	f_l^1 (Hz)
Steel (plate 1)	21	9396	0.3	486	322.9	0.66	1.20	27.010	77.54
Al * (plates 2 & 3)	7	2778	0.34	367	220	0.60	1.06	25.89	139.07
Al* (plate 4)	7	2778	0.34	367	220	0.60	1.16	25.89	152.20
Al* (plate 5)	7	2778	0.34	367	220	0.60	0.51	25.89	66.91

Table 3.1. Mechanical and geometrical characteristics of the isotropic plates tested.

* Aluminium alloy DTDS070

i	v_i
1	4.73004075
3	10.99560784
5	17.27875966
7	23.56194490
9	29.84513021
11	36.12831552

Table (4.1.1): Symmetric eigenfunction parameters for a clamped-clamped beam.

i	v_i
2	7.85320462
4	14.13716549
6	20.42035225
8	26.70353756
10	32.98672286
12	39.26990817

Table (4.1.2): Antisymmetric eigenfunction parameters for a clamped-clamped beam.

$\left(\frac{\omega^*_{nl}}{\omega^*_1}\right)$	a_1	a_3	a_5	a_7	a_9	a_{11}
1.001	.5000E-01	.4765E-05	.5944E-06	.1374E-06	.4423E-07	.1749E-07
1.005	.1000E+00	.3801E-04	.4752E-05	.1099E-05	.3540E-06	.1400E-06
1.018	.2000E+00	.3004E-03	.3790E-04	.8798E-05	.2839E-05	.1124E-05
1.040	.3000E+00	.9941E-03	.1273E-03	.2972E-04	.9617E-05	.3815E-05
1.069	.4000E+00	.2295E-02	.2997E-03	.7050E-04	.2291E-04	.9108E-05
1.106	.5000E+00	.4337E-02	.5803E-03	.1378E-03	.4499E-04	.1795E-04
1.148	.6000E+00	.7213E-02	.9921E-03	.2382E-03	.7824E-04	.3131E-04
1.196	.7000E+00	.1097E-01	.1556E-02	.3783E-03	.1250E-03	.5025E-04
1.247	.8000E+00	.1564E-01	.2289E-02	.5642E-03	.1879E-03	.7581E-04
1.303	.9000E+00	.2119E-01	.3207E-02	.8021E-03	.2691E-03	.1091E-03
1.361	.1000E+01	.2760E-01	.4322E-02	.1097E-02	.3713E-03	.1513E-03
1.422	.1100E+01	.3481E-01	.5642E-02	.1456E-02	.4967E-03	.2035E-03
1.550	.1300E+01	.5144E-01	.8920E-02	.2378E-02	.8263E-03	.3422E-03
1.617	.1400E+01	.6073E-01	.1088E-01	.2950E-02	.1035E-02	.4310E-03
1.684	.1500E+01	.7058E-01	.1306E-01	.3599E-02	.1275E-02	.5341E-03
1.753	.1600E+01	.8095E-01	.1544E-01	.4329E-02	.1548E-02	.6526E-03
1.823	.1700E+01	.9177E-01	.1803E-01	.5140E-02	.1856E-02	.7873E-03
1.893	.1800E+01	.1030E+00	.2082E-01	.6033E-02	.2200E-02	.9391E-03
1.964	.1900E+01	.1146E+01	.2380E-01	.7010E-02	.2582E-02	.1109E-02
2.036	.2000E+01	.1265E+00	.2696E-01	.8069E-02	.3001E-02	.1297E-02

Table (4.2.1): **First nonlinear mode shape.** Summary of numerical results from solution of the nonlinear algebraic equations. Model I.

$\left(\frac{\omega^*_{nl}}{\omega^*_1}\right)^2$	a_2	a_4	a_6	a_8	a_{10}	a_{12}
1.002	.5000E-01	.1225E-04	.2313E-05	.6742E-06	.2509E-06	.1129E-06
1.008	.1000E+00	.9739E-04	.1846E-04	.5392E-05	.2009E-05	.9045E-06
1.033	.2000E+00	.7600E-03	.1464E-03	.4307E-04	.1611E-04	.7271E-05
1.072	.3000E+00	.2466E-02	.4873E-03	.1450E-03	.5456E-04	.2472E-04
1.124	.4000E+00	.5547E-02	.1133E-02	.3420E-03	.1298E-03	.5914E-04
1.187	.5000E+00	.1018E-01	.2159E-02	.6636E-03	.2544E-03	.1167E-03
1.258	.6000E+00	.1639E-01	.3624E-02	.1136E-02	.4406E-03	.2036E-03
1.337	.7000E+00	.2413E-01	.5563E-02	.1783E-02	.7001E-03	.3261E-03
1.421	.8000E+00	.3325E-01	.7998E-02	.2621E-02	.1044E-02	.4904E-03
1.510	.9000E+00	.4361E-01	.1093E-01	.3666E-02	.1480E-02	.7022E-03
1.603	.1000E+01	.5502E-01	.1435E-01	.4925E-02	.2018E-02	.9666E-03
1.699	.1100E+01	.6734E-01	.1823E-01	.6402E-02	.2662E-02	.1288E-02
1.797	.1200E+01	.8041E-01	.2254E-01	.8098E-02	.3417E-02	.1670E-02
1.897	.1300E+01	.9410E-01	.2726E-01	.1001E-01	.4286E-02	.2117E-02
1.998	.1400E+01	.1083E+00	.3233E-01	.1212E-01	.5268E-02	.2629E-02
2.101	.1500E+01	.1229E+00	.3774E-01	.1444E-01	.6363E-02	.3208E-02
2.206	.1600E+01	.1379E+00	.4343E-01	.1694E-01	.7570E-02	.3855E-02
2.311	.1700E+01	.1532E+00	.4939E-01	.1961E-01	.8883E-02	.4570E-02
2.418	.1800E+01	.1686E+00	.5557E-01	.2245E-01	.1030E-01	.5352E-02
2.525	.1900E+01	.1843E+00	.6194E-01	.2543E-01	.1182E-01	.6199E-02

Table (4.2.2): **Second nonlinear mode shape.** Summary of numerical results from solution of the nonlinear algebraic equations. Model I.

$\left(\frac{\omega^*_{nl}}{\omega^*_1}\right)_3$	a_1	a_3	a_5	a_7	a_9	a_{11}
1.003	-0.3820E-04	0.50E-01	.1812E-04	.4350E-05	.1489E-05	.6165E-06
1.010	-0.3020E-03	0.10E+00	.1437E-03	.3467E-04	.1190E-04	.4932E-05
1.039	-0.2309E-02	0.20E+00	.1109E-02	.2732E-03	.9463E-04	.3945E-04
1.086	-0.7260E-02	0.30E+00	.3539E-02	.8996E-03	.3163E-03	.1330E-03
1.149	-0.1572E-01	0.40E+00	.7798E-02	.2062E-02	.7393E-03	.3145E-03
1.224	-0.2766E-01	0.50E+00	.1398E-01	.3864E-02	.1417E-02	.6111E-03
1.309	-0.4270E-01	0.60E+00	.2199E-01	.6360E-02	.2390E-02	.1047E-02
1.403	-0.6030E-01	0.70E+00	.3160E-01	.9561E-02	.3687E-02	.1642E-02
1.504	-0.7994E-01	0.80E+00	.4255E-01	.1344E-01	.5321E-02	.2410E-02
1.610	-0.1011E+00	0.90E+00	.5458E-01	.1795E-01	.7291E-02	.3360E-02
1.721	-0.1235E+00	0.10E+01	.6745E-01	.2303E-01	.9586E-02	.4494E-02
1.835	-0.1468E+00	0.11E+01	.8098E-01	.2860E-01	.1219E-01	.5811E-02
1.952	-0.1707E+00	0.12E+01	.9499E-01	.3458E-01	.1507E-01	.7305E-02
2.072	-0.1951E+00	0.13E+01	.1094E+00	.4092E-01	.1820E-01	.8964E-02
2.193	-0.2199E+00	0.14E+01	.1240E+00	.4755E-01	.2156E-01	.1078E-01
2.316	-0.2449E+00	0.15E+01	.1388E+00	.5441E-01	.2511E-01	.1273E-01
2.441	-0.2700E+00	0.16E+01	.1538E+00	.6146E-01	.2882E-01	.1481E-01
2.567	-0.2953E+00	0.17E+01	.1688E+00	.6865E-01	.3268E-01	.1701E-01

Table (4.2.3): **Third nonlinear mode shape.** Summary of numerical results from solution of the nonlinear algebraic equations. Model I.

Curve no.	w^*_{max}	$\left(\frac{\omega^*_{nl}}{\omega^*_1}\right)$
1	0.079	1.001
2	0.789	1.106
3	1.554	1.361
4	2.297	1.684
5	3.028	2.036

Table (4.3.1): Maximum normalised amplitude and nonlinear to linear frequency ratios corresponding to the mode shapes and curvatures plotted in figures (4.4.1) and (4.5.1).

Curve no.	w^*_{max}	$\left(\frac{\omega^*_{nl}}{\omega^*_1}\right)^2$
1	0.075	1.002
2	0.750	1.187
3	1.488	1.603
4	2.217	2.101
5	2.944	2.633

Table (4.3.2): Maximum normalised amplitude and nonlinear to linear frequency ratios corresponding to the mode shapes and curvatures plotted in figures (4.4.2) and (4.5.2).

Curve no.	w^*_{max}	$\left(\frac{\omega^*_{nl}}{\omega^*_1}\right)^2$
1	0.070	1.002
2	0.732	1.223
3	1.532	1.721
4	2.361	2.316

Table (4.3.3): Maximum normalised amplitude and nonlinear to linear frequency ratios corresponding to the mode shapes and curvatures plotted in figures (4.4.3) and (4.5.3).

w^*_{max}	1.2233	0.7191	3.4069
$\frac{\omega^*_{nl}}{\omega^*_l}$	1.0027	1.0893	2.163
a_{11}	0.05	0.3	1.5
a_{12}	-0.7181E-11	-0.5932E-10	-0.6199E-09
a_{13}	0.2870E-03	0.3763E-02	0.6781E-01
a_{14}	-0.3344E-12	-0.4697E-11	-0.1195E-09
a_{15}	0.4128E-04	0.1182E-02	0.4425E-01
a_{21}	-0.3767E-10	-0.2079E-09	-0.9646E-09
a_{22}	-0.3550E-15	-0.1065E-16	0.4235E-17
a_{23}	-0.3916E-12	-0.3997E-11	-0.5604E-10
a_{24}	0.1875E-15	-0.4086E-17	-0.1299E-17
a_{25}	-0.6216E-13	-0.1114E-11	-0.3136E-10
a_{31}	0.1688E-02	0.1724E-01	0.2156E+00
a_{32}	0.8174E-13	-0.2132E-11	-0.1081E-09
a_{33}	-0.9539E-04	0.6749E-04	0.3352E-01
a_{34}	0.5419E-13	0.1010E-11	-0.1960E-11
a_{35}	-0.1959E-04	-0.3164E-03	-0.1273E-02
a_{41}	-0.2333E-11	-0.1736E-10	-0.1587E-09
a_{42}	0.1177E-15	-0.2700E-17	-0.1625E-18
a_{43}	0.1328E-12	-0.1526E-14	-0.2126E-10

a_{44}	0.6341E-16	-0.3852E-17	0.1087E-17
a_{45}	0.3322E-13	0.1759E-12	-0.4603E-11
a_{51}	0.2660E-03	0.2375E-02	0.4858E-01
a_{52}	0.8316E-13	0.1806E-12	-0.2659E-10
a_{53}	-0.5795E-04	-0.3735E-03	0.1058E-01
a_{54}	0.3492E-13	0.1467E-12	-0.4010E-12
a_{55}	-0.1462E-04	-0.7507E-04	0.1114E-03

Table (5.1) :First nonlinear mode shape of a fully clamped rectangular plate $\alpha = 0.6$.
Typical numerical results obtained using 25 basic functions.

	$\frac{\omega^*_{nl}}{\omega^*_l}$	a_{11}	a_{13}	a_{15}	a_{31}	a_{33}	a_{35}	a_{51}	a_{53}	a_{55}
(a)	35.99	1	0.0141	0.0021	0.0141	-0.0030	-0.0009	0.0021	-0.0009	-0.0004
(b)	36.0877	1	0.0142	0.0020	0.0142	-0.0031	-0.0009	-0.0020	-0.0009	-0.0004

Table (5.2) Comparison of contribution coefficients to the first mode shape of a fully clamped square plate: $\alpha = 1.0$

(a) previous results from linear analysis [5.2]

(b) present results obtained from nonlinear analysis for $w^*_{max}=0.12$

aspect ratio α	0.2	0.4	0.6	0.8	1
(a) ω^*_l	22.6325	23.6438	25.8890	29.8881	35.9852
(b) ω^*_{nl}	22.6366	23.6485	25.8942	29.8943	35.9926

Table (5.3) Comparison of nondimensional frequency parameters obtained here for small amplitudes and various aspect ratios with previous linear results

(a) Values published in [5.2] from [5.6]

(b) Values obtained from solutions of nonlinear algebraic equations for $a_{11}=0.05$

w^*_{max}	ω^*_{nl}/ω^*_l	a_{11}	a_{13}	a_{15}	a_{31}	a_{33}	a_{35}	a_{51}	a_{53}	a_{55}
0.1172	1.0027	0.05	0.4072E-04	0.8789E-05	0.5242E-02	-0.1478E-05	-0.1073E-05	0.1283E-02	-0.7878E-05	-0.1125E-05
0.2288	1.0104	0.10	0.1389E-03	0.4603E-04	0.1334E-01	0.6017E-05	-0.4625E-05	0.2897E-02	-0.1484E-04	-0.2918E-05
0.3339	1.0228	0.15	0.3426E-03	0.1367E-03	0.2507E-01	0.3399E-04	-0.7482E-05	0.5307E-02	-0.1703E-04	-0.7333E-05
0.4353	1.0392	0.20	0.6904E-03	0.3026E-03	0.3958E-01	0.9488E-04	-0.2398E-05	0.8850E-02	-0.7724E-05	-0.1545E-04
0.5355	1.0596	0.25	0.1212E-02	0.5633E-03	0.5568E-01	0.1996E-03	0.1807E-04	0.1354E-01	0.2063E-04	-0.2586E-04
0.6360	1.0833	0.30	0.1928E-02	0.9357E-03	0.7251E-01	0.3568E-03	0.5986E-04	0.1916E-01	0.7469E-04	-0.3547E-04
0.7373	1.1102	0.35	0.2848E-02	0.1433E-02	0.8957E-01	0.5723E-03	0.1274E-03	0.2545E-01	0.1594E-03	-0.4085E-04
0.8394	1.1399	0.40	0.3971E-02	0.2066E-02	0.1066E+00	0.8500E-03	0.2241E-03	0.3218E-01	0.2780E-03	-0.3904E-04
0.9423	1.1722	0.45	0.5292E-02	0.2841E-02	0.1236E+00	0.1192E-02	0.3527E-03	0.3916E-01	0.4322E-03	-0.2774E-04
1.0457	1.2066	0.50	0.6797E-02	0.3760E-02	0.1404E+00	0.1597E-02	0.5149E-03	0.4629E-01	0.6224E-03	-0.5264E-05
1.1495	1.2430	0.55	0.8469E-02	0.4826E-02	0.1571E+00	0.2064E-02	0.7125E-03	0.5347E-01	0.8481E-03	0.2954E-04
1.3579	1.3207	0.65	0.1224E-01	0.7383E-02	0.1902E+00	0.3174E-02	0.1217E-02	0.6787E-01	0.1401E-02	0.1389E-03
1.5671	1.4038	0.75	0.1647E-01	0.1048E-01	0.2228E+00	0.4489E-02	0.1870E-02	0.8218E-01	0.2075E-02	0.3035E-03
1.7769	1.4912	0.85	0.2102E-01	0.1405E-01	0.2553E+00	0.5972E-02	0.2669E-02	0.9634E-01	0.2853E-02	0.5236E-03
1.9871	1.5820	0.95	0.2579E-01	0.1805E-01	0.2875E+00	0.7589E-02	0.3605E-02	0.1104E+00	0.3715E-02	0.7976E-03
2.1976	1.6756	1.05	0.3071E-01	0.2240E-01	0.3196E+00	0.9305E-02	0.4669E-02	0.1243E+00	0.4644E-02	0.1123E-02
3.1484	2.1219	1.50	0.5350E-01	0.4484E-01	0.4636E+00	0.1766E-01	0.1068E-01	0.1858E+00	0.9279E-02	0.3120E-02
4.2083	2.6489	2.00	0.7877E-01	0.7225E-01	0.6227E+00	0.2724E-01	0.1871E-01	0.2531E+00	0.1469E-01	0.6018E-02

Table (5.4) Contribution coefficients to the first nonlinear mode shape of a fully clamped rectangular plate: $\underline{\alpha = 0.2}$

w^*_{max}	ω^*_{nl}/ω^*_1	a_{11}	a_{13}	a_{15}	a_{31}	a_{33}	a_{35}	a_{51}	a_{53}	a_{55}
0.1206	1.0027	0.05	0.1352E-03	0.2100E-04	0.2883E-02	-0.3804E-04	-0.7113E-05	0.5337E-03	-0.3964E-03	-0.7297E-05
0.2398	1.0108	0.10	0.3327E-04	0.7163E-04	0.6421E-02	-0.6533E-04	-0.2043E-04	0.1098E-02	-0.7980E-04	-0.1438E-04
0.3565	1.0238	0.15	0.6464E-03	0.1791E-03	0.1112E-01	-0.7004E-04	-0.4405E-04	0.1740E-02	-0.1191E-03	-0.2191E-04
0.4702	1.0415	0.20	0.1117E-02	0.3670E-03	0.1725E-01	-0.3902E-04	-0.7886E-04	0.2520E-02	-0.1530E-03	-0.3164E-04
0.5810	1.0631	0.25	0.1770E-02	0.6543E-03	0.2486E-01	0.4126E-04	-0.1227E-03	0.3506E-02	-0.1744E-03	-0.4595E-04
0.6892	1.0882	0.30	0.2622E-02	0.1056E-02	0.3383E-01	0.1834E-03	-0.1713E-03	0.4760E-02	-0.1743E-03	-0.6713E-04
0.7954	1.1164	0.35	0.3676E-02	0.1584E-02	0.4397E-01	0.3982E-03	-0.2193E-03	0.6321E-02	-0.1430E-03	-0.9672E-04
0.9002	1.1473	0.40	0.4931E-02	0.2247E-02	0.5504E-01	0.6936E-03	-0.2614E-03	0.8205E-02	-0.7166E-04	-0.1353E-03
1.0040	1.1805	0.45	0.6377E-02	0.3048E-02	0.6683E-01	0.1075E-02	-0.2926E-03	0.1041E-01	0.4703E-04	-0.1824E-03
1.1072	1.2159	0.50	0.8002E-02	0.3992E-02	0.7915E-01	0.1545E-02	-0.3087E-03	0.1292E-01	0.2187E-03	-0.2369E-03
1.2102	1.2530	0.55	0.9790E-02	0.5077E-02	0.9185E-01	0.2103E-02	-0.3061E-03	0.1570E-01	0.4471E-03	-0.2973E-03
1.4161	1.3320	0.65	0.1379E-01	0.7660E-02	0.1179E+00	0.3477E-02	-0.2346E-03	0.2193E-01	0.1080E-02	-0.4283E-03
1.6227	1.4162	0.75	0.1825E-01	0.1076E-01	0.1445E+00	0.5165E-02	-0.6353E-04	0.2885E-01	0.1944E-02	-0.5610E-03
1.8302	1.5046	0.85	0.2304E-01	0.1433E-01	0.1711E+00	0.7126E-02	0.2139E-03	0.3623E-01	0.3020E-02	-0.6837E-03
2.0388	1.5962	0.95	0.2807E-01	0.1829E-01	0.1977E+00	0.9311E-02	0.5984E-03	0.4390E-01	0.4284E-02	-0.7880E-03
2.2482	1.6907	1.05	0.3326E-01	0.2260E-01	0.2242E+00	0.1168E-01	0.1087E-02	0.5174E-01	0.5705E-02	-0.8684E-03
3.1980	2.1416	1.50	0.5748E-01	0.4473E-01	0.3421E+00	0.2359E-01	0.4367E-02	0.8759E-01	0.1333E-01	-0.8888E-03
4.2608	2.6746	2.00	0.8455E-01	0.7170E-01	0.4707E+00	0.3763E-01	0.9363E-02	0.1270E+00	0.2275E-01	-0.3407E-03

Table (5.5) :Contribution coefficients to the first nonlinear mode shape of a fully clamped rectangular plate: $\alpha = 0.4$

w^*_{max}	ω_{nl}/ω_l	a_{11}	a_{13}	a_{15}	a_{31}	a_{33}	a_{35}	a_{51}	a_{53}	a_{55}
1.2233	1.0027	0.05	0.2870E-03	0.4128E-04	0.1688E-02	-0.9539E-04	-0.1959E-04	0.2660E-03	-0.5795E-04	-0.1462E-04
0.2441	1.0108	0.10	0.6430E-03	0.1118E-03	0.3626E-02	-0.1723E-03	-0.4638E-04	0.5535E-03	-0.1183E-03	-0.2846E-04
0.3649	1.0239	0.15	0.1129E-02	0.2390E-03	0.6029E-02	-0.2123E-03	-0.8645E-04	0.8849E-03	-0.1822E-03	-0.4108E-04
0.4844	1.0417	0.20	0.1793E-02	0.4471E-03	0.9051E-02	-0.1971E-03	-0.1439E-03	0.1284E-02	-0.2487E-03	-0.5259E-04
0.6025	1.0636	0.25	0.2665E-02	0.7561E-03	0.1278E-01	-0.1091E-03	-0.2206E-03	0.1774E-02	-0.3144E-03	-0.6362E-04
0.7191	1.0893	0.30	0.3763E-02	0.1182E-02	0.1724E-01	0.6749E-04	-0.3164E-03	0.2375E-02	-0.3735E-03	-0.7507E-04
0.8344	1.1181	0.35	0.5089E-02	0.1735E-02	0.2241E-01	0.3460E-03	-0.4292E-03	0.3107E-02	-0.4191E-03	-0.8788E-04
0.9486	1.1499	0.40	0.6637E-02	0.2423E-02	0.2824E-01	0.7369E-03	-0.5560E-03	0.3980E-02	-0.4433E-03	-0.1028E-03
1.0619	1.1840	0.45	0.8396E-02	0.3251E-02	0.3465E-01	0.1247E-02	-0.6930E-03	0.5001E-02	-0.4381E-03	-0.1201E-03
1.1744	1.2203	0.50	0.1035E-01	0.4212E-02	0.4157E-01	0.1882E-02	-0.8359E-03	0.6172E-02	-0.3964E-03	-0.1398E-03
1.2864	1.2584	0.55	0.1248E-01	0.5323E-02	0.4892E-01	0.2640E-02	-0.9809E-03	0.7491E-03	-0.3117E-03	-0.1615E-03
1.5093	1.3392	0.65	0.1719E-01	0.7934E-02	0.6463E-01	0.4525E-02	-0.1262E-02	0.1054E-01	0.5518E-05	-0.2078E-03
1.7316	1.4251	0.75	0.2238E-01	0.1104E-01	0.8130E-01	0.6868E-02	-0.1510E-02	0.1408E-01	0.5390E-03	-0.2512E-03
1.9538	1.5151	0.85	0.2793E-01	0.1458E-01	0.9860E-01	0.9618E-02	-0.1705E-02	0.1802E-01	0.1296E-02	-0.2833E-03
2.1763	1.6085	0.95	0.3375E-01	0.1849E-01	0.1163E+00	0.1271E-01	-0.1836E-02	0.2228E-01	0.2269E-02	-0.2967E-03
2.3992	1.7046	1.05	0.3975E-01	0.2273E-01	0.1342E+00	0.1610E-01	-0.1894E-02	0.2678E-01	0.3442E-02	-0.2862E-03
3.4069	2.1630	1.50	0.6781E-01	0.4425E-01	0.2156E+00	0.3352E-01	-0.1272E-02	0.4858E-01	0.1058E-01	0.1114E-03
4.5320	2.7049	2.00	0.9936E-01	0.7030E-01	0.3055E+00	0.5457E-01	0.7031E-03	0.7362E-01	0.2042E-01	0.1141E-02

Table (5.6) :Contribution coefficients to the first nonlinear mode shape of a fully clamped rectangular plate: $\alpha = 0.6$

w^*_{max}	ω^*_{nl}/ω^*_l	a_{11}	a_{13}	a_{15}	a_{31}	a_{33}	a_{35}	a_{51}	a_{53}	a_{55}
0.1230	1.0027	0.05	0.4873E-03	0.6911E-04	0.1069E-02	-0.1359E-03	-0.3445E-04	0.1570E-03	-0.5667E-04	-0.1915E-04
0.2457	1.0106	0.10	0.1056E-02	0.1663E-03	0.2278E-02	-0.2470E-03	-0.7570E-04	0.3382E-03	-0.1177E-03	-0.3732E-04
0.3679	1.0236	0.15	0.1778E-02	0.3179E-03	0.3751E-02	-0.3091E-03	-0.1297E-03	0.5668E-03	-0.1866E-03	-0.5369E-04
0.4893	1.0413	0.20	0.2709E-02	0.5477E-03	0.5583E-02	-0.2991E-03	-0.2008E-03	0.8646E-03	-0.2652E-03	-0.6770E-04
0.6099	1.0631	0.25	0.3889E-02	0.8754E-03	0.7834E-02	-0.1956E-03	-0.2915E-03	0.1250E-02	-0.3531E-03	-0.7905E-04
0.7297	1.0888	0.30	0.5337E-02	0.1317E-02	0.1053E-01	0.1975E-04	-0.4025E-03	0.1740E-02	-0.4485E-03	-0.8753E-04
0.8487	1.1177	0.35	0.7056E-02	0.1883E-02	0.1368E-01	0.3623E-03	-0.5327E-03	0.2346E-02	-0.5475E-03	-0.9295E-04
0.9670	1.1494	0.40	0.9041E-02	0.2581E-02	0.1725E-01	0.8437E-03	-0.6798E-03	0.3076E-02	-0.6454E-03	-0.9496E-04
1.0848	1.1837	0.45	0.1128E-01	0.3415E-02	0.2122E-01	0.1472E-02	-0.8407E-03	0.3934E-02	-0.7368E-03	-0.9298E-04
1.2022	1.2201	0.50	0.1374E-01	0.4385E-02	0.2554E-01	0.2251E-02	-0.1012E-02	0.4921E-02	-0.8164E-03	-0.8619E-04
1.3193	1.2584	0.55	0.1641E-01	0.5489E-02	0.3017E-01	0.3181E-02	-0.1189E-02	0.6035E-02	-0.8789E-03	-0.7356E-04
1.5532	1.3398	0.65	0.2228E-01	0.8082E-02	0.4022E-01	0.5488E-02	-0.1548E-02	0.8627E-02	-0.9342E-03	-0.2590E-04
1.7869	1.4263	0.75	0.2871E-01	0.1114E-01	0.5105E-01	0.8354E-02	-0.1889E-02	0.1166E-01	-0.8731E-03	0.6020E-04
2.0210	1.5169	0.85	0.3556E-01	0.1462E-01	0.6245E-01	0.1172E-01	-0.2191E-02	0.1507E-01	-0.6773E-03	0.1942E-03
2.2555	1.6109	0.95	0.4272E-01	0.1843E-01	0.7424E-01	0.1551E-01	-0.2437E-02	0.1879E-01	-0.3388E-03	0.3836E-03
2.4906	1.7078	1.05	0.5010E-01	0.2254E-01	0.8628E-01	0.1967E-01	-0.2617E-02	0.2276E-01	0.1415E-03	0.6328E-03
3.5542	2.1697	1.50	0.8467E-01	0.4323E-01	0.1418E+00	0.4124E-01	-0.2568E-02	0.4251E-01	0.3808E-02	0.2496E-02
4.7420	2.7158	2.00	0.1236E+00	0.6803E-01	0.2038E+00	0.6763E-01	-0.1180E-02	0.6579E-01	0.9722E-02	0.5681E-02

Table (5.7) :Contribution coefficients to the first nonlinear mode shape of a fully clamped rectangular plate $\alpha = 0.8$

w^*_{max}	ω^*_{nl}/ω^*_l	a_{11}	a_{13}	a_{15}	a_{31}	a_{33}	a_{35}	a_{51}	a_{53}	a_{55}
0.1231	1.0026	0.05	0.7275E-03	0.1040E-03	0.7275E-03	-0.1481E-03	-0.4717E-04	0.1040E-03	-0.4712E-04	-0.2044E-04
0.2461	1.0105	0.10	0.1556E-02	0.2344E-03	0.1556E-02	-0.2694E-03	-0.1001E-03	0.2344E-03	-0.1001E-03	-0.3986E-04
0.3686	1.0235	0.15	0.2575E-02	0.4163E-03	0.2575E-02	-0.3378E-03	-0.1639E-03	0.4163E-03	-0.1639E-03	-0.5736E-04
0.4904	1.0411	0.20	0.3856E-02	0.6722E-03	0.3856E-02	-0.3288E-03	-0.2419E-03	0.6722E-03	-0.2419E-03	-0.7223E-04
0.6116	1.0629	0.25	0.5444E-02	0.1021E-02	0.5444E-02	-0.2199E-03	-0.3359E-03	0.1021E-02	-0.3359E-03	-0.8392E-04
0.7320	1.0884	0.30	0.7362E-02	0.1479E-02	0.7362E-02	0.8417E-05	-0.4455E-03	0.1479E-02	-0.4455E-03	-0.9195E-04
0.8519	1.1173	0.35	0.9616E-02	0.2057E-02	0.9616E-02	0.3720E-03	-0.5691E-03	0.2057E-02	-0.5691E-03	-0.9577E-04
0.9712	1.1490	0.40	0.1219E-01	0.2763E-02	0.1219E-01	0.8828E-03	-0.7037E-03	0.2763E-02	-0.7037E-03	-0.9470E-04
1.0901	1.1833	0.45	0.1508E-01	0.3599E-02	0.1508E-01	0.1549E-02	-0.8456E-03	0.3599E-02	-0.8456E-03	-0.8781E-04
1.2086	1.2197	0.50	0.1823E-01	0.4567E-02	0.1823E-01	0.2374E-02	-0.9907E-03	0.4567E-02	-0.9907E-03	-0.7396E-04
1.3271	1.2580	0.55	0.2164E-01	0.5664E-02	0.2164E-01	0.3360E-02	-0.1135E-02	0.5664E-02	-0.1135E-02	-0.5183E-04
1.5637	1.3393	0.65	0.2907E-01	0.8228E-02	0.2907E-01	0.5802E-02	-0.1403E-02	0.8228E-02	-0.1403E-02	0.2318E-04
1.8004	1.4258	0.75	0.3716E-01	0.1124E-01	0.3716E-01	0.8833E-02	-0.1623E-02	0.1124E-01	-0.1623E-02	0.1491E-03
2.0377	1.5165	0.85	0.4574E-01	0.1465E-01	0.4574E-01	0.1239E-01	-0.1772E-02	0.1465E-01	-0.1772E-02	0.3366E-03
2.2755	1.6106	0.95	0.5466E-01	0.1838E-01	0.5466E-01	0.1641E-01	-0.1837E-02	0.1838E-01	-0.1837E-02	0.5936E-03
2.5140	1.7076	1.05	0.6382E-01	0.2237E-01	0.6382E-01	0.2080E-01	-0.1810E-02	0.2237E-01	-0.1810E-02	0.9250E-03
3.5936	2.1699	1.50	0.1065E+00	0.4239E-01	0.1065E+00	0.4370E-01	-0.5963E-03	0.4239E-01	-0.5963E-03	0.3325E-02
4.7997	2.7164	2.00	0.1544E+00	0.6620E-01	0.1544E+00	0.7180E-01	0.2292E-02	0.6620E-01	0.2292E-02	0.7348E-02

Table (5.8) :Contribution coefficients to the first nonlinear mode shape of a fully clamped rectangular plate $\alpha = 1.0$

Ref / Year	Present Work 1990	[5.18] 1961(a)	[5.19] 1973(a)	[5.20] 1976	[5.21] 1978(b)	[5.21] 1978(c)	[5.22] 1979(d)	[5.23] 1984	[5.24] 1989(e)	[5.24] 1989(f)
w*(0.5,0.5)										
0.2	1.0070	1.0085	1.0062	1.0070	1.0129	1.0118	1.0062	1.0073	1.0104	1.0078
0.4	1.0276	1.0292	1.0256	1.0276	1.0306	1.0275	1.0245	1.0291	1.0416	1.0326
0.6	1.0607	1.0661	1.0564	1.0608	1.0665	1.0571	1.0540	1.0648	1.0937	1.069
0.8	1.1044	1.1136	1.0970	1.1047	1.1157	1.0984	1.0934	1.1138	1.1666	1.1173
1.0	1.1573	1.1674	1.1429	1.1578	1.1684	1.1450	1.1411	1.1762	1.2602	1.1757
1.5	1.3499				1.3613	1.3159				

Table 5.9.1. Frequency ratio $\frac{\omega_{nl}}{\omega_l}$ for various vibration amplitudes for the fundamental mode of fully clamped square plates.

(a) Values taken from [5.20].
(b) Values taken from [5.21], read from graph, obtained using stress function method
(c) Values taken from [5.21], read from graph, obtained using Berger's approximation.
(d) Values taken from [5.23]
(e) Values obtained using ultraspherical polynomial method, not considered in Table (5.9.2)
(f) Values obtained using elliptic function method.

w^*_{max}	Average	Standard deviation ($\times 10^2$)
0.2	1.0083	0.23
0.4	1.0283	0.23
0.6	1.0617	0.49
0.8	1.1065	0.84
1.0	1.1591	1.3
1.5	1.3423	1.9

Table 5.9.2. Average and standard deviation of values given in Table 5.9.1

w^*_{max}	ref. [5.20] 1976 (a)	ref. [5.21] 1979 (b)	Present Work
0.2	1.0074	1.0129	
0.4	1.0292	1.0306	
0.6	1.0647	1.0665	
0.8	1.1123	1.1157	1.1129
1.0	1.1686	1.1684	1.1715
1.5		1.3613	1.3562

Table 5.9.3 Frequency ratio $\frac{\omega_{nl}}{\omega_l}$ for various vibration amplitudes for fully clamped rectangular plate. b/a = 0.5.

(a) Finite element method
(b) Stress function method

w^*_{max}	Average	Standard deviation ($\times 10^2$)
0.2		
0.4		
0.6		
0.8	1.1136	0.15
1.0	1.1695	0.14
1.5	1.3588	0.26

Table 5.9.4. Average and standard deviation of values given in Table 5.9.3

curve \ α	1	0.8	0.6	0.4	0.2
1	$1.231\ 10^{-2}$	$1.231\ 10^{-2}$	$1.224\ 10^{-2}$	$1.209\ 10^{-2}$	$1.182\ 10^{-2}$
2	1.090	1.085	1.062	1.004	0.942
3	2.156	2.138	2.065	1.934	1.882
4	3.233	3.199	3.070	2.880	2.831
5	4.317	4.266	4.081	3.835	3.784

Table (5.10) Maximum displacement amplitude along the line $y^* = 0.5$ corresponding to the normalised curves given in Figures (5.2.1) to (5.5.5).

$(x^*,y^*) = (0.5, 0.5)$		$(x^*,y^*) = (0.35,0.35)$		$(x^*,y^*) = (0.225, 0.225)$	
w^* (mm/mm)	f (Hz)	w^* (mm/mm)	f (Hz)	w^* (mm/mm)	f (Hz)
0.29	76.7	0.27	76.0	0.20	78.8
0.37	77.4	0.34	77.8	0.28	83.4
0.46	78.6	0.44	80.6	0.41	90.3
0.50	79.0	0.52	83.6	0.44	91.5
0.59	80.1	0.68	88.6		
0.70	81.6				
0.78	83.3				
0.87	85.1				
0.99	87.4				
1.03	88.3				
1.10	88.6				

Table (6.1) : Summary of measured nonlinear frequency-amplitude curves at three points on plate 1.

y*	0.11	0.17	0.28	0.40	0.50	0.62	0.74	0.85	0.89
x*									
0.09	0.008	0.016	0.033	0.046	0.051	0.047	0.028	0.011	0.007
0.13	0.014	0.027	0.056	0.076	0.087	0.077	0.051	0.018	0.013
0.23	0.037	0.069	0.138	0.182	0.202	0.169	0.112	0.046	0.029
0.33	0.060	0.107	0.219	0.299	0.332	0.291	0.192	0.079	0.053
0.42	0.085	0.153	0.288	0.405	0.442	0.382	0.252	0.104	0.062
0.50	0.093	0.157	0.306	0.435	0.469	0.398	0.265	0.107	0.062
0.62	0.073	0.131	0.258	0.360	0.382	0.327	0.213	0.089	0.053
0.71	0.051	0.089	0.176	0.245	0.262	0.225	0.147	0.062	0.033
0.81	0.030	0.052	0.101	0.138	0.150	0.128	0.084	0.034	0.020
0.91	0.009	0.015	0.032	0.044	0.048	0.040	0.026	0.011	0.006

Table (6.2) : First mode shape measurements plate 2
maximum non-dimensional amplitude : 0.47
excitation frequency : 132.9 Hz
input current in the coil : 0.02 Amps

0.014	0.027	0.056	0.078	0.087	0.076	0.049	0.020	0.015
0.026	0.046	0.096	0.130	0.146	0.127	0.086	0.035	0.024
0.063	0.112	0.228	0.298	0.327	0.282	0.187	0.080	0.051
0.102	0.181	0.352	0.476	0.527	0.460	0.305	0.129	0.078
0.131	0.231	0.445	0.618	0.687	0.589	0.394	0.160	0.098
0.136	0.245	0.480	0.669	0.720	0.616	0.402	0.165	0.111
0.122	0.211	0.416	0.558	0.603	0.516	0.338	0.145	0.084
0.087	0.151	0.289	0.398	0.420	0.367	0.245	0.096	0.058
0.047	0.082	0.162	0.225	0.238	0.205	0.136	0.056	0.031
0.015	0.026	0.054	0.074	0.079	0.067	0.044	0.018	0.011

Table (6.3) : First mode shape measurements plate 2
maximum non-dimensional amplitude : 0.72
Excitation frequency : 140.3 Hz
Input current in the coil : 0.02 Amps
maximum non-dimensional amplitude at the end of measurements : 0.73

0.023	0.039	0.078	0.105	0.116	0.102	0.062	0.030	0.020
0.036	0.066	0.126	0.173	0.196	0.168	0.114	0.046	0.034
0.084	0.146	0.285	0.377	0.418	0.354	0.238	0.107	0.067
0.128	0.223	0.433	0.587	0.652	0.569	0.380	0.165	0.105
0.165	0.282	0.558	0.769	0.845	0.734	0.487	0.202	0.129
0.178	0.296	0.583	0.818	0.909	0.780	0.520	0.218	0.131
0.156	0.265	0.514	0.683	0.747	0.654	0.440	0.193	0.107
0.111	0.196	0.371	0.503	0.534	0.463	0.311	0.133	0.080
0.067	0.111	0.222	0.296	0.316	0.278	0.185	0.078	0.044
0.022	0.033	0.073	0.100	0.105	0.091	0.060	0.027	0.017

Table (6.4) : First mode shape measurements plate 2
maximum non-dimensional amplitude : 0.91
Excitation frequency :157 Hz
Input current in the coil : 0.07 Amps
maximum non-dimensional amplitude at the end of measurements : 0.91

0.016	0.034	0.070	0.099	0.109	0.100	0.059	0.023	0.015
0.029	0.057	0.120	0.163	0.185	0.164	0.109	0.039	0.027
0.079	0.147	0.295	0.389	0.430	0.361	0.238	0.098	0.062
0.127	0.228	0.466	0.637	0.709	0.620	0.410	0.168	0.113
0.182	0.327	0.614	0.864	0.943	0.814	0.538	0.221	0.131
0.197	0.335	0.653	0.927	1.000	0.848	0.564	0.227	0.133
0.156	0.280	0.550	0.768	0.815	0.697	0.455	0.190	0.114
0.109	0.190	0.374	0.521	0.559	0.479	0.313	0.133	0.071
0.064	0.110	0.216	0.294	0.319	0.273	0.180	0.072	0.042
0.019	0.032	0.069	0.095	0.101	0.086	0.056	0.023	0.013

Table (6.5) : First mode shape measurements plate 2
normalised values for maximum non-dimensional amplitude : 0.47

0.020	0.038	0.077	0.108	0.120	0.105	0.068	0.028	0.020
0.036	0.064	0.133	0.180	0.202	0.176	0.119	0.048	0.033
0.088	0.156	0.316	0.413	0.454	0.391	0.260	0.111	0.071
0.141	0.251	0.488	0.660	0.731	0.639	0.423	0.179	0.108
0.182	0.321	0.617	0.858	0.954	0.818	0.546	0.222	0.136
0.188	0.340	0.667	0.929	1.000	0.855	0.559	0.228	0.154
0.170	0.293	0.577	0.775	0.836	0.716	0.469	0.201	0.117
0.120	0.210	0.401	0.552	0.583	0.509	0.340	0.133	0.080
0.065	0.114	0.225	0.312	0.330	0.284	0.188	0.077	0.043
0.021	0.035	0.076	0.103	0.110	0.093	0.061	0.025	0.015

Table (6.6) : First mode shape measurements plate 2
normalised values for maximum non-dimensional amplitude : 0.72

0.025	0.043	0.086	0.115	0.127	0.112	0.068	0.033	0.022
0.040	0.072	0.139	0.190	0.215	0.185	0.126	0.051	0.038
0.092	0.160	0.313	0.414	0.459	0.390	0.262	0.118	0.073
0.141	0.245	0.476	0.645	0.716	0.626	0.418	0.181	0.115
0.181	0.311	0.614	0.846	0.929	0.807	0.535	0.222	0.142
0.196	0.325	0.641	0.900	1.000	0.858	0.572	0.240	0.144
0.171	0.291	0.565	0.751	0.822	0.719	0.484	0.213	0.117
0.122	0.215	0.408	0.553	0.587	0.509	0.342	0.147	0.088
0.073	0.122	0.244	0.325	0.347	0.306	0.203	0.086	0.049
0.024	0.037	0.081	0.110	0.115	0.100	0.066	0.029	0.018

Table (6.7) : First mode shape measurements plate 2
normalised values for maximum non-dimensional amplitude : 0.91

w*	a11	a13	a31	a33
0.47	0.176733	-0.003336	-0.007459	0.000318
0.72	0.277946	-0.003800	-0.006260	0.000876
0.91	0.348155	-0.003112	-0.003487	0.001660

Table (6.8) : Estimated contribution coefficients for plate 2

w*	a11	a13	a31	a33
0.47	1.000000	-0.018876	-0.042204	0.001798
0.72	1.000000	-0.013673	-0.022522	0.003151
0.91	1.000000	-0.008939	-0.010016	0.004768

Table (6.9) : Normalised estimated contribution coefficients from Table 6.8

w*	0.72	0.91
a13	27.6 %	52.6 %
a31	46.6 %	76.3 %
a33	75.3 %	165.3 %

Table(6.10) : Rate of increase of normalised estimated contribution coefficients given in Table 6.9 with amplitude of vibration with reference to the value at non-dimensional amplitude 0.47.

w^*_{max}	Theoretical non-dimensional bending stress	Estimated nondimensional bending stress	Normalised theoretical values	Normalised estimated values
0.47	6.841	2.494	1.00	1.00
0.72	10.853	4.401	1.59	1.76
0.91	15.344	5.863	2.24	2.3

Table 6.11. Comparison of theoetical and estimated bending stress at point $(x^*,y^*) = (0.5,0)$. Plate 2.

$a_1(\omega)$	No. of iterations	$a_1(3\omega)$	$a_3(3\omega)$	$a_5(3\omega)$	$a_7(3\omega)$	$a_9(3\omega)$	$a_{11}(3\omega)$
0.05	68	-0.7071 E-5	-0.2219 E-5	-0.2077 E-6	-0.4643 E-7	-0.1483 E-7	-0.5696 E-8
0.30	65	-0.1419 E-2	-0.4743 E-3	-0.4565 E-4	-0.10e6 E-4	-0.336 E-5	-0.1290 E-5
0.55	102	-0.7450 E-2	-0.2834 E-2	-0.2890 E-3	-0.6776 E-4	-0.2222 E-4	-0.8719 E-5
0.80	105	-0.1853 E-1	-0.8253 E-2	-0.9050 E-3	-0.2215 E-3	-0.7441 E-4	-0.2975 E-4
1.05	106	-0.3312 E-1	-0.1729 E-1	-0.2042 E-2	-0.5250 E-3	-0.4452 E-7	0.9142E-8
1.55	105	-0.6678 E-1	-0.4616 E-1	-0.6193 E-2	-0.1763 E-2	-0.6462 E-3	-0.2748 E-3

Table 7.1 Summary of numerical solutions obtained from the nonlinear model for vibration of a clamped-clamped beam vibrations including a spatially distributed harmonic distortion.
First solution. Third harmonic contribution coefficients

$a_1(\omega)$: contribution of the first clamped-clamped beam linear mode to the first harmonic

$a_i(3\omega)$: contribution of the i^{th} clamped-clamped beam linear mode to the first harmonic

The contribution coefficient to the second harmonic is lower than 10^{-13} for all amplitudes considered. The corresponding contribution coefficients of higher modes to the first harmonic are given in Table (4.2.1)

$a_1(\omega)$	No. of iterations	$a_3(3\omega)$	$a_5(3\omega)$	$a_7(3\omega)$	$a_9(3\omega)$	$a_{11}(3\omega)$
0.05	62	-0.2217 E-5	-0.2075 E-6	-0.4640 E-7	-0.1482 E-7	-0.5739 E-8
0.55	101	-0.2613 E-2	-0.2671 E-3	-0.6267 E-4	-0.2055 E-4	-0.8115 E-5
1.05	84	-0.1421 E-1	-0.1705 E-2	-0.4407 E-3	-0.1525 E-3	-0.6250 E-4
1.55	99	-0.3460 E-1	-0.4820 E-2	-0.1388 E-2	-0.5116 E-3	-0.2186 E-3

Table 7.2 Summary of numerical solutions obtained from the nonlinear model for vibration of a clamped-clamped beam vibrations including a spatially distributed harmonic distortion.
Second solution. Third harmonic contribution coefficients

$a_1(\omega)$: contribution of the first clamped-clamped beam linear mode to the first harmonic

$a_i(3\omega)$: contribution of the i^{th} clamped-clamped beam linear mode to the first harmonic

The contribution coefficient to the second harmonic is lower than 10^{-13} for all amplitudes considered. The corresponding contribution coefficients of higher modes to the first harmonic are given in Table (4.2.1)

$a_{11}(\omega)$	$\alpha_{11}(3\omega)$	$a_{12}(3\omega)$	$a_{13}(3\omega)$	$a_{21}(3\omega)$	$a_{22}(3\omega)$	$a_{23}(3\omega)$	$a_{31}(3\omega)$	$a_{32}(3\omega)$	$a_{33}(3\omega)$
0.2	-0.1038 E-2	-0.3956 E-11	-0.3814 E-3	-0.7558 E-12	-0.3240 E-12	-0.1009 E-13	0.6754 E-3	-0.1355 E-11	-0.4258 E-4
0.55	-0.1476 E-1	-0.5040 E-10	-0.5374 E-2	-0.1319 E-10	-0.9849 E-14	0.1217 E-11	0.5431 E-2	-0.2875 E-10	-0.1564 E-2
1.05	-0.5793 E-1	-0.1561 E-9	-0.1897E-1	-0.7110 E-10	0.1649 E-15	0.1937 E-10	0.8062 E-2	-0.3517 E-9	-0.9696 E-2
1.50	-0.1094 E0	0.4085 E-9	-0.3149 E-1	-0.1598 E-9	-0.7649 E-13	0.5927 E-10	0.4730 E-2	-0.3057 E-8	-0.1909 E-1
2.0	-0.1724 E0	-0.2915 E-8	-0.4328 E-1	-0.2802 E-9	-0.1377 E-13	0.1176 E-9	-0.2229 E-2	0.5987 E-8	-0.2763 E-1

Table 8. Contribution coefficients to the third harmonic component in the free response of a fully clamped rectangular isotropic plate of an aspect ratio of 0.6.

$a_{11}(\omega)$: contribution coefficient of the first basic function to the first harmonic

$a_{ij}(3\omega)$: contribution coefficient of the ij^{th} plate function to the third harmonic

The contribution coefficients to the second harmonic were, in all cases, lower than 10^{-11}

The number of iterations for the five above cases were: 77, 72, 83, 79, 73.

a_{11}	ω^*	a_{13}	a_{15}	a_{31}	a_{33}	a_{35}	a_{51}	a_{53}	a_{55}
0.005	0.5833 E+2	0.1447 E-4	0.1867 E-5	0.2525 E-3	-0.4897 E-5	-0.7689 E-6	0.4590 E-4	-0.4473 E-5	-0.8628 E-6
0.10	0.6153 E+2	0.4882 E-3	0.1310 E-3	0.6492 E-2	-0.7954 E-4	-0.3497 E-4	0.1157 E-2	-0.9077 E-4	-0.1500 E-4
0.20	0.7064 E+2	0.1965 E-2	0.7642 E-3	0.1821 E-1	-0.1819 E-4	-0.1530 E-3	0.3422 E-2	-0.1735 E-3	-0.2993 E-4
0.30	0.8423 E+2	0.4764 E-2	0.2197 E-2	0.3347 E-1	0.3715 E-3	-0.3492 E-3	0.6994 E-2	-0.1755 E-3	-0.6064 E-4
0.40	0.1039 E+3	0.8716 E-2	0.4516 E-2	0.4975 E-1	0.1211 E-2	-0.5796 E-3	0.1144 E-1	-0.2196 E-4	-0.1092 E-3
0.65	0.1708 E+3	0.2153 E-1	0.1359 E-1	0.9007 E-1	0.5249 E-2	-0.9869 E-3	0.2492 E-1	0.1210 E-2	-0.2426 E-3
1.05	0.3346 E+3	0.4471 E-1	0.3336 E-1	0.1530 E0	0.1513 E-1	-0.3396 E-3	0.4471 E-1	0.5145 E-2	-0.1992 E-3

Table 9 Summary of numerical results obtained from solution of the theoretical model for CFRP plates presented in Chapter IX. The corresponding estimated stiffnesses are given in Appendix J.

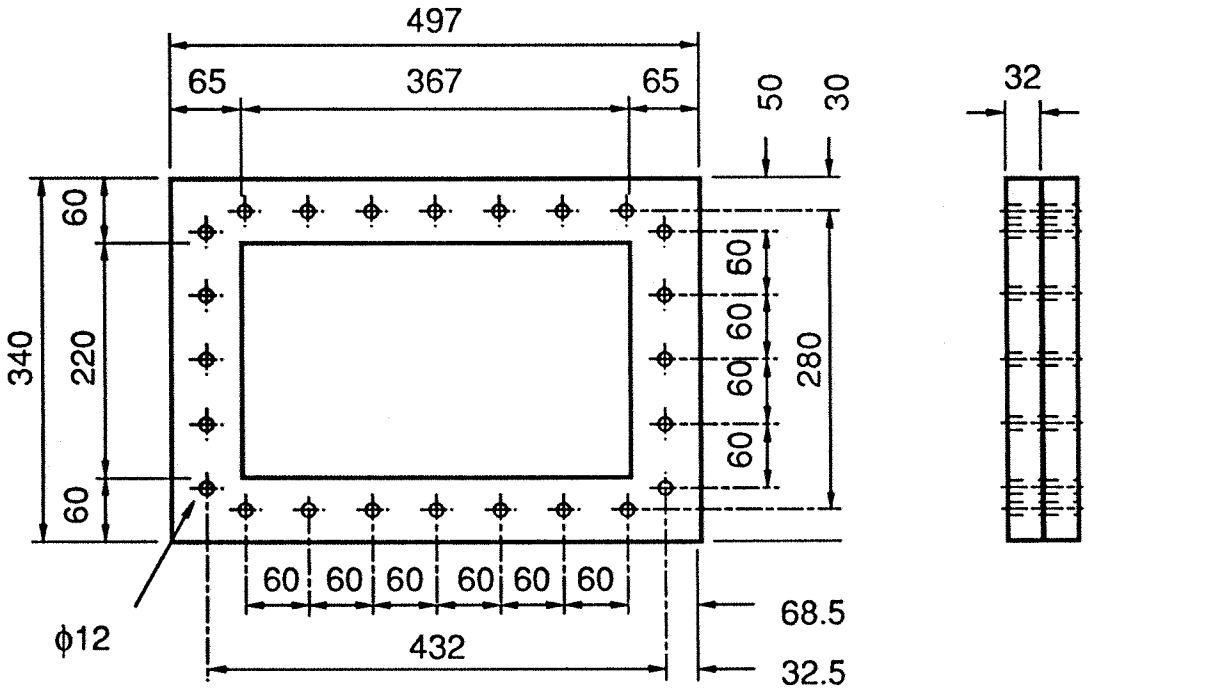

Dimensions in mm

Figure 3.1 RIG 1 FRAME DIMENSIONS

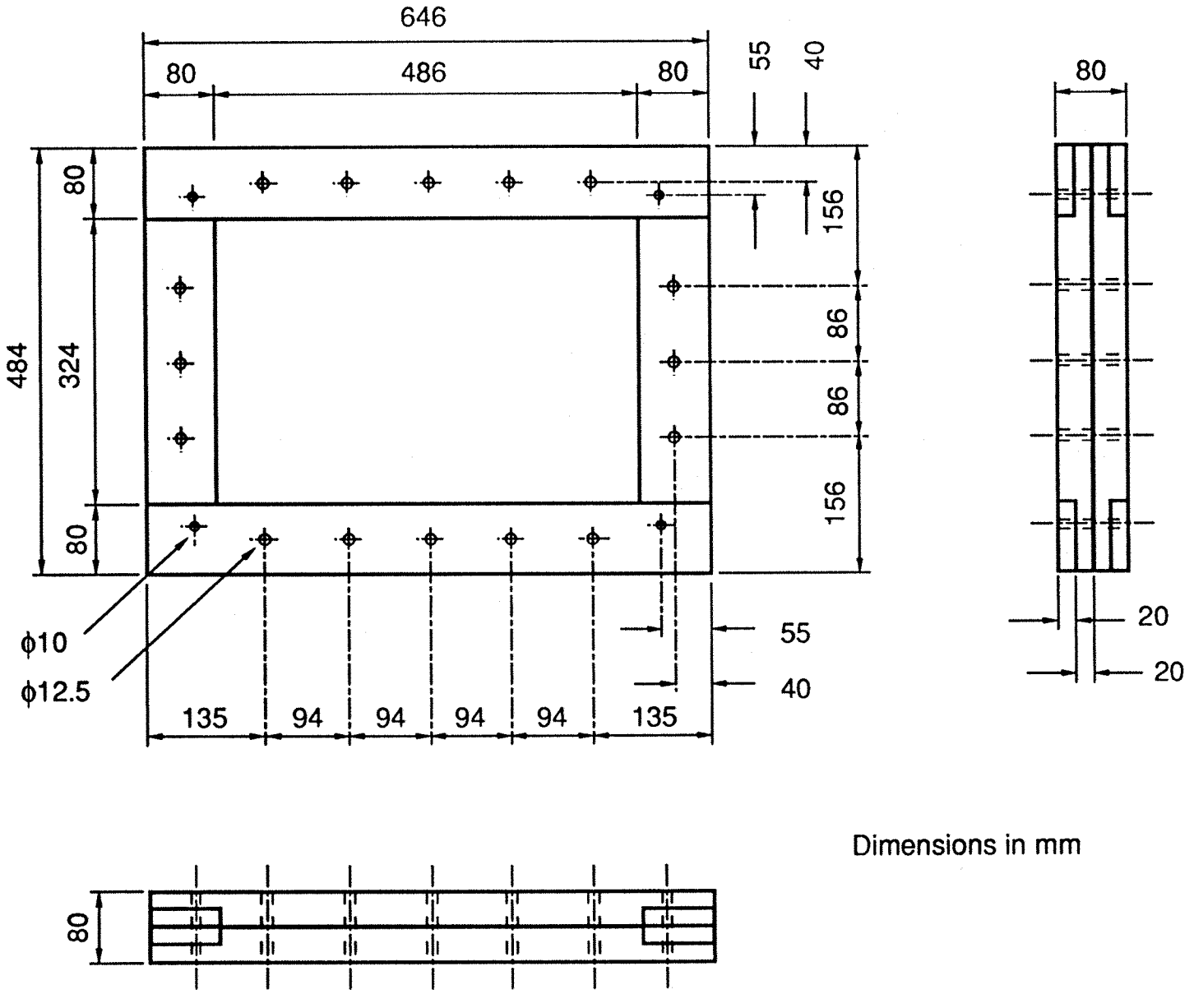

Dimensions in mm

Figure 3.2 RIG 2 FRAME DIMENSIONS

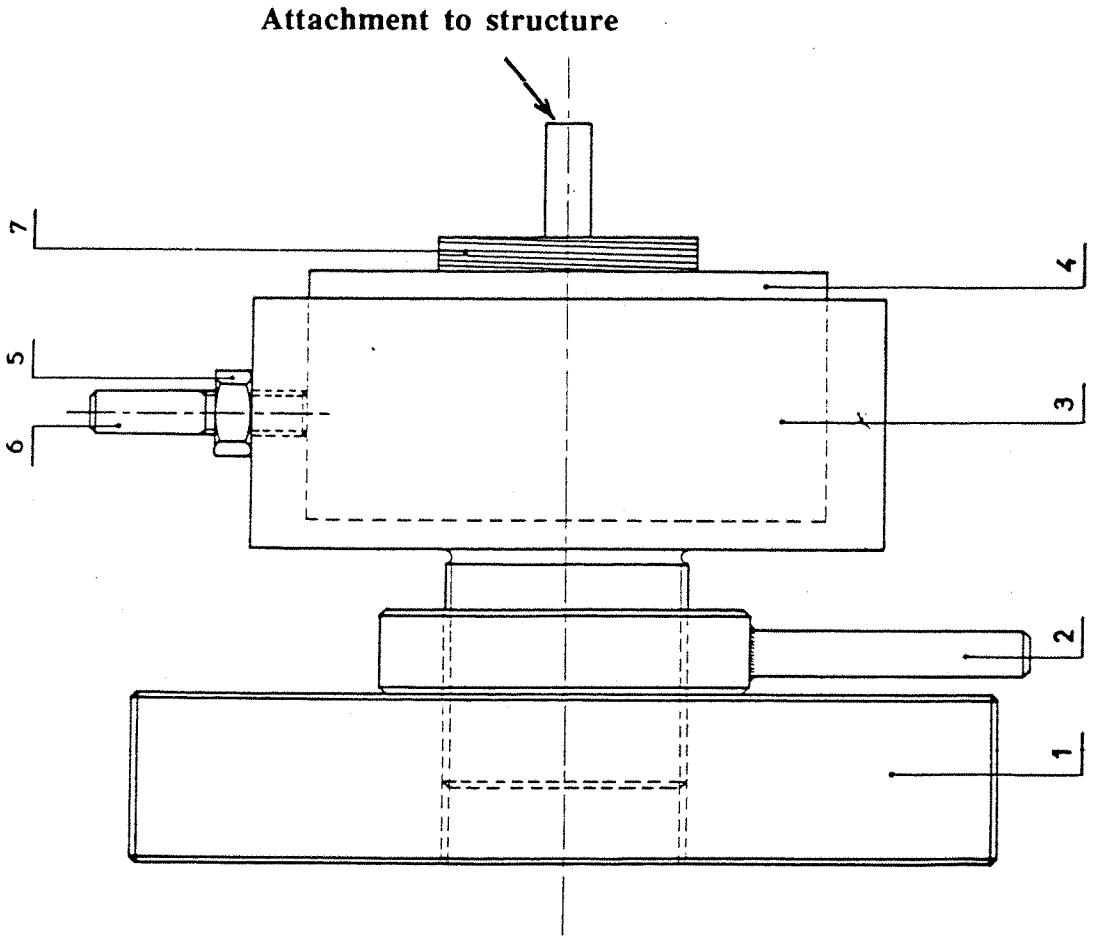

Figure 3.3 COIL AND MAGNET ARRANGEMENT

(1) Base
(2) Coil adjustment ring
(3) Magnet housing
(4) Annular magnet
(5)(6) Magnet locking device
(7) Coil

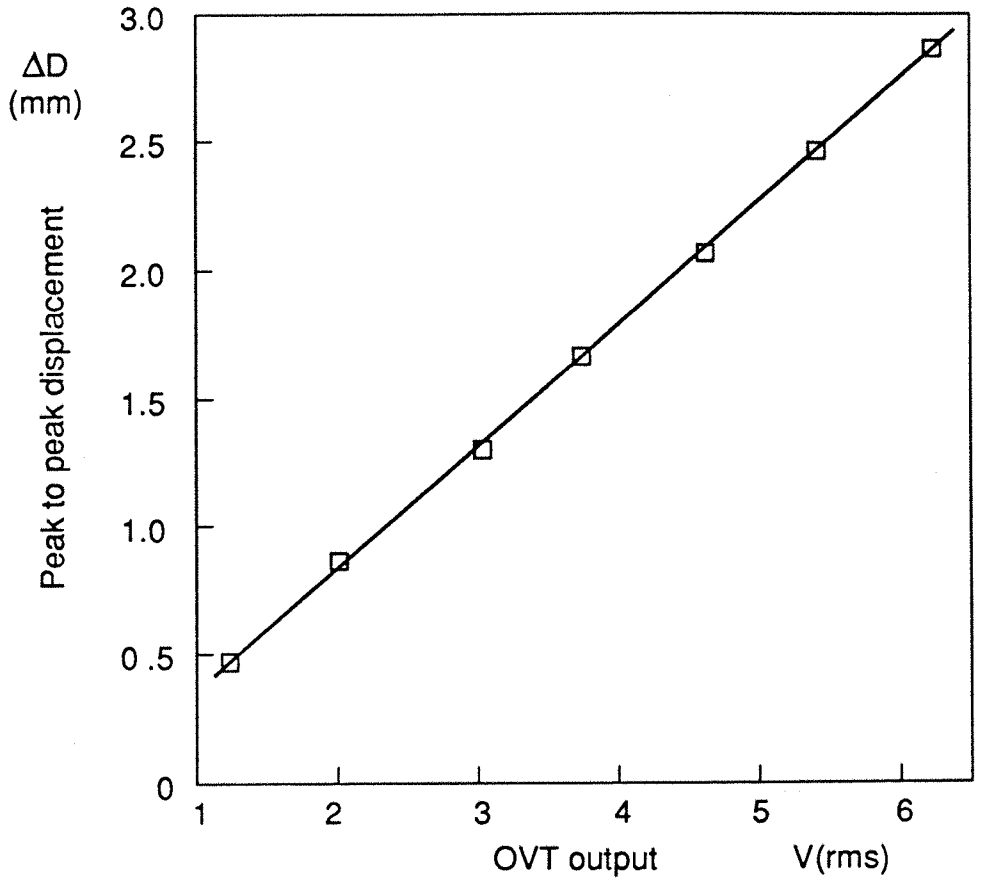

Figure 3.4 O.V.T. 1 DYNAMIC CALIBRATION FOR d_0 = 7.9 mm f=64Hz

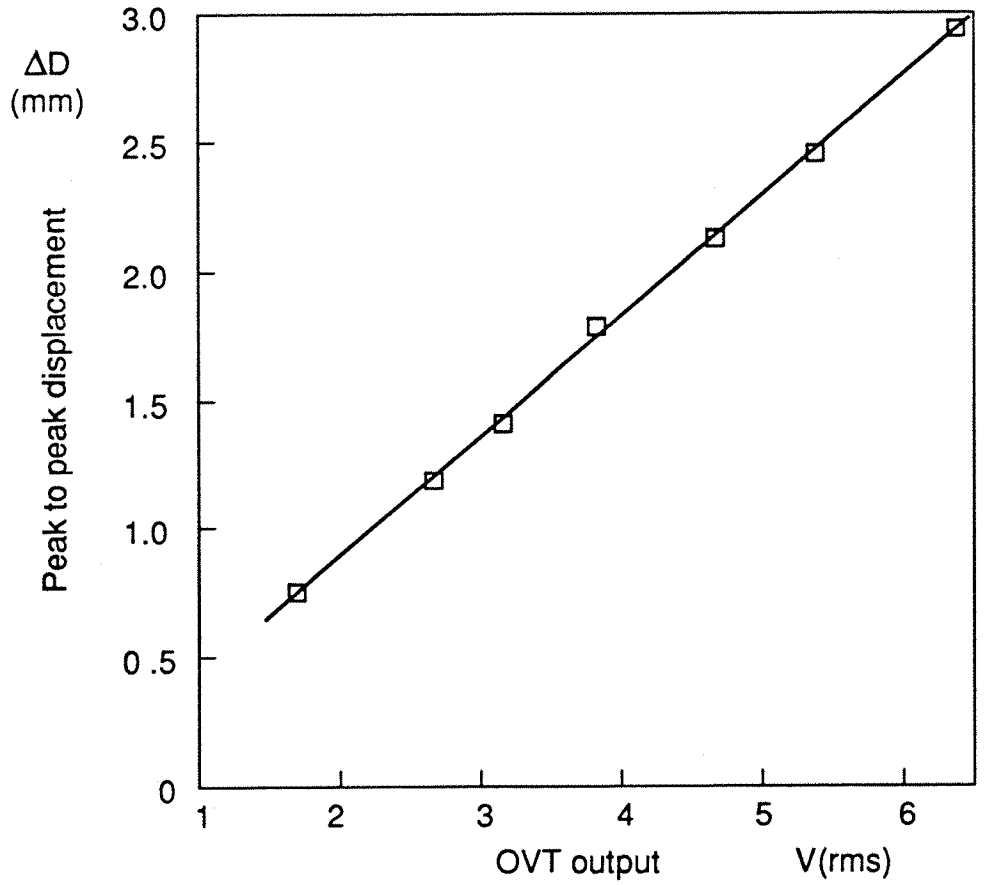

Figure 3.5 O.V.T. 1 DYNAMIC CALIBRATION FOR d_0 = 11.6 mm f=62 Hz

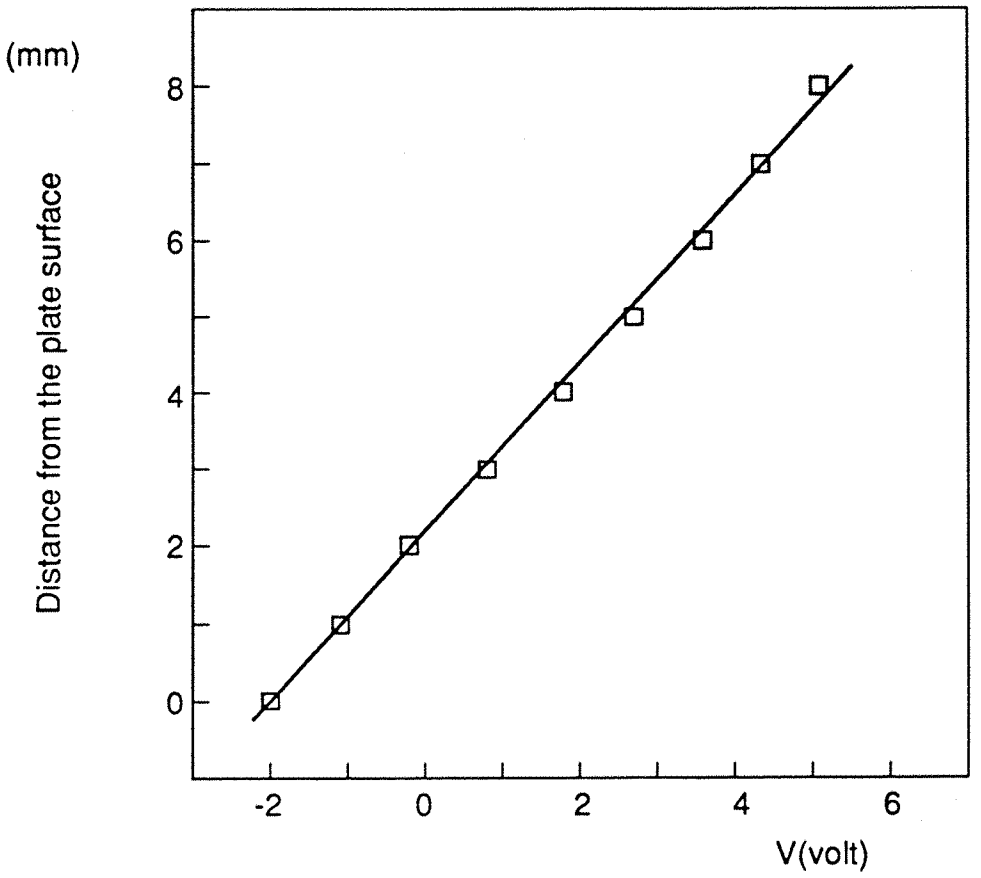

Figure 3.6 OPTICAL VIBRATION TRANSDUCER 2 STATIC CALIBRATION

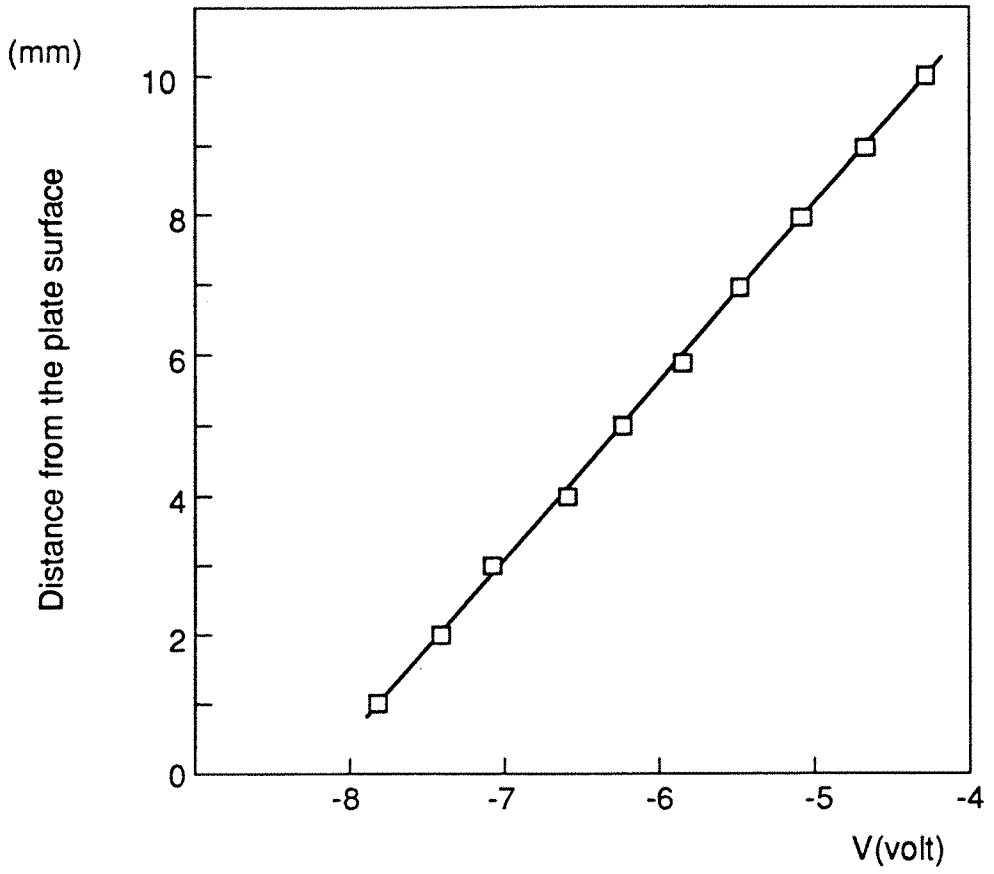

Figure 3.7 OPTICAL VIBRATION TRANSDUCER 3 STATIC CALIBRATION

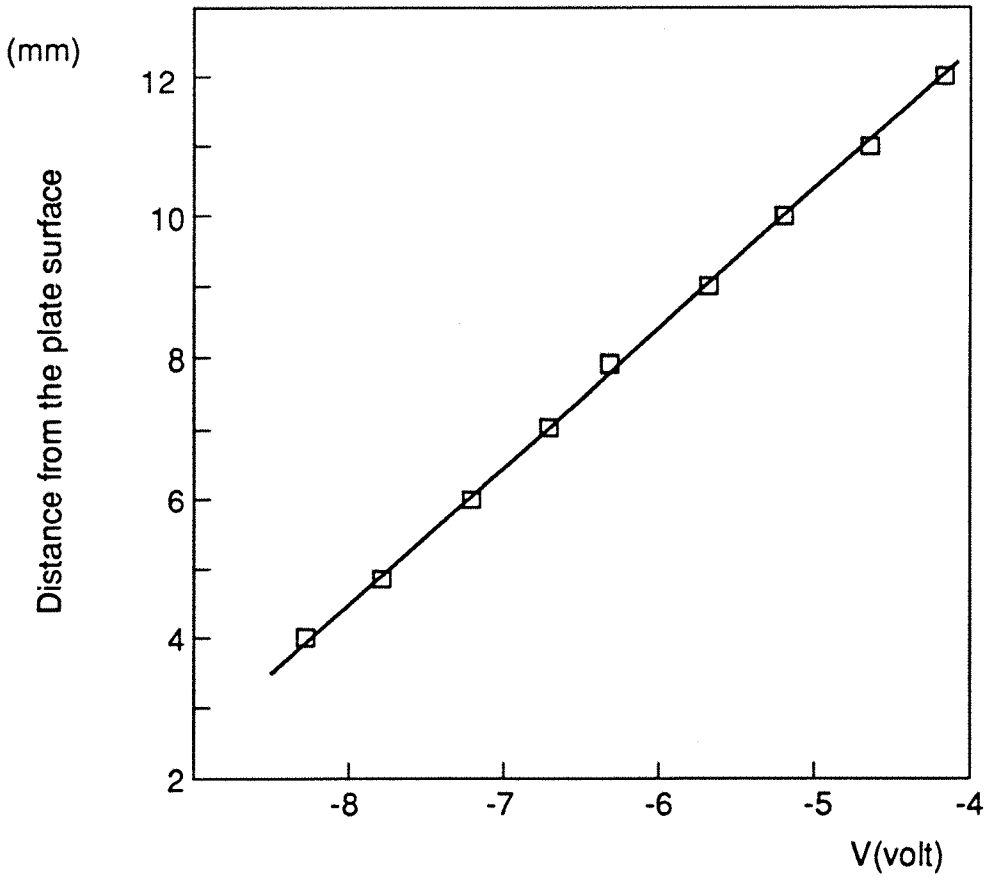

Figure 3.8 OPTICAL VIBRATION TRANSDUCER 4 STATIC CALIBRATION

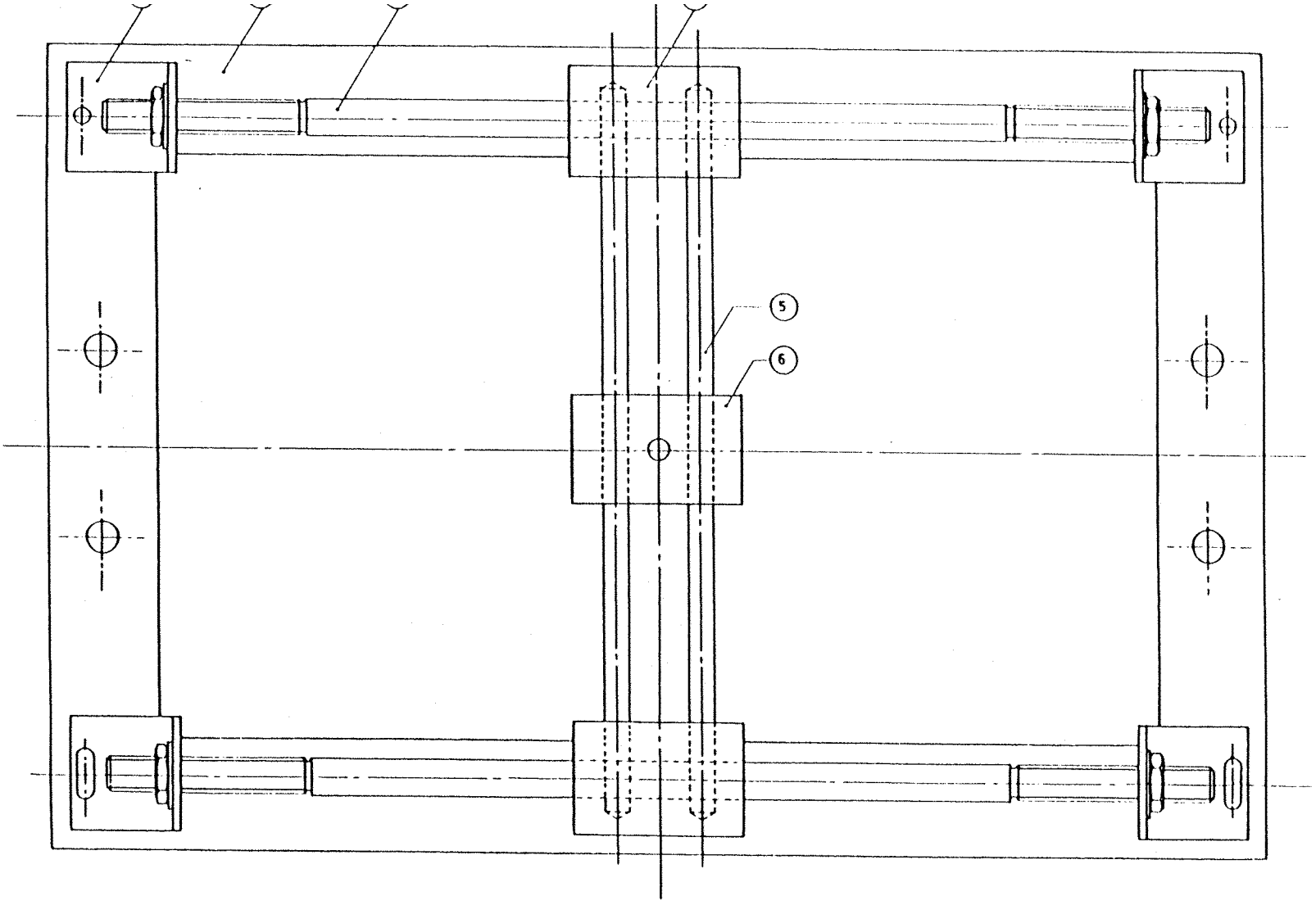

(1) Frames
(2) Length guides
(3) Guide support
(4) Length sliders
(5) Width guides
(6) Width slider

Figure (3.9) : Guided support for the O.V.T.

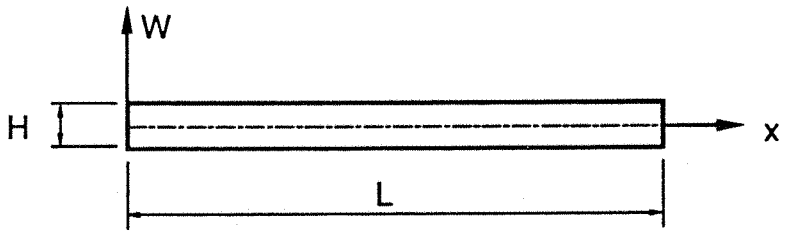

Figure (4.1) : BEAM NOTATION

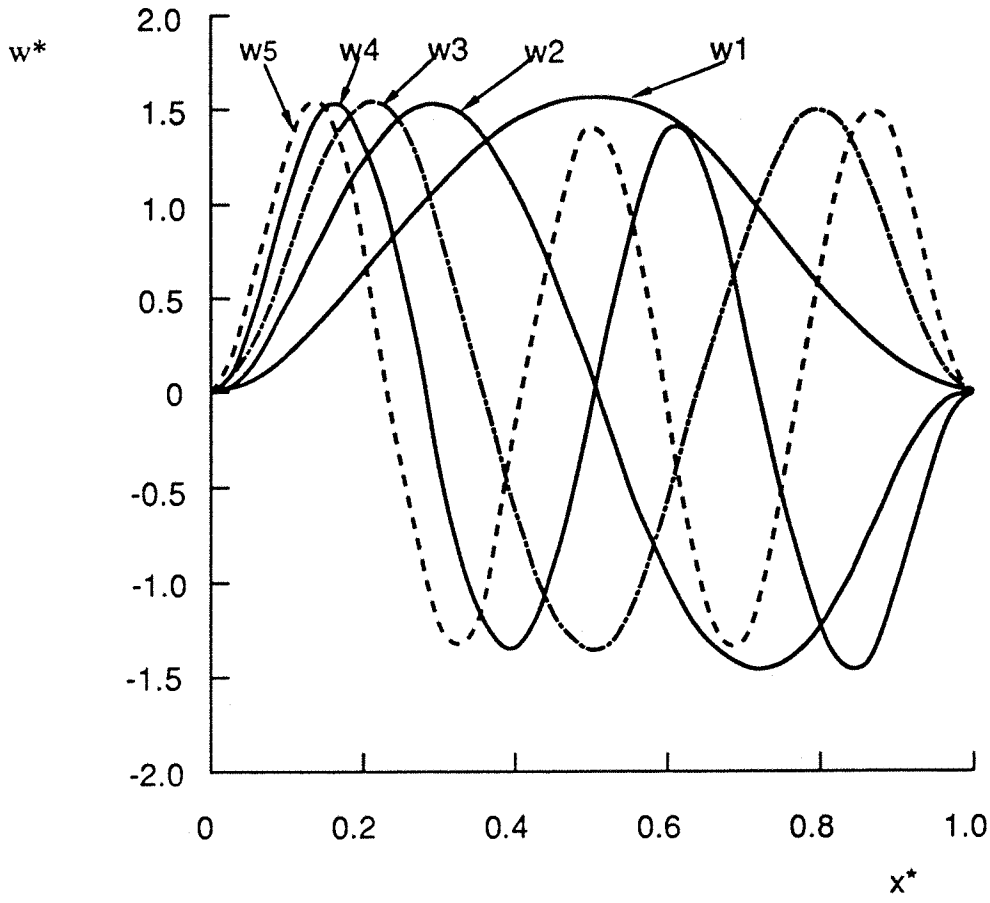

Fig. (4.2) NORMALISED CLAMPED-CLAMPED BEAM FUNCTIONS w_i^* FOR i = 1 to 5.

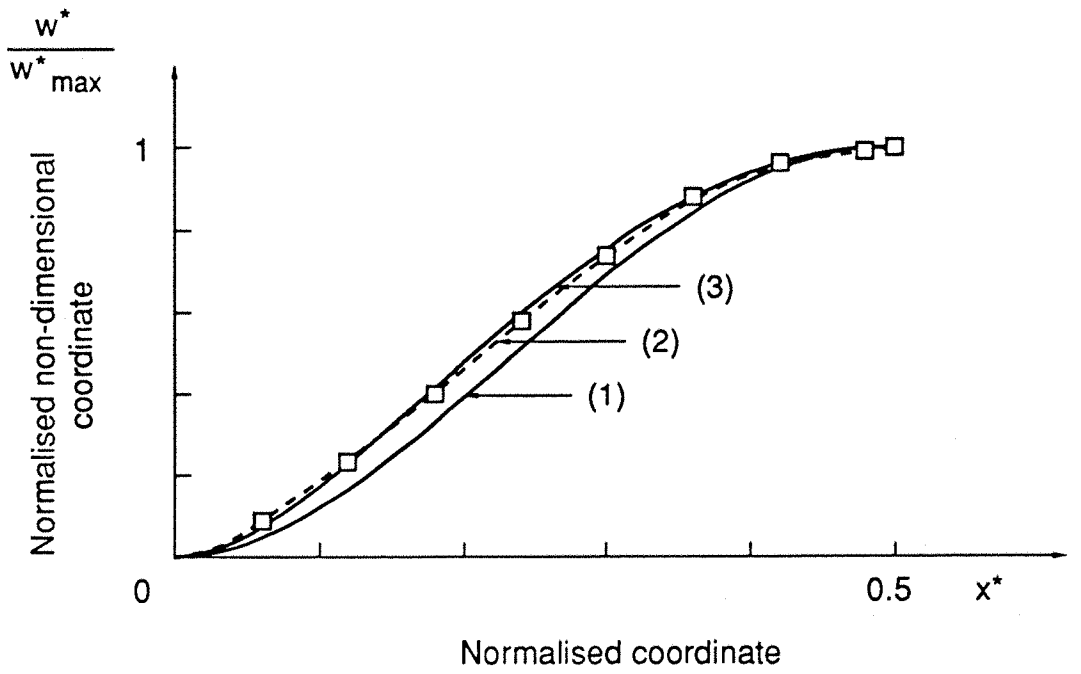

(1) Theoretical linear mode

(2) Experimental data (from [4.2])

(3) Theoretical nonlinear mode calculated for $w^*_{max} = 2.04$

Figure 4.3 COMPARISON OF THEORETICAL AND MEASURED NORMALISED NONLINEAR MODE SHAPE OF A CLAMPED-CLAMPED BEAM AT A MAXIMUM NON-DIMENSIONAL AMPLITUDE $w^*_{max} = 2.04$.

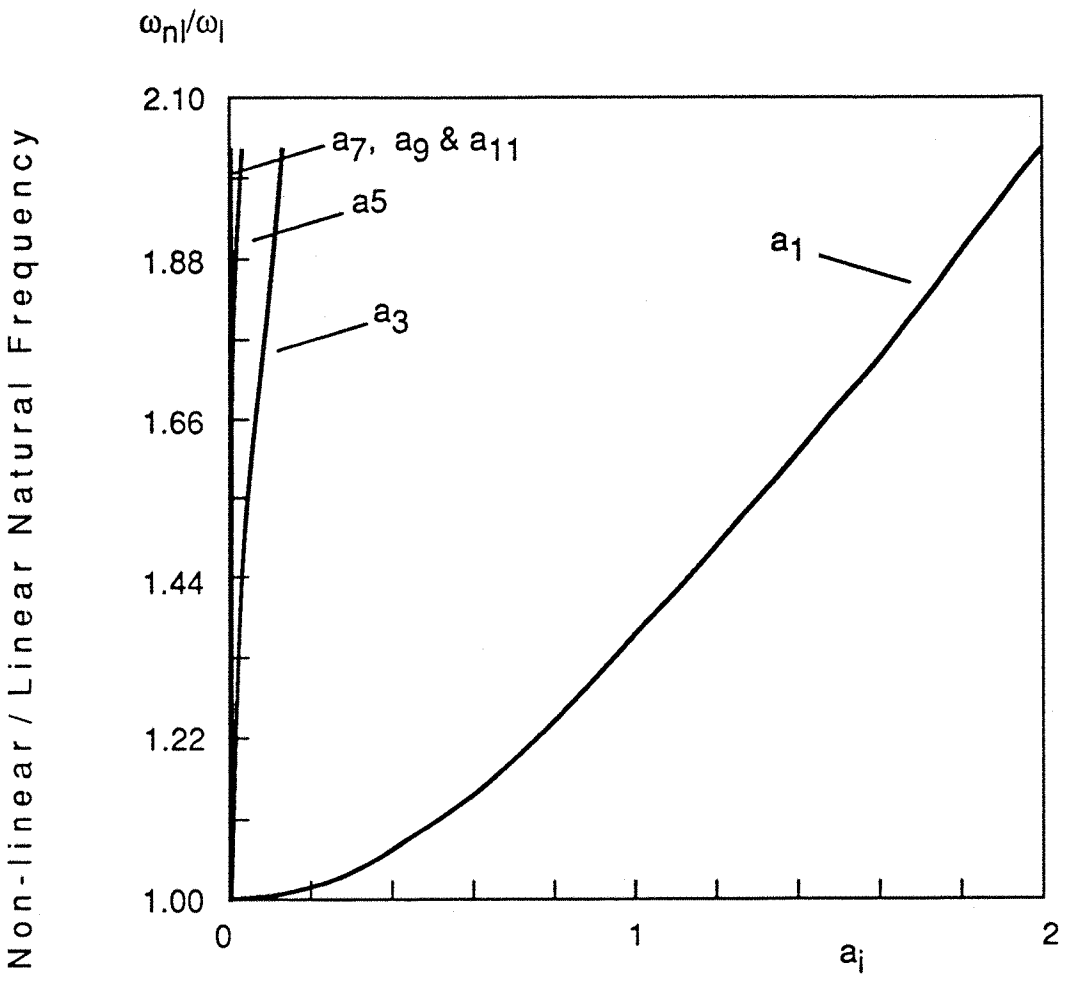

Fig. (4.3.1) BASIC FUNCTION CONTRIBUTION COEFFICIENTS TO THE **FIRST NONLINEAR MODE SHAPE** OF A CLAMPED-CLAMPED BEAM $\alpha = 3$

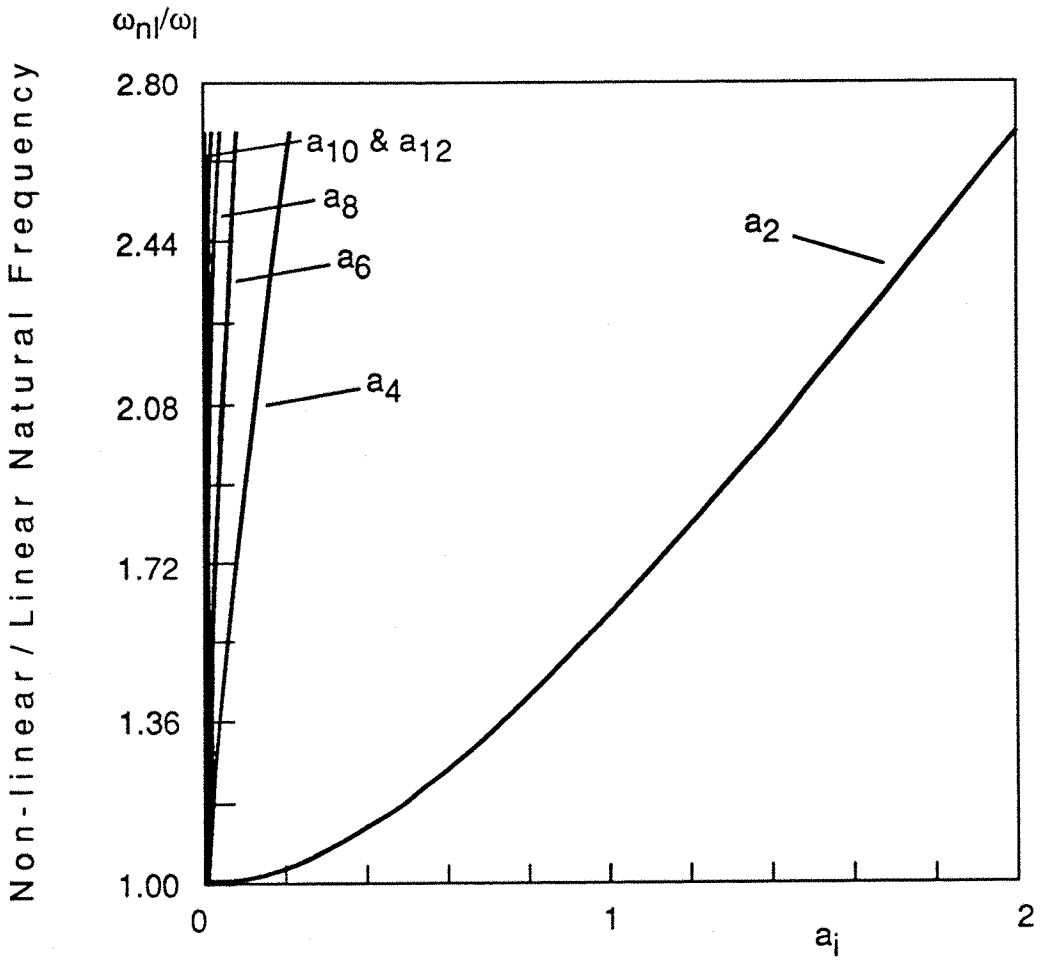

Fig. (4.3.2) BASIC FUNCTION CONTRIBUTION COEFFICIENTS TO THE **SECOND NON-LINEAR MODE SHAPE** OF A CLAMPED-CLAMPED BEAM. $\alpha = 3$

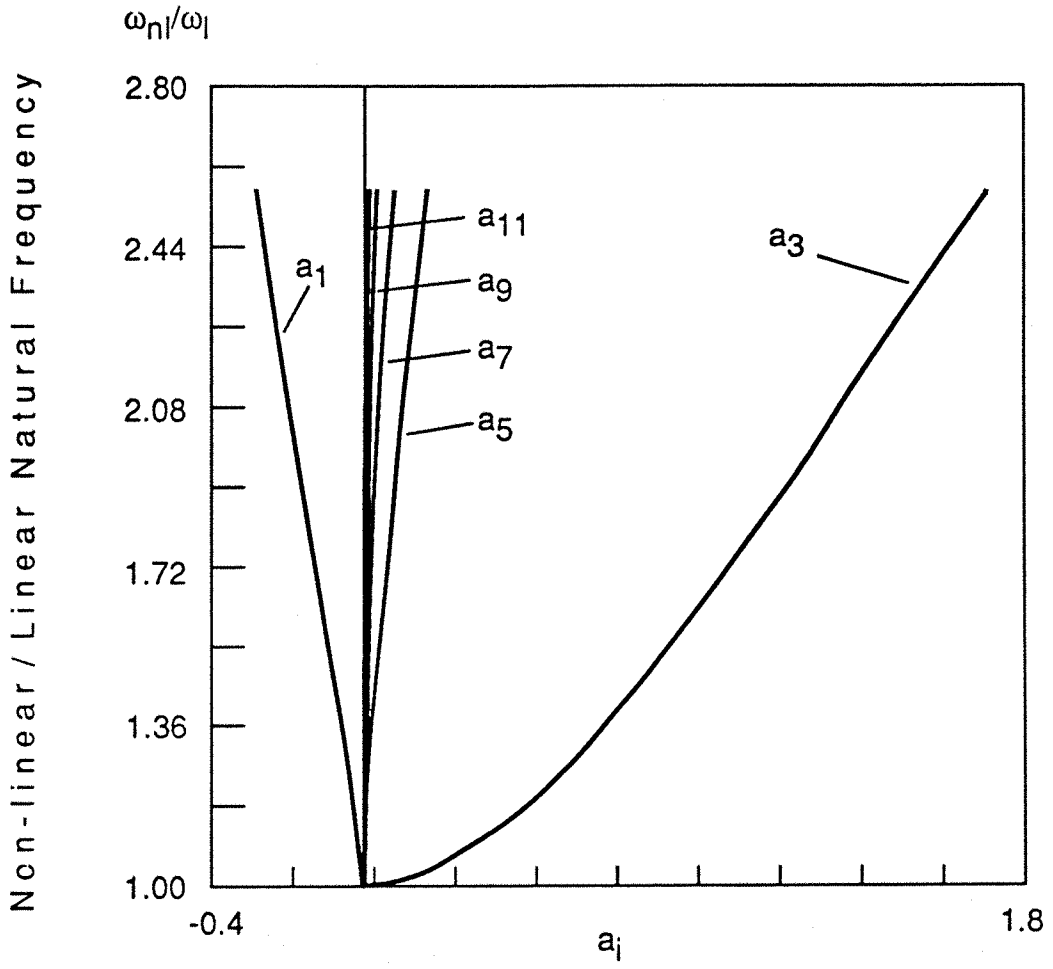

Fig. (4.3.3) BASIC FUNCTION CONTRIBUTION COEFFICIENTS TO THE **THIRD NONLINEAR MODE SHAPE** OF A CLAMPED-CLAMPED BEAM. $\alpha = 3$

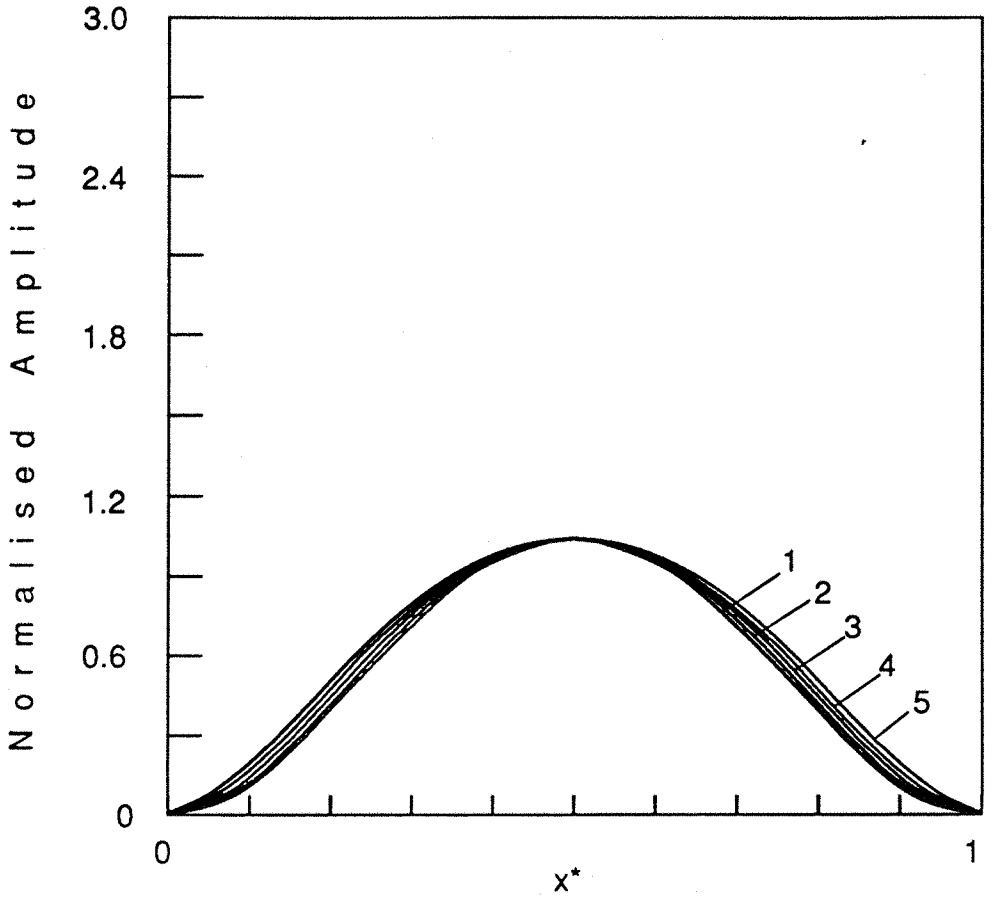

Fig. (4.4.1) THEORETICAL NON-LINEAR FIRST MODE SHAPE OF A CLAMPED-CLAMPED BEAM.

The maximum nondimensional amplitudes corresponding to curves 1 to 5 are given in Table 4.3.1

Curve 1: lowest amplitude

Curve 5: Highest amplitude

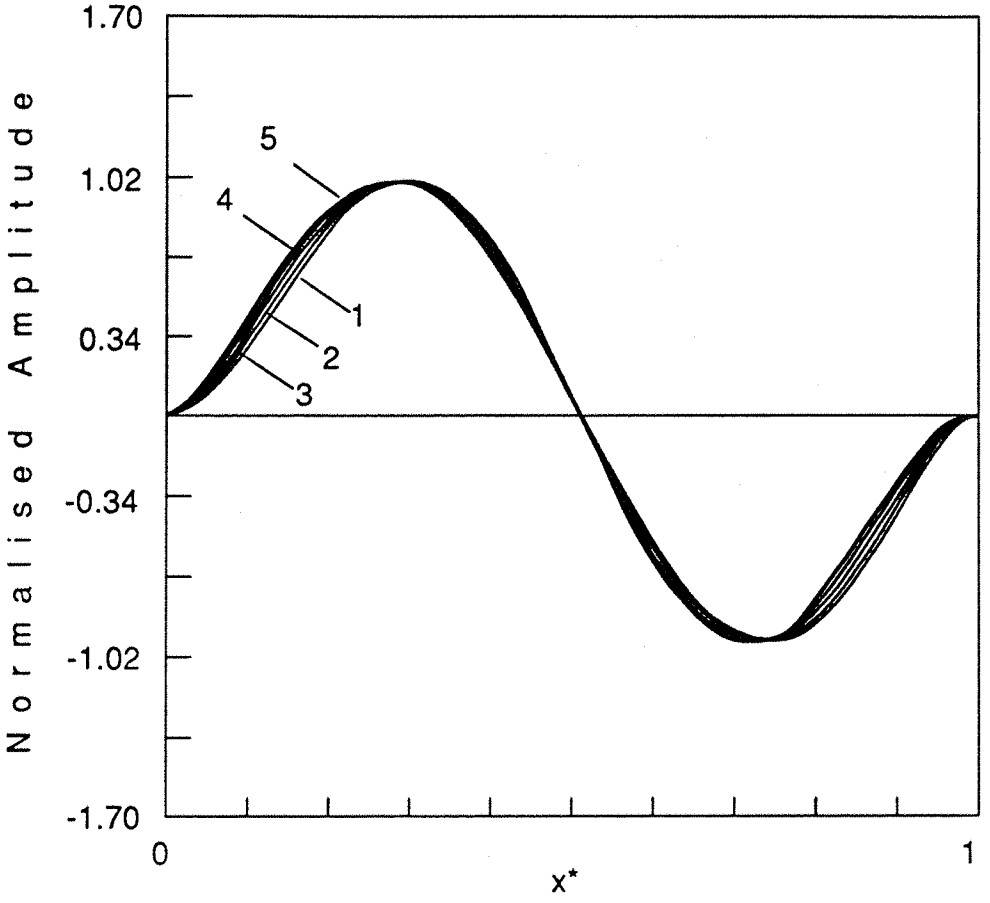

Fig. (4.4.2) THEORETICAL NON-LINEAR SECOND MODE SHAPE OF A CLAMPED-CLAMPED BEAM.

The maximum nondimensional amplitudes corresponding to curves 1 to 5 are given in Table 4.3.2

Curve 1: lowest amplitude

Curve 5: highest amplitude

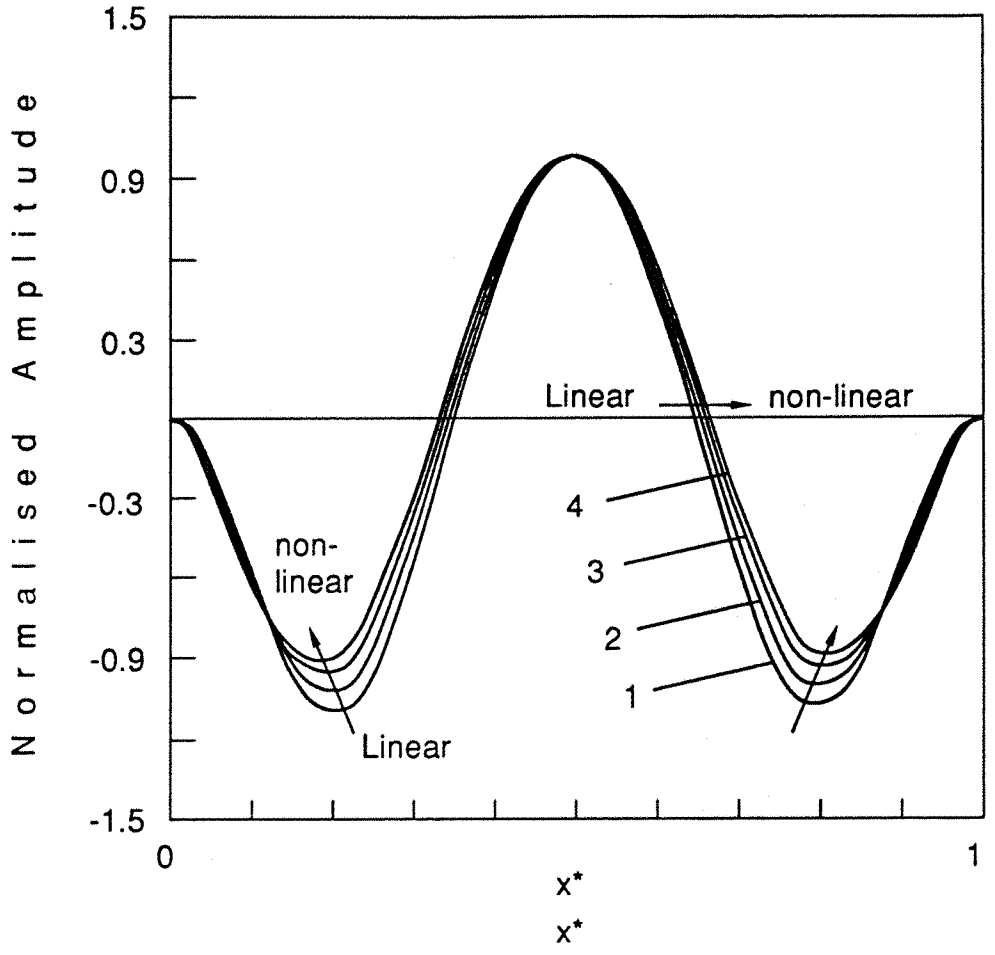

Fig. (4.4.3) THEORETICAL NON-LINEAR THIRD MODE SHAPE OF A CLAMPED-CLAMPED BEAM.

The maximum nondimensional amplitudes corresponding to curves 1 to 5 are given in Table 4.3.3

Curve 1: lowest amplitude

Curve 5: highest amplitude

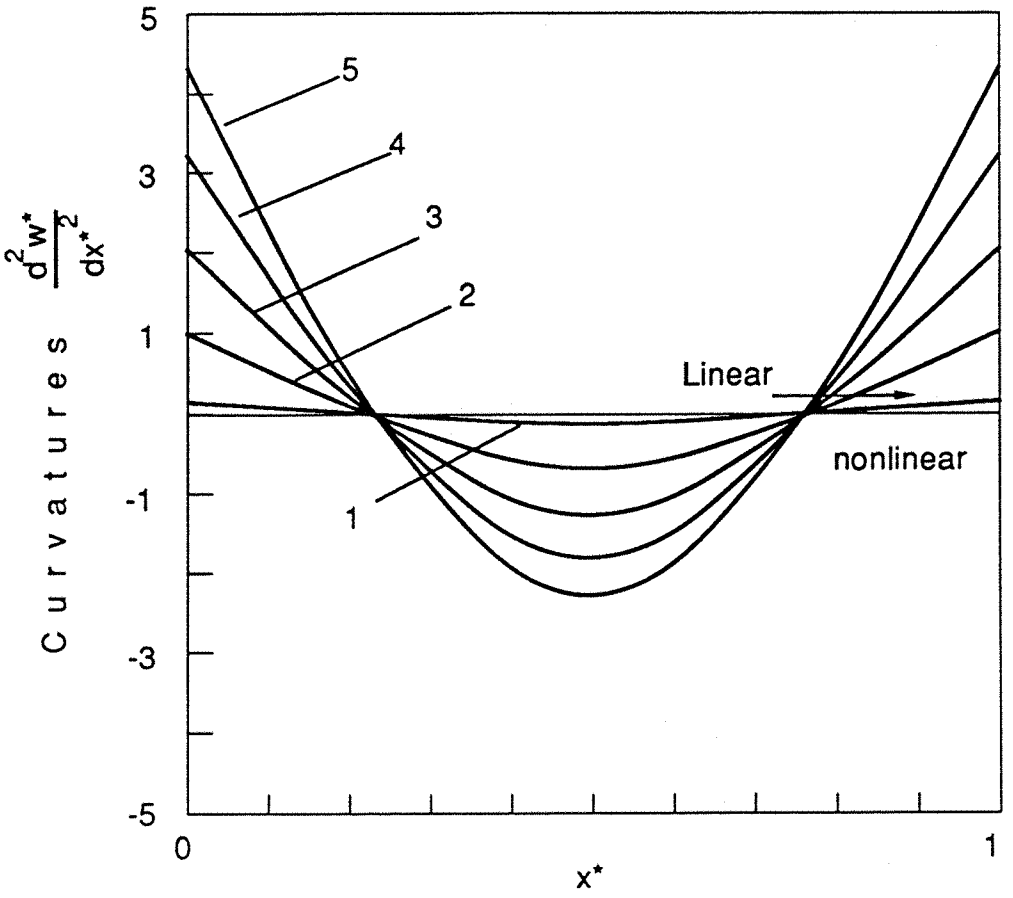

Fig.(4.5.1) CURVATURES OF THE FIRST NON-LINEAR MODE SHAPE OF A CLAMPED-CLAMPED BEAM.

The maximum nondimensional amplitudes corresponding to curves 1 to 5 are given in Table 4.3.1

Curve 1: lowest amplitude

Curve 5: highest amplitude

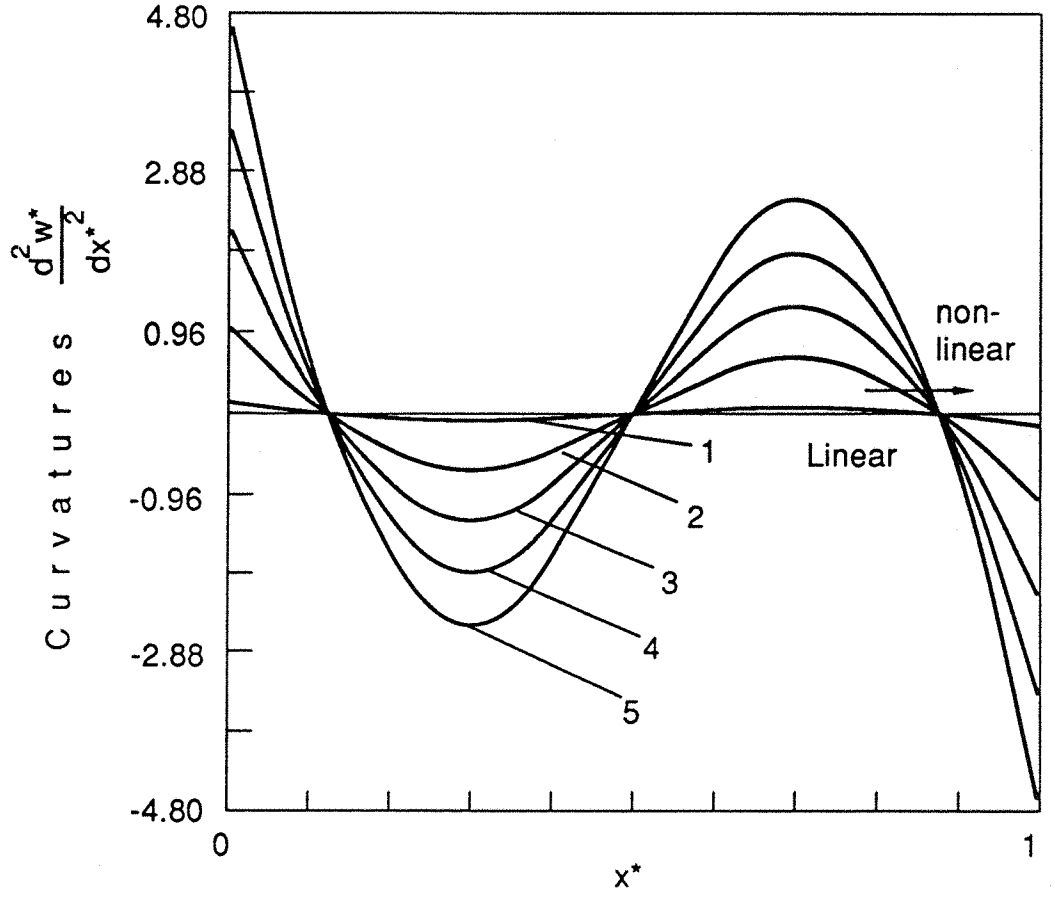

Fig.(4.5.2) CURVATURES OF THE SECOND NONLINEAR MODE SHAPE OF A CLAMPED-CLAMPED BEAM.

The maximum nondimensional amplitudes corresponding to curves 1 to 5 are given in Table 4.3.1

Curve 1: lowest amplitude

Curve 5: highest amplitude

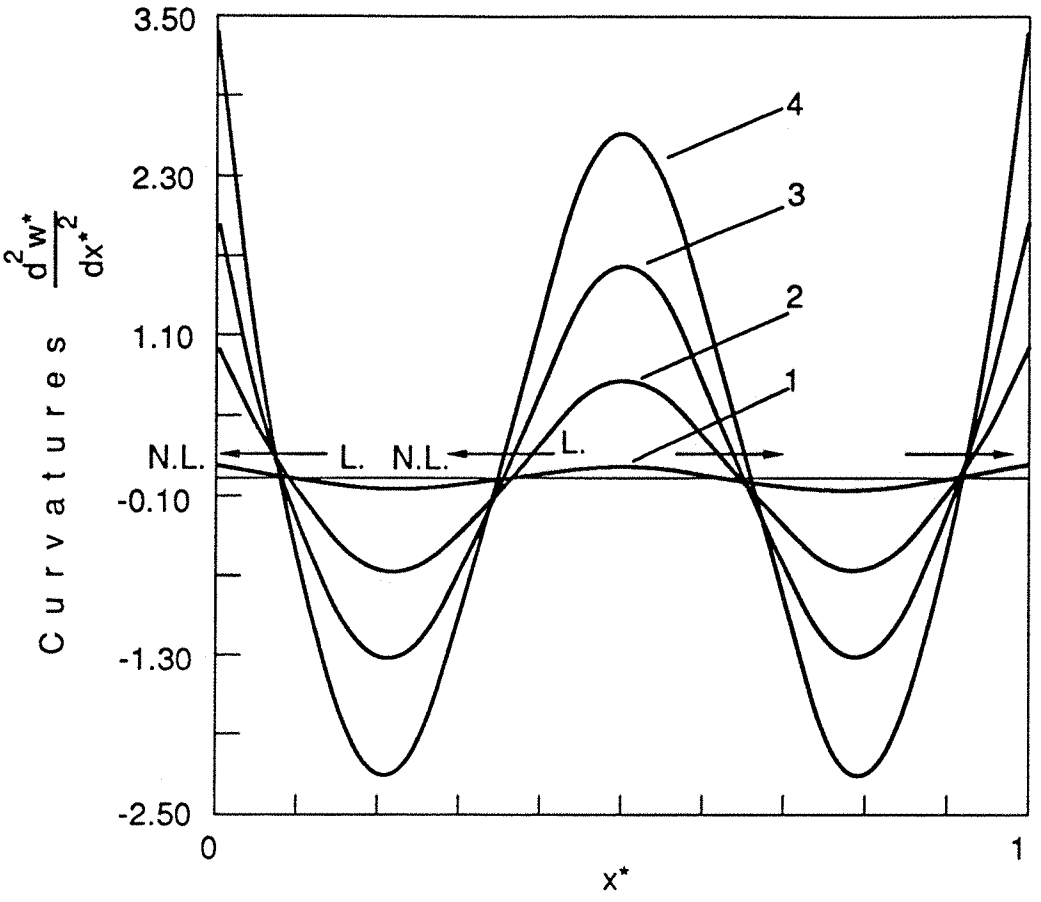

Fig.(4.5.3) CURVATURES OF THE THIRD NON-LINEAR MODE SHAPE OF A CLAMPED-CLAMPED BEAM.

The maximum nondimensional amplitudes corresponding to curves 1 to 5 are given in Table 4.3.3

Curve 1: lowest amplitude

Curve 5: highest amplitude

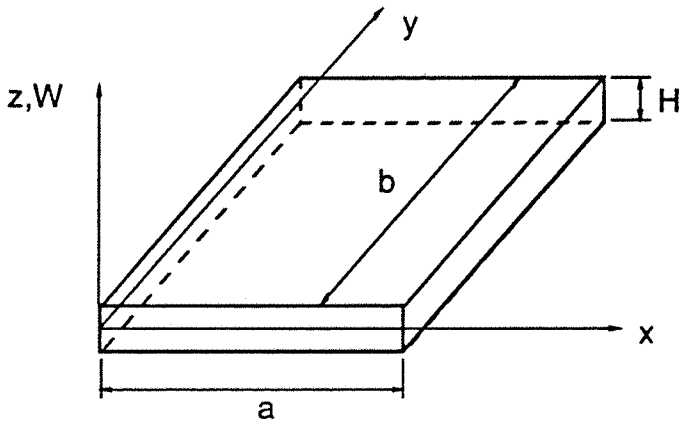

Fig. 5.1 PLATE NOTATION

The maximum nondimensional displacement amplitudes corresponding to curves 1 to 5 of Figures 5.2.1 to 5.5.5 are summarised in Table 5.10.

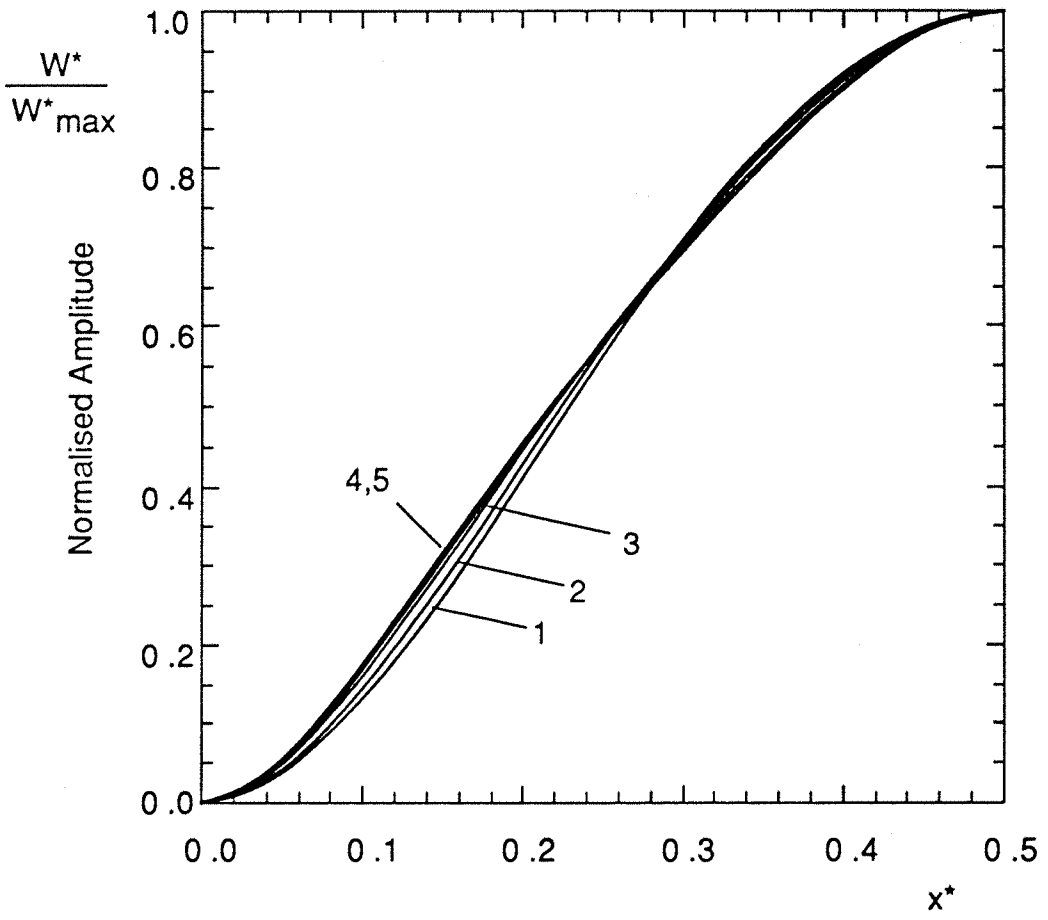

Fig. 5.2.1 NORMALISED SECTIONS OF THE FIRST NON-LINEAR MODE SHAPE CORRESPONDING TO $y^* = 0.5$ AND $\alpha = 1$

Curve 1: lowest amplitude

Curve 5: highest amplitude

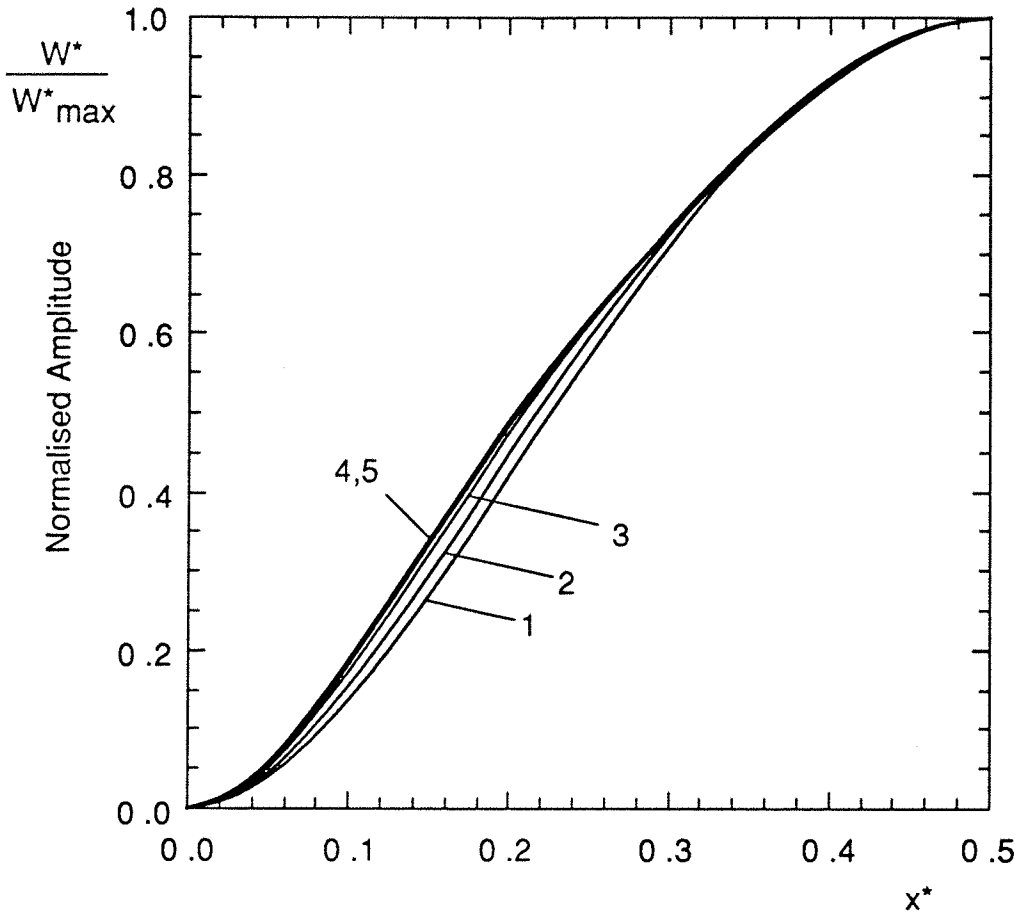

Fig. 5.2.2 NORMALISED SECTIONS OF THE FIRST NON-LINEAR MODE SHAPE CORRESPONDING TO $y^* = 0.5$ AND $\alpha = 0.8$

Curve 1: lowest amplitude

Curve 2: highest amplitude

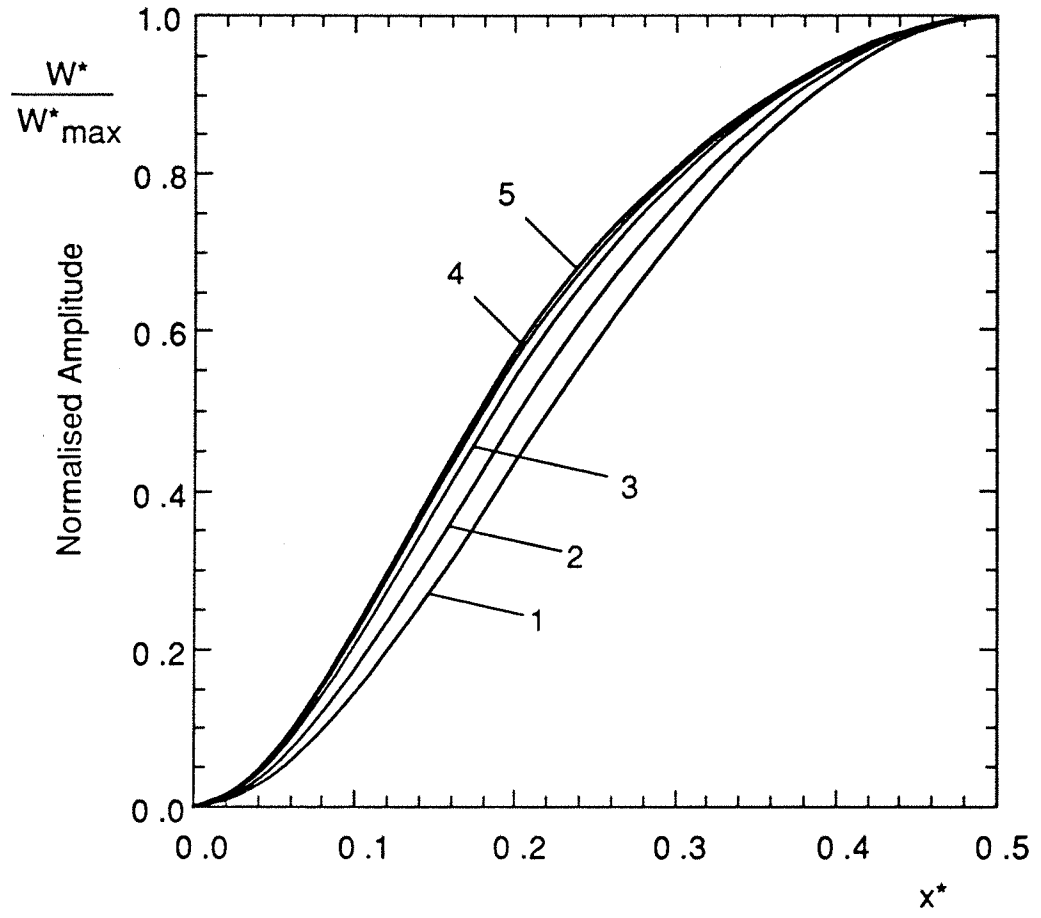

Fig. 5.2.3 NORMALISED SECTIONS OF THE FIRST NON-LINEAR MODE SHAPE CORRESPONDING TO $y^* = 0.5$ AND $\alpha = 0.6$

Curve 1: lowest amplitude

Curve 5: highest amplitude

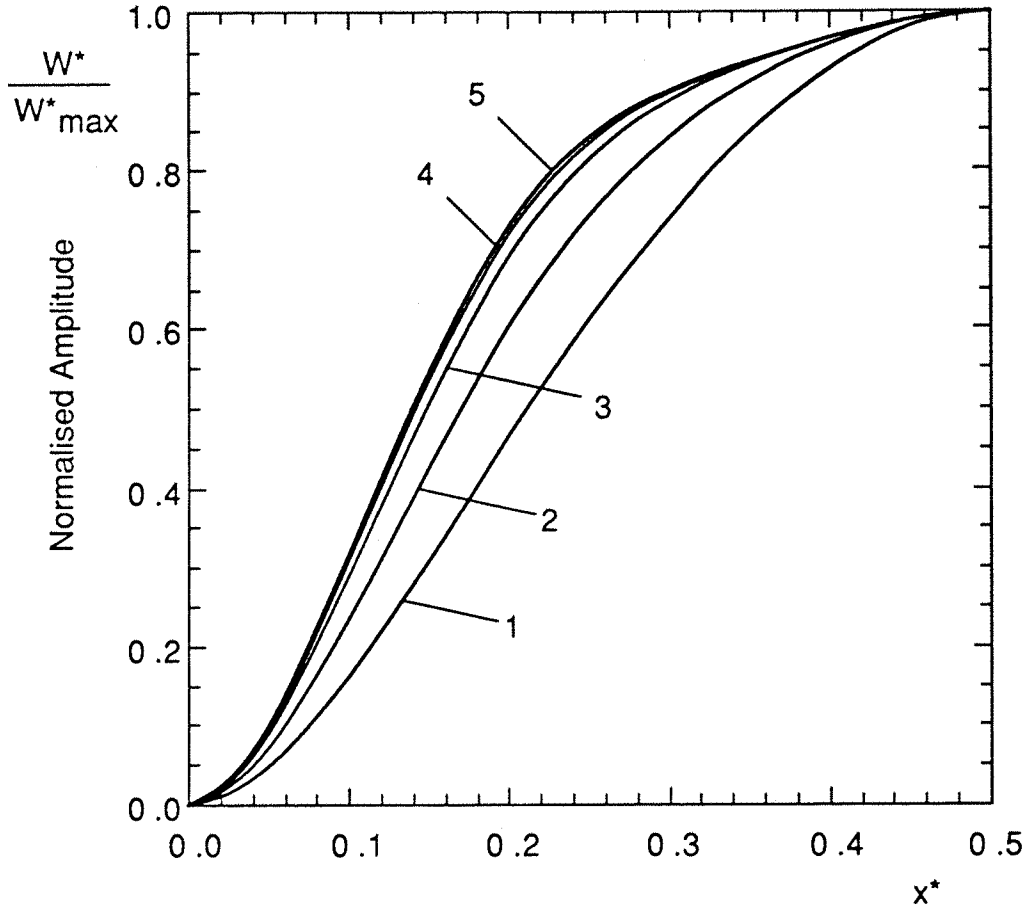

Fig. 5.2.4 NORMALISED SECTIONS OF THE FIRST NON-LINEAR MODE SHAPE CORRESPONDING TO $y^* = 0.5$ AND $\alpha = 0.4$

Curve 1: lowest amplitude

Curve 5: highest amplitude

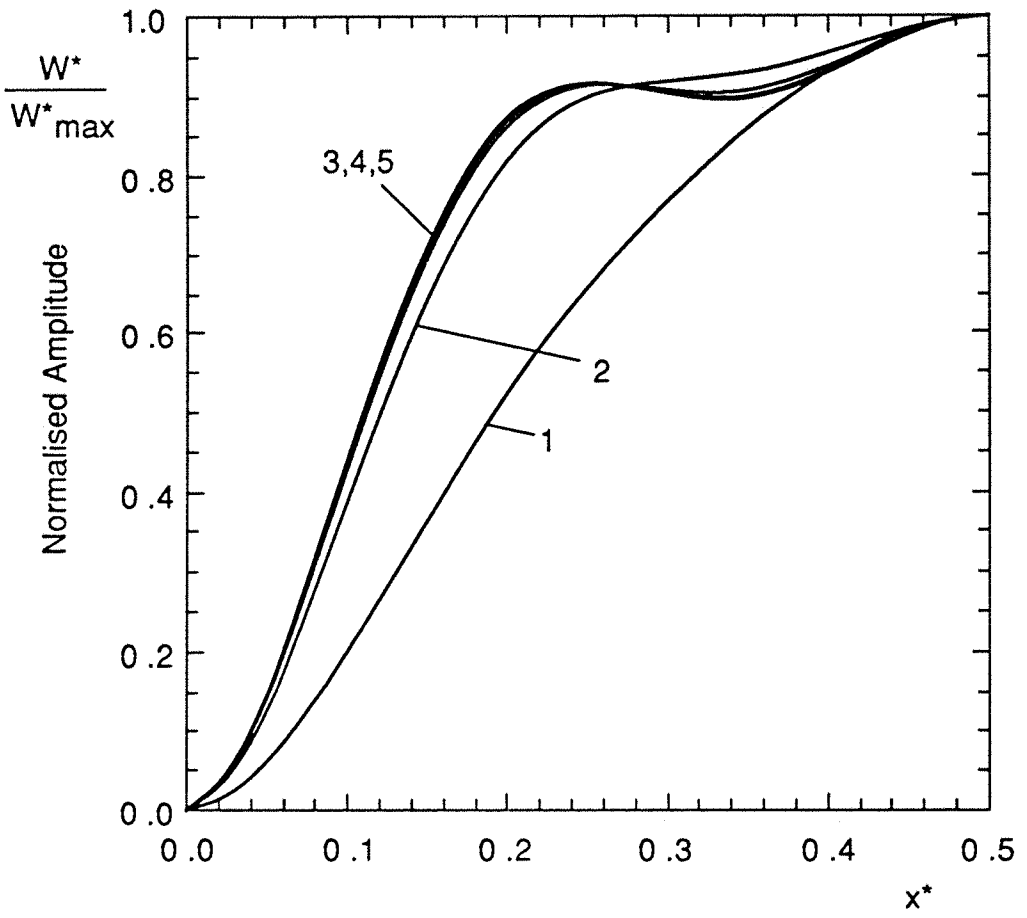

Fig. 5.2.5 NORMALISED SECTIONS OF THE FIRST NON-LINEAR MODE SHAPE CORRESPONDING TO $y^* = 0.5$ AND $\alpha = 0.2$

Curve 1: lowest amplitude

Curve 5: highest amplitude

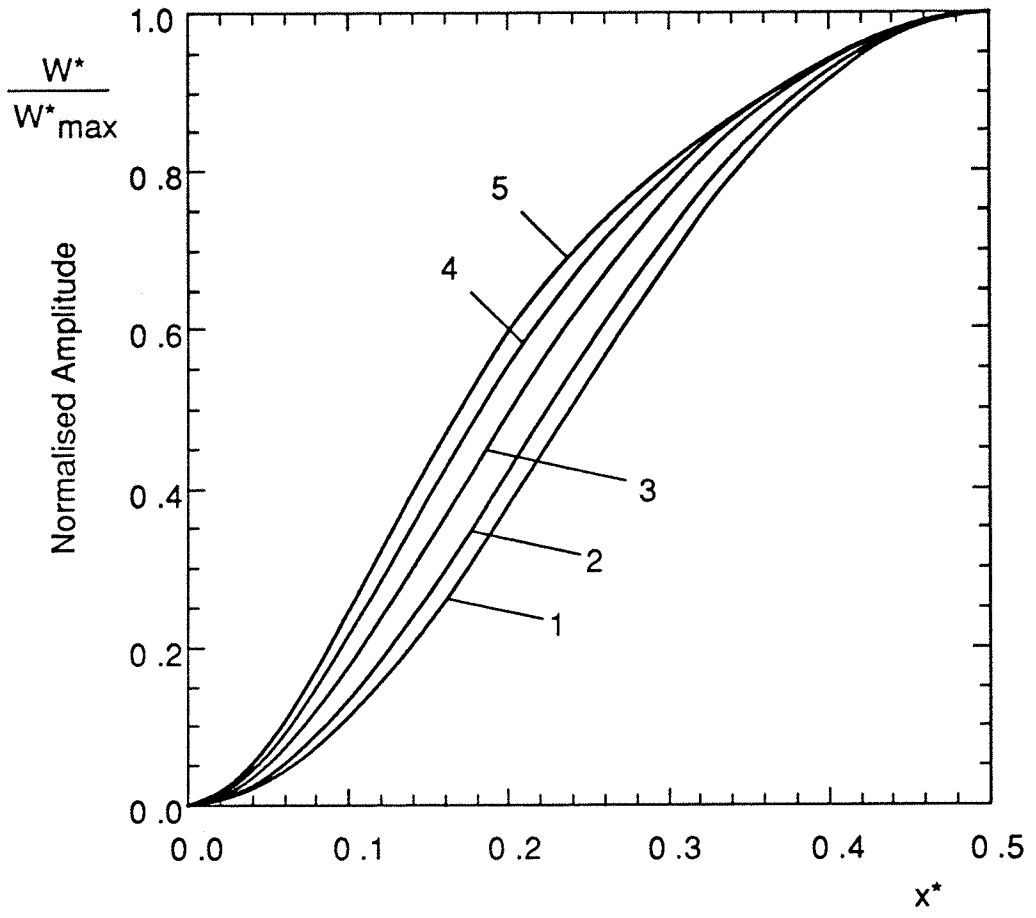

Fig. 5.3.1 NORMALISED SECTIONS OF THE FIRST NON-LINEAR MODE SHAPE CORRESPONDING TO $y^* = 0.05$ AND $\alpha = 1$

Curve 1: lowest amplitude

Curve 5: highest amplitude

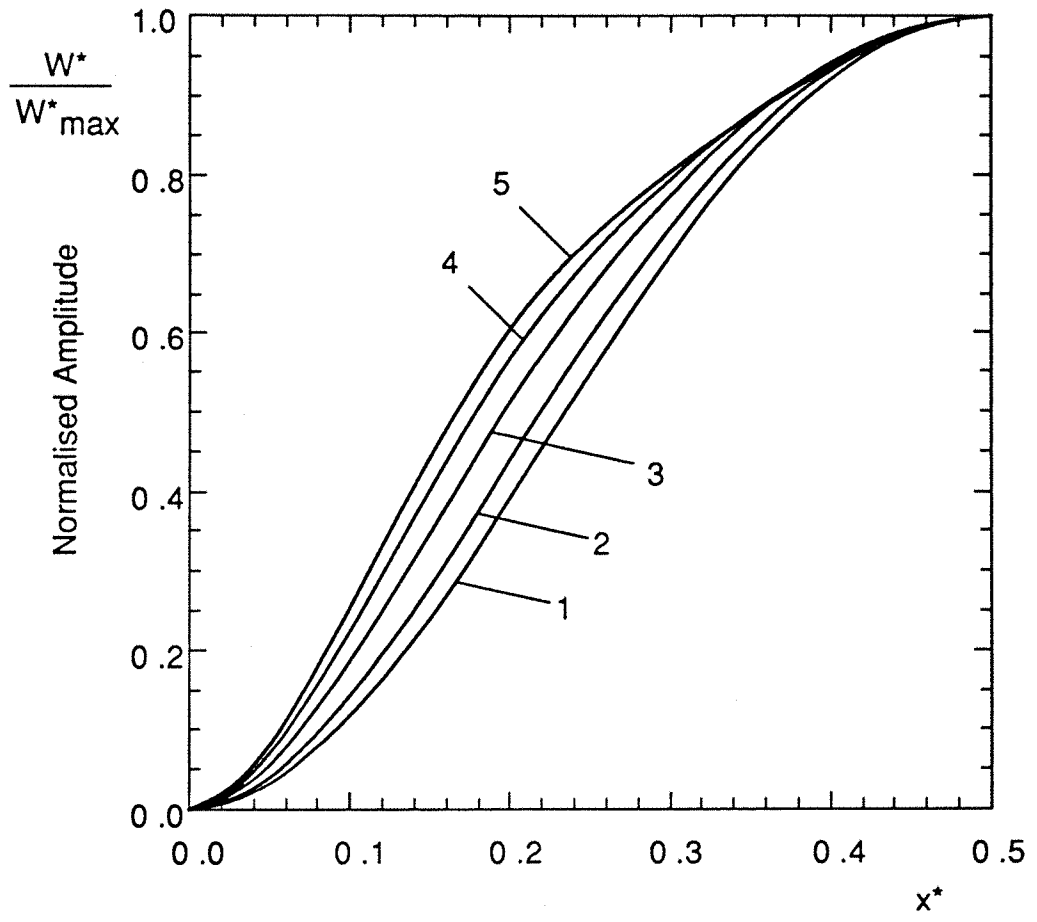

Fig. 5.3.2 NORMALISED SECTIONS OF THE FIRST NON-LINEAR MODE SHAPE CORRESPONDING TO $y^* = 0.05$ AND $\alpha = 0.8$

Curve 1: lowest amplitude

Curve 5: highest amplitude

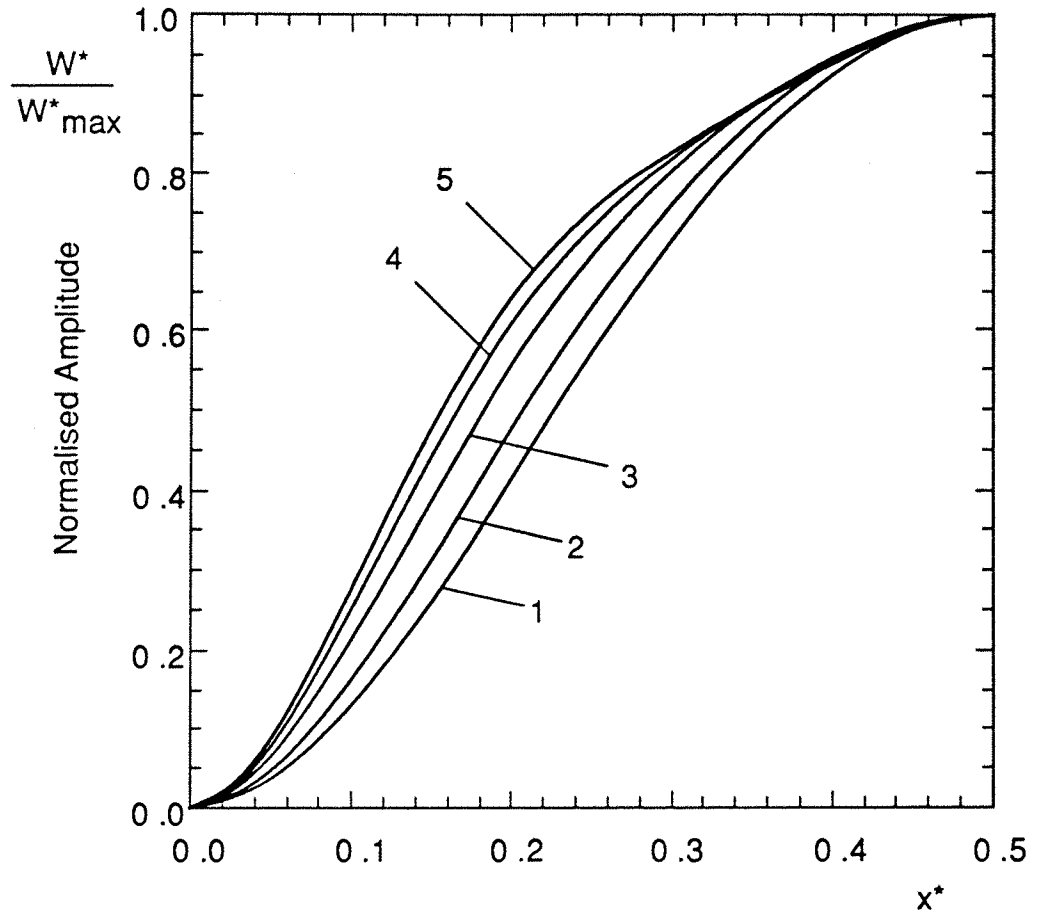

Fig. 5.3.3 NORMALISED SECTIONS OF THE FIRST NON-LINEAR MODE SHAPE CORRESPONDING TO $y^* = 0.05$ AND $\alpha = 0.6$

Curve 1: lowest amplitude

Curve 2: highest amplitude

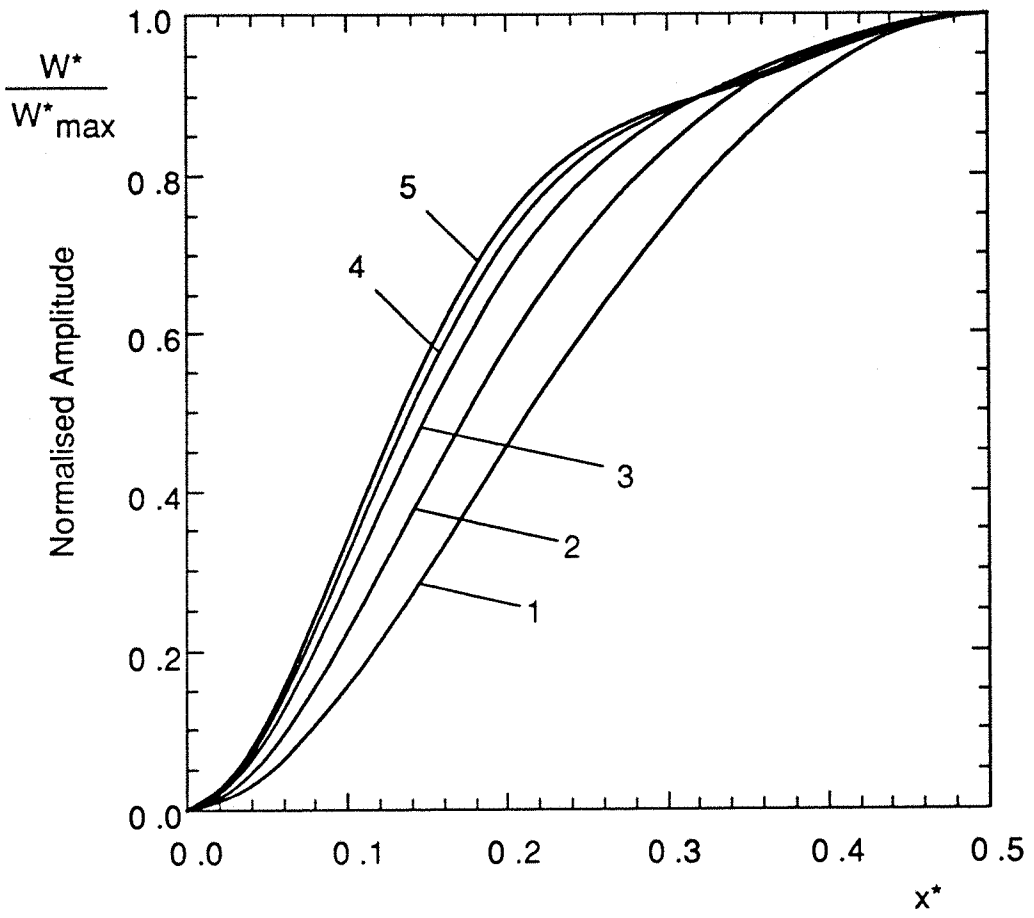

Fig. 5.3.4 NORMALISED SECTIONS OF THE FIRST NON-LINEAR MODE SHAPE CORRESPONDING TO $y^* = 0.05$ AND $\alpha = 0.4$

Curve 1: lowest amplitude

Curve 5: highest amplitude

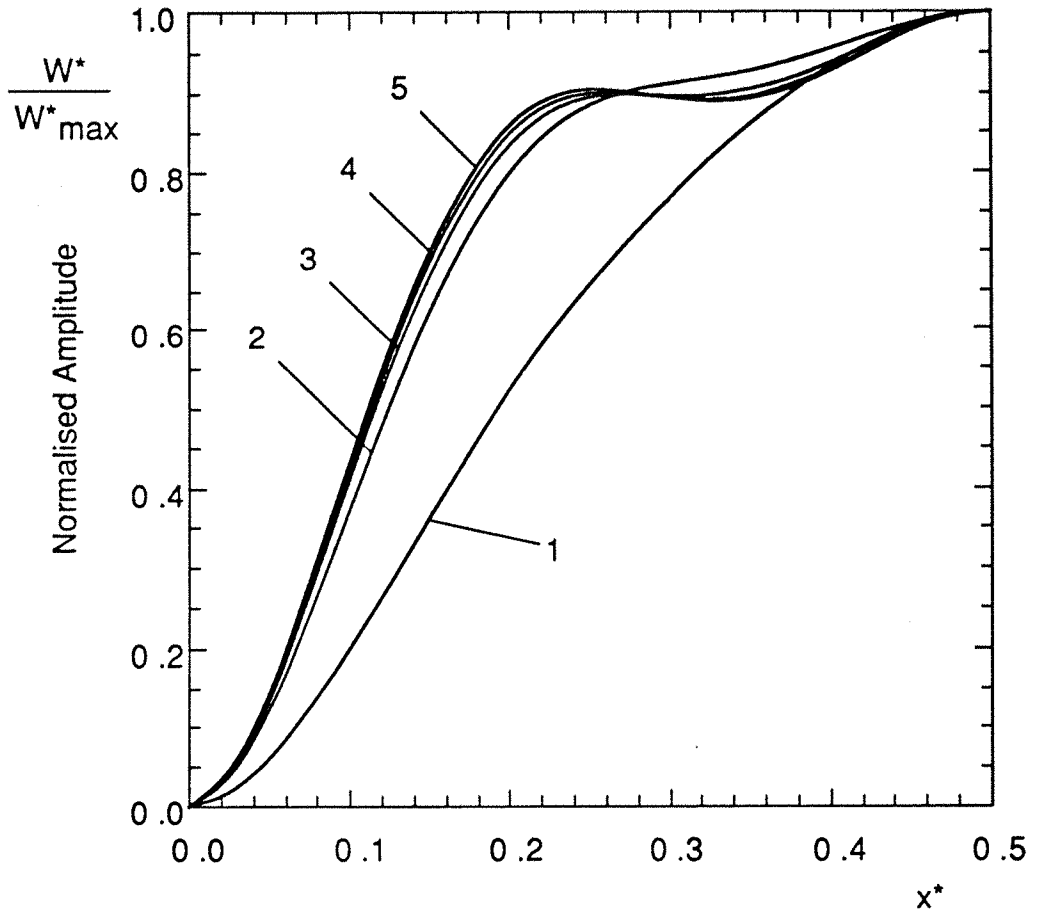

Fig. 5.3.5 NORMALISED SECTIONS OF THE FIRST NON-LINEAR MODE SHAPE CORRESPONDING TO $y^* = 0.05$ AND $\alpha = 0.2$

Curve 1: lowest amplitude

Curve 5: highest amplitude

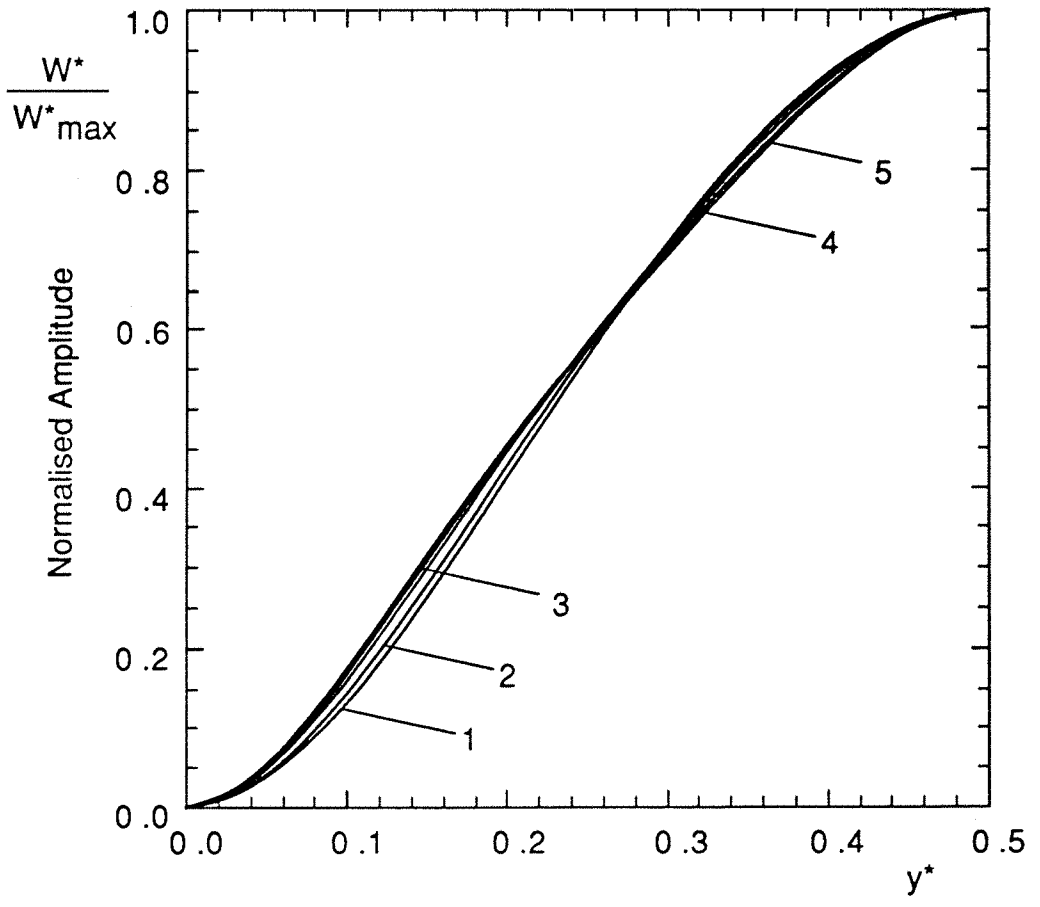

Fig. 5.4.1 NORMALISED SECTIONS OF THE FIRST NON-LINEAR MODE SHAPE CORRESPONDING TO $x^* = 0.5$ AND $\alpha = 1$

Curve 1: lowest amplitude

Curve 5: highest amplitude

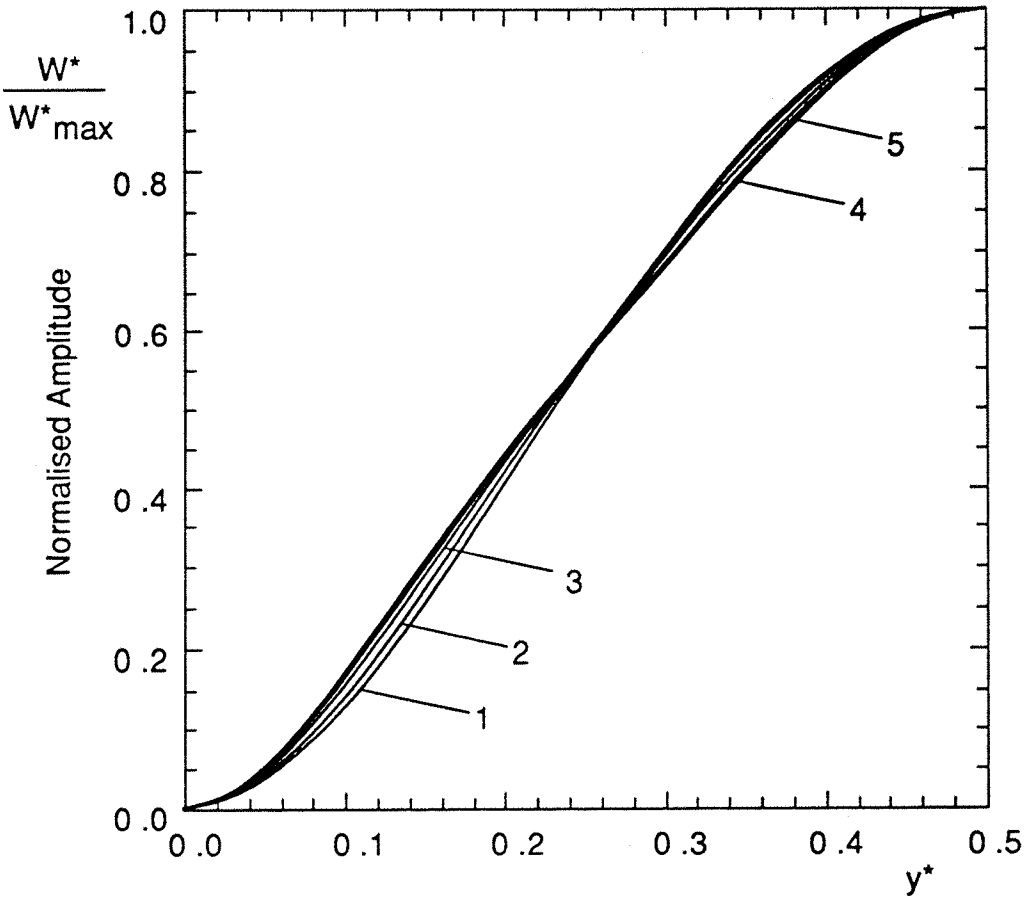

Fig. 5.4.2 NORMALISED SECTIONS OF THE FIRST NON-LINEAR MODE SHAPE CORRESPONDING TO $x^* = 0.5$ AND $\alpha = 0.8$

Curve 1: lowest amplitude

Curve 5: highest amplitude

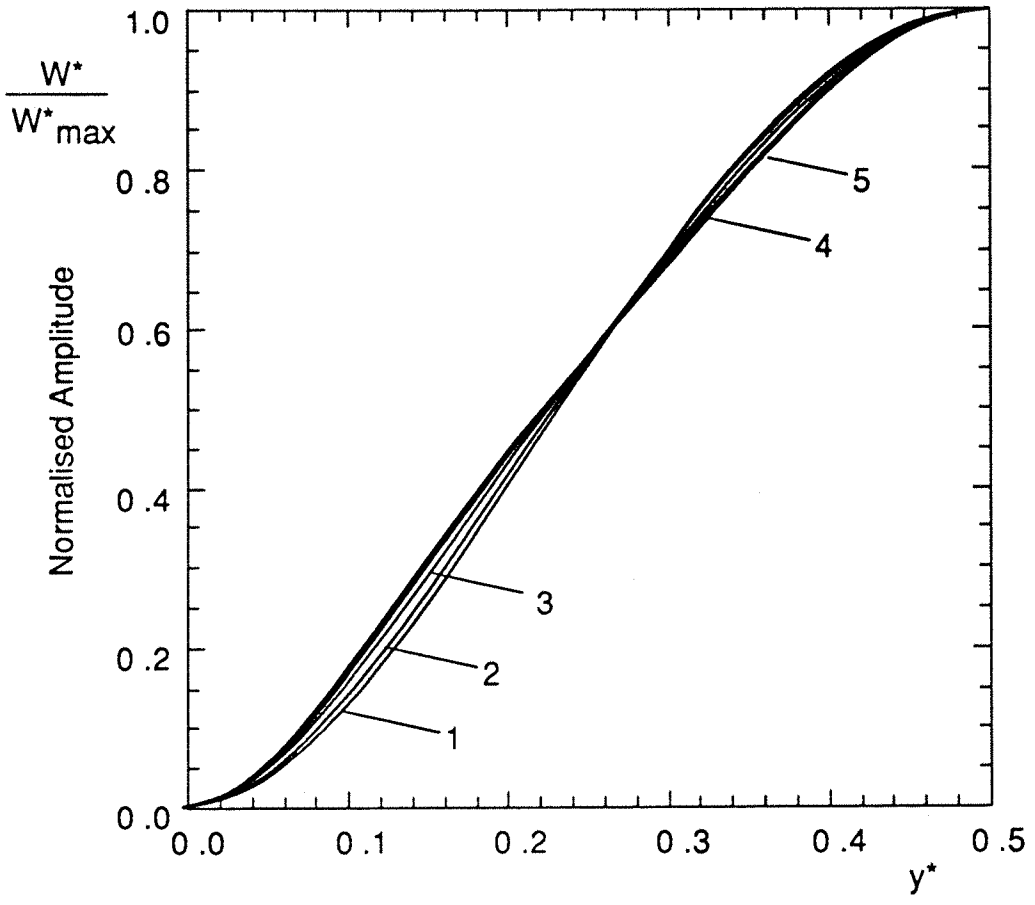

Fig. 5.4.3 NORMALISED SECTIONS OF THE FIRST NON-LINEAR MODE SHAPE CORRESPONDING TO $x^* = 0.5$ AND $\alpha = 0.6$

Curve 1: lowest amplitude

Curve 5: highest amplitude

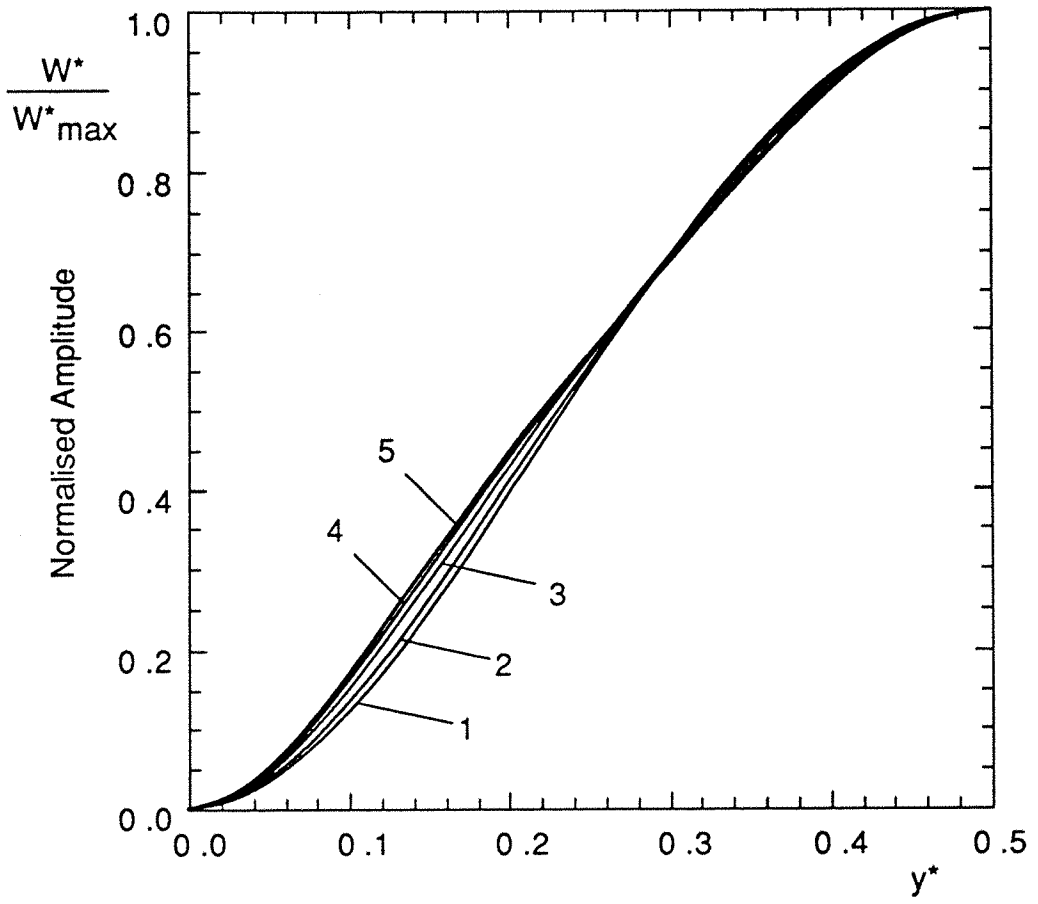

Fig. 5.4.4 NORMALISED SECTIONS OF THE FIRST NON-LINEAR MODE SHAPE CORRESPONDING TO $x^* = 0.5$ AND $\alpha = 0.4$

Curve 1: lowest amplitude

Curve 5: highest amplitude

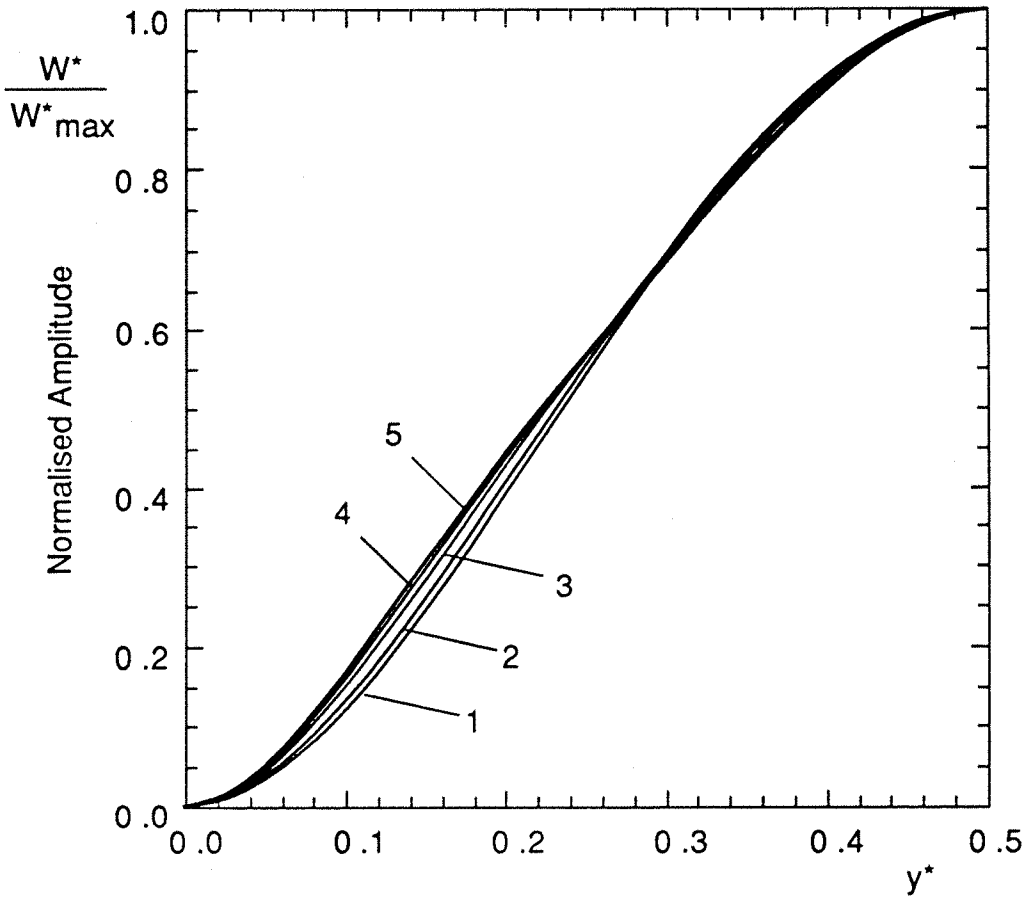

Fig. 5.4.5 NORMALISED SECTIONS OF THE FIRST NON-LINEAR MODE SHAPE CORRESPONDING TO $x^* = 0.5$ AND $\alpha = 0.2$

Curve 1: lowest amplitude

Curve 5: highest amplitude

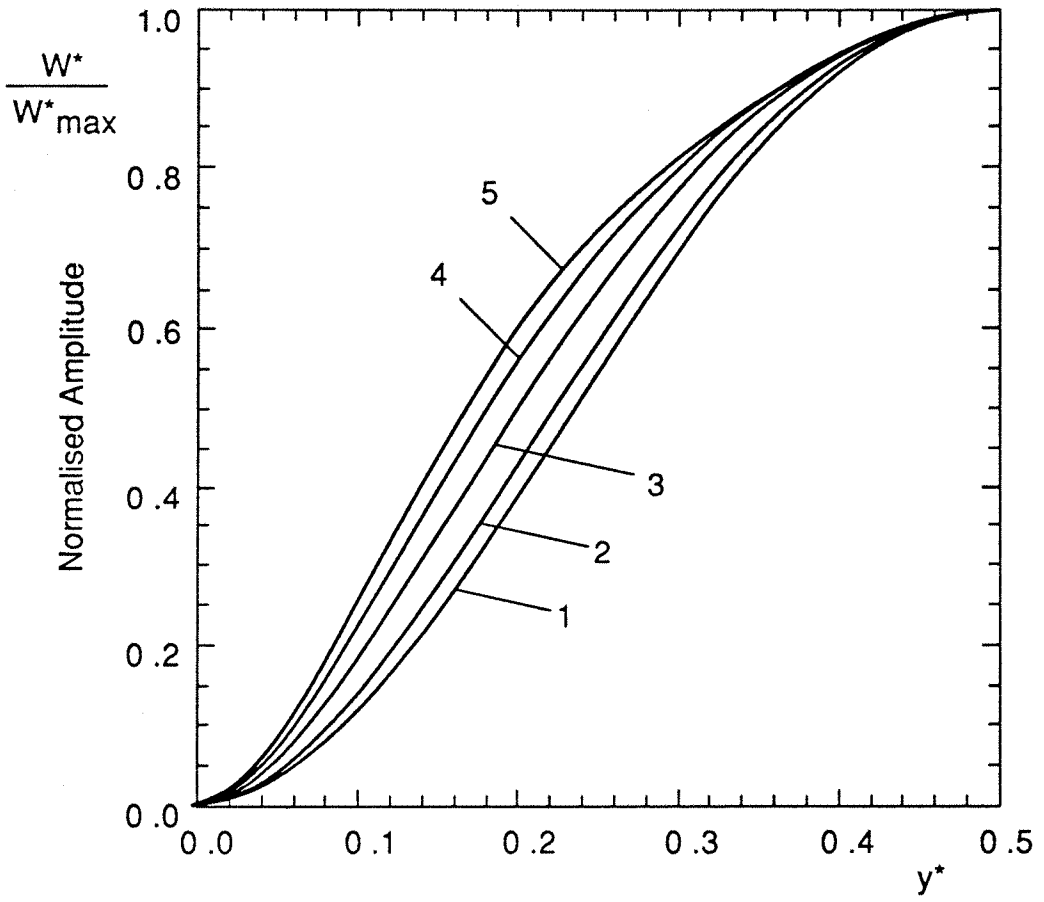

Fig. 5.5.1 NORMALISED SECTIONS OF THE FIRST NON-LINEAR MODE SHAPE CORRESPONDING TO $x^* = 0.05$ AND $\alpha = 1$

Curve 1: lowest amplitude

Curve 5: highest amplitude

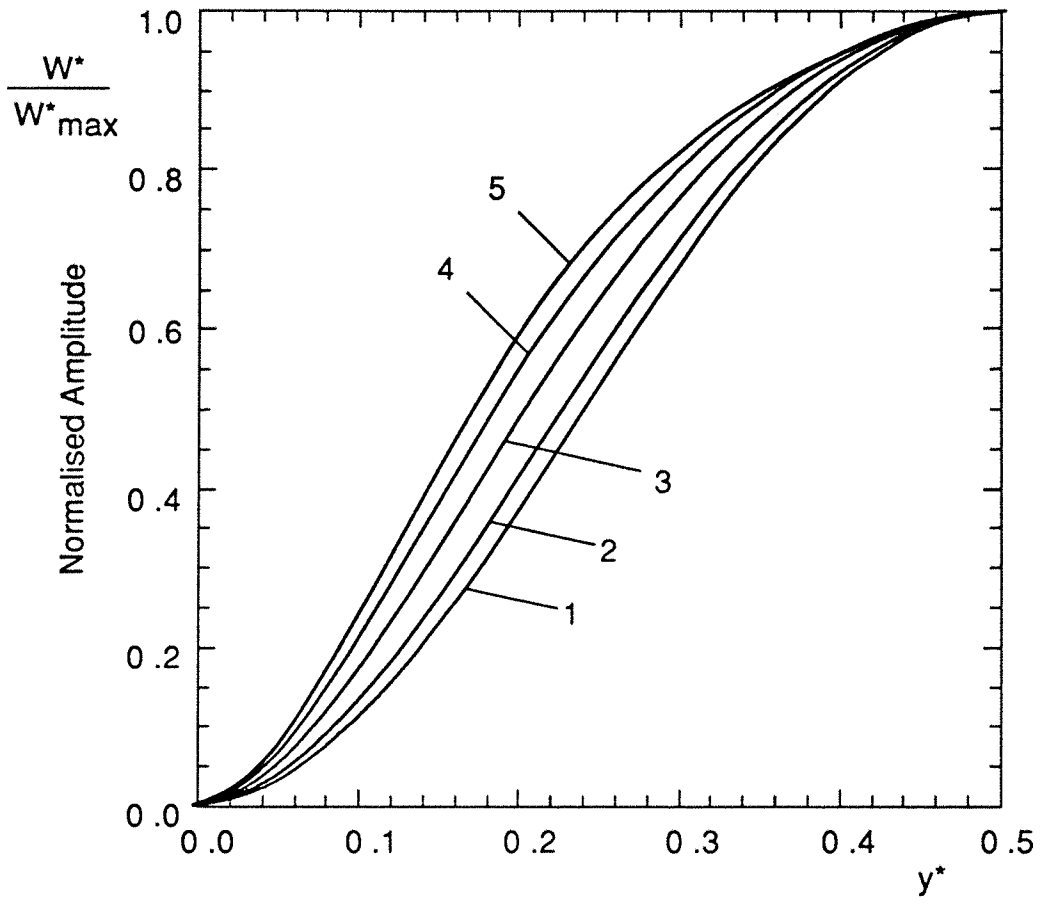

Fig. 5.5.2 NORMALISED SECTIONS OF THE FIRST NON-LINEAR MODE SHAPE CORRESPONDING TO $x^* = 0.05$ AND $\alpha = 0.8$

Curve 1: lowest amplitude

Curve 5: highest amplitude

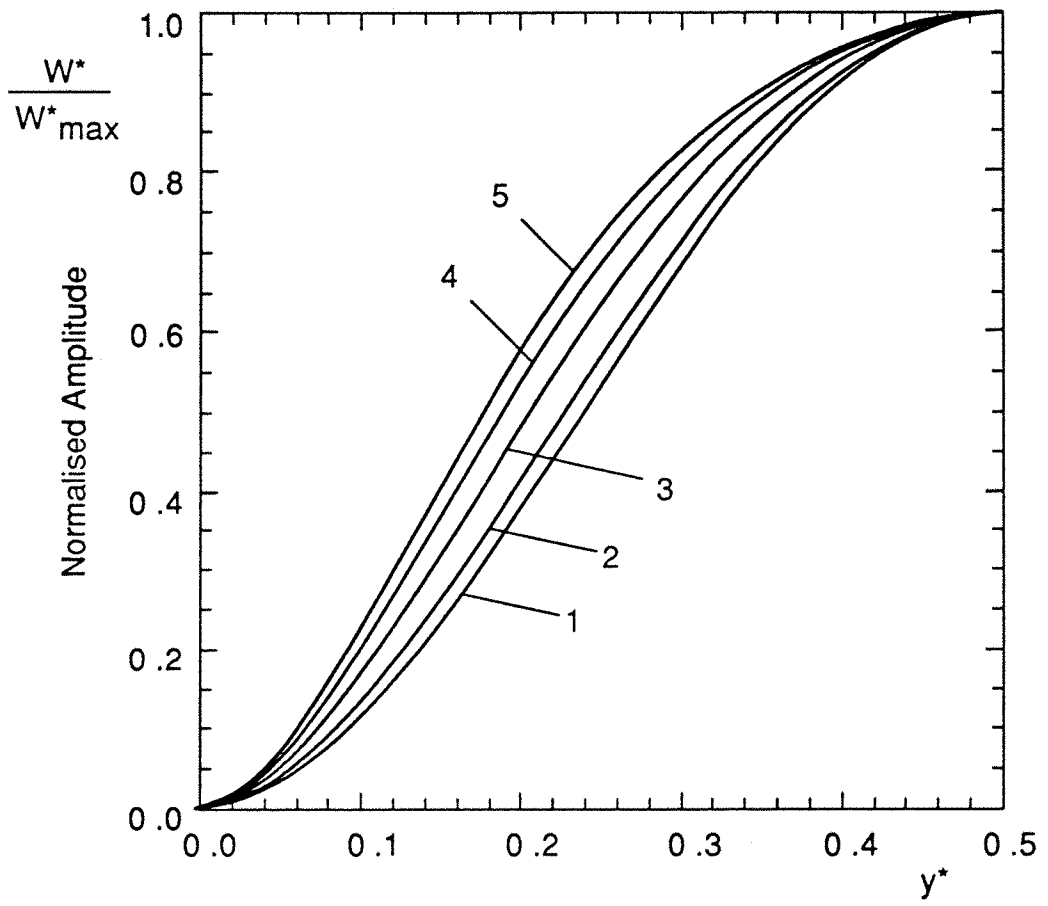

Fig. 5.5.3 NORMALISED SECTIONS OF THE FIRST NON-LINEAR MODE SHAPE CORRESPONDING TO $x^* = 0.05$ AND $\alpha = 0.6$

Curve 1: lowest amplitude

Curve 5: highest amplitude

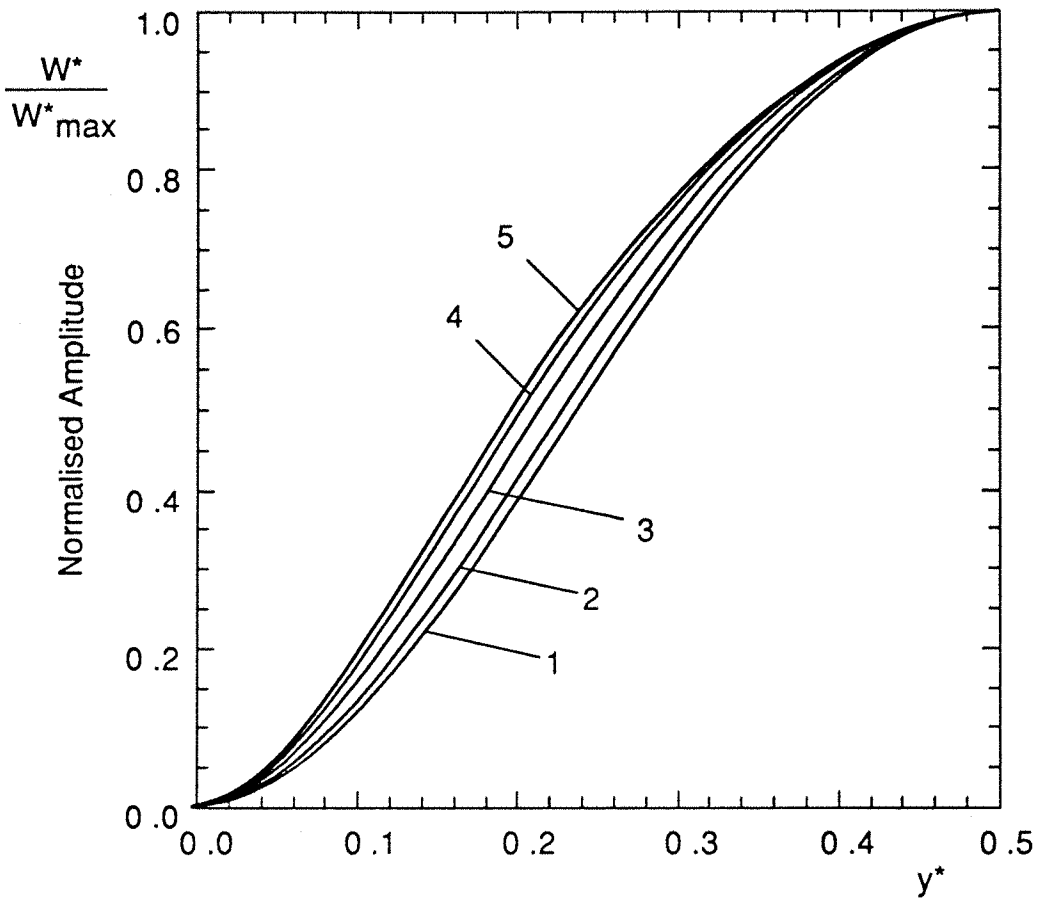

Fig. 5.5.4 NORMALISED SECTIONS OF THE FIRST NON-LINEAR MODE SHAPE CORRESPONDING TO $x^* = 0.05$ AND $\alpha = 0.4$

Curve 1: lowest amplitude

Curve 5: highest amplitude

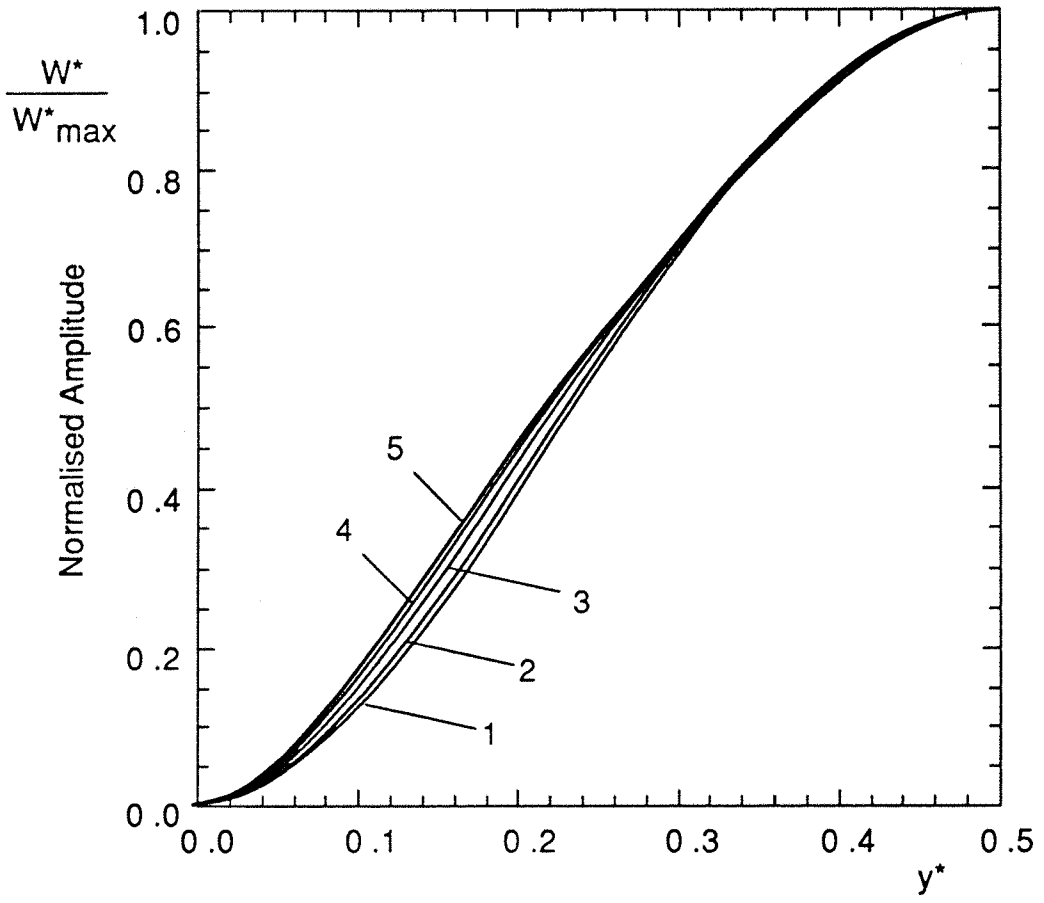

Fig. 5.5.5 NORMALISED SECTIONS OF THE FIRST NON-LINEAR MODE SHAPE CORRESPONDING TO $x^* = 0.05$ AND $\alpha = 0.2$

Curve 1: lowest amplitude

Curve 5: highest amplitude

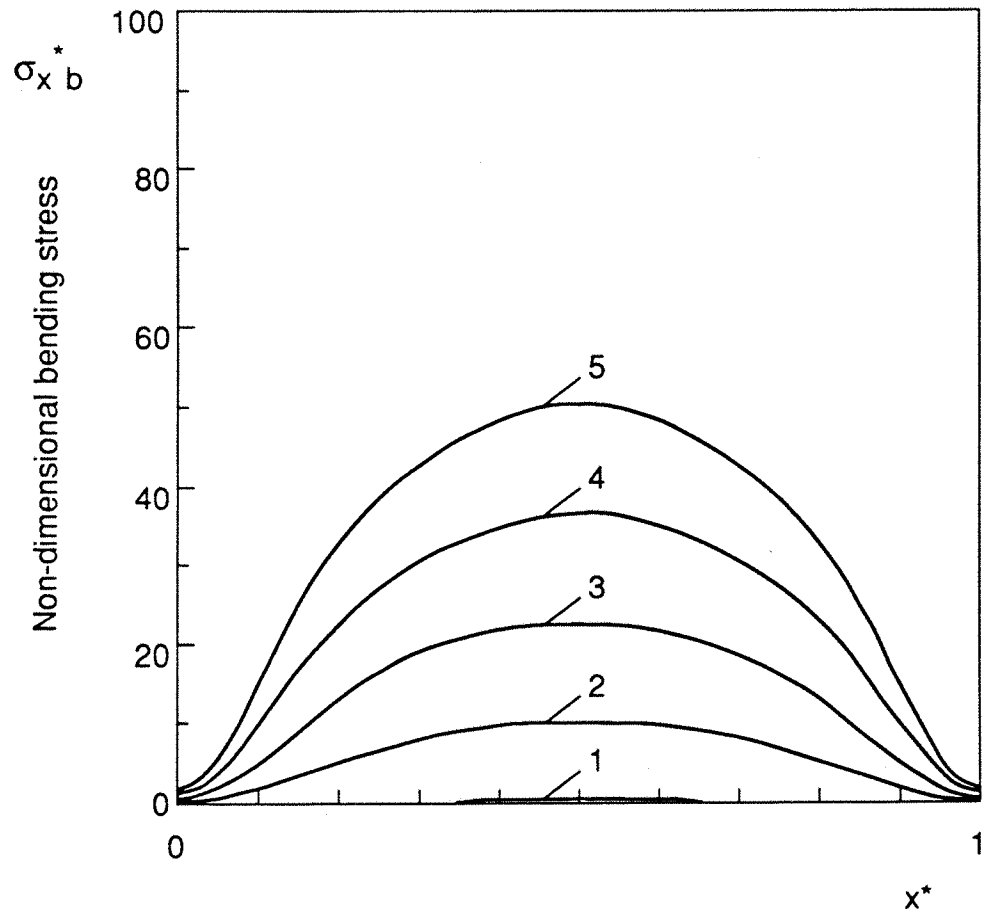

Fig. 5.6.1 NON-DIMENSIONAL BENDING STRESS DISTRIBUTION ALONG THE SECTION $y^* = 0.05$ OF A FULLY CLAMPED RECTANGULAR PLATE, $\alpha = 0.6$.

Curve 1: lowest amplitude

Curve 5: highest amplitude

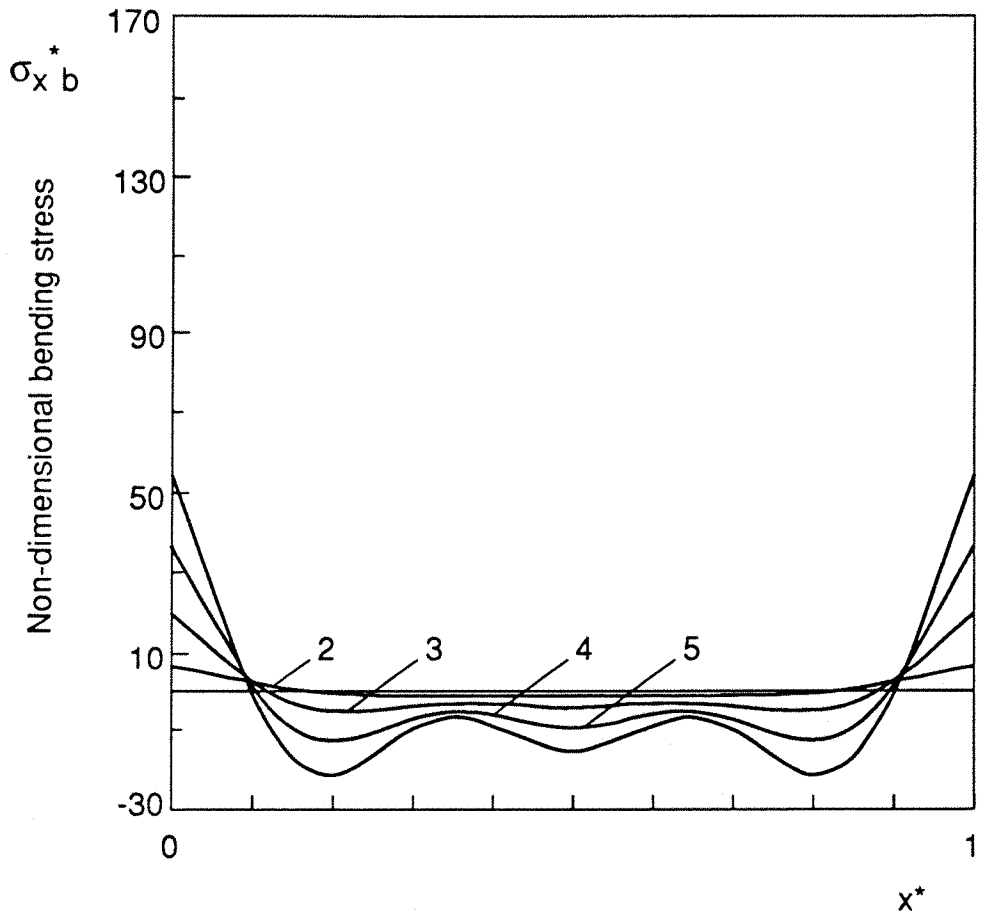

Figure 5.6.2 NON-DIMENSIONAL BENDING STRESS DISTRIBUTION ALONG THE SECTION $y^* = 0.2$ OF A FULLY CLAMPED RECTANGULAR PLATE, $\alpha = 0.6$.

Curve 1: lowest amplitude

Curve 5: highest amplitude

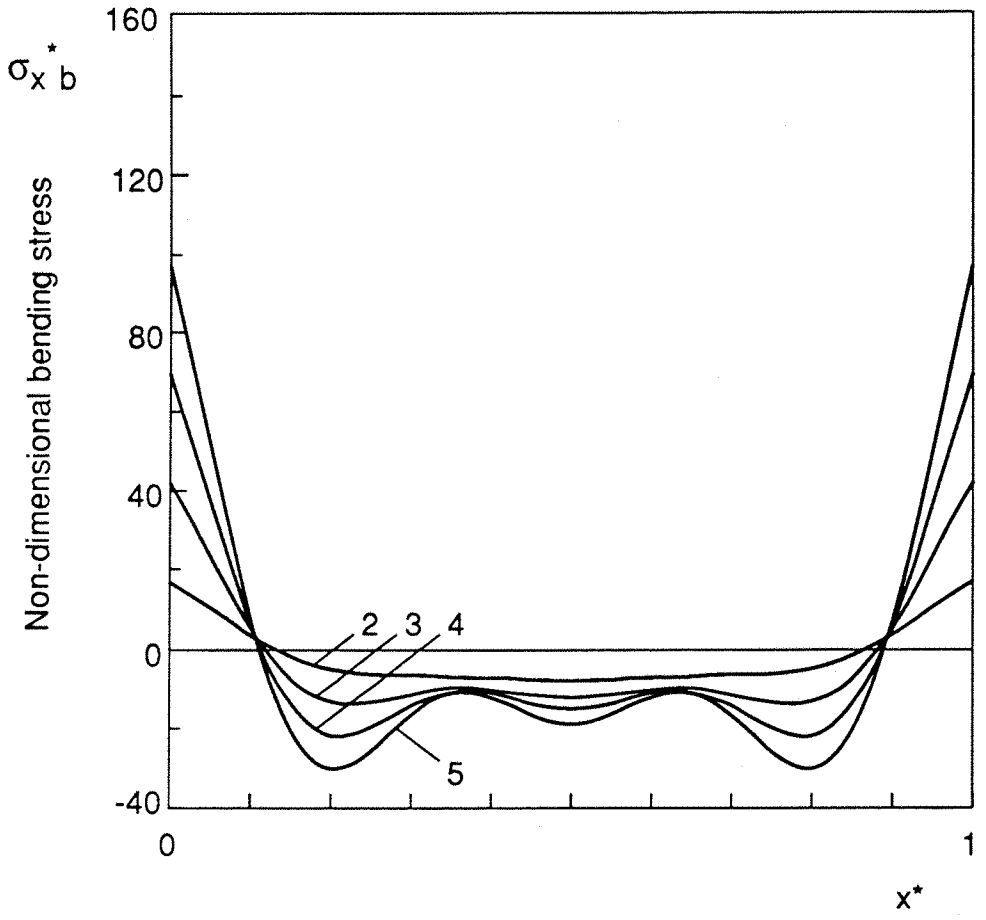

Figure 5.6.3 NON-DIMENSIONAL BENDING STRESS DISTRIBUTION ALONG THE SECTION $y^* = 0.375$ OF A FULLY CLAMPED RECTANGULAR PLATE, $\alpha = 0.6$.

Curve 1: lowest amplitude

Curve 5: highest amplitude

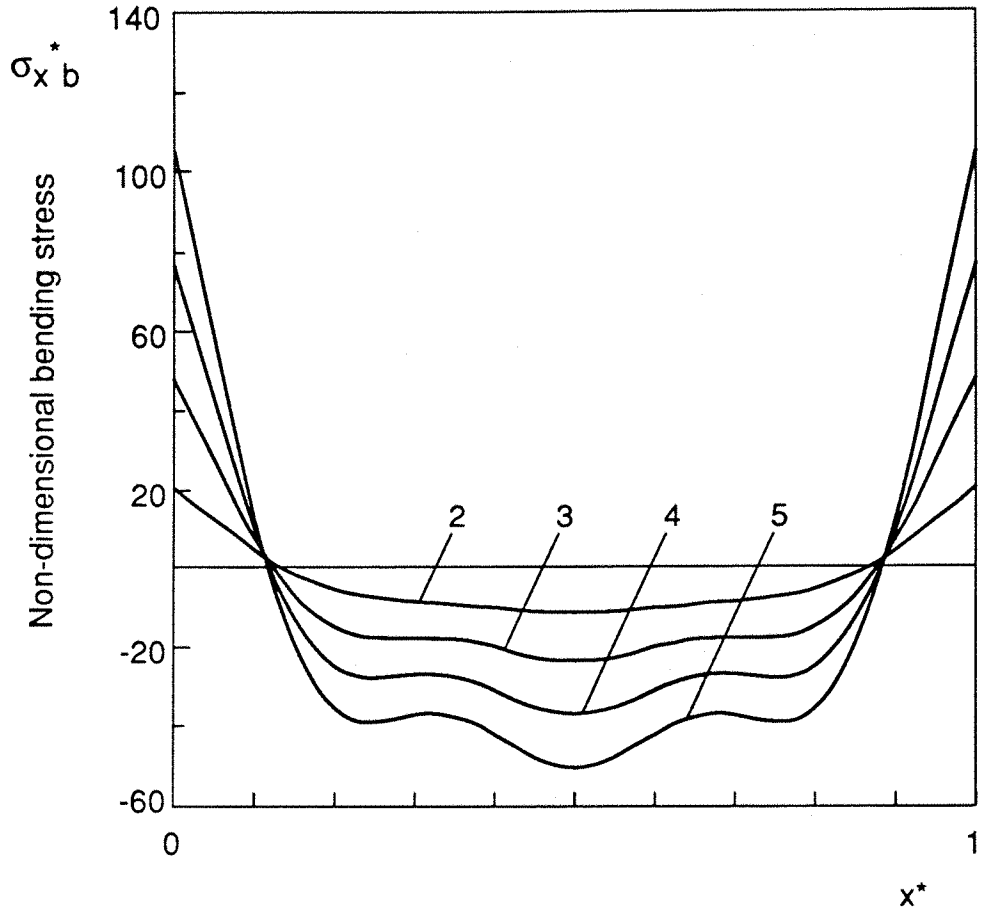

Figure 5.6.4 NON-DIMENSIONAL BENDING STRESS DISTRIBUTION ALONG THE SECTION $y^* = 0.5$ OF A FULLY CLAMPED RECTANGULAR PLATE, $\alpha = 0.6$.

Curve 1: lowest amplitude

Curve 5: highest amplitude

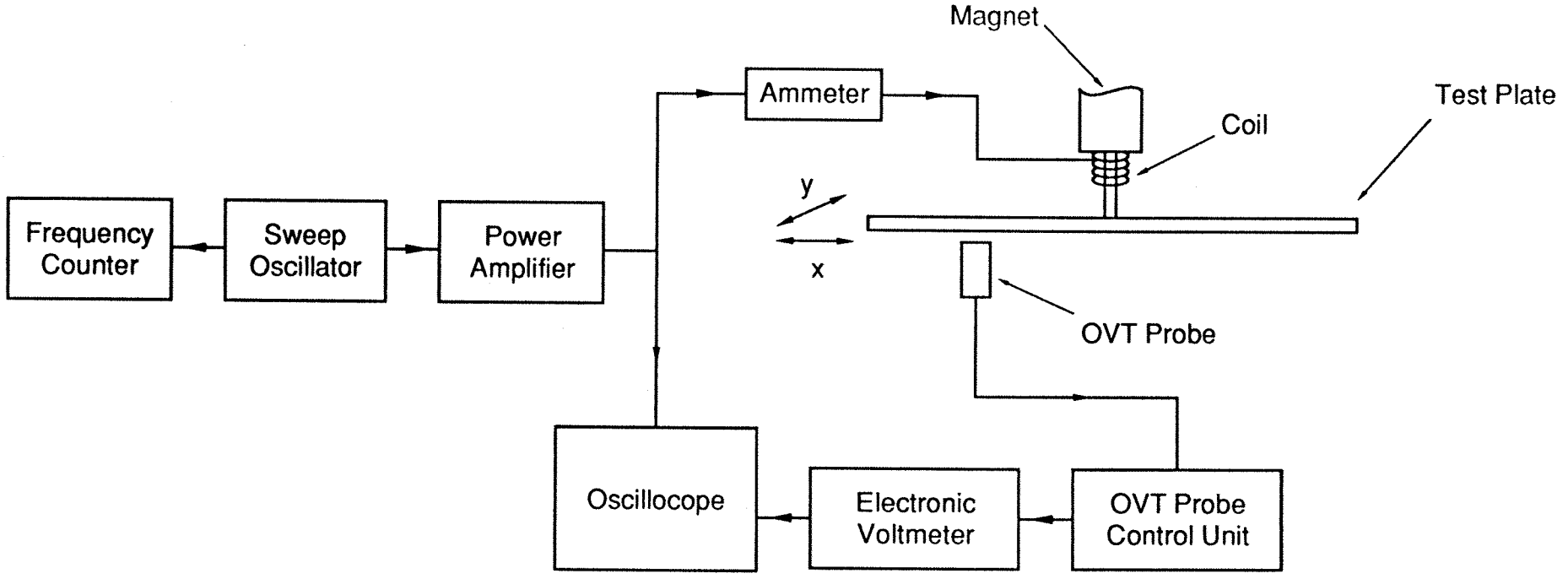

FIG. 6.1 INSTRUMENTATION LAYOUT FOR AMPLITUDE DEPENDENCE OF RESONANCE FREQUENCY MEASUREMENTS.

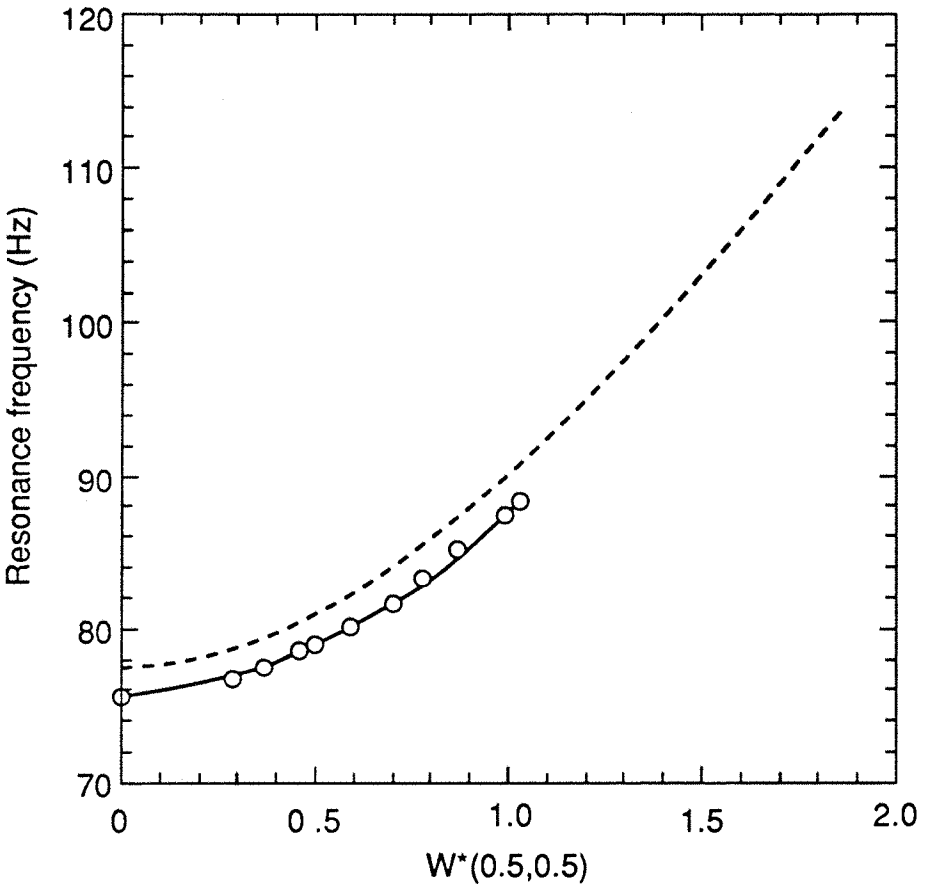

Figure 6.2 INCREASE OF FUNDAMENTAL RESONANCE FREQUENCY WITH INCREASE OF AMPLITUDE TO THICKNESS RATIO AT POINT $(x^*,y^*) = (0.5,0.5)$. - - - - Theoretical; —— Experimental.

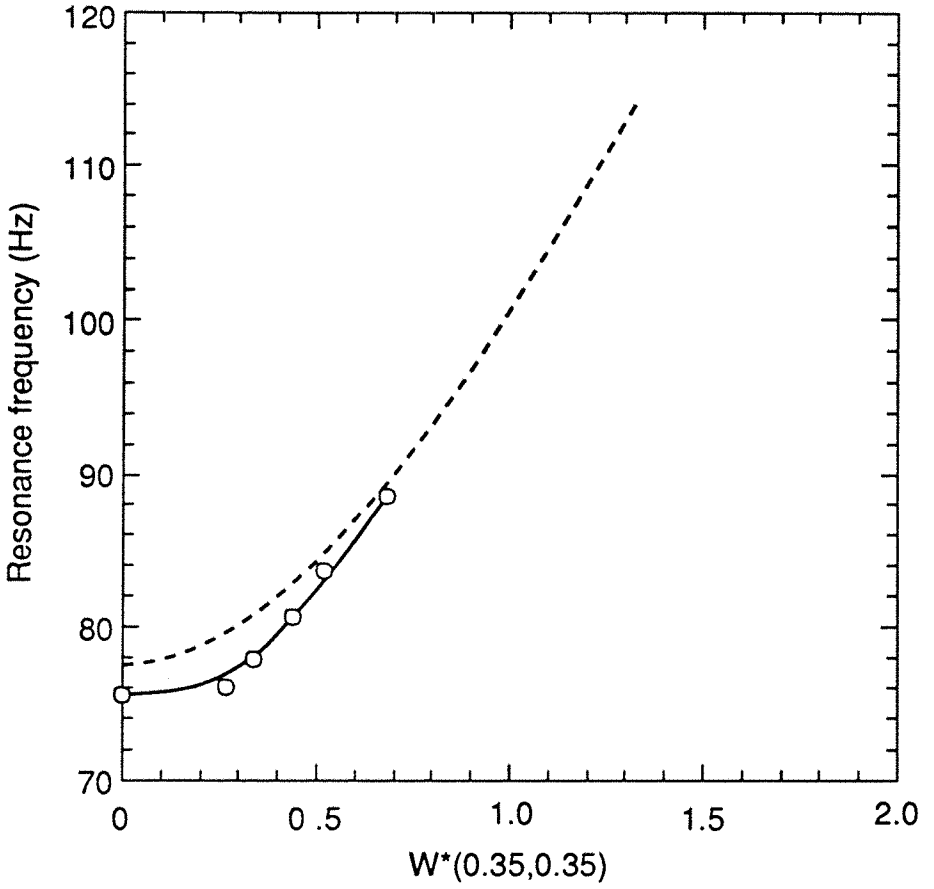

Figure 6.3 INCREASE OF FUNDAMENTAL RESONANCE FREQUENCY WITH INCREASE OF AMPLITUDE TO THICKNESS RATIO AT POINT (x*,y*) = (0.35,0.35). - - - - Theoretical; —— Experimental.

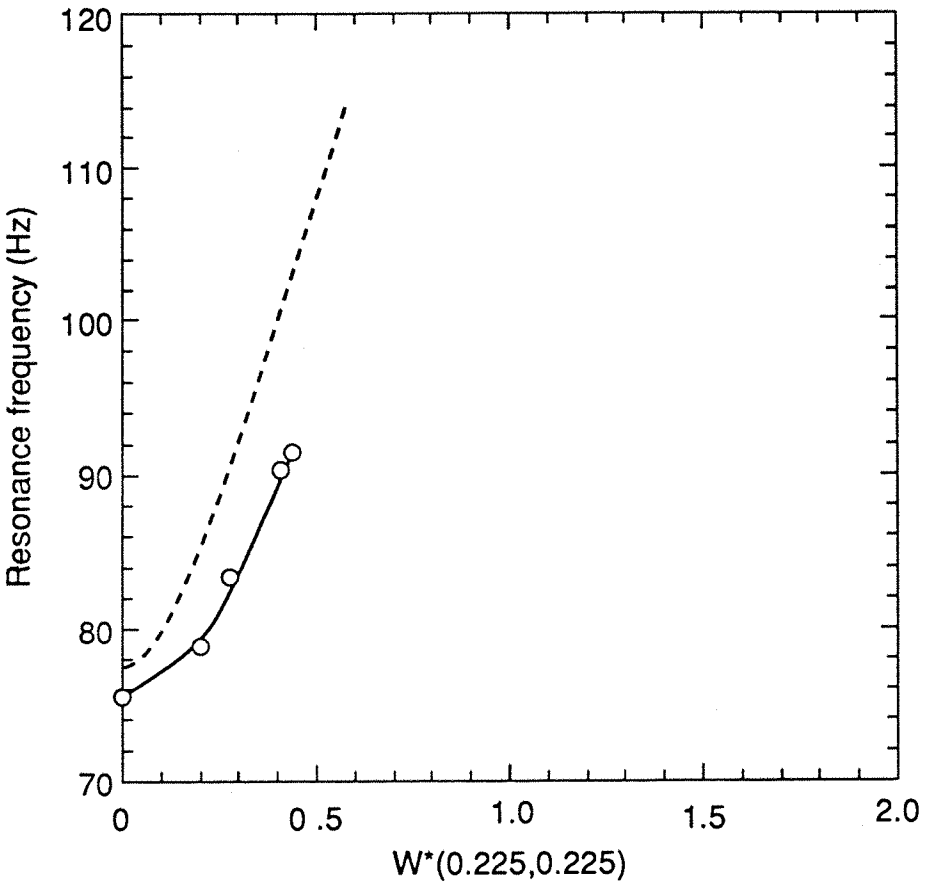

Figure 6.4 INCREASE OF FUNDAMENTAL RESONANCE FREQUENCY WITH INCREASE OF AMPLITUDE TO THICKNESS RATIO AT POINT (x*,y*) = (0.225,0.225). - - - - Theoretical; —— Experimental.

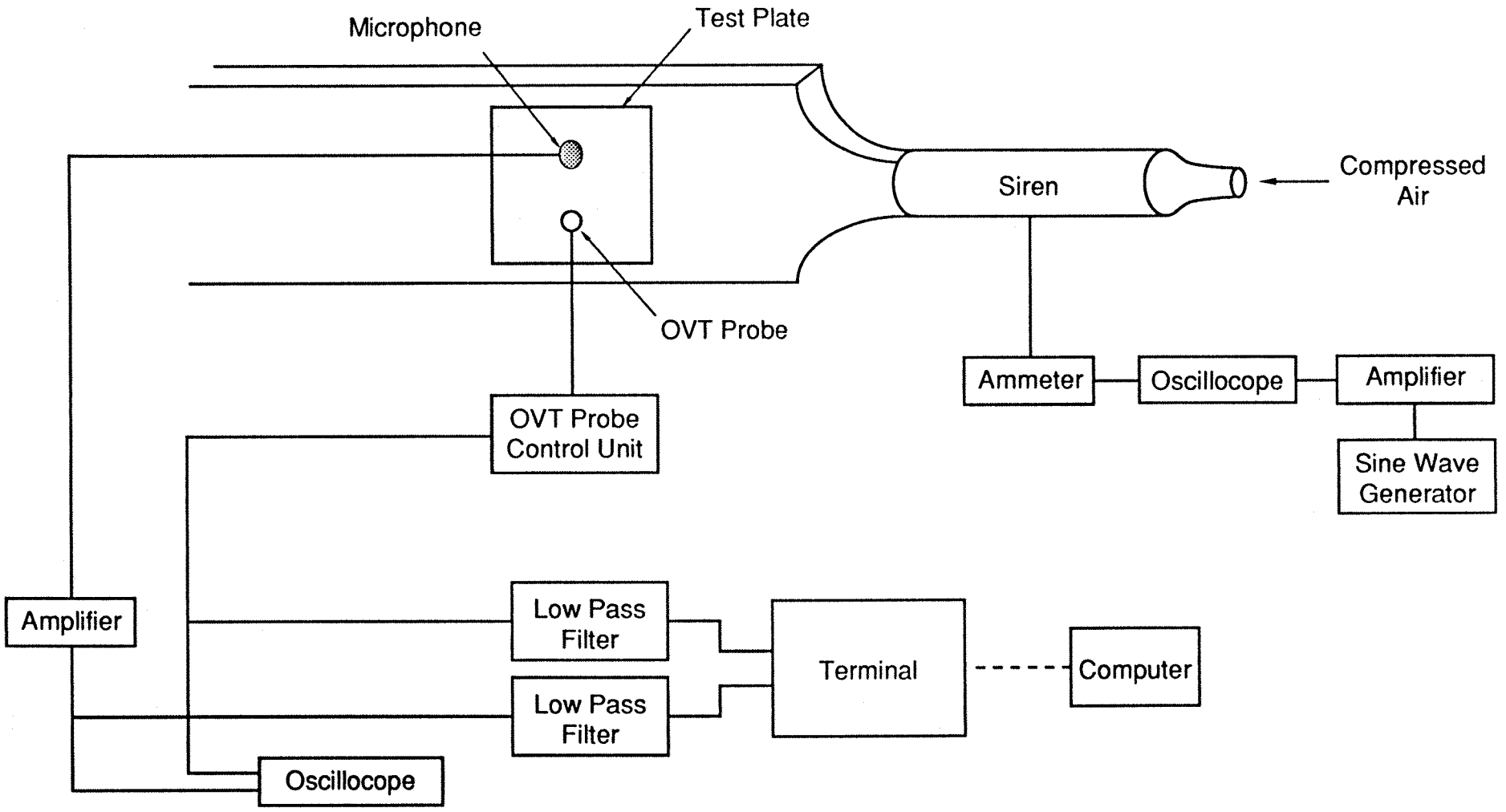

FIG. 6.5.1 SCHEMATIC DIAGRAM GF THE EXPERIMENTAL APPARATUS FOR ACOUSTIC EXCITATION AND DIGITAL DATA ACQUISTION.

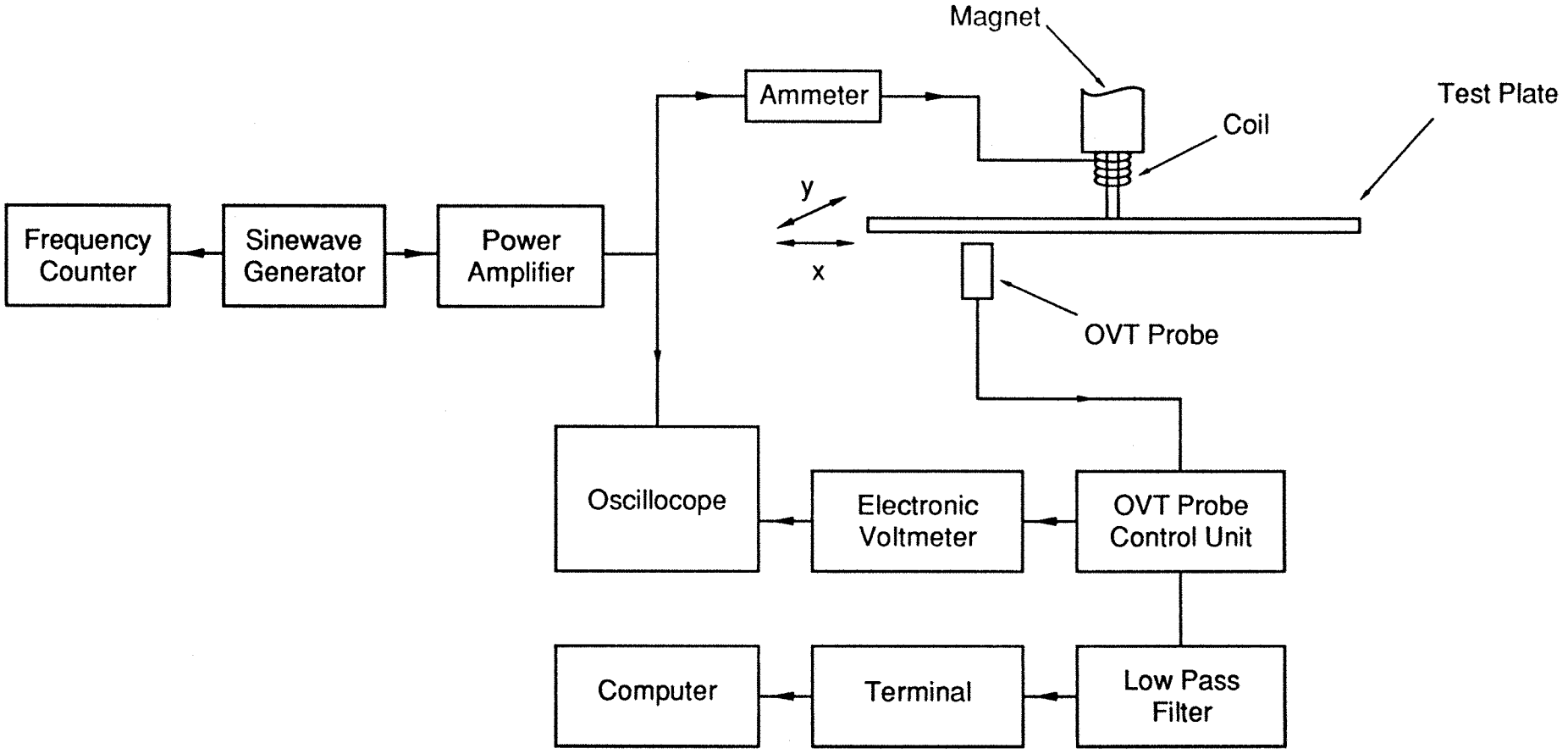

FIG. 6.5.2 INSTRUMENTATION LAYOUT FOR MODE SHAPE MEASUREMENTS USING DIGITAL DATA ACQUISITION.

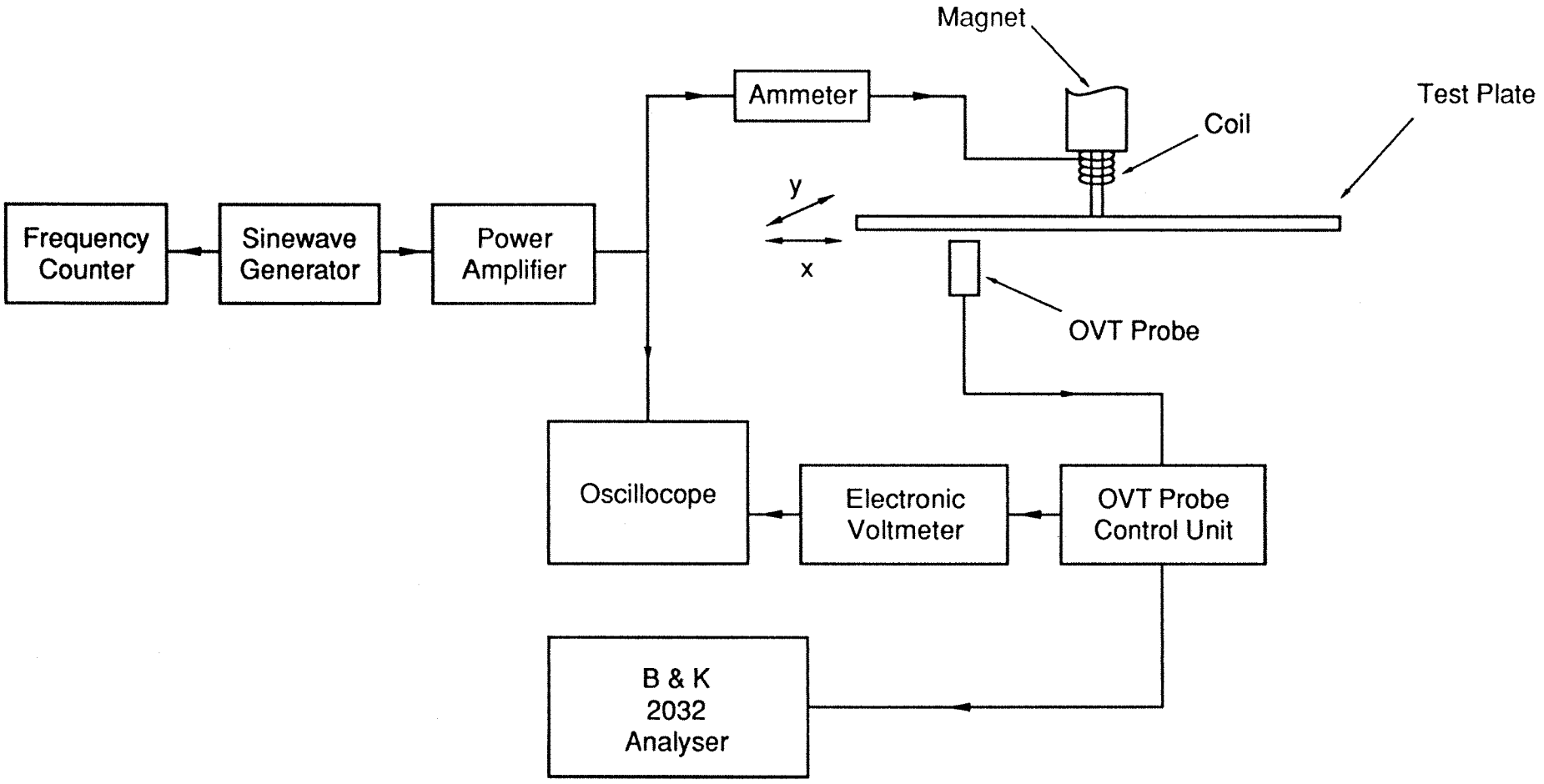

FIG. 6.5.3 INSTRUMENTATION LAYOUT FOR MODE SHAPE MEASUREMENTS USING B & K 2132 ANALYSER.

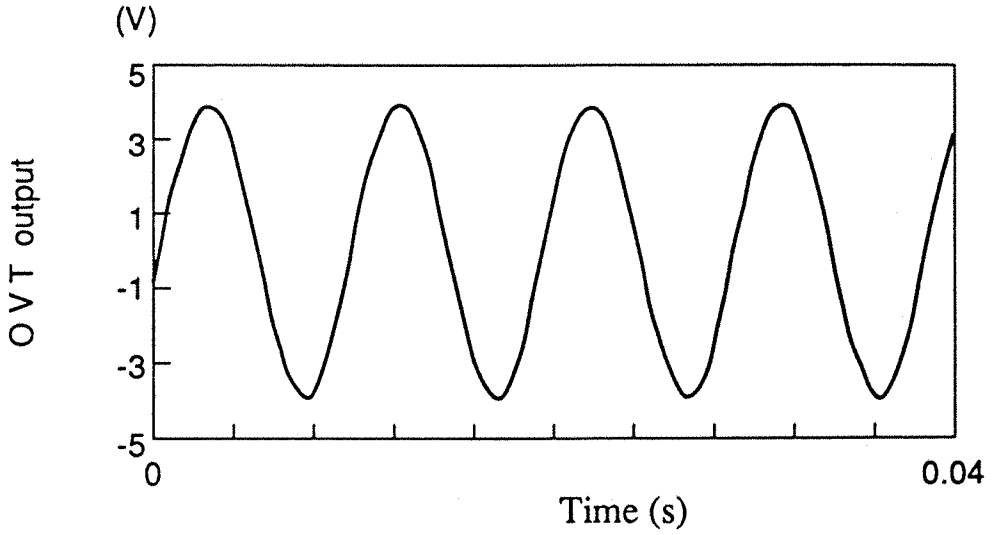

Figure 6.6.1 TIME HISTORY OF SIGNAL PROPORTIONAL TO PLATE DISPLACEMENT AT (x*,y*) = (0.5,0.5).

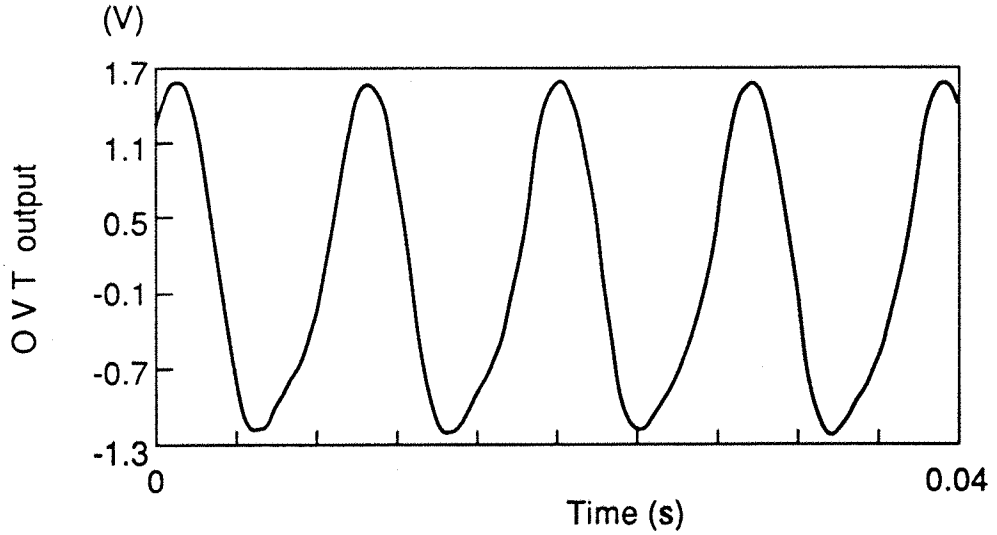

Figure 6.6.2 TIME HISTORY OF SIGNAL PROPORTIONAL TO PLATE DISPLACEMENT AT (x*,y*) = (0.80,0.50).

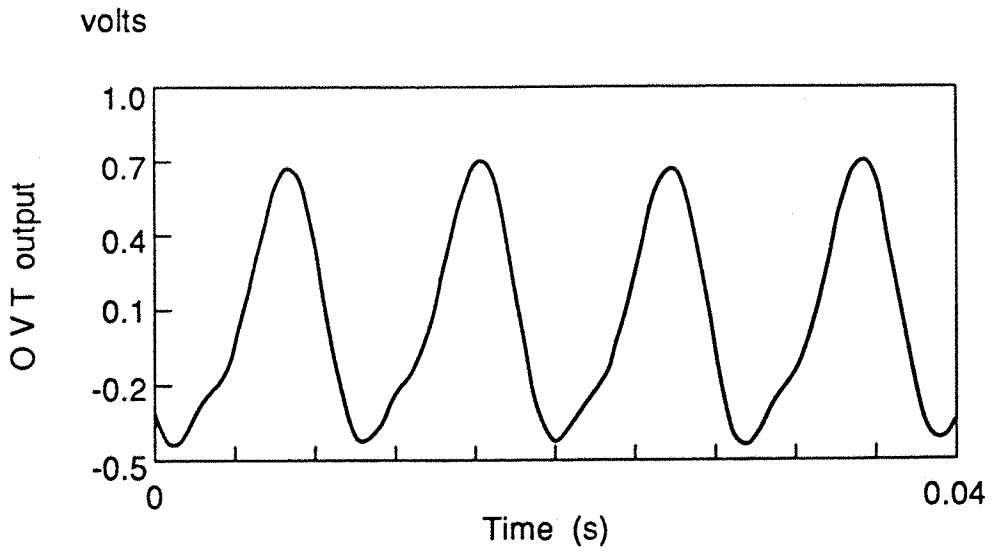

Figure 6.6.3 TIME HISTORY OF SIGNAL PROPORTIONAL TO PLATE DISPLACEMENT AT $(x^*,y^*) = (0.88,0.50)$.

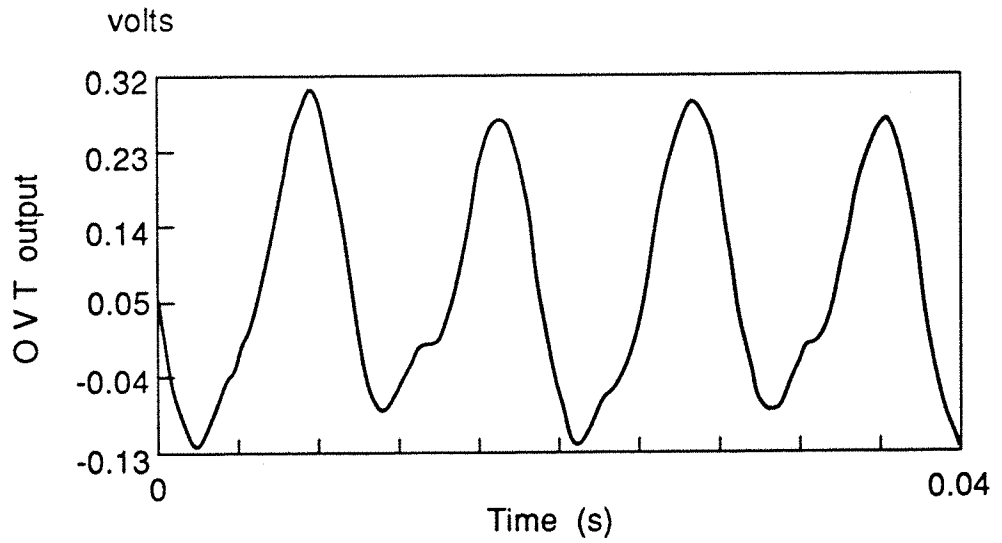

Figure 6.6.4 TIME HISTORY OF SIGNAL PROPORTIONAL TO PLATE DISPLACEMENT AT $(x^*,y^*) = (0.936,0.50)$.

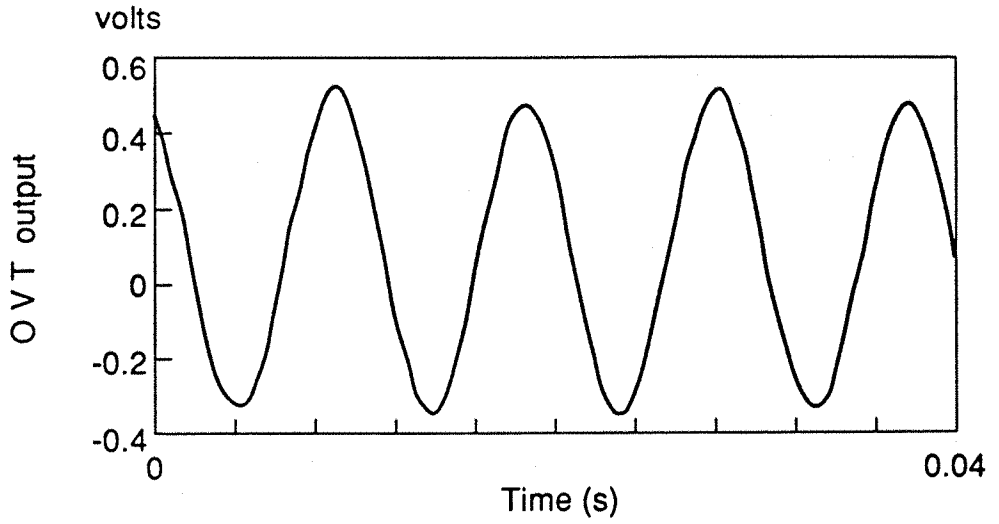

Figure 6.6.5 TIME HISTORY OF SIGNAL PROPORTIONAL TO PLATE DISPLACEMENT AT $(x^*,y^*) = (0.5,0.091)$.

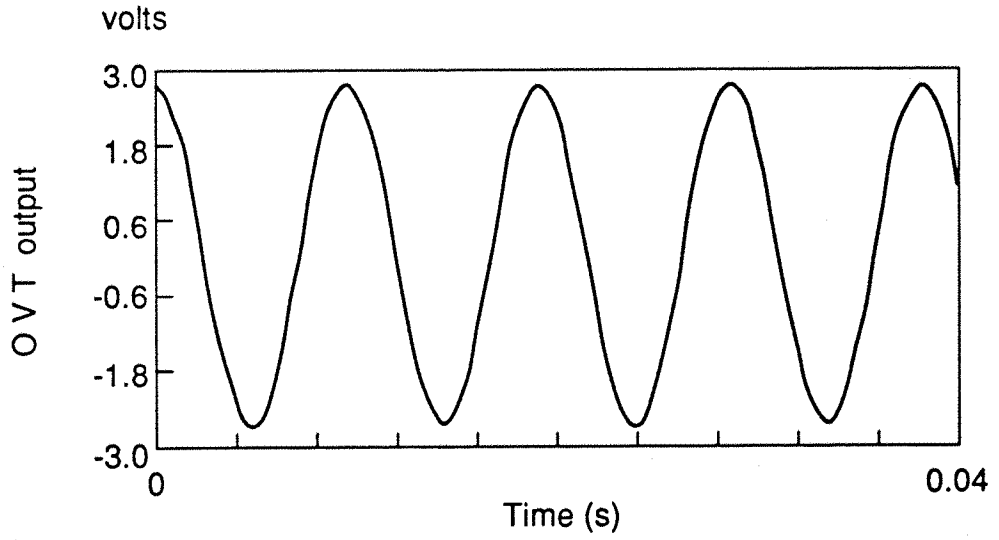

Figure 6.6.6 TIME HISTORY OF SIGNAL PROPORTIONAL TO PLATE DISPLACEMENT AT $(x^*,y^*) = (0.5,0.318)$.

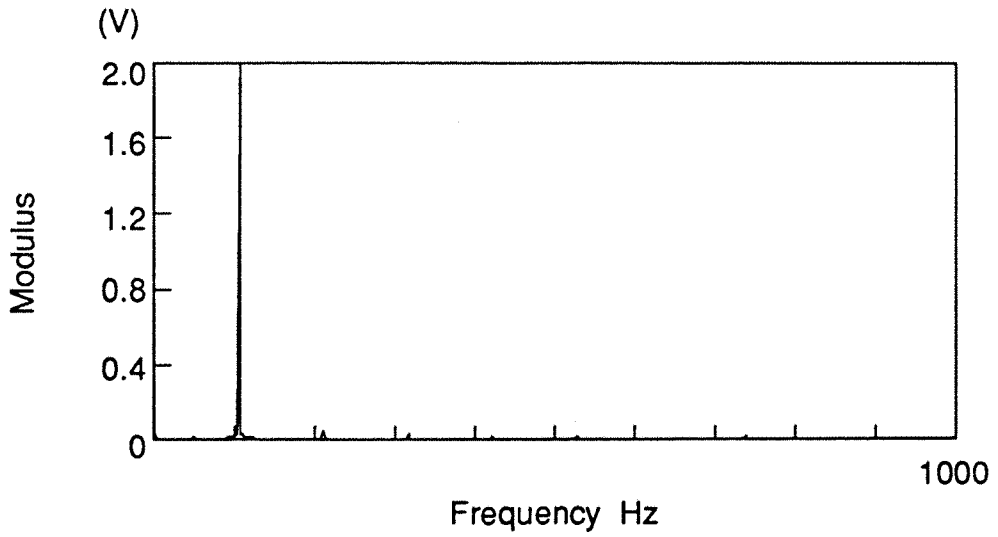

Figure 6.7.1 MODULUS OF THE FAST FOURIER TRANSFORM OF THE PLATE RESPONSE AT $(x^*,y^*) = (0.5,0.5)$.

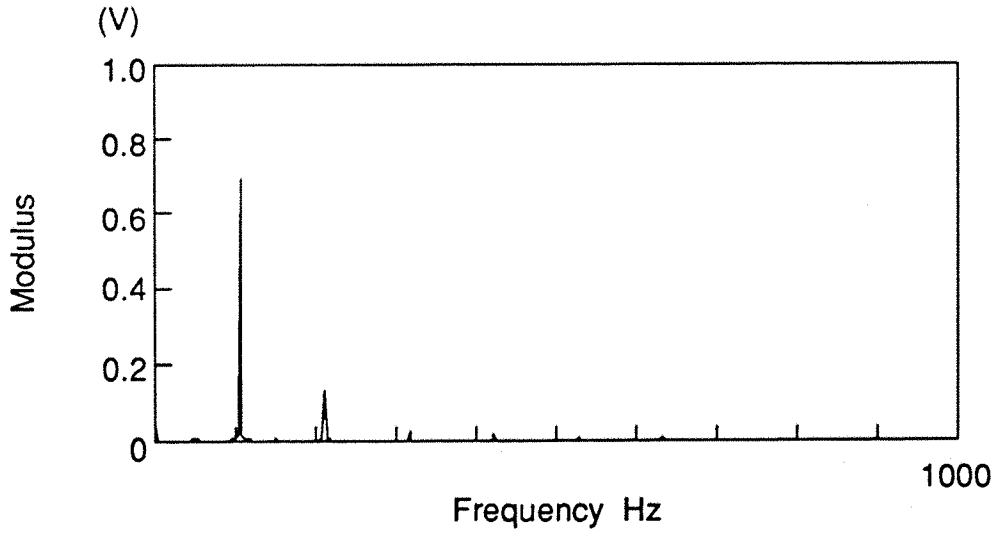

Figure 6.7.2 MODULUS OF THE FAST FOURIER TRANSFORM OF THE PLATE RESPONSE AT $(x^*,y^*) = (0.80,0.50)$.

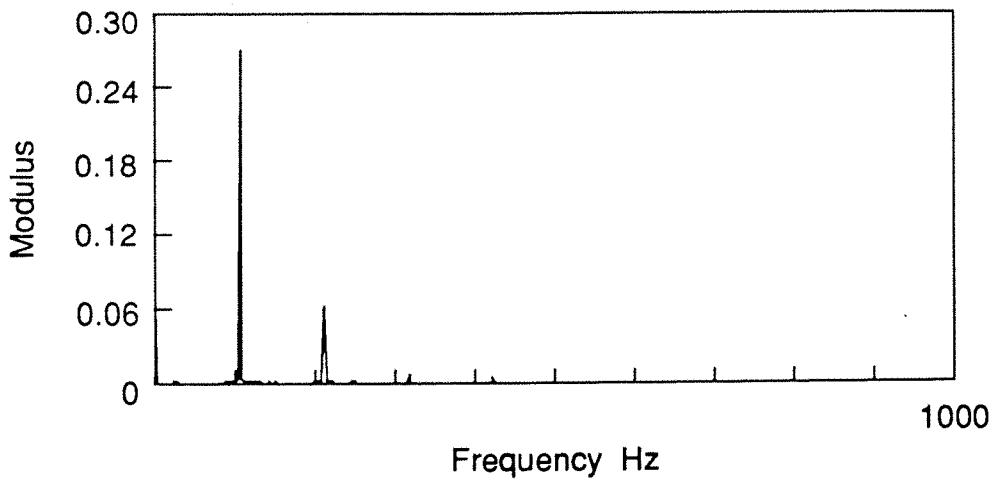

Figure 6.7.3 MODULUS OF THE FAST FOURIER TRANSFORM OF THE PLATE RESPONSE AT $(x^*,y^*) = (0.88,0.50)$.

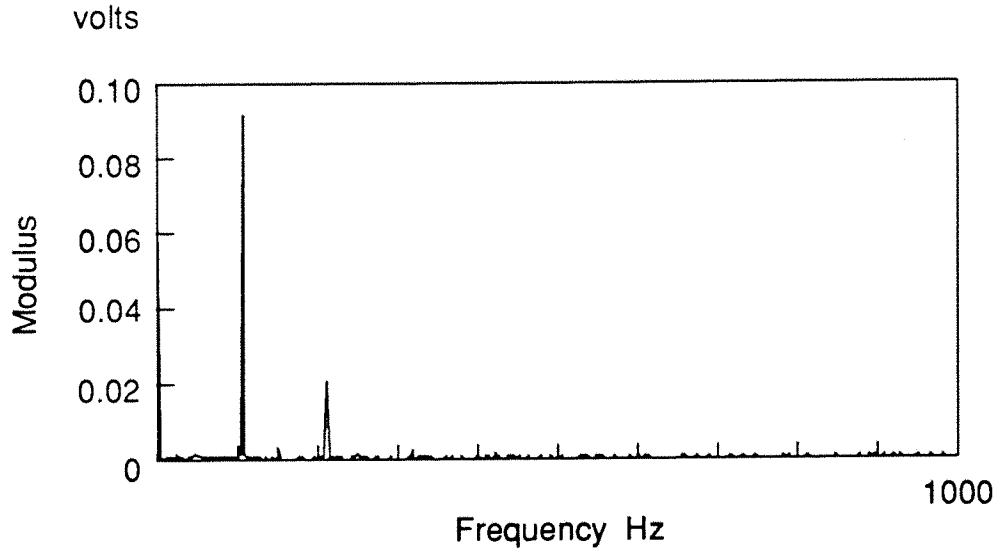

Figure 6.7.4 MODULUS OF THE FAST FOURIER TRANSFORM OF THE PLATE RESPONSE AT $(x^*,y^*) = (0.936,0.50)$.

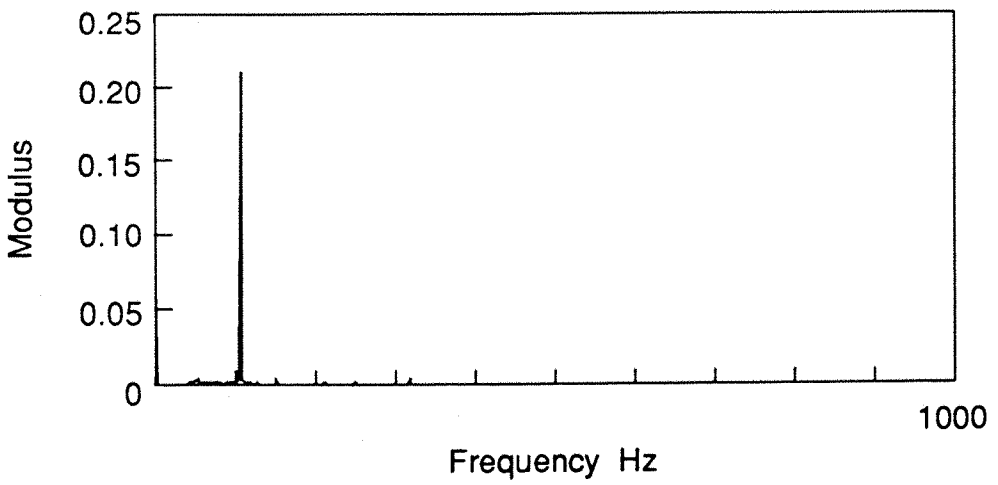

Figure 6.7.5 MODULUS OF THE FAST FOURIER TRANSFORM OF THE PLATE RESPONSE AT $(x^*,y^*) = (0.5,0.091)$.

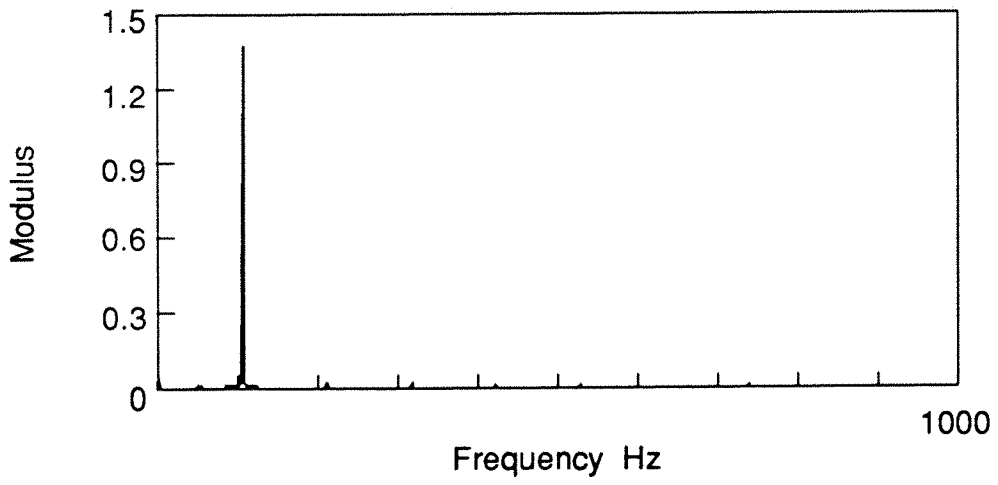

Figure 6.7.6 MODULUS OF THE FAST FOURIER TRANSFORM OF THE PLATE RESPONSE AT $(x^*,y^*) = (0.5,0.318)$.

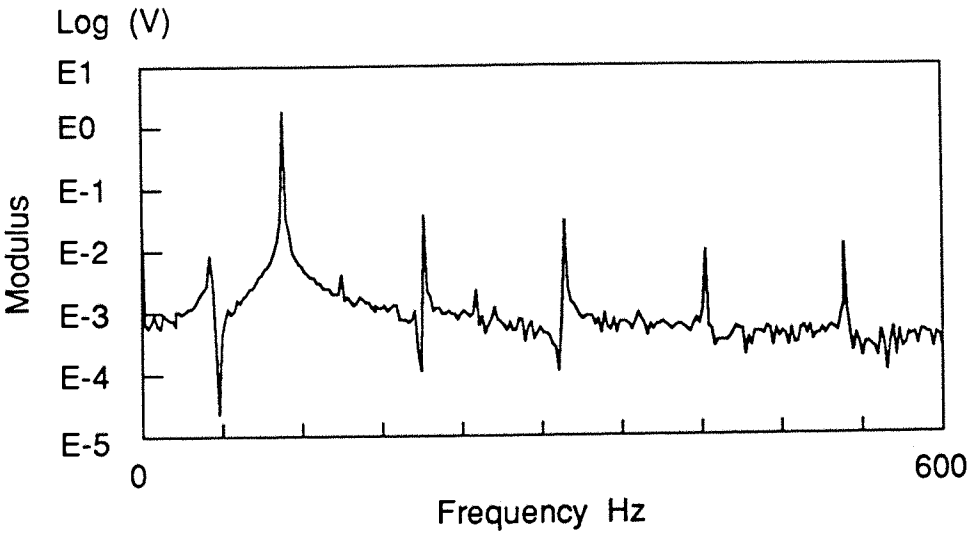

Figure 6.8.1 MODULUS OF THE FAST FOURIER TRANSFORM OF THE PLATE RESPONSE AT $(x^*,y^*) = (0.5,0.5)$.

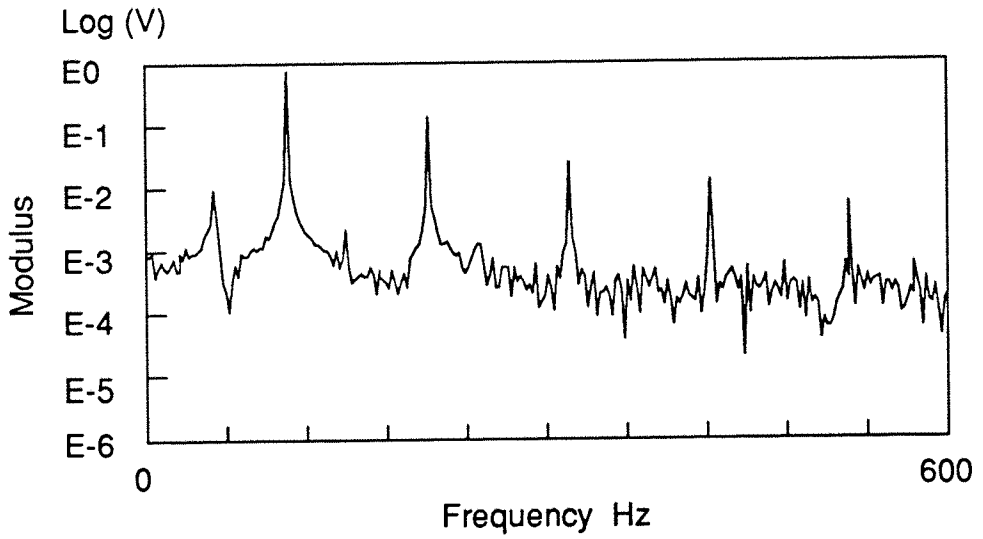

Figure 6.8.2 MODULUS OF THE FAST FOURIER TRANSFORM OF THE PLATE RESPONSE AT $(x^*,y^*) = (0.80,0.50)$.

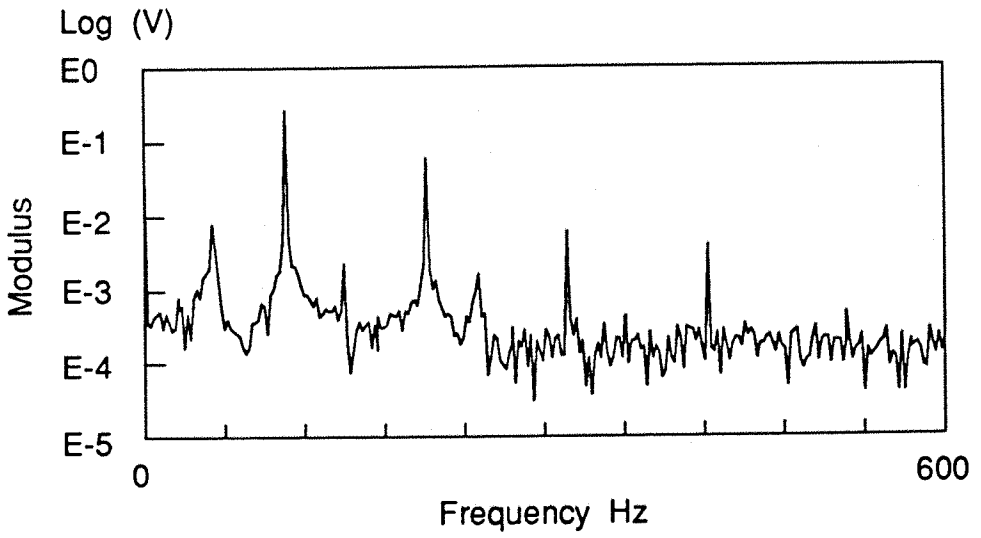

Figure 6.8.3 MODULUS OF THE FAST FOURIER TRANSFORM OF THE PLATE RESPONSE AT $(x^*,y^*) = (0.88,0.50)$.

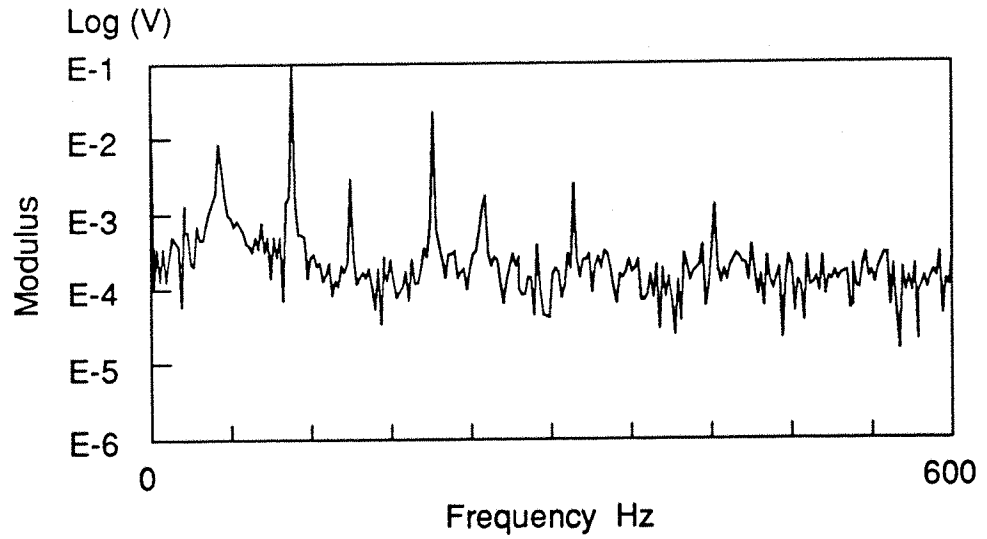

Figure 6.8.4 MODULUS OF THE FAST FOURIER TRANSFORM OF THE PLATE RESPONSE AT $(x^*,y^*) = (0.936,0.50)$.

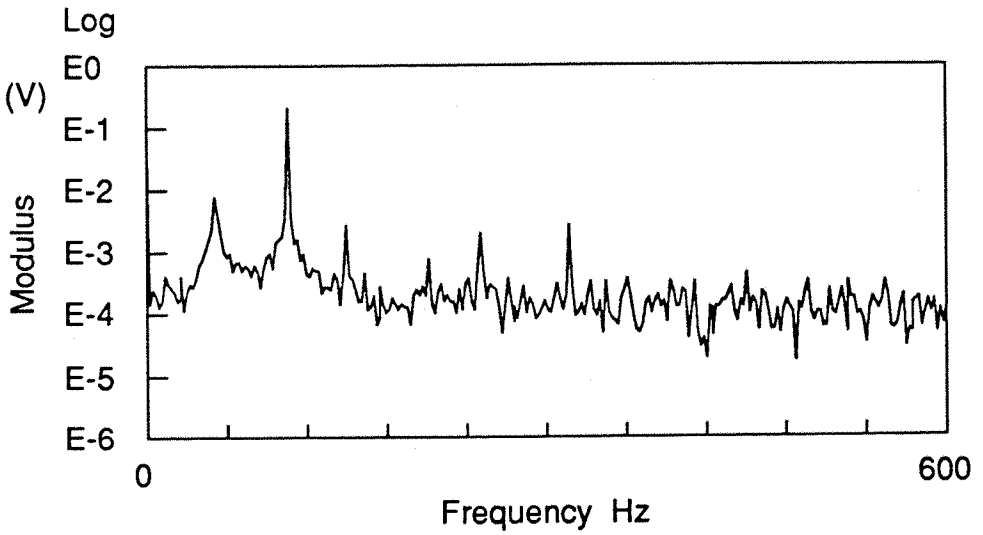

Figure 6.8.5 MODULUS OF THE FAST FOURIER TRANSFORM OF THE PLATE RESPONSE AT $(x^*,y^*) = (0.5,0.091)$.

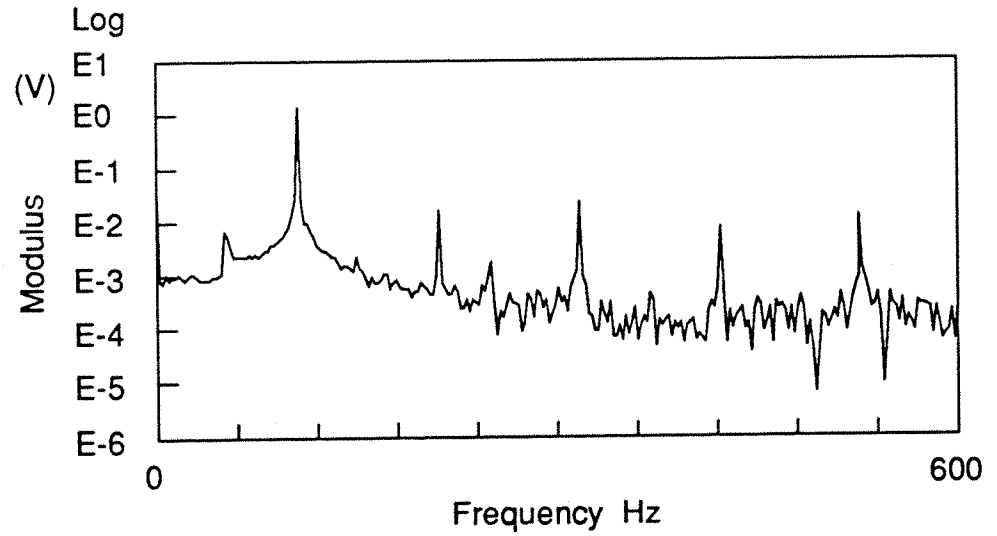

Figure 6.8.6 MODULUS OF THE FAST FOURIER TRANSFORM OF THE PLATE RESPONSE AT $(x^*,y^*) = (0.5,0.318)$.

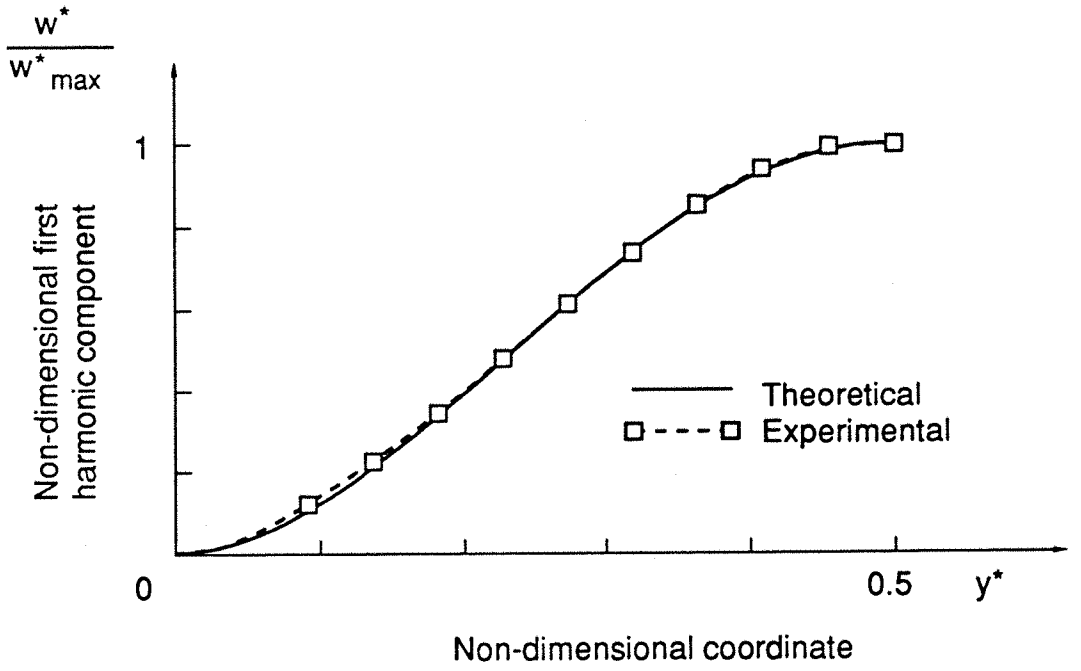

Figure 6.9.1 NORMALISED FIRST HARMONIC COMPONENT ALONG THE PLATE WIDTH DIRECTION FOR $x^* = 0.5$. ISOTROPIC PLATE 3 $w^*_{max} = 0.3$. A COIL AND MAGNET EXCITER AND A B & K ANALYSER. EXCITATION FREQUENCY: 116 Hz.

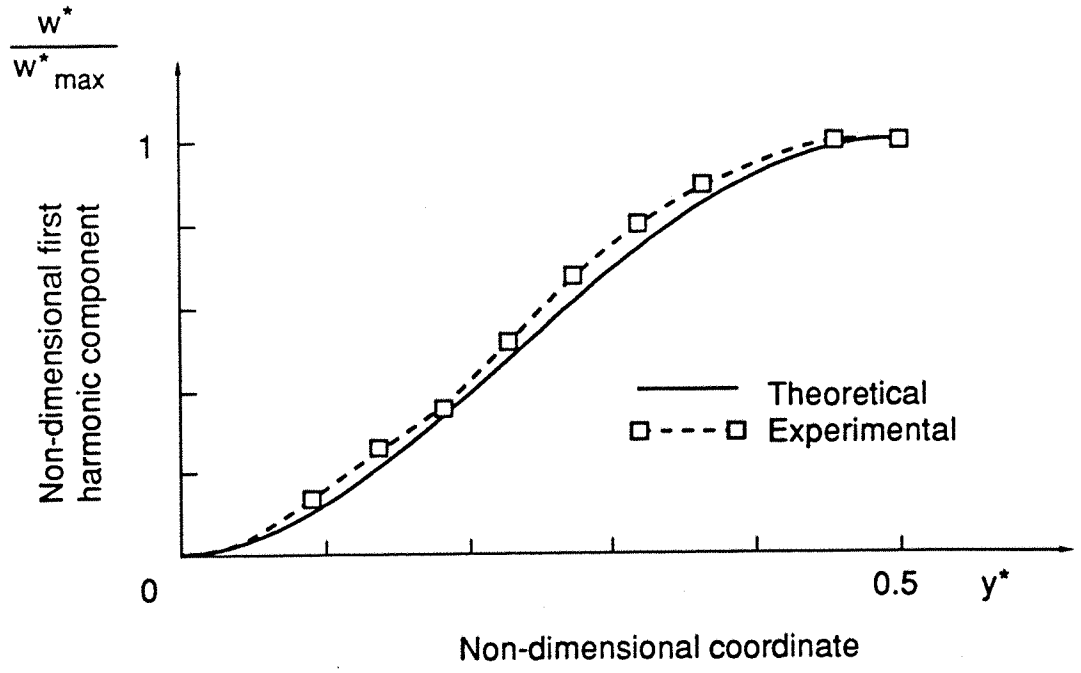

Figure 6.9.2 NORMALISED FIRST HARMONIC COMPONENT ALONG THE PLATE WIDTH DIRECTION FOR $x^* = 0.5$. ISOTROPIC PLATE 3 $w^*_{max} = 0.7$. A COIL AND MAGNET EXCITER AND A B & K ANALYSER. EXCITATION FREQUENCY: 119.8 Hz.

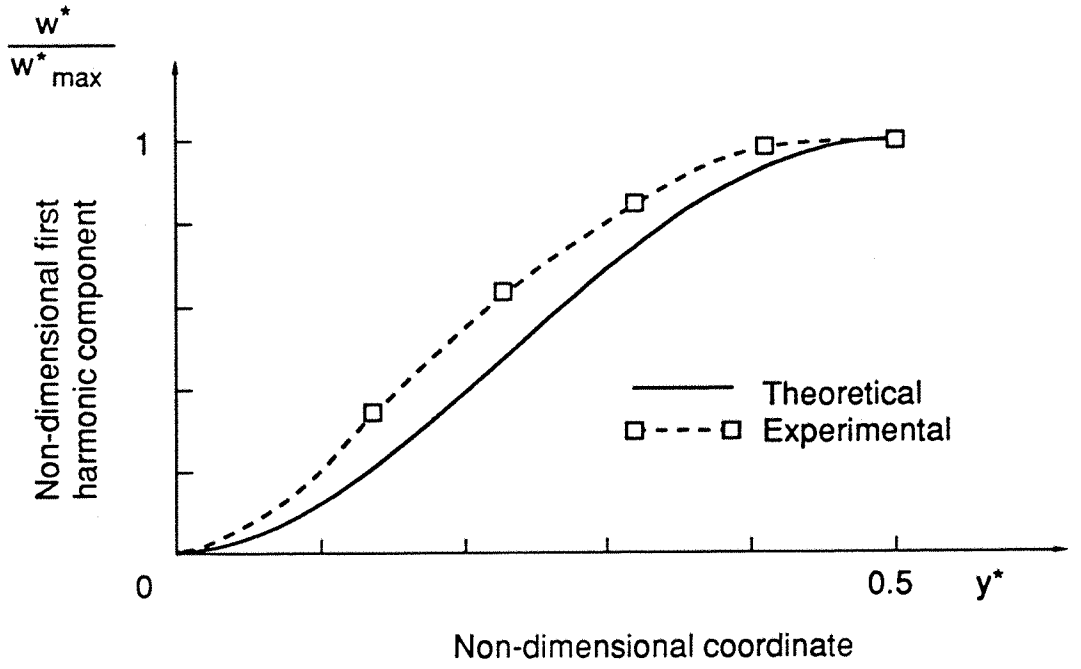

Figure 6.9.3 NORMALISED FIRST HARMONIC COMPONENT ALONG THE WIDTH DIRECTION FOR $x^* = 0.5$. ISOTROPIC PLATE $w^*_{max} = 1.7$. ACOUSTIC EXCITATION: 155 dB. EXCITATION FREQUENCY: 190 Hz.
PLATE 4

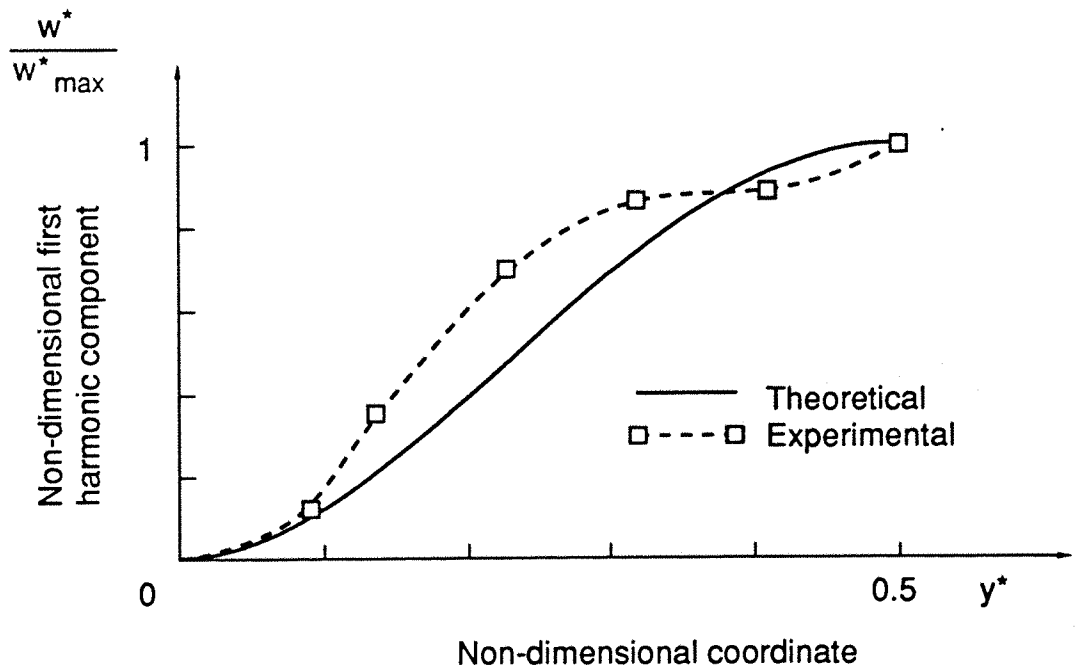

Figure 6.9.4 NORMALISED FIRST HARMONIC COMPONENT ALONG THE WIDTH DIRECTION FOR $x^* = 0.28$. ISOTROPIC PLATE $w^*_{max} = 1.8$. ACOUSTIC EXCITATION: 145 dB. EXCITATION FREQUENCY: 208 Hz.
PLATE 5

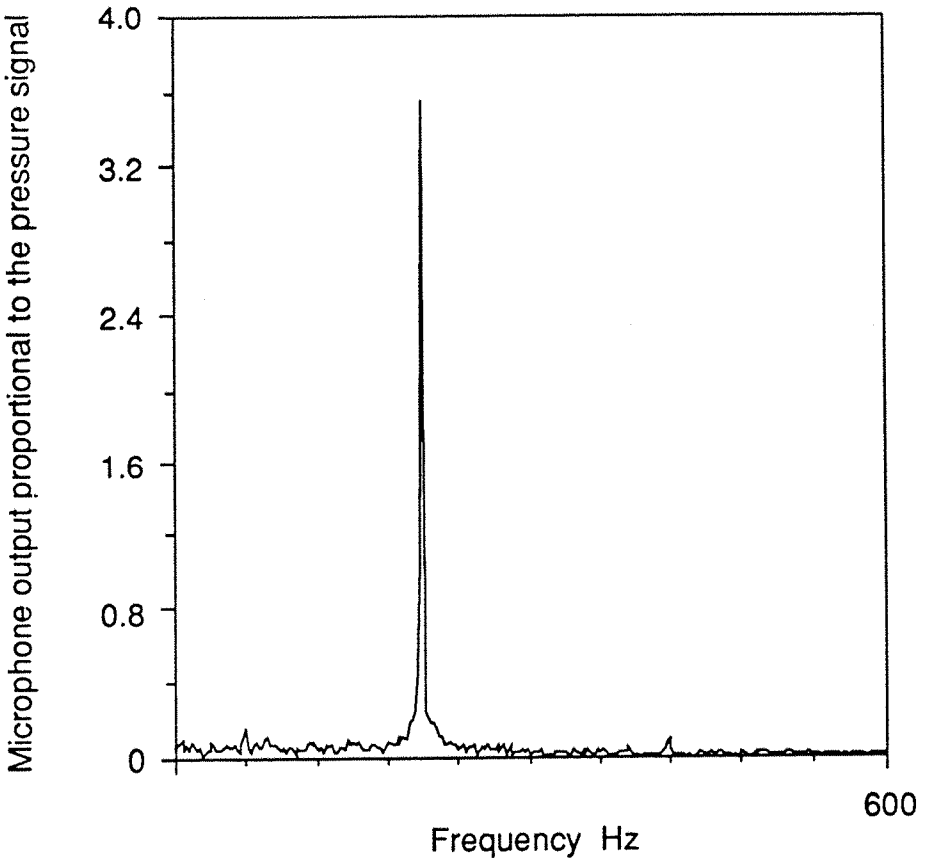

Figure 6.10 FOURIER TRANSFORM OF THE PRESSURE SIGNAL IN THE ACOUSTIC TUNNEL. 155 dB.

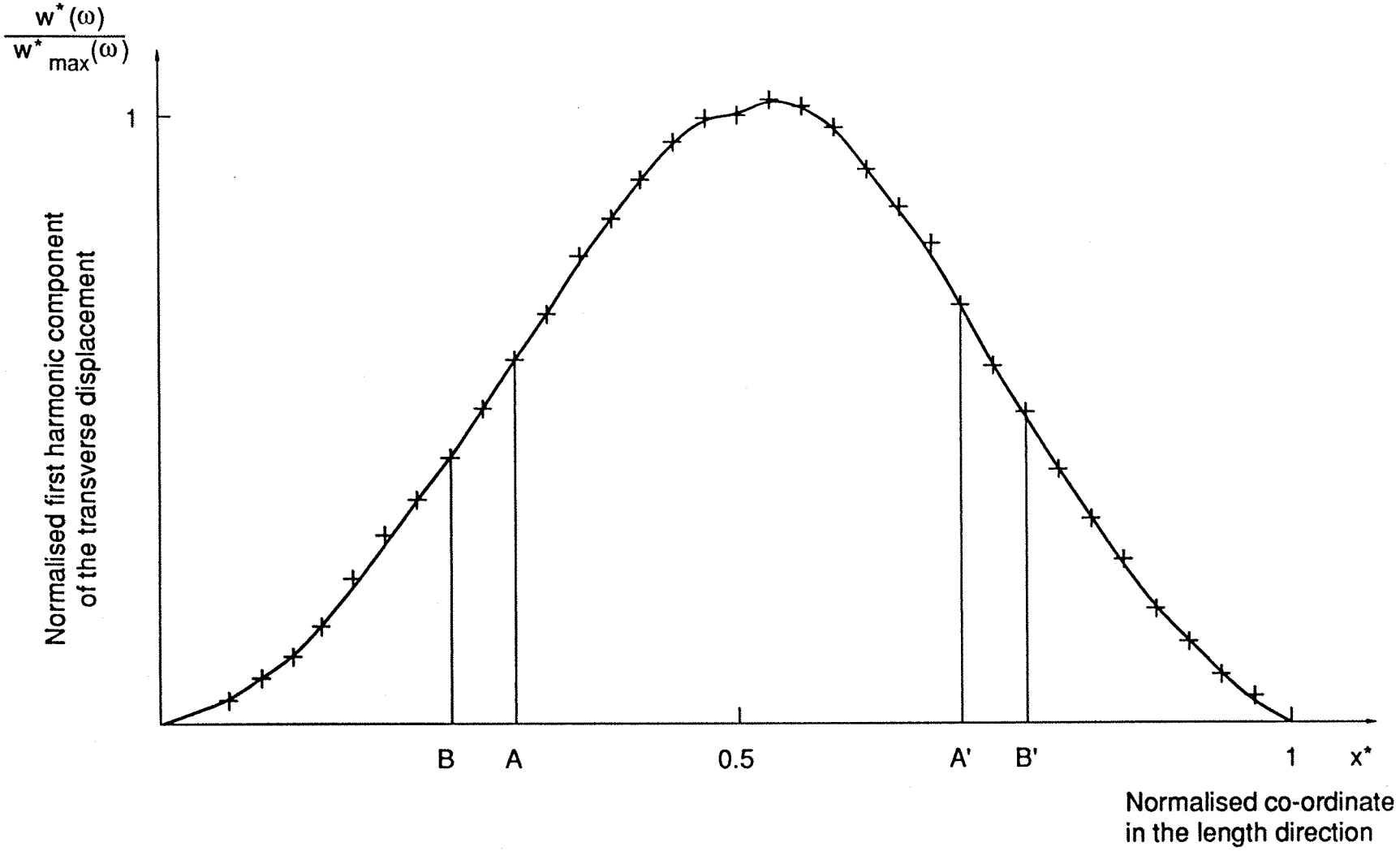

w^*_{max} at $(x^*,y^*) = (0.5,0.5)$ is 0.9

phase at A - phase at A' = 0.05 rad

phase at B - phase at B' = 0.06 rad

Fig. 6.11.1 MEASURED NORMALISED FIRST HARMONIC DISTRIBUTION AT $y^* = 0.5$

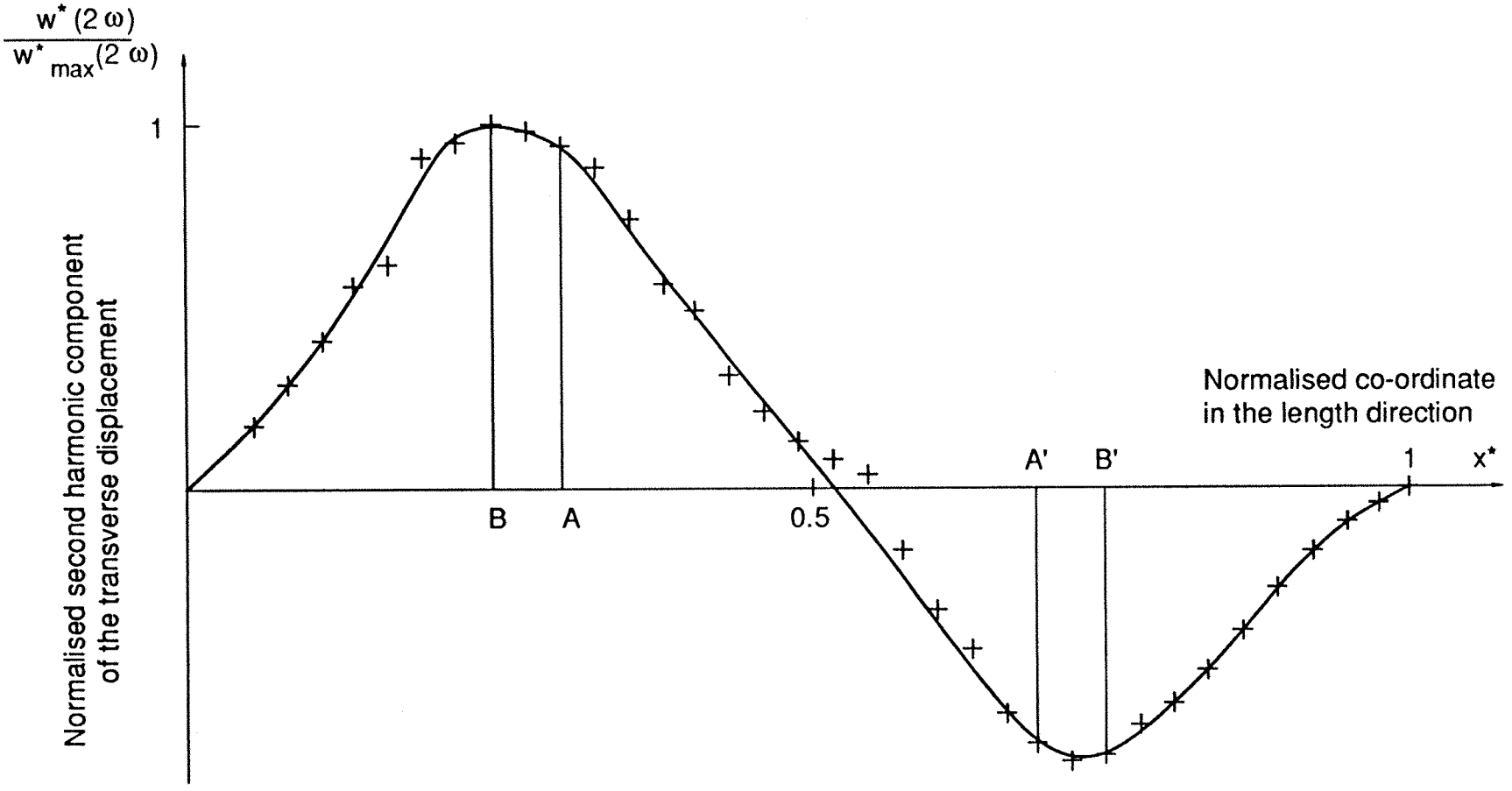

Fig. 6.11.2 MEASURED NORMALISED SEOND HARMONIC DISTRIBUTION AT y* = 0.5

Fig. 6.12.1

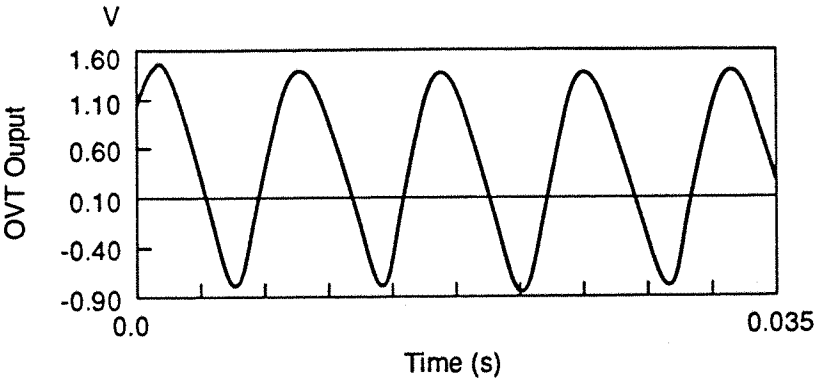

Fig. 6.12.2

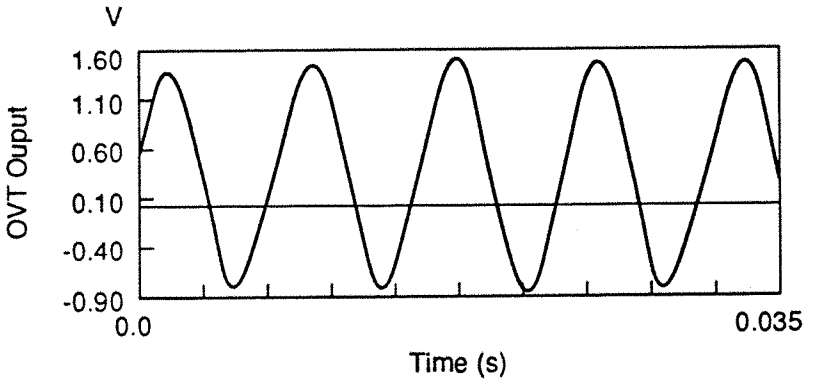

TIME HISTORY OF SIGNAL PROPORTIONAL TO PLATE DISPLACEMENT AT $(x^*,y^*) = (0.72,0.5)$ AND $(x^*,y^*) = (0.28,0.5)$.

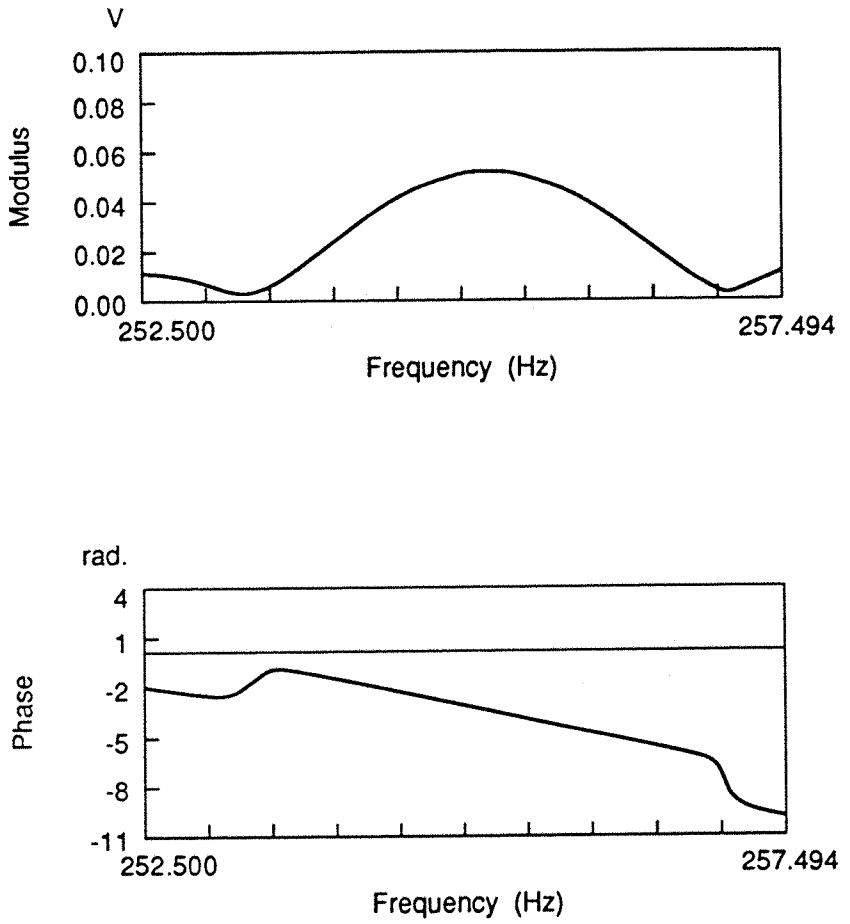

Fig. 6.13.1

MODULUS AND PHASE PLOTS AT THE POINT (x*,y*) = (0.72,0.5) NEAR TO THE SECOND HARMONIC OBTAINED FROM THE ZOOM ANALYSIS. PHASE AT THE MAXIMUM = -3.14 rad.

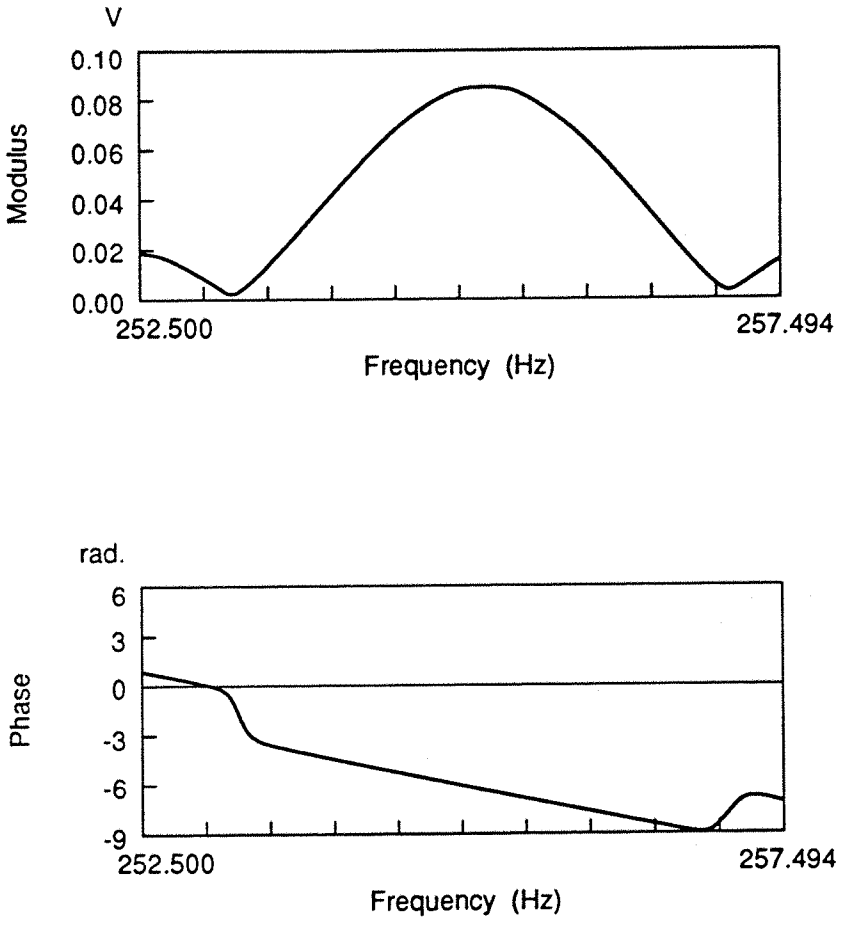

Fig. 6.13.2

MODULUS AND PHASE PLOTS AT THE POINT (x*,y*) = (0.28,0.5) NEAR TO THE SECOND HARMONIC OBTAINED FROM THE ZOOM ANALYSIS. PHASE AT THE MAXIMUM = -6.39 rad.

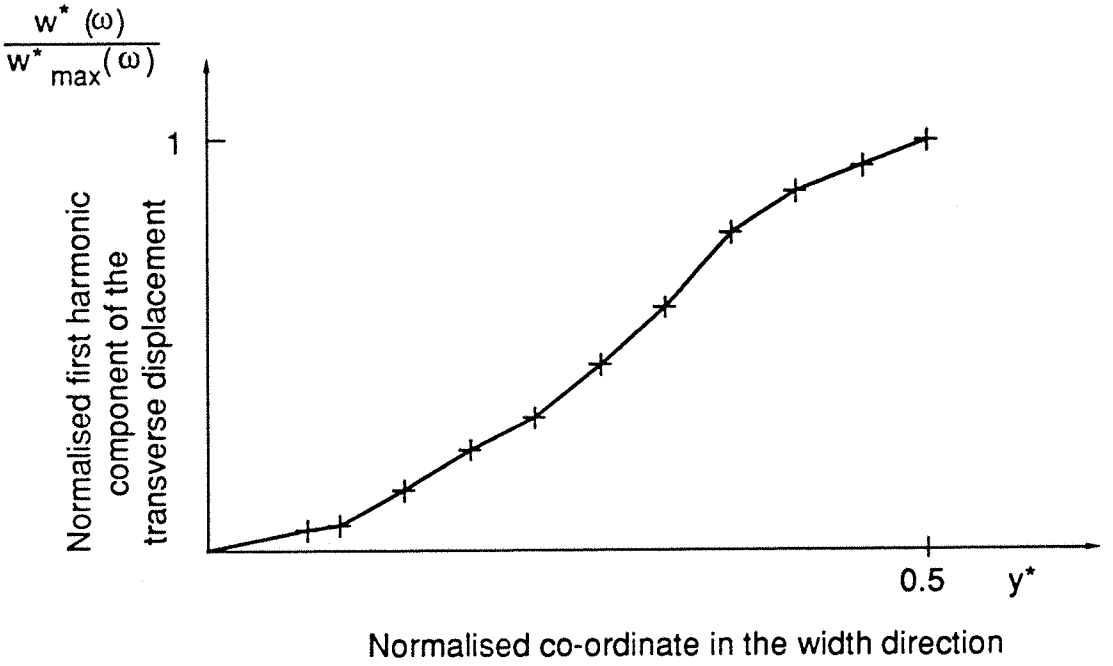

Fig. 6.14.1 MEASURED NORMALISED FIRST HARMONIC DISTRIBUTION AT $x^* = 0.3$, $w^*_{max}(\omega)$ at $(x^*,y^*) = (0.3,0.5)$ is 0.5 .

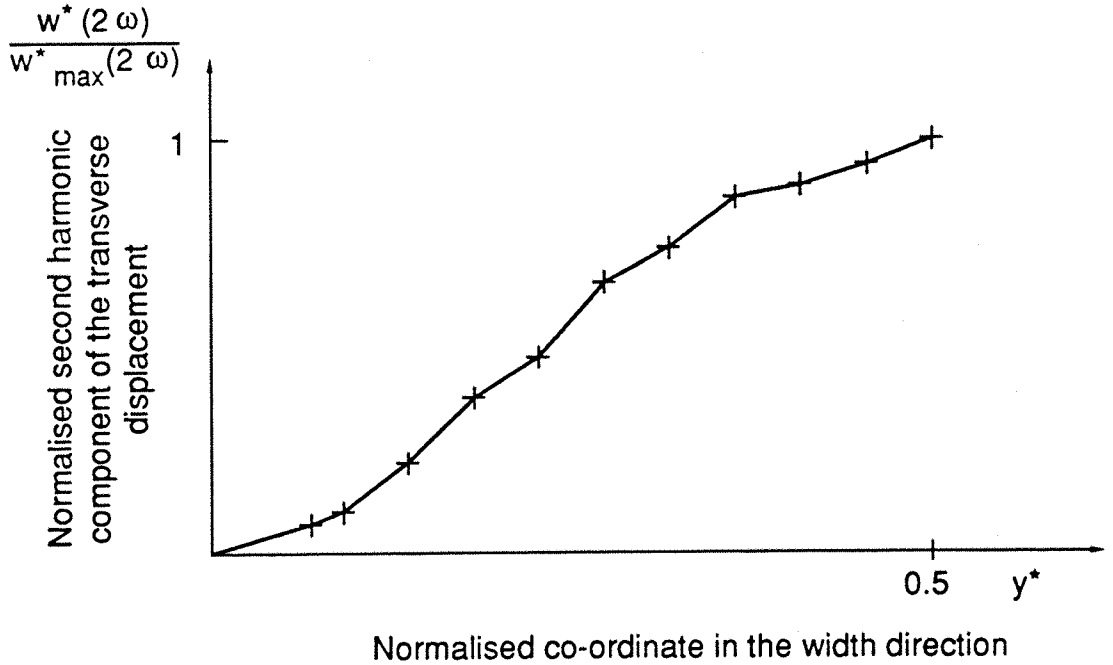

Fig. 6.14.2 MEASURED NORMALISED SECOND HARMONIC DISTRIBUTION AT $x^* = 0.3$, $w^*_{max}(2\omega) = 0.1$.

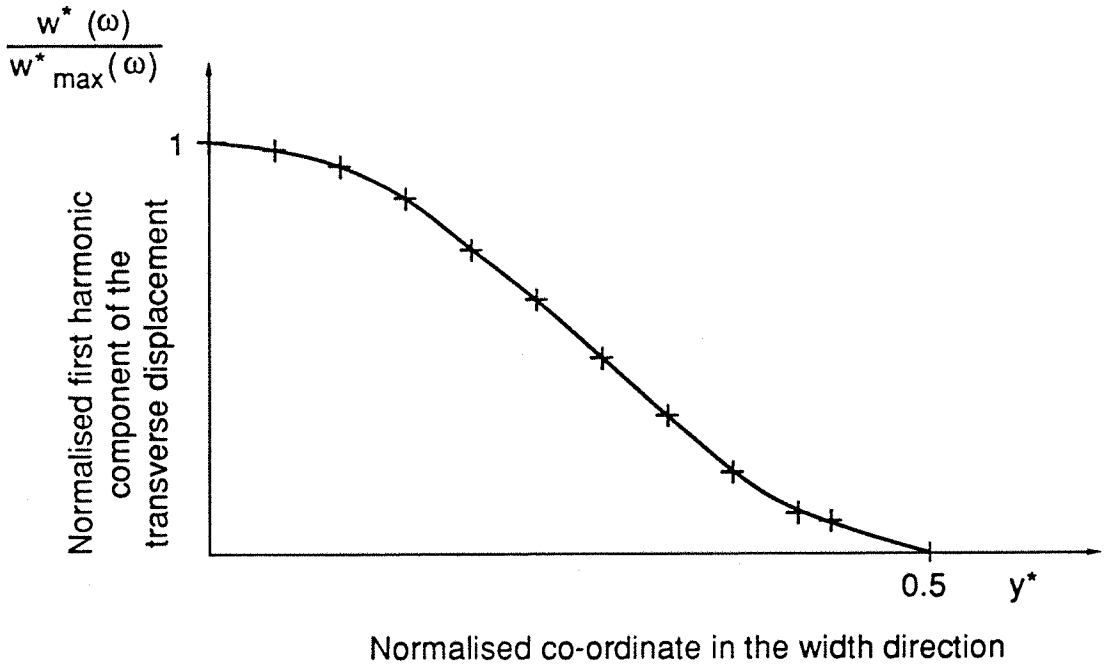

Fig. 6.14.3 MEASURED NORMALISED FIRST HARMONIC DISTRIBUTION AT $x^* = 0.7$, $w^*_{max}(\omega)$ at $(x^*,y^*) = (0.7,0.5)$ is 0.6 .

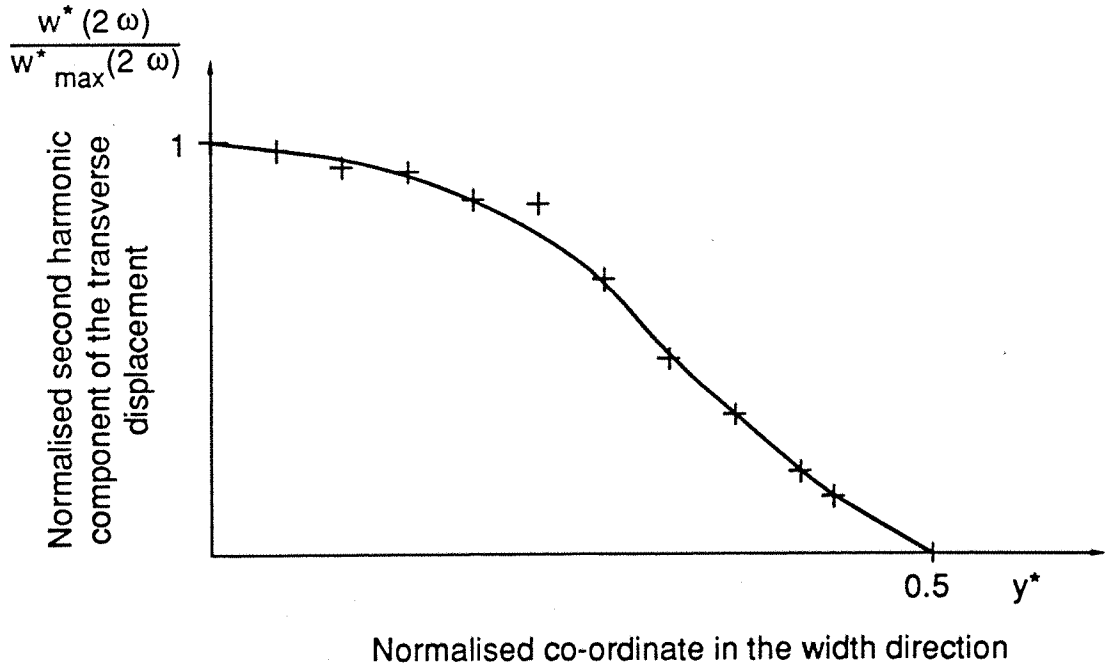

Fig. 6.14.4 MEASURED NORMALISED SECOND HARMONIC DISTRIBUTION AT $x^* = 0.7$, $w^*_{max}(2\omega) = 0.1$.

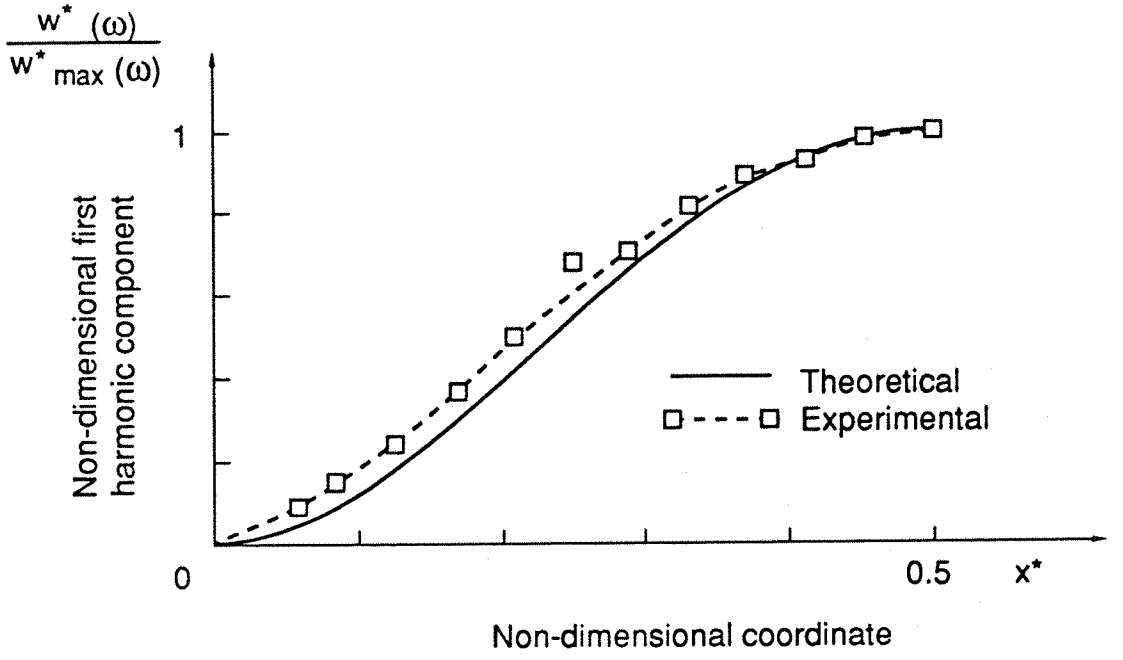

Figure 6.15.1 NORMALISED FIRST HARMONIC COMPONENT ALONG THE LENGTH DIRECTION FOR $y^* = 0.5$. C F R P PLATE . A COIL AND MAGNET EXCITER AND B & K ANALYSER. EXCITATION FREQUENCY: 56 Hz. $w^*_{max} = 0.5$.

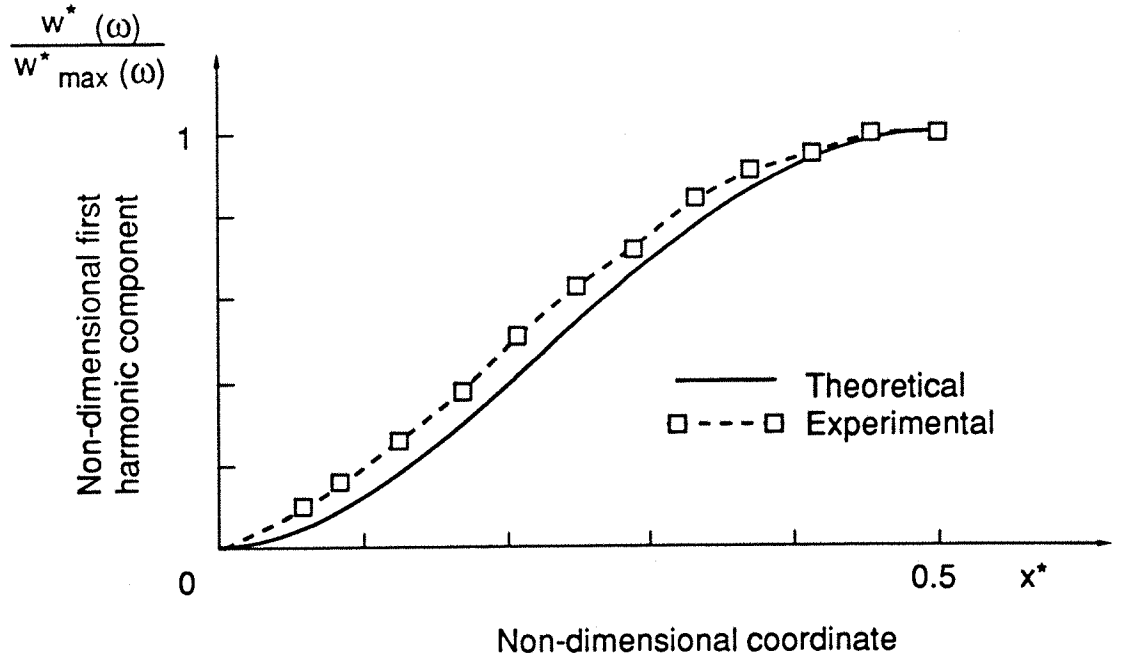

Figure 6.15.2 NORMALISED FIRST HARMONIC COMPONENT ALONG THE LENGTH DIRECTION FOR $y^* = 0.5$. C F R P PLATE . A COIL AND MAGNET EXCITER AND B & K ANALYSER. EXCITATION FREQUENCY: 66 Hz. $w^*_{max} = 0.8$.

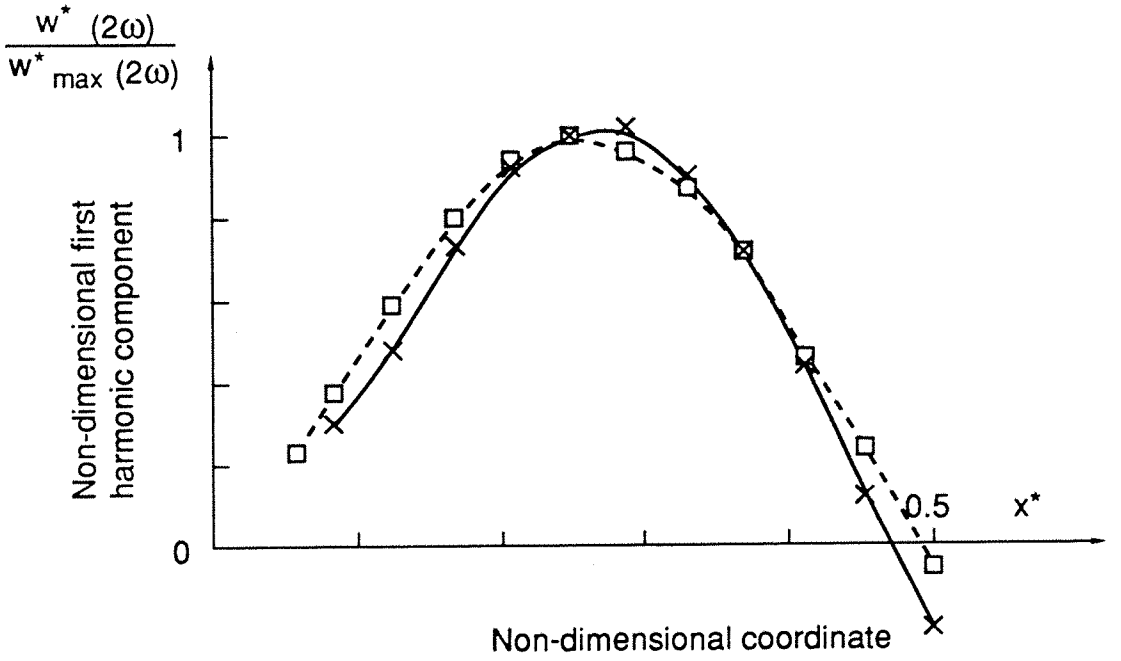

Fig. 6.15.3 NORMALISED SECOND HARMONIC COMPONENT ALONG THE LENGTH DIRECTION FOR $y^* = 0.5$. CFRP PLATE

×——× Second harmonic associated with the first harmonic plotted in Figure 6.15.1.

□- - - □ Second harmonic associated with the first harmonic plotted in Figure 6.15.2

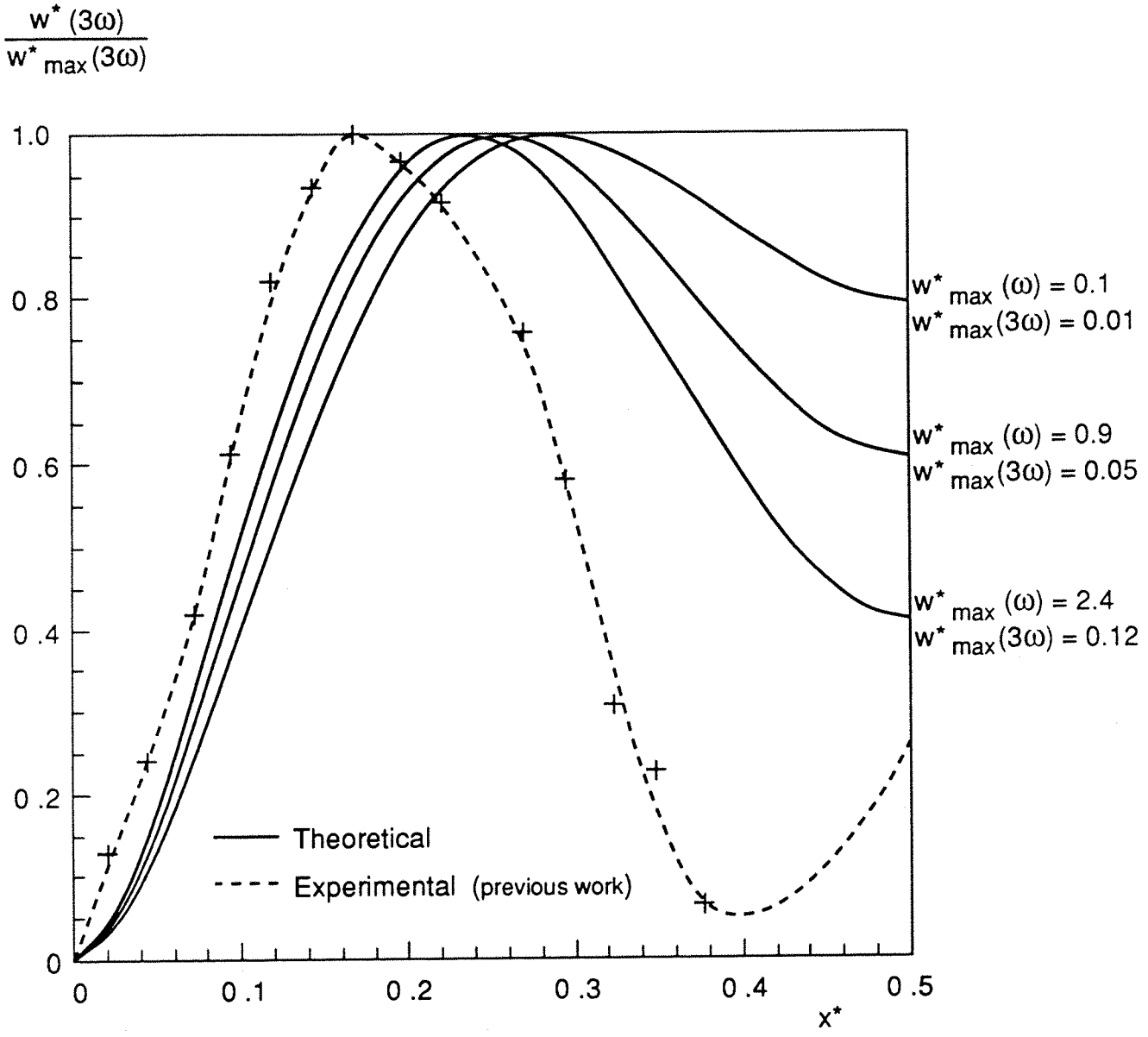

Figure 7.1 MEASURED AND CALCULATED NORMALISED THIRD HARMONIC DISTRIBUTION FOR VARIOUS VALUES OF VIBRATION AMPLITUDES OF A FULLY CLAMPED BEAM.

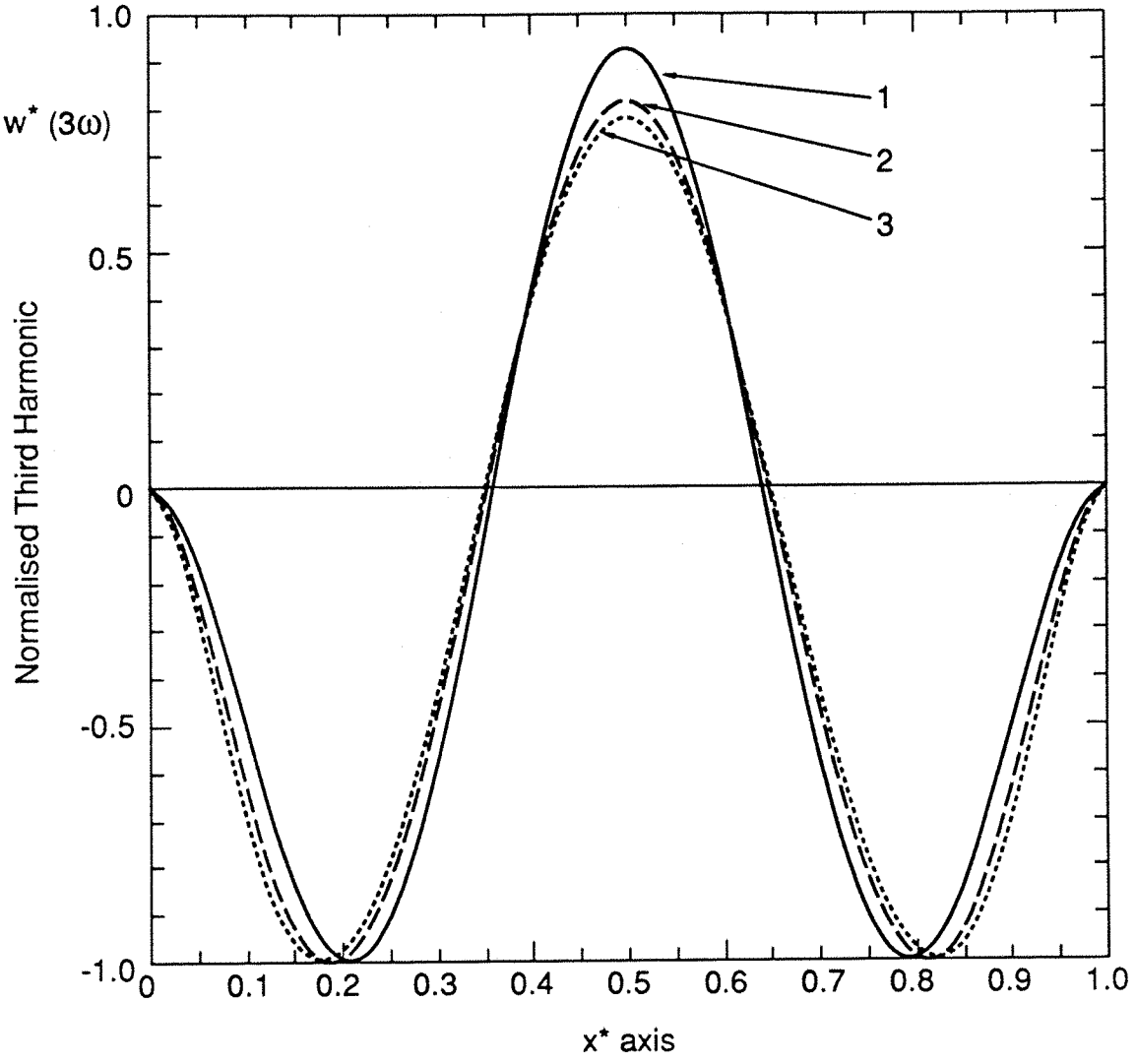

1 ——— { $w^*_{max}(\omega) = 0.8$; $w^*_{max}(3\omega) = 0.310^{-5}$

2 – – – { $w^*_{max}(\omega) = 1.6$; $w^*_{max}(3\omega) = 0.02$

3 ..... { $w^*_{max}(\omega) = 3.7$; $w^*_{max}(3\omega) = 0.13$

Figure 7.2 CALCULATED NORMALISED THIRD HARMONIC SPATIAL DISTRIBUTION FOR CLAMPED-CLAMPED BEAM.

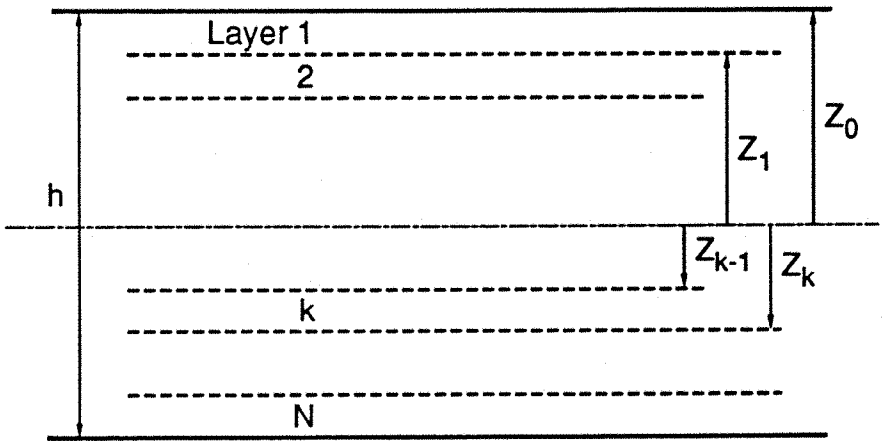

Figure 9.1 GEOMETRY OF N LAYERED LAMINATED PLATE

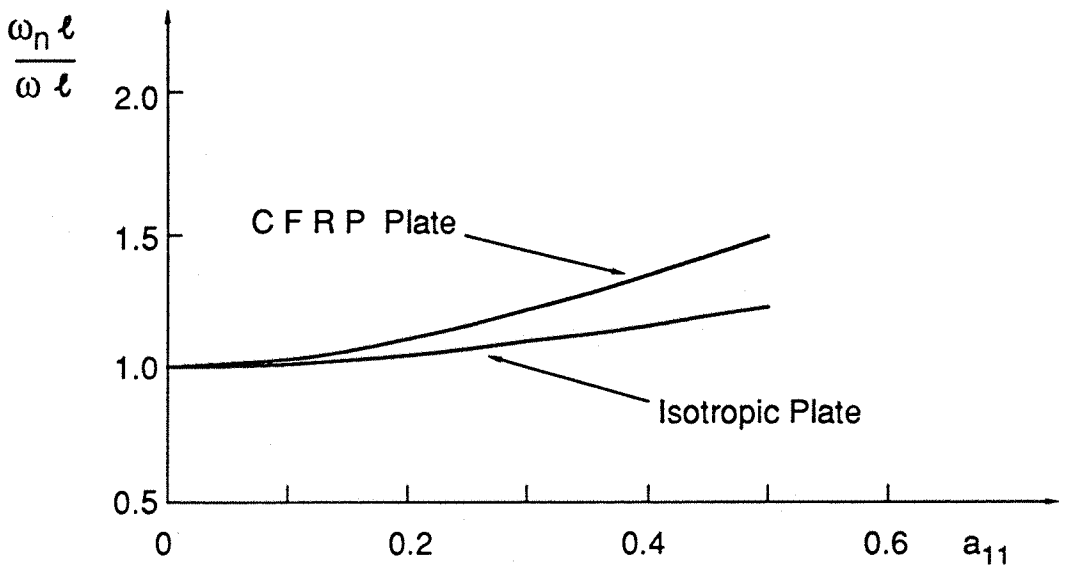

Figure 9.2 COMPARISON OF THE CHANGE IN NATURAL FREQUENCY AT LARGE AMPLITUDES FOR ISOTROPIC AND C F R P PLATES.